UNIVERSITY OF STRATHCLYDE

DEPARTMENT OF ELECTRICAL ENGINEERING

TRANSIENTS AND FERRORESONANCE IN SINGLE PHASE TRANSFORMERS

Being a study of methods of analytical and numerical calculations of the transient and ferroresonance phenomena including the nonlinearity and hysteresis effects.

by

A. Sefa Akpınar

Thesis presented for the degree of Doctor of Philosophy

in Electrical Engineering of the University of Strathclyde

March 1980

CONTENTS

SUMMARY

Initially the fundamental equations are derived from the physical system which provide a basis to draw the equivalent circuit diagram. Then the previous analytical and numerical works on transient current and ferroresonance phenomena are reviewed and the aim of the present investigation is given in Chapter 1.

In order to reduce the number of circuit parameters, the parameters are generalized making use of the "standard coefficients". Thus, in Chapter 2 the differential equations obtained in Chapter 1 are put into new forms.

Since there are a number of methods of representing the B/H characteristics the possibilities are compared at the beginning of Chapter 3 to choose the most suitable one. To estimate the coefficients of the functions representing the characteristics the experimental B/H pattern is required. Therefore, the method used to obtain these characteristics is explained.

The main purpose of Chapter 3 is actually to calculate the transient current. So analytical and numerical techniques are developed.

In Chapter 4 fundamental ferroresonance is investigated. To visualize the jump phenomena a graphical solution is presented and used to predict the jump points. To achieve more accurate results, additional terms are included in the expressions of flux linkages.

Subharmonic ferroresonance is, in fact, a part of ferroresonance but, since its nature differs from fundamental ferroresonance, it is studied separately in Chapter 5. In this chapter, using the Preisach model and experimental series method

for the B/H representation, the hysteresis effect on subharmonic ferroresonance is examined. By an analytical method the stability of this phenomenon is investigated.

Although there is "analysis" and "comparisons" sections at the end of each chapter, general conclusions are drawn and some suggestions are made for the future work in Chapter 6.

All the explanatory figures are located in the text side and the experimental and computed figures are presented in a separate "diagrams" section.

LIST OF PRINCIPAL SYMBOLS

A	Cross-sectional area
B	Flux density
C	Capacitance
H	Magnetic field strength
I	RMS current
i	Instantaneous current
L	Length
ℓ	Leakage inductance
M	Mutual inductance
N	Turns
p	$\frac{d}{dt}$
q	Instantaneous charge
R	Resistance
t	Time
V	RMS voltage
v	Instantaneous voltage
X	Reactance
Z	Impedance
α	Switching angle
$\emptyset$	Flux
Ψ	Flux linkages
μ	Permeability

SUBSCRIPTS

A	Primary winding quantities
a	Secondary winding quantities
m	Magnetising

CHAPTER 1

INTRODUCTION

The early experimental investigations on transient and ferroresonance phenomena led the investigators to find out the fundamental principles underlying the phenomena. But, besides understanding the principles, a prediction of these phenomena which require a mathematical analysis as well as experiments to define some parameters of the system were also in question.

From this standpoint, the basic point for the prediction is to represent the devices which will be used by an adequate mathematical model. Such a model for a single phase shell type transformer,whose physical model is shown in Fig. 1.1,and constructional details are given in Appendix A1 may be derived in two parts.

1.1 Electric Circuit Equations

From the consideration of the magnetic flux paths shown in Fig. 1.2 the following voltage equations for each coil can be written.

$$v_A = R_A i_A + \ell_A . \; pi_A + N_A . p\phi$$
$$v_a = R_a i_a + \ell_a . \; pi_a + N_a . p\phi \qquad 1.1$$

Since the B/H characteristic is normally given the flux ϕ should be expressed in terms of B and H. This can be established by using the magnetic circuit equations.

1.2 Magnetic Circuit Equations

The flux associated with the coil on any limb consists of two components, one of them links with other coils on the other limbs, which is defined as mutual flux and corresponds to the mutual inductance. The other component has a path mainly in air, so it is

defined as leakage flux,and the corresponding leakage inductance is taken as being constant, whereas mutual inductance is a function of magnetising current. In reality, the leakage flux is not constant because of passing through the core. It, therefore, varies with the voltage applied to the coil.

Now, if the Ampere Turns rule is applied to the path 4 in Fig. 1.2,

$$N_A\, i_A + N_a\, i_a = L.\, H \qquad 1.2$$

where

$$L = 2\, L_2 + 2\, L_1$$

the average length of flux path in metres.

The flux equation for the junction (1) in Fig. 1.2 is

$$\phi = \phi_1 + \phi_2 \qquad 1.3$$

since the magnetic circuit is completely symmetrical and the relation between cross sectional areas is

$$A = 2\, A_1 \qquad 1.4$$

The flux density B is the same in all limbs. Therefore we can use the B/H characteristic obtained from the central limb for the other limbs and yokes.

Substituting the relations obtained from magnetic circuit

$$\phi = 2\, \phi_1$$

and

$$\phi_1 = B\, \frac{A}{2}$$

into the equation 1.3 we can get

$$\phi = B.A$$

In this equation B is a function of field strength H. So, differentiating flux ϕ with respect to time yields

$$p\, \phi = A.\, \mu.\, pH \qquad 1.5$$

where

$$\mu = \frac{dB}{dH}$$

is the differential permeability or the slope of the B/H characteristic.

Combining equations 1.1, 1.2 and 1.5, and referring all the secondary quantities to the primary turns N_A, the following set of simultaneous differential and algebraic equations are obtained.

$$\begin{aligned} v_A &= R_A\, i_A + \ell_A \cdot pi_A + M(i_m) \cdot p\, i_m \\ v_a &= R_a\, i_a + \ell_a \cdot pi_a + M(i_m) \cdot p\, i_m \\ i_m &= i_A + i_a \end{aligned} \qquad 1.6$$

where

$$M(i_m) = \frac{N_A^2 \cdot A}{L} \cdot \mu(i_m)$$

is the mutual inductance which is function of magnetising current defined by

$$i_m = \frac{L}{N_A} \cdot H.$$

In regard to equations 1.6 an equivalent circuit as in Figure 1.3 may be given for the transformer. When the secondary side of the transformer is open circuited ($i_a = 0$), as will be considered in this investigation, the performance equations of the transformer become

$$\begin{aligned} v_A &= R_A \cdot i_A + \ell_A \cdot pi_A + M(i_m) \cdot pi_m \\ v_a &= M(i_m) \cdot pi_m \\ i_m &= i_A \end{aligned} \qquad 1.7$$

Now, in order to write the equations of the series resonance circuit shown in Figure 1.4, the resistance and inductance of the circuit are added to the resistance and leakage inductance of the transformer respectively provided that they are linear. Hence

$$v_A = R_A \cdot i_A + \ell_A \cdot pi_A + M(i_m) \cdot pi_m + v_c$$

$$v_a = M(i_m) \cdot pi_m$$

$$v_c = \frac{1}{C} \int i_A dt + v_c(0^+)$$

$$i_m = i_A \qquad 1.8$$

It is clear that to solve either equations 1.7 (as in the transient problem) or equations 1.8 (as in the ferroresonance problem) the relation $M = f(i_m)$, in other words, $B = f(H)$ must be known.

1.3 Previous Work

It is convenient to classify the previous work on transient current and ferroresonance as analytical work and numerical work.

1.3.1 Previous Analytical Work on Transient Currents

The first systematical experimental investigation on transient current was made by Turner[1]. In the paper published in 1931 he gave the factors affecting transient current experimentally.

Blume et al[2] made the first attempt to calculate the transient current and they suggested some method to reduce it. In the text book of Blume et al[3], the exciting current and transient current are studied in detail.

Since the protection equipment in a system must be capable of carrying the transient current its shape is also important as well as its peak values in order to select the fuses and relays. So, Specht[4] gave a method to determine the shape of the transient current in single phase transformer using "The Experience Factors". He tried to improve the results obtained from a linear approximation. Although the error for the first peak in the calculated results is $\pm$ 27% it is about $\pm$ 17% for the later peaks. It was assumed that there was no current flowing till flux reaches its saturation value.

That is to say, the B/H characteristic is represented as in Fig. 1.5.

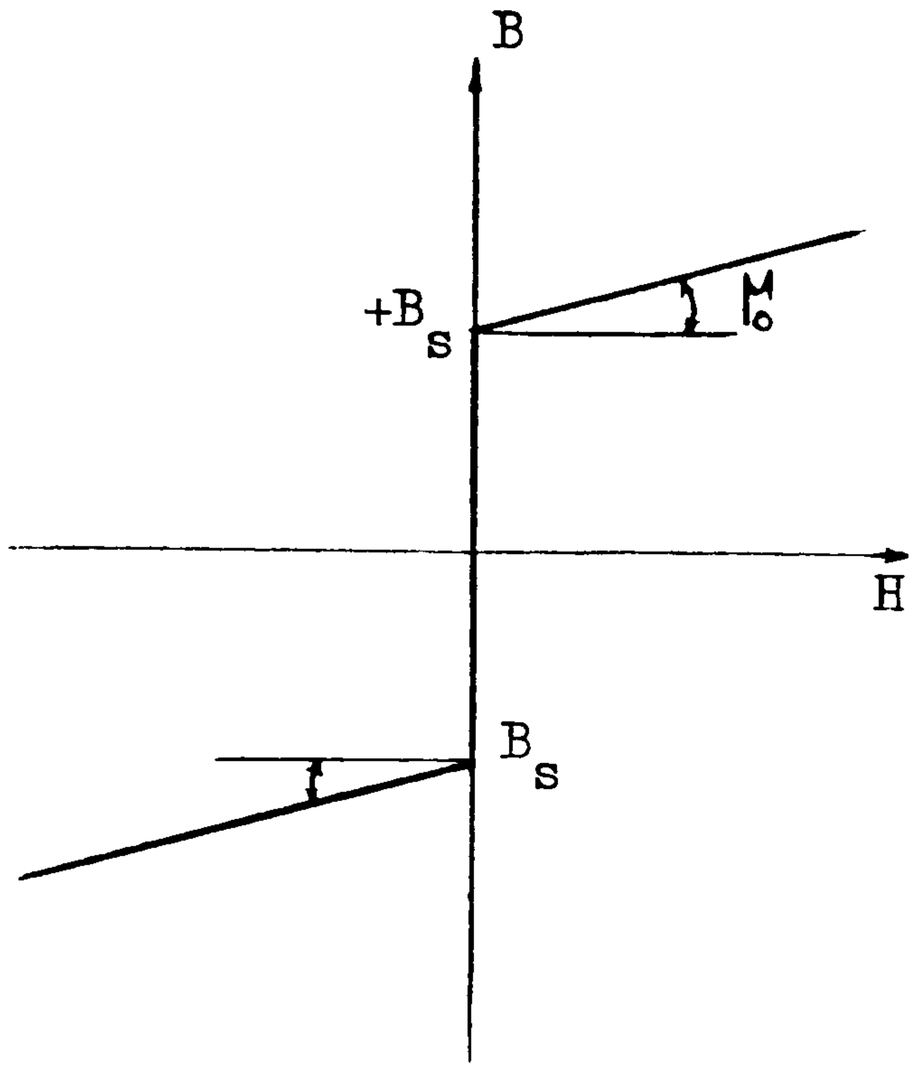

Fig. 1.5

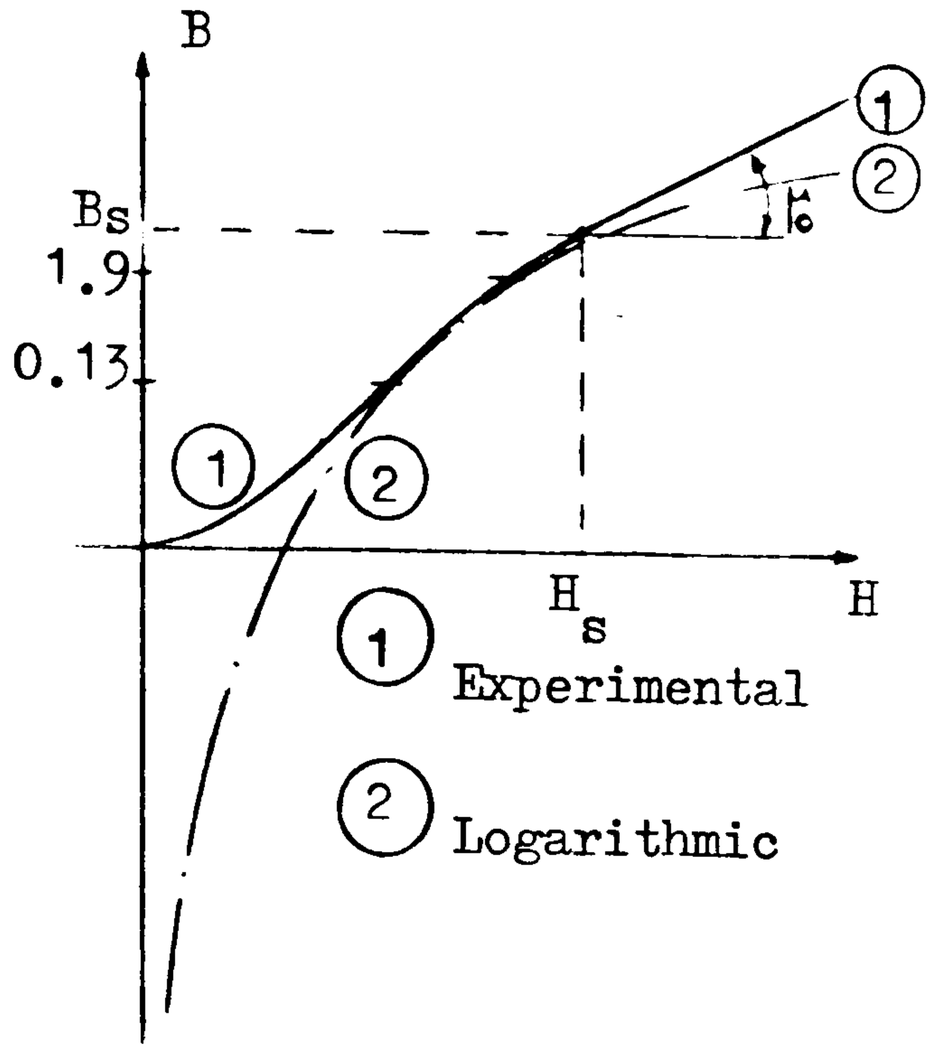

Fig. 1.6

Holcomb[5], Drozdov et al[6] used a method similar to Specht, but Holcomb's method produces more accurate results and needs less time for the calculation.

Malyshev[7] represents the B/H characteristic by a Logarithmic relation as in Fig. 1.6 and, neglecting the leakage inductance of the system, he reduces the voltage equation 1.7 to the well-known "Bernouilli Equation". The analytic expression of the B/H relation used is

$$B = c_1 \, \mathrm{Log}_{10} (c_2 \, H) \qquad 1.9$$

Sarkar et al[8] apply Kron's tensorial method to analyse the transient currents of a loaded transformer, neglecting the magnetising current and using the Laplace transformation.

1.3.2 Previous Analytical Work on Ferroresonance

Although Martienssen[9] also has done experimental work on ferroresonance, especially on jumping phenomena, the first systematic experimental investigation on ferroresonance was performed by Rouelle[10]. He described all the factors affecting jumping phenomena

Duffing[11] gave a method for the solution of the equation, so called "Duffing Equation",

$$F \cos \omega t = p^2 X + k_1 X + k_2 X^3 \qquad 1.10$$

where F, k_1, k_2 are constants.

Although Duffing gives this equation for the mechanical oscillations, neglecting the leakage inductance, the voltage equations 1.8 can also be put into the above form if the B/H characteristic is represented by a single-valued power series.

$$H = c_1 B + c_3 B^3 \qquad 1.11$$

where c_1, c_3 are constants.

Odessey et al[12] and Thomson[13] use the volt-ampere characteristic instead of B/H to describe the critical point (only jumping-up conditions). They mainly use two independent relations, namely the volt-ampere characteristic of the transformer and the voltage equations 1.8 in terms of 'fundamental harmonic'.

Rudenberg[14] describes the jumping-up point by a graphical construction but using volt-ampere characteristic and the voltage equations 1.8 in terms of fundamental harmonic again.

Keller[15] displays six different methods of solution including perturbation and Galarking methods for the discrete non-linear problems in electrical engineering, but in a second paper Keller[16] employs a method similar to perturbation to solve equations 1.8.

Hayashi[17] investigates the forced oscillations with non-linear restoring forces and analyses their stability by means of integral curves. He uses a cubical form given by equation 1.11 for the B/H representation.

In a second and third paper of Hayashi[18,19] the stability problem of fundamental and subharmonic oscillations are discussed by the variational method. The principle of the method is to reduce

a differential equation

$$p^2X + 2\delta \cdot pX + c_1X + c_2X^3 = f(t) \qquad 1.12$$

to an equation of Hill's type.

In a fourth paper[20] of Hayashi, a method of representing the B/H hysteresis loop is proposed to examine the influence of hysteresis on non-linear resonance and the energy losses. The B/H loop is represented by an ellipse and magnetisation curve by a cubical form as in equation 1.11. The following figure illustrates how to get a loop according to this method.

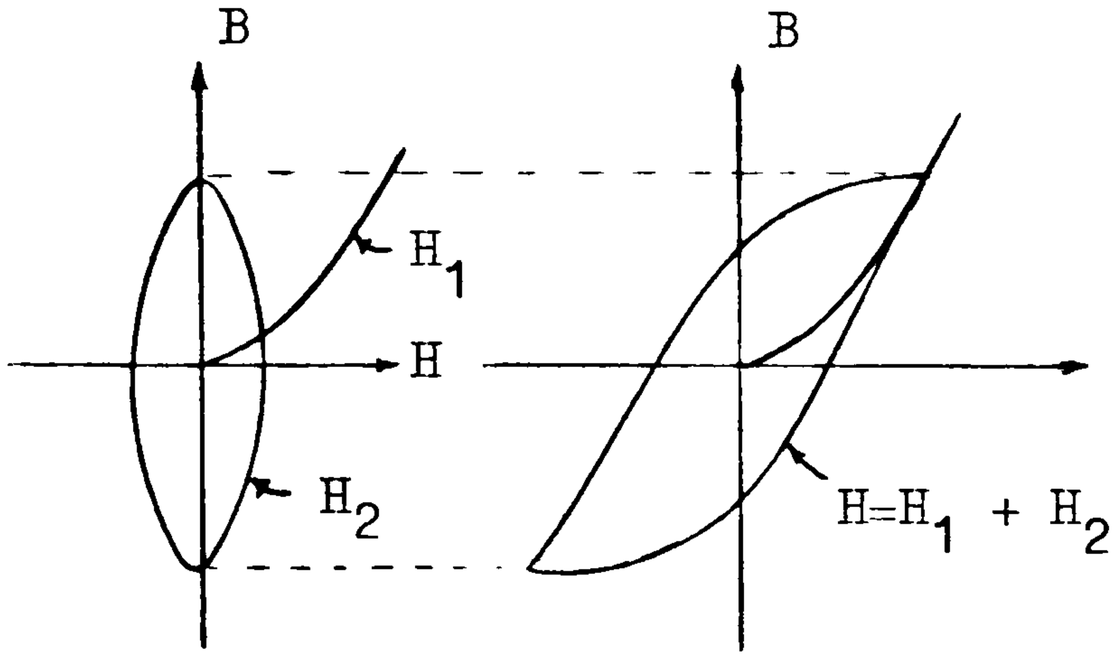

$H_1 = c_1B + c_3B^3$

$H_2 = \frac{1}{\omega} \frac{c_4}{(1+c_5B_m^2)} \frac{dB}{dt}$

B_m = Max.value of B

c_1, c_3, c_4, c_5: constants

Fig. 1.7

Ku[21, 22] develops the "phase plane method" to apply to circuits with non-linear elements such as non-linear capacitance and non-linear inductance. He examines the differential equation in the form of equation 1.12 from the topologic point of view, i.e. instead of solving directly by inserting new variables

$$V = \frac{dx}{dt}, \quad g = \frac{dV}{dt} \quad \text{and} \quad \frac{g}{V} = \frac{dV}{dx}$$

He derives

$$g = f(t) - 2\delta V - c_1X - c_2X^3 \qquad 1.13$$

So, for given initial conditions X_o, t_o, V_o, the corresponding acceleration g is calculated from equation 1.13. Then choosing an increment ΔX ($\Delta X = X_1 - X_o$) the new set of variables are found

so that

$$\Delta V = V_1 - V_o = \left(\frac{g_o}{V_o}\right) \Delta X \quad \text{or} \quad V_1 = V_o + \left(\frac{g_o}{V_o}\right) \Delta X$$

$$\Delta t = t_1 - t_o = \frac{\Delta X}{\Delta V} \quad \text{or} \quad t_1 = t_o + \frac{\Delta X}{\Delta V}$$

and acceleration g_1 is obtained by substituting X_1, V_1, t_1 into equation 1.13. Thus, proceeding in this way, further points are obtained. Then plotting v and g against X and analysing the graphs, some qualitative information about ferroresonant conditions is obtained.

Huey et al[23], Swift[24,25] and Kumar et al[26] view the ferroresonance problem as a control-system problem and apply the "Describing Function Technique". According to this technique the flux linkage is supposed to have the following form:

$$\Psi = A \cos(\omega t + \alpha) + B \cos \omega t \qquad 1.14$$

and the "Describing Function" is defined as

$$K = \frac{\text{Fundamental of output phasor}}{\text{Input phasor}}$$

The relation $i = f(\Psi)$ is converted to a block which has a gain of K. Thus, the block diagram of series resonance circuit is

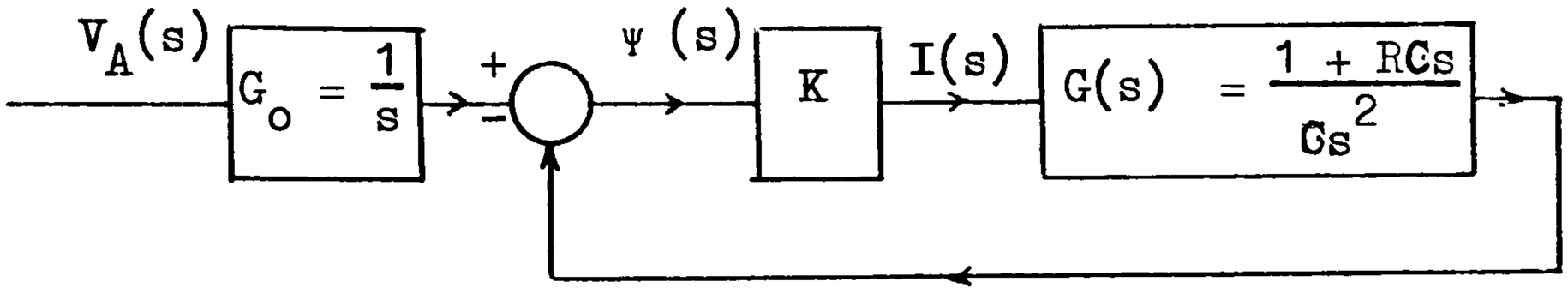

Fig. 1.8

G_o and G(s) in this block diagram are found from voltage equation 1.8 neglecting leakage induction c_e and applying Laplace transformation. By Nyguist criteria the stability of system is then studied.

They also use a cubical form as in equation 1.11 for the relation $i = f(\Psi)$.

Baycura[27] offers a qualitative explanation of the unsymmetrical mode of ferroresonance and an approximate solution

using "The Reversion Method of Series". In order to apply this technique he puts the voltage equation 1.1 in the form of

$$a_1 \psi + a_2 \psi^3 = k f(t) \qquad a_1 \neq 0 \qquad 1.15$$

where a_1 and a_2 are functions of operator $p = \frac{d}{dt}$, and k a constant, f(t) a given function of time.

Reversion method [28] assumes that the form of solution of the differential equation 1.15 is

$$\psi(t) = k A_1 + k^2 A_2 + k^3 A_3 + \text{- - - - -} \qquad 1.16$$

The unknown coefficients A_1, A_2, A_n are determined by substituting equation 1.16 into 1.15 and equating coefficients of equal powers of k. Consequently, the problem of solving the non-linear differential equations becomes a problem of solving a set of linear differential equations.

To put the voltage equation 1.8 into the form as in equation 1.15 a cubical relation is taken for $i = f(\psi)$.

On subharmonic resonance, the first systematical experimental work belongs to Fallou[29]. Rouelle[10] determined the effects of frequency variation on subharmonic resonance and gave a test circuit by which it was easy to initiate the subharmonic resonance.

Travis[30], Angello[31] (analytically) and Spitzer[32] (experimentally) determine the initial conditions.

Hayashi[19], Wright[33] and Shenkman[34] give stability criteria by means of Hill's equations.

Norimatsu et al[35] introduce a method of prevention of subharmonic resonance.

1.3.3 Previous Numerical Work on Transient Current

In all the calculation methods given by the authors mentioned in the preceding section the analytical technique was employed and did not produce accurate results because the representation

of the B/H characteristics could not be given by a function which yields a differential equation capable of solution. But, since 1960, the developments in computers and computing technique allow the use of numerical method to solve differential equations. Thus, a wealth of methods of representing the magnetisation curve and B/H loop by complicated functions has arisen. For example, MacFadyen[36] represents the magnetisation characteristic by an exponential series such as

$$B_1(H) = \mu_o H + \sum_{i=1}^{3} c_{2i-1} (1 - \exp(-c_{2i} \cdot H)) \qquad 1.17$$

and produces very accurate results. Without computer, it is impossible to solve the differential equation containing such a representation analytically.

Since this expression fails to represent the region around the origin MacFadyen makes use of

$$\Delta B = c_7 \cdot H \cdot \exp(-c_8 \cdot H^{c_9}) \qquad 1.18$$

for the difference.

$$\Delta B = B_1(H) - B \text{ experimental}$$

Thus, the whole expression is

$$B(H) = B_1(H) - \Delta B \qquad 1.19$$

and differential permeability

$$\mu(H) = \frac{d\, B_1(H)}{dH} - \frac{d(\Delta B)}{dH}$$

or

$$\mu(H) = \mu_o + \sum_{2i-1}^{3} c_{2i-1} \cdot c_{2i} \cdot \exp(-c_{2i} \cdot H)$$

$$- c_7 \cdot \exp.(-c_8 \cdot H^{c_9}) \cdot (1 - c_8\, c_9\, H^{c_9}) \qquad 1.20$$

where $c_1, \ldots c_9$ are coefficients to be determined and μ_o the final slope of experimental B/H characteristic.

Neape[37] presents another method representing the whole B/H loop in addition to magnetisation characteristic using the same idea,

i.e. the exponential series. In this method the basic idea is to shift the particular part of magnetisation curve to produce a loop. This method is also capable of expressing the minor loops.

MacFadyen and Teape both study the transient current in single phase and three phase transformers at the loaded and unloaded conditions by their representation methods.

Yamashita et al[38] investigate the transient phenomenon by signal flow graphs, and represent the transformer in the experiments by a simulator, and B/H loop and magnetisation characteristic by straight line segments.

1.3.4 Previous Numerical Work on Ferroresonance

Teape[37] studies the ferroresonance phenomena using his own B/H representation method and, in the three-phase case, a model which allows for inter-phase leakage flux thereby catering for unbalance during transient conditions.

Reducing all the different combination of circuit to a single phase form, Germay et al[39] analyse the ferroresonance phenomena on high-voltage power system applying Preisach Theory.

1.3.5 Preisach Theory

In the Preisach Theory[40,41,42] the magnetic material is considered to be an assembly of dipoles, each of which exhibits a square-loop hysteresis characteristic determined by two independent parameters H_m and H_c. H_m represents the fields of neighbouring dipoles and H_c the coercivity. It is assumed that the dipoles are distributed statistically in the magnetic material. So, defining the distribution function

$$\gamma (H_m, \ H_c)$$

Preisach gives

$$B = \mu_o H + 2 B_s \iint \gamma (H_m, H_c). \, d H_c \, d H_m \qquad 1.21$$

for the calculation of the flux density. The essential principles and basic theory are detailed in Appendix A3.

Felltkeller et al[43] used the analytical expression

$$\gamma\ (H_m, H_c) = \exp\ (\ -((\frac{H_m}{a})^2 \ + \ (\frac{H_c}{b})^2\ )\ )$$

(a, b constants)

for the distribution function. But they noticed that this expression has two maxima for the soft material. However, Girke et al[44] experimentally showed that some soft material also has one or two maxima.

On the other hand, introducing new variables

$$H_1 = H_m - H_c$$

$$H_2 = H_m + H_c$$

which are independent from each other. A new distribution function

$$\overline{\gamma}\ (H_1,\ H_2) = \ \gamma\ (\frac{H_1 + H_2}{2}\ ,\ \ \ \frac{H_2 - H_1}{2})$$

is derived. Biorci and Pescetti[45] separate this new function into independent functions with one variable so that

$$\overline{\gamma}\ (H_1,\ H_2) = \ \overline{\gamma}_1\ (H_1)\ .\ \overline{\gamma}_2\ (H_2) \qquad 1.22$$

Germay et al[46] define $\overline{\gamma}1$ and $\overline{\gamma}2$ numerically from the experimental B/H characteristic. An example is given in Appendix A3.

Coulson[47] has given the following expression for γ

$$2Bs\ \gamma\ (H_m, H_c) = \sum_{i=1}^{m} c_{1i}\ c_{2i}\ c_{3i}\ \frac{(c_{1i}\ H_c)^n}{n_i}\ \exp(-c_{1i}\ H_c).\ \exp(-c_{2i}|H_m|) \qquad 1.23$$

where m : number of terms to be used

c_{1i}, c_{2i}, c_{3i} and n coefficients.

For a hard magnetic material, Coulson found that one term gives an

acceptable representation but soft magnetic materials require additional terms.

1.4 Purpose of the Present Investigation

In power system engineering it is well known that the energy transportation can be economized by increasing the impressed voltage of the transmission line, and the power factor of the distribution system can be improved by a group of condensers. But, increasing the voltage of the system consisting of generator, transmission line and transformer may cause the operating conditions to reach critical points at which abnormal phenomena, such as ferroresonance and subharmonic resonance, may occur. Similar phenomena are observed in distribution systems.

In order to protect the system from these abnormal phenomena protection equipment, such as fuses, relays, are installed. But these equipments should permit the transient current due to switching of the supply. That means the designer should have some information about the amount of transient current and corresponding time.

Thus, it is seen that there are mainly two problems. One the abnormal phenomena and conditions referred to above, and the other the normal transient current.

As given in the sections on previous work, some authors investigate these phenomena purely experimentally - for example, references 1, 9, 10, 29. Some of them take the problems from the purely mathematical points of view, as in references 15, 17, 21, 22. However, in references such as 24, 25, 36, 37 and 39 the theory is accompanied by experiments, and comparisons are made.

It is the purpose of the present investigation to explore alternative analytical solutions and stability criteria for these phenomena. The possibility of applying Preisach theory as the basis for allowing for magnetic non-linearities will be given particular attention. By using the normalised loop, the performance equations will be generalised, thus more general solutions will be sought. Finally, comparisons will be made between computed and experimental results for single-phase systems.

CHAPTER 2

2. GENERALIZATION OF THE PARAMETERS

In order to study the response of the circuit to any change in the circuit parameters, the performance equations of the circuit need to be examined. If the circuit to be studied is composed of many parameters it is rather difficult to exhibit the effects of the change in each parameter. However, using mathematical rules it is not only possible to reduce the number of parameters and to generalize them, but also much computing time may be saved.

Plotting the results thus obtained, and analysing the graphs, some general information about response of the circuit may be derived. Therefore, first the normalized loop will be considered.

2.1 Normalized Loop

If the H axis in Figure 2.1a is divided by H_c and B axis by B_s the Figure 1b is obtained. From now on this loop is to be called the "Normalized Loop" and the coefficients to be used in the representation of it "Standard Coefficients".

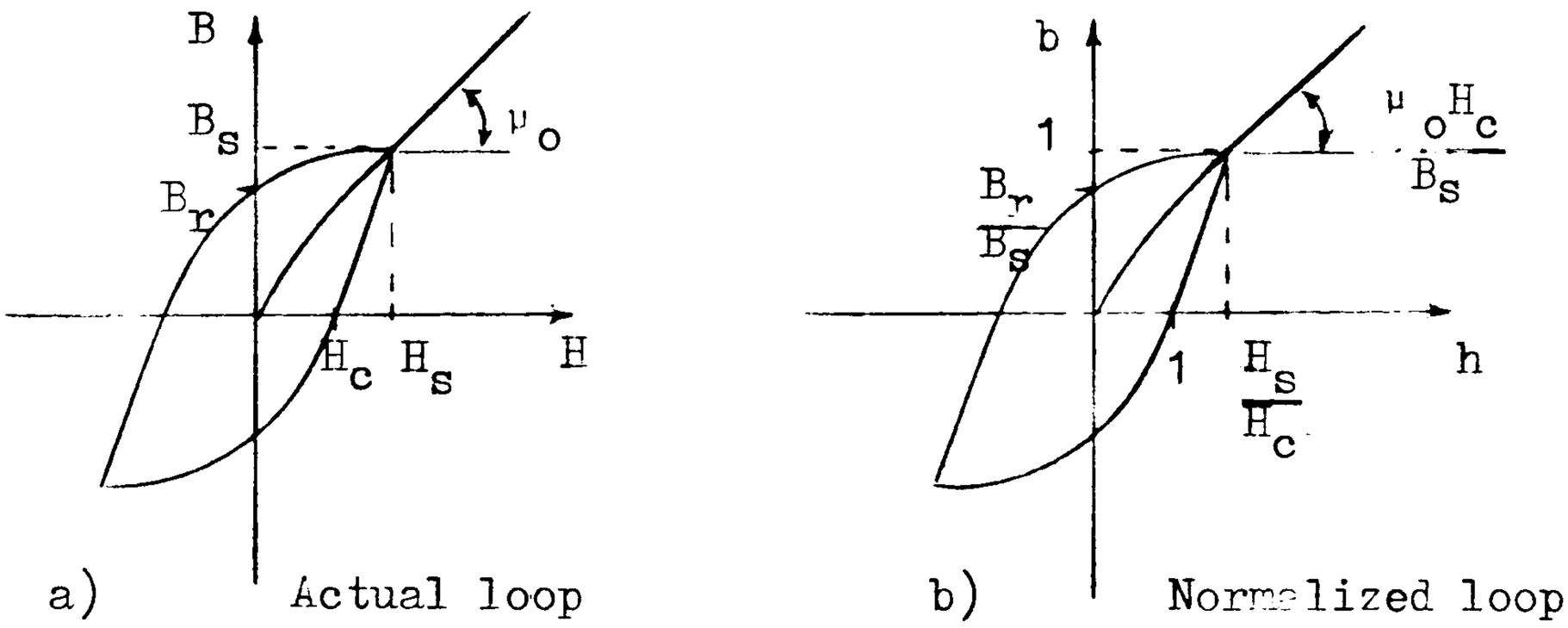

a) Actual loop b) Normalized loop

Fig. 2.1

If the normalized loop is expressed by

$$b = f(h) \qquad 2.1$$

then the corresponding actual loop becomes

$$B = B_s \cdot f(h) \qquad 2.2$$

where

$$b = \frac{B}{B_s} \qquad 2.3$$

$$h = \frac{H}{H_c} \qquad 2.4$$

The differential permeability can be derived from equation 2.2 so that

$$\mu = \frac{dB}{dH} = B_s \cdot \frac{df(h)}{dh} \cdot \frac{dh}{dH}$$

or

$$\mu = \frac{B_s}{H_c} \quad f'(h) \qquad 2.5$$

Thus, knowing only the saturation flux density B_s and coercive force H_c, and using the standard coefficients given by Coulson[47], tabulated in Table 2.1, it is possible to transfer the actual loop to a normalized loop. Of course, the loop or magnetisation characteristic obtained by using the standard coefficients will not be as accurate as the one obtained using the actual coefficients estimated over the actual loop. But, as will be seen in sections of the later chapters where results are compared, the accuracy is not too bad.

Since f(h), the function representing the non-linearity and hysteresis, is now independent from the material, the results of the performance equations only depend on parameters which include B_s, H_c.

Terms	Coefficients		
	First (c_{1i})	Second (c_{2i})	Third (c_{3i})
First (n = 12)	14	14	0.599
Second (n = 0)	0.34	1	0.415
Third (n = 0)	1.1	0.26	0.478
Fourth (n = 0)	10	$5.9\ 10^{-3}$	0.254

c_{1i}, c_{2i}, c_{3i} are the coefficients of the equation 1.23.

Table 2.1 Standard Coefficients

2.2 Generalized Parameter for the Transient Current

For the numerical prediction of the transient current in the single phase transformer with secondary open circuited, the equations 1.6 are utilized. But for $\mu(H)$, the differential permeability, either the actual loop representation or normalized loop representation can be used. If the normalized loop is employed, the main voltage equation

$$\sqrt{2}\,.\,V \sin(\omega t + \alpha) = Ri + \ell \frac{di}{dt} + N \frac{d\phi}{dt}$$

becomes

$$\sqrt{2}\,.\,V \sin(\omega t + \alpha) = \frac{R.L.H.}{N} + \frac{\ell.L}{N} \frac{dH}{dt} + N.A. \frac{dB}{dH} \cdot \frac{dH}{dt}$$

by substituting $i = \frac{L.H}{N}$

Using the relation 2.4 and 2.5 we get the following equation

$$\sin(\omega t + \alpha) = \frac{R.L.H_c}{\sqrt{2}\,V.N.} \cdot h + \frac{\ell.L.H_c}{\sqrt{2}\,V.N.} \frac{dh}{dt} + \frac{A.N.B_s}{\sqrt{2}.\,V.} f'(h) \frac{dh}{dt} \qquad 2.6$$

Inserting the new parameters

$$\tau = \omega t + \alpha$$

$$d\tau = \omega dt$$

$$P_1 = \frac{R.L.H_c}{\sqrt{2}\,V.N}$$

$$P_2 = \frac{\omega.\ell.L.H_c}{\sqrt{2}\,V.N.}$$

$$P_3 = \frac{\omega.\,A.N.B_s}{\sqrt{2}\,V}$$

The new form of the voltage equation is

$$\sin \tau = P_1.\, h(\tau) + [P_2 + P_3.\, f'(h)] \frac{dh(\tau)}{dt} \qquad 2.7$$

Thus we have reduced nine parameters such as the construction parameters N, A, L, the material parameters B_s, H_c, the circuit parameters R, ℓ and supply parameters ω, V to only three parameters P_1, P_2, P_3 which are, from now on, to be called the "Generalized Parameters".

It must be noticed that P_1, P_2 and P_3 are independent from each other because each one has one independent actual parameter.

Another point to be observed is that τ is not in time dimension any longer; its dimension is degree.

Since there is no analytical solution of equation 2.7 due to representing f(h) by very complicated functions, it is only solved by numerical technique.

Once the results are produced by changing the parameters P_1, P_2, P_3 for one transformer, then the transient current for

another transformer can be easily found by just calculating the parameters P_1, P_2, P_3 from the actual parameters of the new transformer. That means there is no need to run the programme for the new transformer.

2.3 Generalized Parameters for Ferroresonance Circuit

With the same idea explained in the foregoing section we can derive the generalized form of the performance equations of the ferroresonance circuit.

From equation 1.8

$$\sqrt{2}\ V \sin(\omega t + \alpha) = Ri + \ell \frac{di}{dt} + N \frac{d\phi}{dt} + \frac{Q}{C}$$

$$\frac{dQ}{dt} = i \qquad 2.8$$

Substituting the relations 2.4, 2.5 and $i = \frac{L.H.}{N}$ into the above equation we have the equation

$$\sin(\omega t + \alpha) = \frac{R.L.H_c}{\sqrt{2}\ V.\ N.} . h + \frac{\ell\ .L.H_c}{\sqrt{2}\ V.N.} \frac{dh}{dt} + \frac{A.N.B_s}{\sqrt{2}\ V.} . f'(h) \frac{dh}{dt} + \frac{Q}{C}$$

$$\frac{dQ}{dt} = \frac{L.H_c}{N} . H \qquad 2.9$$

By the transformations

$$\tau = \omega t + \alpha$$

$$d\tau = \omega dt$$

$$q = \frac{\omega.N}{L.H_c} . Q$$

$$P_1 = \frac{R.L.H_c}{\sqrt{2}\ V.N.}$$

$$P_2 = \frac{\omega\ell\ .L.H_c}{\sqrt{2}\ V.N.}$$

$$P_3 = \frac{\omega.A.N.B_s}{\sqrt{2}\ .V.}$$

$$P_4 = \frac{L.\ H_c}{\sqrt{2}\ V.\omega.C.N.}$$

The equations 2.8 become

$$\sin \tau = P_1 h(\tau) + [P_2 + P_3 f'(h)] \frac{dh(\tau)}{dt} + P_4 q(\tau)$$

$$\frac{dq(\tau)}{d\tau} = h(\tau) \qquad 2.10$$

Thus ten parameters consisting of R, ℓ , C, N, A, L, H_c, B_s, ω and V are reduced to four parameters P_1, P_2, P_3 and P_4. Again we call these the "Generalized Parameters" for ferroresonance circuit.

It must be remembered that we cannot neglect any generalized parameter because of it being smaller than any of the actual parameters whereas external resistance or leakage inductance may be neglected for the steady-state operating case because they are small in such a circuit. The main reason for this is that the generalized parameters are composed of more than one actual parameter. For instance, even if R is small P_1 cannot be neglected, because for small V, P_1 will have a high value.

Within a restricted region it is observed that the current, or flux, in ferroresonance circuits has two values corresponding to one value of voltage.This is also true if ω or C are considered as the variables in place of voltage. Therefore, although we have reduced the number of parameters, this characteristic feature of the current is still valid in the equation 2.10 with the generalized parameters.

It is obvious that the effects of new parameters on performance are totally different from that of the actual parameters' effects.

CHAPTER 3

3. TRANSIENT CURRENT

3.1 Numerical Solution

In the application of the mathematical model of the system the equations 1.6 and 1.7 require the differential permeability - $\mu(H)$.

In the numerical calculations there are mainly two possible ways to get the differential permeability. These are:

A) storing a number of (B, H) points experimentally obtained and making use of the mathematical fact that

$$\frac{dB}{dH} = \frac{\Delta B}{\Delta H} = \frac{B_{n+1} - B_n}{H_{n+1} - H_n}$$

where n is the number of points and ΔH must be very small.

B) representation of the B/H characteristic by continuous curves using the stored experimental points and one of the curve fitting methods.

In the first way which leads to the linear interpolation, each point on the B/H characteristic will have two different differential permeabilities, that is, if μ were plotted against H there would be some discontinuities just due to the method.

On the other hand, as is well known, the solution of any differential equation by a numerical technique is strictly dependent on the initial value of the variable to be solved. In other words, the initial value must be unique and correct. Otherwise, any incorrect initial value will affect the next step in the calculation and consequently the results will be wrong.

Now, in the light of this fact it is quite possible to

have some unstable solutions during the process if the first way is followed. Therefore, the continuous expressions for the representation of B/H characteristic will be chosen to get the differential permeability.

3.1.1 Selection of the Method Representing the B/H Characteristic

Although there are many methods of representing the B/H characteristic by continuous functions, a number of them have been compared[36] with each other and it has been proved that these methods are not able to represent this characteristic accurately.

In fact, the comparison should be carried out depending on the purpose of using these representations. If it is preferable to use the analytical techniques, the present mathematics may not be sufficient to solve either the transient current or the ferro-resonance problem using the expressions given by Macfadyen[36], Teape[37], Coulson[47], even the polynomial form of higher order such as

$$B = a_o + a_1 H + \ldots + a_n H^n ,$$

or

$$H = b_o + b_1 B + \ldots + b_n B^n , \qquad 3.1$$

or

Frohlich formula

$$B = \frac{B_s . H}{c_1 + c_2 H} + \mu_o H \qquad 3.2$$

But, if a numerical technique will be employed, in this case, the computing time for the comparison should be considered as well as the accuracy of the methods.

In the present investigation, for the numerical calculations, the Frohlich formula, which requires less computing time compared to other methods, and Macfadyen's exponential

expression, which is the best in accuracy, will be used for the representation of the magnetisation characteristic.

In order to observe the effects of hysteresis on the calculation, the Preisach Theory will be applied.

Since Frohlich formula requires only two coefficients (see Equation 3.2) it is relatively simple in form and these coefficients c_1, c_2 can even be evaluated by hand just taking two experimental points (B_1, H_1), (B_2, H_2). But, for a set of data points c_1 and c_2 can be defined by the least square method. By this method the error between the fitted curve and experimental curve is minimized.

As will be seen from expressions 1.19 and 1.20 there are nine coefficients to be determined in Macfadyen's exponential series. These coefficients may also be evaluated by least-square method. But Macfadyen used the iteration method given in Appendix A2, illustrated in Figures 3.1, 3.2 and 3.3, which is relatively simple and saves more computing time.

The method of calculating B and μ developed by Coulson[47] from Preisach Theory, the estimation of the coefficients in Appendix A3, and related illustrative diagrams in Figures 3.4, 3.5, 3.6, 3.7, 3.8 and 3.9 are given in detail.

3.1.2 Reason for and Method of Obtaining the Experimental B/H Characteristic

As it is understood from the above discussions, in any case, any representation method requires an experimental B/H curve and B/H loop to get the data points for the evaluations of the coefficients.

The B/H characteristic was obtained in two stages using

two systems as in Figures 3.10 and 3.11. The region up to the saturation point (B_s, H_s) was obtained by the former system and the remainder, which is a straight line, by the later system.

Before the experiment is carried out two requirements need to be fulfilled. These are calibration and demagnetisation.

A. Calibration of Equipment

Since

$$\Psi = N.A.B.$$

$$v_y = k.\Psi = k.N.A.B.$$

k = Gain of Integrator

and N, A are known, for a given value of B the input voltage to the Y - terminal is calculated. By the same manner, from equations

$$i = (L.H)/N$$

$$v_x = R_{sh}.i = \frac{R_{sh}.L}{N} . H$$

R_{sh} = Shunt Resistance

v_x, the input voltage to x terminal, can be calculated for a given value of H and known values of R_{sh}, L, N. Thus, by means of the above relations, the plotter and oscilloscope are calibrated.

B. Demagnetisation of the Transformer

Any residual flux density in the transformer core will cause an unsymmetrical form of B/H characteristic and, consequently, affect the accuracy of the coefficients. Therefore, the core is demagnetised before obtaining the whole B/H characteristic, either by applying an A.C or D.C voltage. In the former case, the applied voltage is gradually reduced from saturation level to zero flux density. In the latter case, the D.C voltage is also gradually reduced from saturation level to zero but by constructing loops within loops. The latter method is more reliable but it is

a lengthy and laborious process.

It is important to notice that at the moment the transformer is energised to obtain B/H characteristic, the capacitor of the integrator should have no initial charge, otherwise the characteristic will not be perfectly symmetrical.

After calibration and demagnetisation, the set is ready for obtaining the B/H characteristic. So, applying D.C voltages, the magnetisation characteristic (Fig. 3.12), the loops (Fig. 3.13 and 3.14) are obtained, and applying A.C voltages the straight line section of the B/H characteristic (Fig. 3.15) is obtained.

It should be observed that for the estimation of the coefficients only the outermost loop is required.

3.1.3 Comparison of the Methods Chosen

Since the Frohlich formula fits the upper region of magnetisation characteristic satisfactorily but fails for the lower region, it is suitable for transient current calculation but not for the steady-state solution. On the other hand, the exponential series fits perfectly at each point. That is to say, it gives good results for the steady-state current as well as transient current.

The Preisach Theory does not fit as well as the exponential series, especially in the region about the origin. As will be seen from Figures 3.4 and 3.5, this method gives a characteristic abruptly rising about the origin. This is a very important feature of this method because it will force us to use smaller time steplength for this region.

One of the vital features of the various representation methods for the numerical calculation is that they give different values of differential permeability at the origin (H = 0).

Therefore, let us consider the expressions of the slope functions at this point.

From Equation 3.2 for Frohlich formula

$$\mu(0) = \frac{B_s}{c_1} + \mu_o \qquad c_1 >> B_s \qquad 3.3$$

From Appendix A3 for Preisach model

$$\mu(0) = \mu_1(0) = \mu_o \qquad 3.4$$

From Equation 1.20 for exponential series

$$\mu(0) = \mu_o + c_1 c_2 + c_3 c_4 + c_5 c_6 - c_7 \qquad 3.5$$

Since the exponential series represents the characteristic very well its slope should be correct. So, comparing Equations 3.3 and 3.4 with Equation 3.5, it is seen that the Preisach Theory gives a low value. In fact, the analytical expression of the distribution function given by Coulson is not satisfactory at the origin.

Now, if we write the derivative of the current with respect to time from Equation 1.7

$$\frac{di}{dt} = \frac{v_A - R_A . i_A}{\ell + M(i_A)}$$

or

$$\frac{di}{dt} = \frac{V_m \sin(\omega t + \alpha) - R_A . i_A}{\ell + \frac{N^2 . A . \mu(H)}{L}}$$

Since $i = 0$, $H = 0$ at $t = 0$ the above relation becomes

$$\frac{di}{dt} = \frac{V_m \sin \alpha}{\ell + \frac{N^2 . A . \mu(0)}{L}} \qquad 3.6$$

From this relation it is clear that for a small value of $\mu(0)$ the derivative of the current will be large. Consequently, this incorrect initial value results in incorrect solution because the first step of the method of numerical solution (Runge-Kutta) is

directly equal to this derivative and other steps are functions of the first step.

It is not the purpose of this investigation to deal with the B/H representation. Therefore, instead of improving the B/H model, we will overcome the above difficulty by supposing that there is very small current flowing in the circuit at the instant $t = 0$. Thus, the slope will become bigger than μ_o. For example, for the initial condition $t = 0$, $i = 0$, $\alpha = \frac{\pi}{4}$, $B_r = 0$, $V = 250$ V, the first peak of current is $Ip_1 \cong 130$ A which is very far removed from the experimental one. But, if the initial current $i = 0.03$ A is taken at the same condition, the first peak becomes $Ip_1 \tilde{=} 79$ A which is closer to the experimental value.

Now, if an error statement is described as below

$$\text{Error} = \frac{\sum_{i=1}^{k} \frac{BE_i - BC_i}{BE_i}}{\sum_{i=1}^{k} i} \quad 100\% \qquad 3.7$$

where BE : experimental flux density

BC : computed flux density

i : number of points used

Using the least-square technique for the estimation of the coefficients and the 6000 - Honeywell Computer, the following table of comparison is obtained. But, for this, the coefficients of the Preisach model have been estimated using only magnetisation curve and remanent flux density (see Appendix A3 for detail).

All the coefficients computed for the sample transformer are given in Appendix A1.

	Computing Time for coefficients (in second)	Error for the same number of points (%)
Frohlich Formula	0.0366	27.57
Exponential Series	2.71	2.32
Preisach Theory	1.5	9.07

TABLE 3.1

3.1.4 The Selection of the Time Steplength

For the numerical solution of the differential equation the four-step Runge-Kutta method will be used.

Since there is no iteration process in this method the approach to the solution depends on the nature of the function to be solved, and to the time steplength to be selected.

The other method of solution, predictor-corrector method includes a process of iteration. Therefore, by the iteration more accurate results may be produced but, unfortunately, this method requires two initial values for each of dependent and independent variables while Runge-Kutta needs only one. Furthermore, predictor-corrector consumes more computing time compared to the former method.

For the time steplength there is no explicit method given for the right size but it can be chosen by trial and error. However, we can write the factors affecting steplength in our calculation.

A) The variation of the current by time. If the current is varying very quickly by time the steplength should be small. If not, it can be enlarged.

B) The B/H representation. If this characteristic is rising abruptly from one step to another as in Coulson's model (around the origin) the steplength must be small, otherwise corresponding slope will be very different from one point to another which will result in larger values. For that reason, in the numerical calculations we choose dt = 0.05 ms for lower region and dt = 0.2 ms for upper region of B/H characteristic. If dt = 0.02 ms is taken for the lower region as well, the result will be larger.

For the purpose of comparison, we can give the following tables 3.2 and 3.3 obtained using the 6000 - Honeywell computer. First table is for Preisach model, second for exponential series method.

Computed Current (A)	Steplength (ms)				Experimental Current (A)
	0.1	0.05,* 0.1	0.2	0.05,* 0.2	
First peak	109.13	103.74	134.0	103.71	102
Second peak	33.44	32.36	36.75	32.18	33
Third peak	16.8	16.62	17.09	16.36	17
Steady-state	7.8	7.8	7.8	7.8	8
Job Time** (in sec.)	31.31	45.12	15.64	36.55	-

Table 3.2

First peak	103.04	103.04	103.00	103.01	102
Second peak	31.98	31.90	30.94	31.94	33
Third peak	17.04	16.80	21.66	16.77	17
Steady-state	8.2	8.2	8.2	8.2	8
Job Time** (in sec.)	21.57	28.32	10.72	20.38	-

Table 3.3

* (The first steplength for the region < 0.17)
(The second one for the region < 0.17)

** Job time is measured over the time period t = 0.2 sec.

$V = 250V$, $\alpha = 0$, $B_r = 0$, $R = 1.64$, $\ell = 0.00265$, $f = 50$ Hz

As it is seen from these tables, the change in steplength does not considerably affect the results if the exponential series representation is used. But, if Coulson's representation is employed, attention should be paid to choosing the time steplength as, in this case, the first peak of the current strictly depends on it.

Comments on the programme for the computer, establishment of initial flux density by Preisach Theory and other related matters are given in Appendix A4.

3.2 Analytical Solution

In the analytical calculations it is necessary to represent the B/H characteristic by continuous functions, then differentiating this with respect to H, the required differential permeability (slope function) - $\mu(H)$ is found. But, as is mentioned before, it is impossible to make an analytical calculation using the expressions given by Macfadyen, Teape and Coulson, even the higher order polynomial forms as in Equations 3.1. Therefore, the function representing the B/H characteristic should be simple in form and should be able to put the performance equations in readily solvable form.

Before becoming involved in analytical expressions, let us analyse the effect of the circuit resistance on transient current by numerical programme.

3.2.1 Effect of Resistance on Transient Current

In the open circuited condition, the voltage drop due to the primary resistance is usually small compared to the voltage across the transformer's terminals. Therefore this voltage drop, $R_A\ i_A$, can be neglected until the current flowing in primary circuit reaches

a certain limit.

On the other hand, from our accurate numerical calculation we know that the current and corresponding time for any point (B_1, H_1) on the B/H plane, near the point (B_s,H_s) are

T_1 = 5.55 ms I_1 = 22.74A

and the first peak of current

T_p = 8.35 ms I_p = 102.54A

with R = 1.64 Ω , V = 250V, α = 0, B_r = 0.

If R = 0 is taken

T_1 = 5.55 ms I_1 = 25.01A

T_p = 9.95 ms I_p = 197.95A

Now, if we take R = 0 for the region $0 \leqslant H \leqslant H_1$, then R = 1.64 for the region $H_1 \leqslant H$, we find

T_1 = 5.55 ms I_1 = 25.26A

T_p = 8.35 ms I_p = 104.98A

So, it is seen that the resistance has a large effect on peak current and corresponding time, but has not a perceptible effect within limits which will now be indicated. The whole B/H characteristic can be split into two parts as shown in Fig. 3.16. The voltage drop due to resistance can be neglected until the saturation point (B_s, H_s) and included in calculations after this point.

3.2.2 Representation of the Rising Curves

In the following analytical expression to be derived the B/H characteristic will be represented by Frohlich formula given by Equation 3.2. But, in order to take into account the initial flux density we add an extra term to the Frohlich formula.

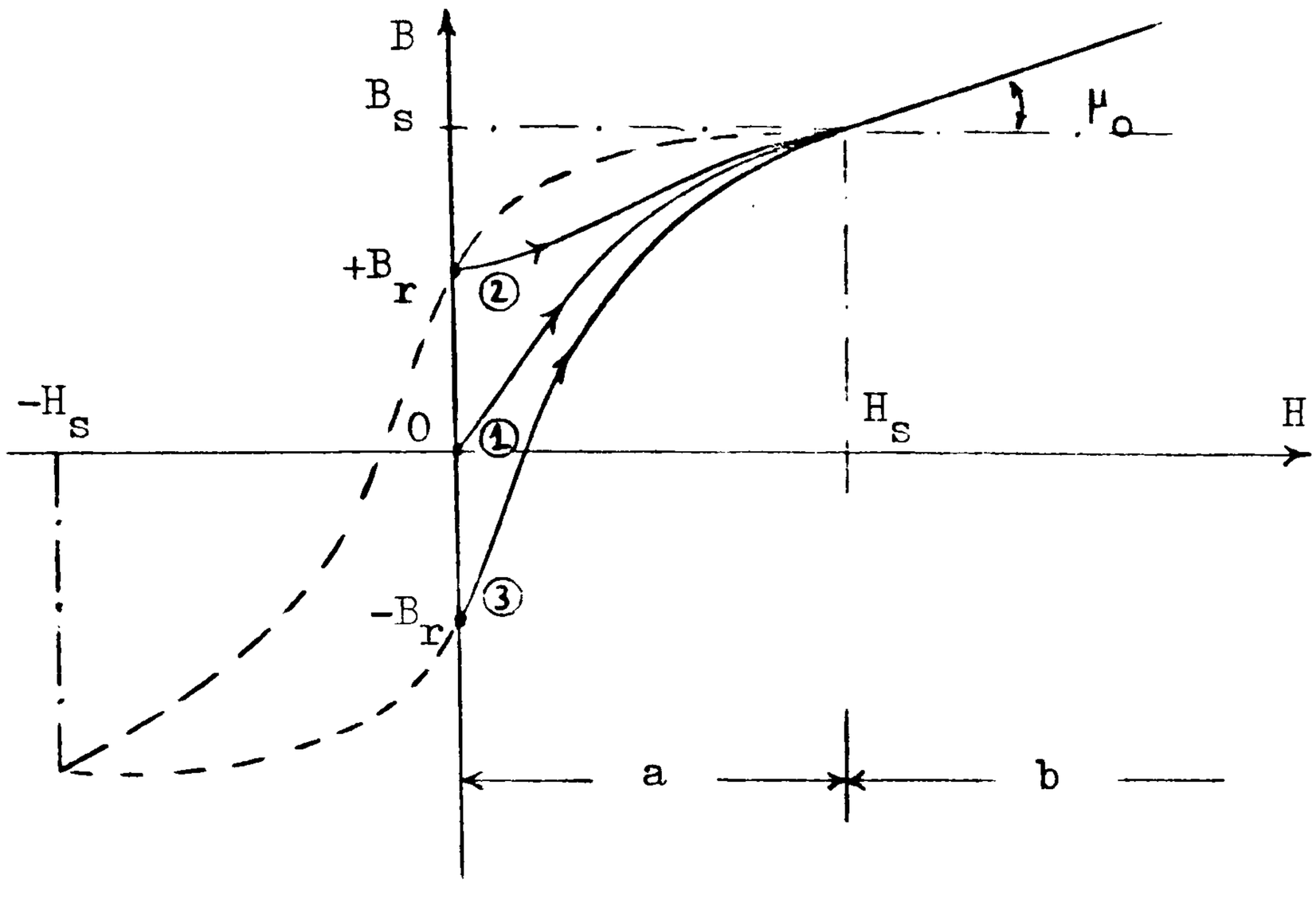

Fig. 3.16

Thus, the new form of Frohlich formula becomes

$$B = \frac{B_s . H}{c_1 + c_2 H} + \mu_o H + B_o \qquad 3.8$$

and slope function

$$\mu = \frac{dB}{dH} = \frac{c_1 B_s}{(c_1 + c_2 H)^2} + \mu_o \qquad 3.9$$

where

for the rising curve (1) (magnetisation curve) $B_o = 0$

for the rising curve (2) (positive residual condition) $B_o = +B_r$

for the rising curve (3) (negative residual condition) $B_o = -B_r$

μ_o : the final slope of the B/H characteristic c_1, c_2 the coefficients to be determined.

It is noticed that for all these three curves the same expression is given for the slope function (Equation 3.9), but, of course, the coefficients will have different values in each case.

The coefficients can be defined by hand selecting two points from each experimental curve.

So for $H_1 = 14000, \quad B_1 = 2.09, \quad B_s = 2.08$

$H_2 = 500, \quad B_2 = 1.41, \quad B_o = 0$

The coefficients of curve (1)

$c_1 = 223.6$

$c_2 = 1.03$

for

$H_1 = 14000, \quad B_1 = 2.09, \quad B_s = 2.08$

$H_2 = 500, \quad B_2 = 1.45, \quad B_o = +0.95$

The coefficients of curve (2)

$c_1 = 1131.29$

$c_2 = 1.928$

for

$H_1 = 14000, \quad B_1 = 2.09, \quad B_s = 2.09$

$B_2 = 500, \quad B_2 = 1.37, \quad B_o = -0.95$

The coefficients of the curve (3)

$c_1 = 98.16$

$c_2 = 0.7$

However, it is not necessary to have three experimental curves if the second point is selected nearer to the first point, which must be around the saturation point (B_s, H_s). The same flux density can be used for three curves. That means if the magnetisation curve and the residual condition of core are known, the coefficients can be calculated choosing two points from this magnetisation curve.

Above the saturation point Equation 3.8 becomes

$$B = B_s + \mu_o H + B_o \qquad 3.10$$

because for high value of H the limit of the first term of Equation 3.8 is equal to B_s.

The corresponding slope function is

$$\mu = \mu_o \qquad 3.11$$

3.2.3 Derivation of the Analytical Expressions

Since we neglect the voltage drop on resistance in the region

$$0 \leq H \leq H_s$$

from the performance Equation 1.1 we have

$$V_m \sin(\omega t + \alpha) = \ell \frac{di}{dt} + \frac{N^2 A \mu(H)}{L} \frac{di}{dt}$$

Substituting the Equation 3.9 and the relation Ni = LH into the above equation and denoting

$$k_1 = \frac{N^2 A}{L} c_1 B_s$$

$$k_2 = c_1$$

$$k_3 = \frac{c_2 . N}{L}$$

$$k_4 = \frac{N^2 A \mu_o}{L} + \ell$$

we get

$$V_m \sin(\omega t + \alpha)\, dt = \left[\frac{k_1}{(k_2 + k_3 i)^2} + k_4\right] di$$

Integrating both sides within the integration limits

$$0 \leq t \leq t$$

$$0 \leq i \leq i$$

we find the relation

$$-\frac{V_m}{\omega}[\cos(\omega t + \alpha) - \cos(\alpha)] = \left[-\frac{k_1}{k_3(k_2+k_3 i)} + k_4 i + \frac{k_1}{k_3 k_2}\right] \qquad 3.12$$

When the current reaches a value of

$$I_s = \frac{L . H_s}{N} \qquad 3.13$$

which corresponds to the saturation point, the corresponding time as obtained from Equations 3.12 and 3.13 will be

$$T_s = \frac{\arccos\left[-\frac{\omega}{V_m}\left[-\frac{k_1}{k_3(k_2+k_3 I_s)} + k_4 I_s + \frac{k_1}{k_2 k_3}\right] + \cos(\alpha)\right] - \alpha}{\omega} \qquad 3.14$$

From the trigonometry we know that the argument of the inverse function "arc cos" in the expression of T_s must be

$$-1 \leq \text{ARGUMENT} \leq +1 .$$

So, if the argument is equated to " -1" we find

$$\cos\alpha = -1 + \frac{\omega}{V_m}\left[-\frac{k_1}{k_3(k_2+k_3 I_s)} + k_4 I_s + \frac{k_1}{k_2 k_3}\right]$$

and

$$\omega T_s + \alpha = \pi \qquad 3.15$$

Hence the switching angle corresponding to this argument is

$$\alpha_s = \arccos\left[-1 + \frac{\omega}{V_m}\left[-\frac{k_1}{k_3(k_2+k_3 I_s)} + k_4 I_s + \frac{k_1}{k_2 k_3}\right]\right] \qquad 3.16$$

In order to discover the physical meaning of this angle we should return to the first derivative of the current. So, the early expression of this derivative, for a peak current equal to saturation current I_s, must be equal to zero, i.e.

$$\left.\frac{di}{dt}\right|_{\substack{i = I_{p1} = I_s \\ t = T_p = T_s}} = 0$$

or

$$\frac{V_m \sin(\omega T_s + \alpha)}{\left[\frac{k_1}{(k_2+k_3 I_s)^2} + k_4\right]} = 0 .$$

Hence, since

$$k_1, k_2, k_3, k_4, I_s \neq 0$$

the angle of sin function above must be equal to π, i.e.

$$\omega T_s + \alpha = \pi .$$

Thus we see that this equation is exactly the same as the equation

3.15 so the interpretation of the expression 3.16 is that α_s is the switching angle at which the first peak of the transient current being equal to $I_{p1} = I_s$ occurs. The corresponding instant

$$T_s = \frac{\pi - \alpha_s}{\omega} \qquad 3.17$$

A comparison will be made when we plot the peak current against switching angle α at the different residual conditions by numerical solution of performance equation.

By this analysis we have established an accurate relation between the saturation current I_s and switching angle α at the various residual conditions. Thus, one can determine within which limits of switching angle the largest positive peak currents appear. As soon as the current exceeds I_s the performance equation becomes

$$V_m \sin(\omega t + \alpha) = \ell \frac{di}{dt} + \frac{N^2 A \mu(H)}{L} \frac{di}{dt} + R i$$

Again, substituting the relation $Ni = LH$ and Equation 3.11 into this equation we obtain the differential equation

$$V_m \sin [\omega (t + T_s) + \alpha] = \ell_t \cdot \frac{di}{dt} + R i$$

where

$$\ell_t = \frac{N^2 A \mu_o}{L} + \ell$$

The solution of this differential equation with the initial values

$$t = 0 \quad , \quad i(0) = I_s$$

is

$$i(t) = k_c . \exp\left(- \frac{R}{\ell_t} . t\right) + \frac{V_m}{Z} \sin(\omega t + \beta) \qquad 3.18$$

where

$$Z = \sqrt{R^2 + (\omega \ell_t)^2}$$

$$\theta = \arctan \left(\frac{\omega \ell t}{R}\right)$$

$$\beta = \omega . T_s + \alpha - \theta$$

$$k_c = I_s - \frac{V_m}{Z} \sin (\beta)$$

Any peak value of current, and the corresponding time, can be found by taking the first derivative of the current function $i(t)$ with respect to time and equating to zero, i.e. from Equation 3.18

$$\frac{di}{dt} = - k_c \frac{R}{\ell_t} \exp\left(-\frac{R}{\ell_t}. t\right) + \frac{\omega V_m}{Z} \cos(\omega t + \beta) = 0$$

denoting

$$K_g = \frac{\omega . \ell . V_m}{Z . R . |k_c|}$$

and remembering that k_c is always negative we get

$$\exp\left(-\frac{R}{\ell_t} . t\right) = - K_g . \cos(\omega t + \beta) \qquad 3.19$$

To solve the time t from this equation we plot both sides in the same plane against time as illustrated in Figure 3.17.

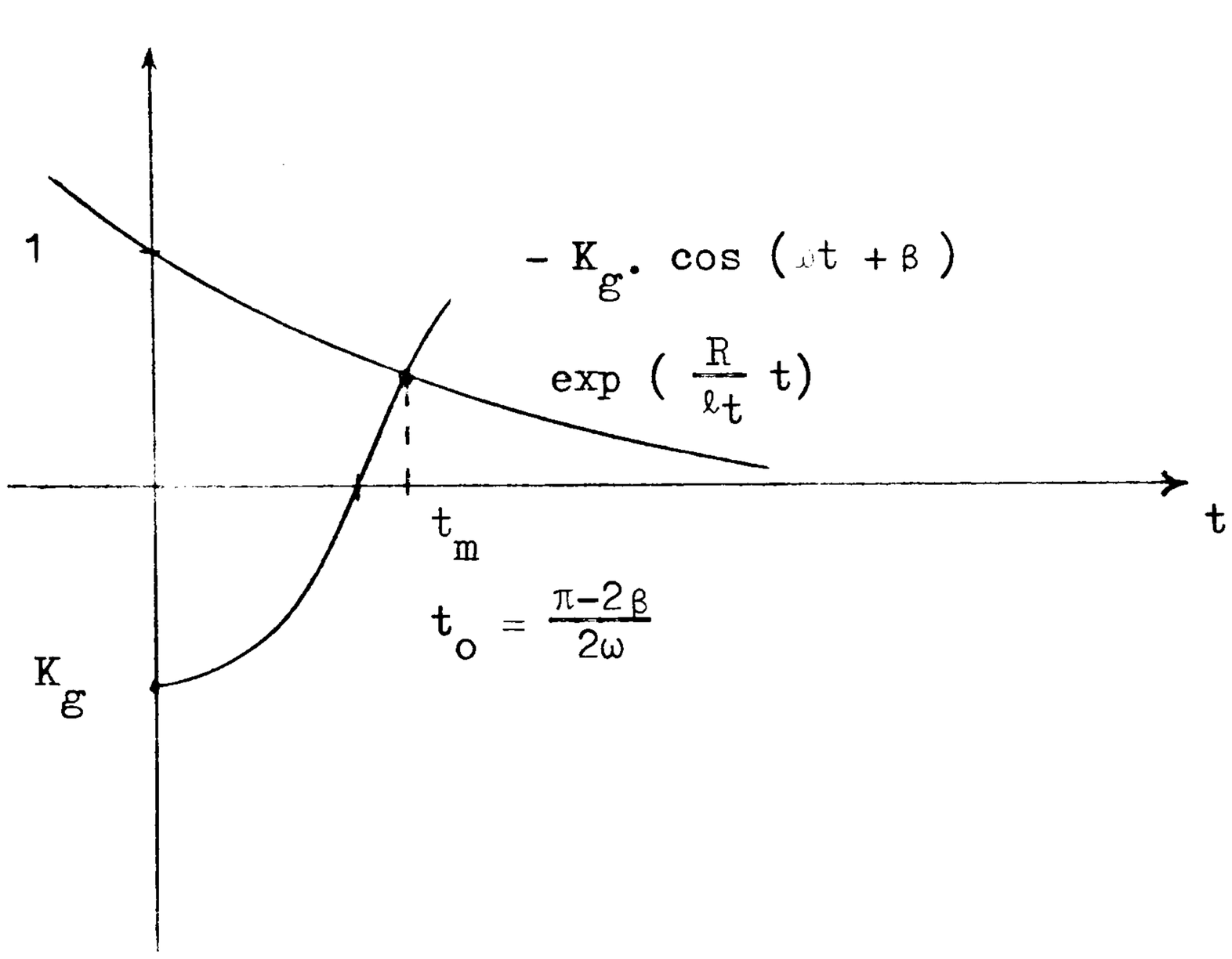

Fig. 3.17

Thus, the solution point $t = t_m$ is easily obtained graphically.

Then the peak value of current, from the expression 3.15 is

$$I_p = i(t_m) \qquad 3.20$$

and the total time from the instant at which the circuit is switched

on to the instant of the peak point is

$$T_p = T_s + t_m \qquad 3.21$$

For

$N = 240.0$, $L = 0.4059$, $A = 0.0024774$,

$V = 250$, $\omega = 314$, $R = 1.64$, $\ell = 0.00265$

$\alpha = 0$, $B_s = 2.08$, $H_s = 14000$, $B_r = 0$

$c_1 = 224$, $c_2 = 1.037$

The performance equation 1.7 is solved both by numerical method and analytical method, as described above. The results are shown in the following table

	T_s (ms)	I_s (A)	T_p (ms)	I_p (A)	Experimental I_p (A)
Numerical Solution	5.6	23.67	8.35	102.54	102.0
Analytical Solution	5.51	23.67	8.37	105.5	

$\alpha = 0$, $B_r = 0$, $V = 250V$

Table 3.4

3.3 Comparisons and Analysis of The Results

In order to compare the results of different computational techniques, it is necessary to produce experimental results for various conditions. Therefore, we will now give brief information about what technique was used to get the transient current, and how the parameters were measured.

3.31 Experimental Requirements

A. - Transformer Parameters

First d.c. values of winding resistance, using a

Kelvin-double bridge, then leakage inductance by means of a conventional short circuit test, were obtained. The results are given in Appendix A1.

B. - External Impedance

The first peak of transient current is considerably affected by the impedance of the circuit and so, in addition to the internal impedance of the transformer, the external impedance of the circuit used has to be taken into account.

Figure 3.18 shows the circuit to record the transient current. Referring to Thevenin's theorem the external circuit shown in this figure can be reduced to an equivalent circuit which consists of an open-circuit voltage E_e and equivalent impedance Z_e provided that the supply transformer and its source and supply are assumed to be linear elements. So the function $V_L = f(I_L)$ shown on the same figure is plotted by measuring the voltage across the load and the load current.

For two different resistive loads and fixed voltage E_e

$$Re = \sqrt{\frac{E_e^2 \left(1 - \left({}^{I_2}/_{I_1}{}^2\right) + V_1^2 \left({}^{I_2}/_{I_1}\right)^2 - V_2^2\right.}{2 V_2 I_2 - 2 V_1 I_1 \left(I_2/I_1\right)^2}}$$

and

$$\ell_e = \frac{\sqrt{E_e^2 - (V_1 + I_1 R_e)^2}}{\omega I_1}$$

For further detail regarding the derivation of these relations refer to reference 37.

Since the switching angle selector cannot work at the high current for very long, its impedance was found separately and plotted in Figure 3.19.

Teape[37] expresses this characteristic by

$$V = \left(b + \frac{a}{|i|}\right) i$$

Hence the impedance of switching angle selector is

$$R = b + \frac{a}{|i|}$$

External resistance and reactance values,and the coefficients a and b, are given in Appendix A1.

C. - Recording of the Transient Current

In the experiments a Tektronix 5013 storage oscilloscope was used to take transient patterns and recorded by means of a polaroid camera. Before recording the patterns, first the transformer is put into the required residual condition by demagnetisation using the d.c. circuit shown in Figure 3.10. Then the switching angle selector is adjusted to the required angle, and for various voltages applied the transient patterns were produced.

In Figure 3.20 the experimental and computed transient patterns are given and in Figure 3.21 the corresponding experimental and computed B/H patterns are shown.

3.3.2 Analysis of the Results

In order to observe the hysteresis effect on transient current two programmes have been made. In one the magnetisation curve is taken for the whole B/H characteristic, and in the other one the B/H loop is represented by Preisach model. The results are tabulated in Table 3.5. It is observed that there is no perceptible effect of hysteresis on the first three positive peaks. This is as expected because the corresponding field strengths all fall on the straight line section of the B/H characteristic. On the other hand, the residual flux, as will be seen from Figure 3.20, has a significant effect on the first peak of current. In the table 3.5 the effects

of the various residual conditions on first three positive peaks are given.

In fact, the effects of residual flux depend on the switching angle. For instance, if the circuit is switched on when the flux produced by the applied voltage is in the same direction as the residual flux in the core, so that they will add, the combination of these fluxes will give the maximum transient current.

In Figure 3.22 the computed and experimental first peaks of the transient current are plotted against switching angle α at the different residual flux densities. Up to $\alpha = 90^{o}$ the largest peak is positive and occurs at the positive residual flux density. But, for the bigger angles, the largest peak is negative and occurs when B_r is negative.

In order to define the switching angle α_s from this figure and to compare with the analytic one, a horizontal line is drawn so that the peak current will be equal to the saturation current $I_s = 23.67A$. Thus, we can tabulate α_s's obtained from the numerical results and these obtained by analytical solution as shown in table 3.6.

(1)	Experimental			Frohlich Formula (numerical solution)	Exponential Series	Preisach Theory			Parametric Method		
	B_r= -0.958	B_r=0	B_r=0.958			B_r= -0.958	B_r=0	B_r=0.958	B_r= -0.958	B_r=0	B_r=0.958
Ip_1(A)	55	102	137	102.5	103	57	103.7	137.9	54.5	102.8	138.5
Ip_2(A)	22	33	37	33.6	31.94	22.6	32.2	38.1	23.9	32.	36.6
Ip_3(A)	16	17	18	16.95	16.7	13.9	16.4	17.95	16.57	18.7	19.8
I_{ssp}(A)	8	8	8	4.5	8.2	7.8	7.8	7.8	11.5	11.5	11.5
(2)											
Ip_1(A)	0.77	19	64	19.8	19.9	0.76	19.6	63.5	0.55	23.4	68.1
Ip_2(A)	0.76	11	18.5	8.6	10.5	0.75	10.1	16.2	0.53	13.27	21.4
Ip_3(A)	0.74	7	11	5.1	7.1	0.74	7.	9.2	0.53	9.17	12.6
I_{ssp}(A)	0.72	0.72	0.72	0.45	0.73	0.74	0.74	0.74	0.5	0.5	0.5

Table 3.5

α = 0. (1) V = 250 V (2) V = 150 V

	$B_r = -0.95$	$B_r = 0$	$B_r = 0.95$
From Figure 3.22	$48^{\circ}.7$	$79^{\circ}.5$	111°
From Expression 3.16	48°	$80^{\circ}.8$	110°

Table 3.6 α_s at the various residual conditions V = 250 V

	Numerical		Analytical		Experimental	
	$\alpha = 0$	$\alpha = \pi/4$	$\alpha = 0$	$\alpha = \pi/4$	$\alpha = 0$	$\alpha = \pi/4$
$B_r = 0.95$	137	120	139.2	120.8	137	122
$B_r = 0$	103.7	79.7	105.5	80.7	102	82.5
$B_r = -0.95$	57	28.9	60.3	27.2	55	33

Table 3.7

Effect of switching angle on peak transient current at the different residual conditions. V = 250 V.

In Table 3.7 the experimental, computed and analytical results are introduced to see the accuracy of the analytical method.

On the other hand, the analytical method proposed produces accurate results only under the condition

$$i \geq I_s ,$$

$$0 \leq \alpha \leq \alpha_s$$

If the switching angle is bigger than α_s, then the current will be less than I_s and must be calculated directly from the Equation 3.12.

As indicated in Table 3.5 the results of the generalized parametric method explained in Chapter 2 are generally in good agreement with the experimental results. But this method gives about 37% error for steady-state current whereas the exponential series method gives 2.5%, Preisach model 5%.

Figures 3.23, 3.24, 3.25, 3.26, 3.27, 3.28, 3.29 and 3.30 show the variation of the first peak and steady-state value of the generalized-dependent variable h (see Equation 2.4) with the generalized parameters.

Analysing these figures the following conclusions can be drawn:

A) In the region

$$0 \leq P_3 \leq 0.5$$

there is no significant variation in hp_1's (first peak of h) obtained from the various residual conditions. It seems this is a general rule because for the different values of P_1 and P_2 this property of h is not affected.

B) In the region

$$0.5 \leq P_3 \leq 2.5$$

there is considerable variation in hp_1's. For instance, at

$P_3 = 2.5$ for $B_r = 0$, $B_r = -1$ hp_1 is almost zero but hp_1 for $B_r = +1$ has still large value.

C) Generally, for all values of P_2 and P_3, hp_1 tends to zero for $B_r = 0$ at $P_1 = 3.0$, and for $B_r = -1$ at $P_1 = 2$.

D) In the region

$$0 \leq P_3 \leq 1$$

the steady-state peak value of h, i.e. h_{sp} is very dependent on P_2 and P_3.

It is interesting to point out that in this region there is not much difference between the steady-state value and the transient value. That means the oscillations are very stable.

E) In the region

$$i \leq P_3$$

the steady-state peak value h_{sp} is not significantly affected by parameters P_1, P_2 and P_3.

F) In the region

$$05. \leq P_3 \leq 1$$

the variation of h_{sp} from one step to another is very large.

3.3.3 Comparisons

For the calculation of the first peak Blume et al[2,3] method gives about 30% error between calculated and test results, Specht[4] method 27% and Holcomb 9%.

On the other hand, the accuracy of the method presented by Malyshev[7] for the first peak is variable. Because the expression 1.9 (given in Chapter 1) representing B/H curve agrees with the experimental curve within region

$$0.13 \leq B \leq 1.9$$

so this method gives accurate results within this region but not

over the region B > 1.9. In the transient current case, as is well known, B is much bigger than 1.9. Therefore, this method fails for high value of B.

The common point of Specht's and Holcomb's methods is that there is no current flowing until the saturation point (B_s, H_s) beyond which the permeability of the core is assumed to be constant. That means they are taking the B/H characteristic as in Figure 1.5.

Assumption of no current flowing until saturation cannot be valid, especially for the medium and small size transformer, because, as mentioned before, the current and the time corresponding to the saturation point (B_s, H_s) are

$$T_s = 5.6 \text{ ms} \quad , \quad I_s = 23.6 \text{ A}$$

and the first peak current and corresponding time

$$T_p = 8.35 \text{ ms} \qquad I_p = 102 \text{ A}$$

By the comparison of T_s to T_p, I_s to I_p it is realised that I_s is not a negligible amount.

The analytical method developed in this investigation enables us to get an accuracy of 3% error without neglecting the current I_s.

The most important contribution of this method is that knowing only magnetisation characteristic and residual conditions of core, the initial flux density can be taken into account by the presentation of the function B = f (H). It must be noticed that by the representation H = f (B) it is easy to take into account the initial flux in solving the differential equations 1.1 but not by B = f (H).

This method can be extended to establish the other peak values as well.

From the analysis of the results it is seen that the Preisach model provides high accuracy (see Table 3.5) and enables us to take into account the hysteresis effects, but it requires laborious work to estimate the coefficients and to set up the B/H model in the computer programme.

This model also explains the crossing-over phenomena as given in detail in Appendix A3, and produces results closer to experimental ones as shown in Figure 3.2.1.

The generalized parametric method is not as accurate as the normal method but it enables us to have a compact solution to the transient phenomena. However, at high voltages this method is quite accurate but only the first peaks (see Table 3.5 for comparison).

CHAPTER 4

FUNDAMENTAL FERRORESONANCE

4.1 Definitions

In order to avoid any ambiguity and misunderstanding in notations which will be used in this chapter it is necessary to give definitions.

Resonance: It is associated with a linear circuit condition whereby the inductive and capacitive impedance components of a circuit are balanced. Since, at this condition, the voltage drop due to the inductive impedance is compensated by the voltage drop due to the capacitive impedance, the total impedance to the supply is only the resistance of the circuit which is very small in many cases in practice. Therefore the current continually rises and reaches a large value.

At the resonance condition the stored energy makes an oscillation between the magnetic and electric field of ℓ and C respectively. That is, during the half period energy is stored in the field of the capacitor and during the next half period energy is stored in the field of the inductor.

Ferroresonance: This is a resonance condition occurring in a circuit containing an iron core, i.e. a nonlinear inductive element and has several different modes, as explained below.

Fundamental Ferroresonance: This is a kind of ferro-resonance phenomenon where the quantities such as flux in the core, current flowing in the circuit, consist essentially of a component at supply frequency. That is, the predominant components of these quantities are at the supply frequency.

Subharmonic Resonance: This is also a kind of ferro-resonance phenomenon but, in this case, the quantities mentioned above contain a large component (i.e. predominant component) whose frequency is lower than the supply frequency.

Unsymmetrical Mode of Ferroresonance: This is, in fact, a case of fundamental ferroresonance occurring with higher voltages applied but the current and flux have an unsymmetrical waveform. That is, the waveforms of these quantities in a half period are not similar and equal to the one appearing in the next half period.

In this case, the current and flux contain a number of harmonics but still the predominant component is at the supply frequency.

Jump Phenomenon: In a ferroresonant circuit at some certain conditions, which are called "the critical conditions", an infinitesimal change in the driving signal amplitude, or frequency, or in one of the circuit parameters, causes the current and flux to take new values. In other words, a transition from the previous value to the new one takes place with a jump.

In the case of fundamental ferroresonance there are three kinds of jump phenomena[48]. These are:

A) the transition from the inductive to capacitive state.

It can be illustrated by the following figure 4.1a.

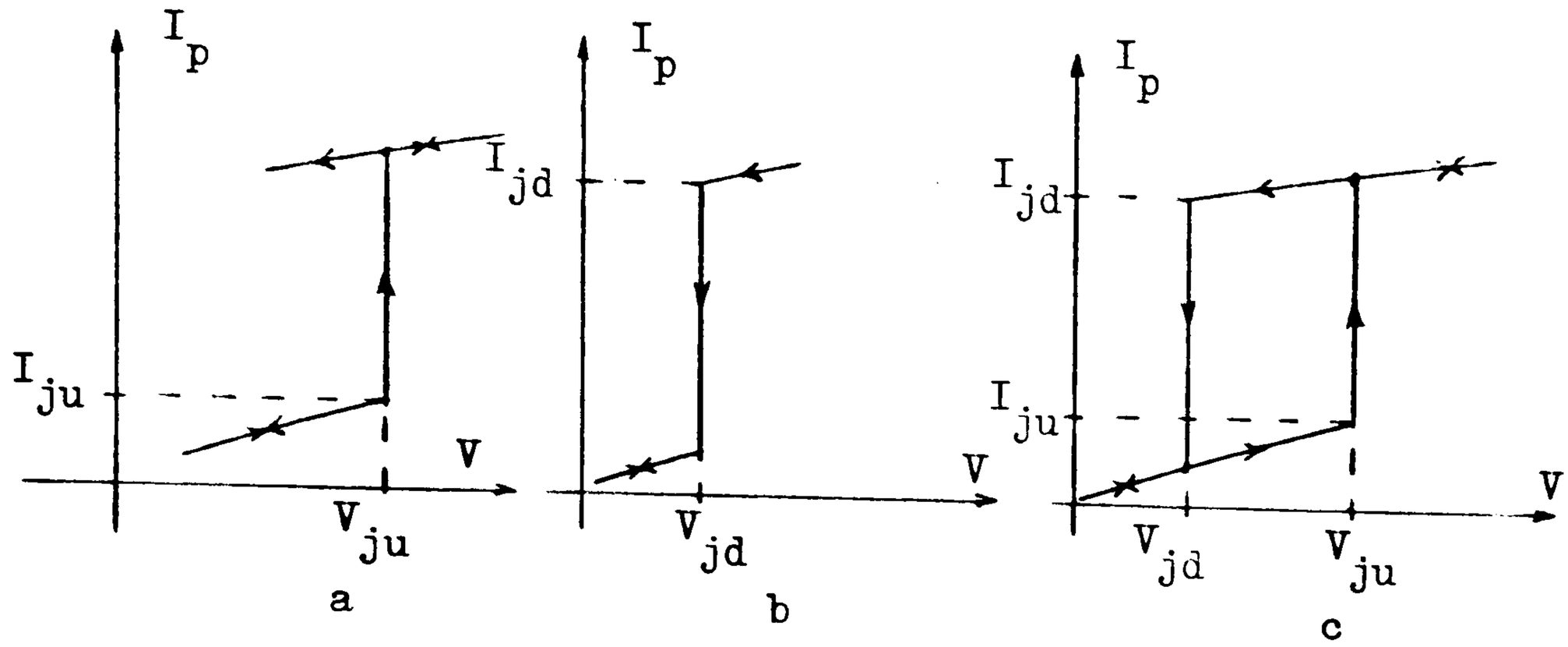

Subscript ju indicates the jump-up

Subscript jd indicates the jump-down

Figure 4.1

B) the transition occuring with the high values of applied voltage in the capacitive state.

C) the transition from the capacitive to inductive state as illustrated by Figure 4.1b.

Thus, it is seen that the entire I/V characteristic consists of two parts as shown in Figure 4.1c. The upper part corresponds to the capacitive state, the lower one to the inductive state.

In this present investigation we will especially be dealing with the first and third kinds of jump phenomena and related critical conditions since they are more important than the second kind in practice.

It is observed that the transition does not always take place with a jump. As will be examined in detail later, this characteristic feature of transition depends on the circuit resistance.

For instance, for higher values of the resistance the transition has a continuous nature.

In the case of subharmonic resonance, the jump-up phenomenon takes place as soon as the circuit is switched. That is, the existence of subharmonic resonance depends on the initial conditions such as the switching angle, applied voltage, the capacitance of circuit, initial flux (residual flux) in the core. But the jump-down phenomenon is only the function of the condition of the circuit at the present time.

4.2 Differences between Resonance and Ferroresonance

In order to compare these two similar phenomena, let us consider the series resonance circuit consisting of supply, resistor, capacitor and inductor. In both cases the resistance and capacitance of the circuit are linear but the inductance in the resonance circuit is a linear element; in the ferroresonance circuit it is a nonlinear element due to being a function of the current.

In a resonance circuit at the resonance condition the current theoretically goes to infinity and the resonance occurs only when the supply frequency ω is equal to the natural frequency of the circuit defined by $\omega_n = 1 / \sqrt{\ell.C}$.

On the other hand, the current never takes an infinite value in a ferroresonance circuit and within a certain region, as seen from the Figure 4.1c, it has two distinct values for a given voltage applied.

Ferroresonance phenomena is not only dependent on the supply frequency but also dependent on the applied voltage while ordinary resonance is only a function of the supply frequency.

Another salient difference between these two phenomena is the jump phenomenon which occurs only in the ferroresonance circuit.

4.3 Laboratory Model

Besides the single phase ferroresonance circuits there are a number of three phase ferroresonance circuits which can be reduced to a single phase form, or can be resolved into three single-phase points. Two examples of such circuits are shown in Figures 4.2 and 4.3. Germay et al[39] classifies all these three-phase circuits and reduces them to a single phase configuration.

On the other hand, Swift[24] suggests that the series circuit is ideal for the investigation of the ferroresonance phenomena rather than the parallel circuit. Therefore, we will use a single phase series circuit as shown in Figure 1.4 for laboratory experiments to study ferroresonance phenomena.

The technique used to measure all the parameters and characteristics which are required for the solution of the performance equations 1.8 and to record the experimental results is exactly the same as for the transient current.

4.4 Numerical Solution for Fundamental Ferroresonance

Unfortunately, there is no analytical method to analyse the transient state during the transition, the hysteresis effect and accurate prediction of the jump conditions. Only Hayashi[20] gives a method of representing the B/H loop in the analytical calculation. But this method may be valid for only steady-state cases because he uses a symmetrical ellipse (see Fig. 1.7).

We will employ the exponential series method and the Preisach model to represent the magnetisation curve and B/H loop

respectively in equation 1.8. Thus, using two representations, we can observe the hysteresis effect and the transition at all states, at all conditions. But in this case, as we have explained in Chapter 3, we can solve these equations only by a numerical method, not an analytical method.

We will use the Runge-Kutta method (four steps) as a numerical method, and choose dt = 0.05 msec for the lower region, dt = 0.2 msec for the upper region of the B/H characteristic as time step lengths.

The details of the programme for the numerical solution by the computer are given in Appendix A4.

The results produced by this numerical solution will be analysed and compared with the experimental results at the end of this chapter.

To observe the effect of hysteresis losses and resistance on fundamental ferroresonance and subharmonic resonance phenomena, especially at jump-down points, the following steps must be carried out in the numerical programme.

a) First, programme must follow the inductive state characteristic shown in Figure 4.1 by increasing the voltage from zero to the jump-up point as in the experiment.

b) Second, after jump-up phenomenon has taken place the voltage must be decreased to the value required.

If this process is applied to both programmes involving magnetisation curve and loop representation it is seen that for zero external resistance in the programme involving magnetisation curve represent-ation the jump down never happens, but in the other one it does. Thus, the effect of hysteresis losses on jump-down point is confirmed.

4.5 Analytical Solution

In a ferroresonance circuit, if the transition takes place with a jump the waveform of the flux linkage ψ in the inductive state is totally different to the one in the capacitive state. The following figures a and b display the waveform of ψ in inductive and capacitive states respectively.

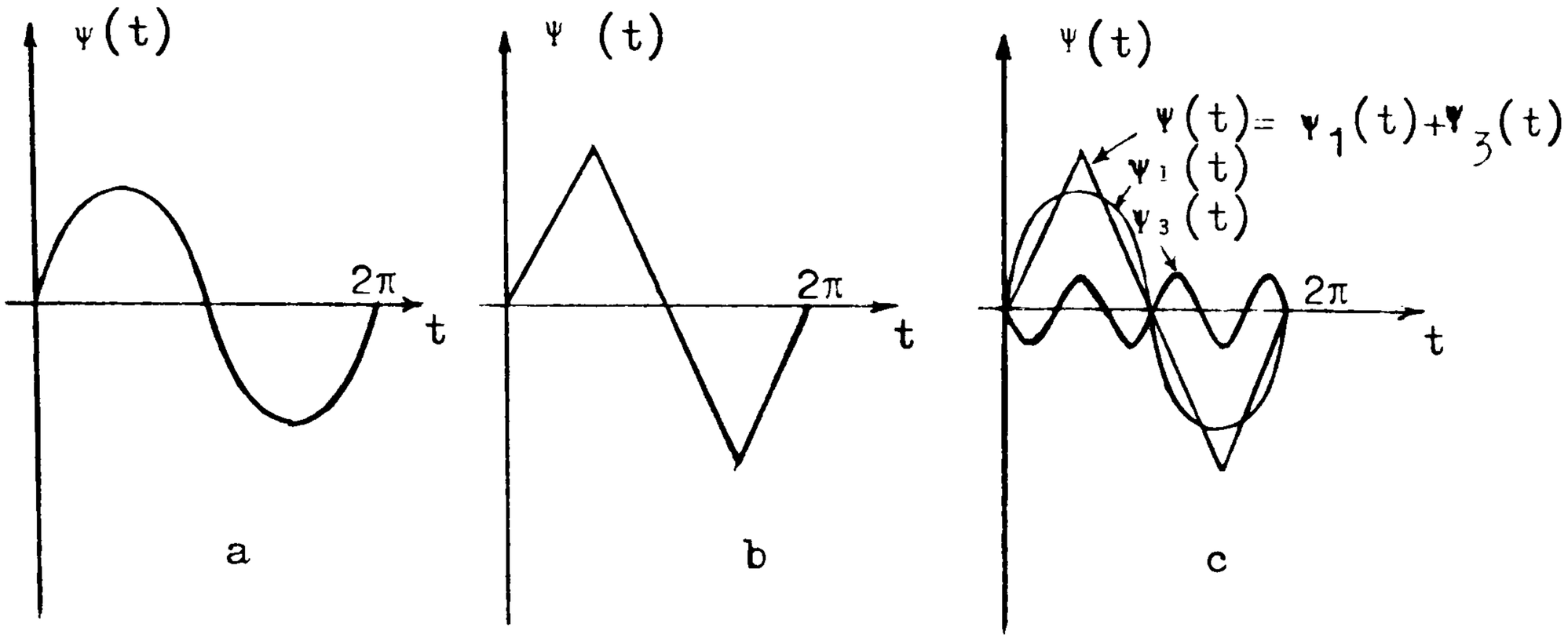

Figure 4.4

Both the figures 4.4a and 4.4b can be expressed by means of Fourier series, but it is found that the first two odd terms of this series are sufficient to reconstruct the experimental waveform of ψ as illustrated in Figure 4.4c. These two terms

$$\Psi_1(t) = \sqrt{2}\ \Psi_1 \sin(\omega t + \theta_1) \quad .. \quad 4.1$$

$$\Psi_3(t) = \sqrt{2}\ \Psi_3 \sin(3\omega t + \theta_3) \quad .. \quad 4.2$$

provide a basis for analytical expressions which will be developed.

4.5.1 The Derivation of the Analytical Expressions

From the above relation, as specified in Figure 4.4c, the resultant flux linkage is

$$\Psi(t) = \Psi_1(t) + \Psi_3(t) \quad .. \quad 4.3$$

On the other hand, the magnetisation curve experimentally obtained will be represented by a cubical polynomial

$$H = a_1 B + a_3 B^3 \qquad .. \qquad 4.4$$

where a_1 and a_3 designate the coefficients to be determined. Here, we will modify this polynomial to get the current-flux linkage relationship. So, substituting the relations

$$H = (N.\ i\ ) / L \quad ,$$

$$B = \phi / A \quad ,$$

and

$$\Psi = N.\ \phi$$

into the above polynomial we obtain the relation

$$i = c_1 \Psi + c_3 \Psi^3 \qquad .. \qquad 4.5$$

where

$$c_1 = (a_1.\ L) / (N^2.\ A)$$

$$c_3 = (a_3.\ L) / (N^4.\ A^3)$$

Thus, we have the following equations for the series ferroresonance circuit shown in Figure 1.8.

$$\sqrt{2}\ V.\ \sin(\omega t) = Ri(t) + \ell\ .pi(t) + \frac{1}{C} \int i(t)dt + p\,\Psi(t)$$

$$i(t) = c_1\ \Psi(t) + c_3\, \Psi^3(t)$$

$$\Psi(t) = \Psi_1(t) + \Psi_3(t)$$

From these equations, using the harmonic balance rule we derive the following system of equations with complex coefficients (see Appendix A5 for detail) for fundamental ferroresonance.

$$\bar{V} = \bar{Z}_1.\ \bar{I}_1 + j\ \omega\ \bar{\Psi}_1 \qquad .. \qquad 4.6$$

$$0 = \bar{Z}_3.\ \bar{I}_3 + j3\omega\ \bar{\Psi}_3 \qquad .. \qquad 4.7$$

where $\bar{I}_1$ and $\bar{I}_3$ are function of $\bar{\Psi}_1$ and $\bar{\Psi}_3$. For their expressions in terms of $\bar{\Psi}_1$ and $\bar{\Psi}_3$ refer to the appendix A5.

If the equations 4.6 and 4.7 are examined closely it will be seen that by this method we can take into account all the circuit parameters.

We have made only two approximations, one for the representation of B/H characteristic by a cubical polynomial which is not suitable for higher values of H and B, and one for the reconstruction of the waveform of flux linkage, but the former is more influential on results to be produced. Therefore, if there are large differences between the experimental and calculated results it must be due to the representation of B/H characteristic.

4.5.2 A Method for the Solution of the System of Equations with Complex Coefficients

Equations 4.6 and 4.7 might be solved by Newton-Raphson[49,50] method dividing these into the real and imaginary parts. But, in this case, we would have four equations with four unknowns such as Ψ_1, Ψ_3, θ_1, θ_3. Of course it would not only be a complicated problem but also it would take a lot of computing time. Using the complex form leads to only two unknowns such as $\bar{\Psi}_1$ and $\bar{\Psi}_3$. But the solution of $\bar{\Psi}_1$ and $\bar{\Psi}_3$ from these equations still requires the derivatives

$$\frac{\partial \bar{F}}{\partial \bar{\Psi}_1}, \quad \frac{\partial \bar{F}}{\partial \bar{\Psi}_3}, \quad \frac{\partial \bar{G}}{\partial \bar{\Psi}_1}, \quad \frac{\partial \bar{G}}{\partial \bar{\Psi}_3}$$

where

$$\bar{F} = \bar{Z}_1 . \bar{I}_1 + j\omega \bar{\Psi}_1 - \bar{V} \qquad .. \qquad 4.8$$

$$\bar{G} = \bar{Z}_3 . \bar{I}_3 + j3\omega \bar{\Psi}_3 \qquad .. \qquad 4.9$$

Replacing the derivatives by finite differences Brown[51] produces a method based on Taylor's theorem. This method is very useful when the computer is employed for the calculations since it saves time, but the accuracy is not as good as that of the ordinary method.

According to this method

$$\frac{\partial \bar{F}}{\partial \bar{\Psi}_1} = \frac{\bar{F}(\bar{\Psi}_1 + \Delta\bar{\Psi}_1, \bar{\Psi}_3) - \bar{F}(\bar{\Psi}_1 - \Delta\bar{\Psi}_1, \bar{\Psi}_3)}{2\,\Delta\bar{\Psi}_1},$$

$$\frac{\partial \bar{F}}{\partial \bar{\Psi}_3} = \frac{\bar{F}(\bar{\Psi}_1, \bar{\Psi}_3 + \Delta\bar{\Psi}_3) - \bar{F}(\bar{\Psi}_1, \bar{\Psi}_3 - \Delta\bar{\Psi}_3)}{2\,\Delta\bar{\Psi}_3},$$

$$\frac{\partial \bar{G}}{\partial \bar{\Psi}_1} = \frac{\bar{G}(\bar{\Psi}_1 + \Delta\bar{\Psi}_1, \bar{\Psi}_3) - \bar{G}(\bar{\Psi}_1 - \Delta\bar{\Psi}_1, \bar{\Psi}_3)}{2\Delta\,\bar{\Psi}_1},$$

$$\frac{\partial \bar{G}}{\partial \bar{\Psi}_3} = \frac{\bar{G}(\bar{\Psi}_1, \bar{\Psi}_3 + \Delta\bar{\Psi}_3) - \bar{G}(\bar{\Psi}_1, \bar{\Psi}_3 - \Delta\bar{\Psi}_3)}{2\,\Delta\bar{\Psi}_3}.$$

Thus knowing the initial values of $\bar{\Psi}_1$ and $\bar{\Psi}_3$, and choosing appropriate $\Delta\bar{\Psi}_1$ and $\Delta\bar{\Psi}_3$ we can calculate all derivatives required, and $\bar{F}$ and $\bar{G}$. Hence by the Newton rule

$$\begin{bmatrix} \frac{\partial \bar{F}}{\partial \bar{\Psi}_1} & \frac{\partial \bar{F}}{\partial \bar{\Psi}_3} \\ \frac{\partial \bar{G}}{\partial \Psi_1} & \frac{\partial \bar{G}}{\partial \bar{\Psi}_3} \end{bmatrix} \begin{bmatrix} \bar{D}\Psi_1 \\ \bar{D}\Psi_3 \end{bmatrix} = \begin{bmatrix} -\bar{F} \\ -\bar{G} \end{bmatrix}$$

$D\bar{\Psi}_1$ and $D\bar{\Psi}_3$ can be evaluated so the new values of $\bar{\Psi}_1$ and $\bar{\Psi}_3$ are

$$\bar{\Psi}_1 = \bar{\Psi}_{10} + \bar{D}\bar{\Psi}_1$$

$$\bar{\Psi}_3 = \bar{\Psi}_{30} + \bar{D}\bar{\Psi}_3$$

Where $\bar{\Psi}_{10}$ and $\bar{\Psi}_{30}$ are the initial values of $\bar{\Psi}_1$ and $\bar{\Psi}_3$ respectively. For the next step of calculations these new values will be taken as initial values for Ψ_1 and $\bar{\Psi}_3$. By an iteration process the calculations are repeated till $\bar{D}\bar{\Psi}_1$ and $\bar{D}\bar{\Psi}_3$ become reasonably small.

Now, at this stage, the problem is to find out a set of initial values. For the fundamental resonance we have to give two different initial values to each variable. For instance, it has been observed that in the capacitive state initial values

$$\Psi_{10} = \frac{V}{\omega} \quad , \qquad \theta_{10} = + \pi/2$$

$$\Psi_{30} = 0.1 \, . \, \Psi_{10} \, , \; \theta_{30} = + \pi/2$$

and inductive state

$$\Psi_{10} = 10 . \frac{V}{\omega} \quad , \qquad \theta_{10} = - \pi/2$$

$$\Psi_{30} = 0.1 \, \Psi_{10} \, , \quad \theta_{30} = - \pi/2$$

yield stable and accurate results.

4.5.3 The Stability of the Fundamental Ferroresonance

The solution of the equations 4.6 and 4.7 by the method proposed above reveals that the third harmonic Ψ_3 does not have a considerable contribution to the resultant flux linkage Ψ around the region specified by the jump-up and jump-down points in Figure 4.1c.

For instance, for

$$C = 20 \; \mu F \qquad \ell = 2.65 \; mH \qquad R = 1.64 \Omega \qquad V = 100 \text{ volt}$$

before jump up $\quad \Psi_3 \simeq 0.005 \, . \, \Psi_1$

after jump up $\quad \Psi_3 \simeq 0.06 \, . \, \Psi_1$

Therefore, neglecting the third harmonic we have only one equation with complex coefficients which is

$$\bar{V} = \bar{Z}_1 \, . \, \bar{I}_1 + j\omega\bar{\Psi}_1$$

splitting this into real and imaginary parts then taking the square of both sides we arrive at the equation

$$A\Psi_1^{\,6} + B\,\Psi_1^{\,4} + C\,\Psi_1^{\,2} + D = 0 \qquad .. \qquad 4.10$$

where

$$D_1 = c_1 \, Z_1 + \omega . \sin \zeta_1$$

$$E_1 = \omega \, . \cos \zeta_1$$

$$F_1 = \frac{3 . c_3 . Z_1}{2}$$

$$A = F_1^2$$

$$B = 2F_1 . D_1$$

$$C = D_1^2 + E_1^2$$

$$D = -V^2$$

From equation 4.10, if $V = f(\Psi_1)$ is sketched, the following Figure 4.5 is obtained

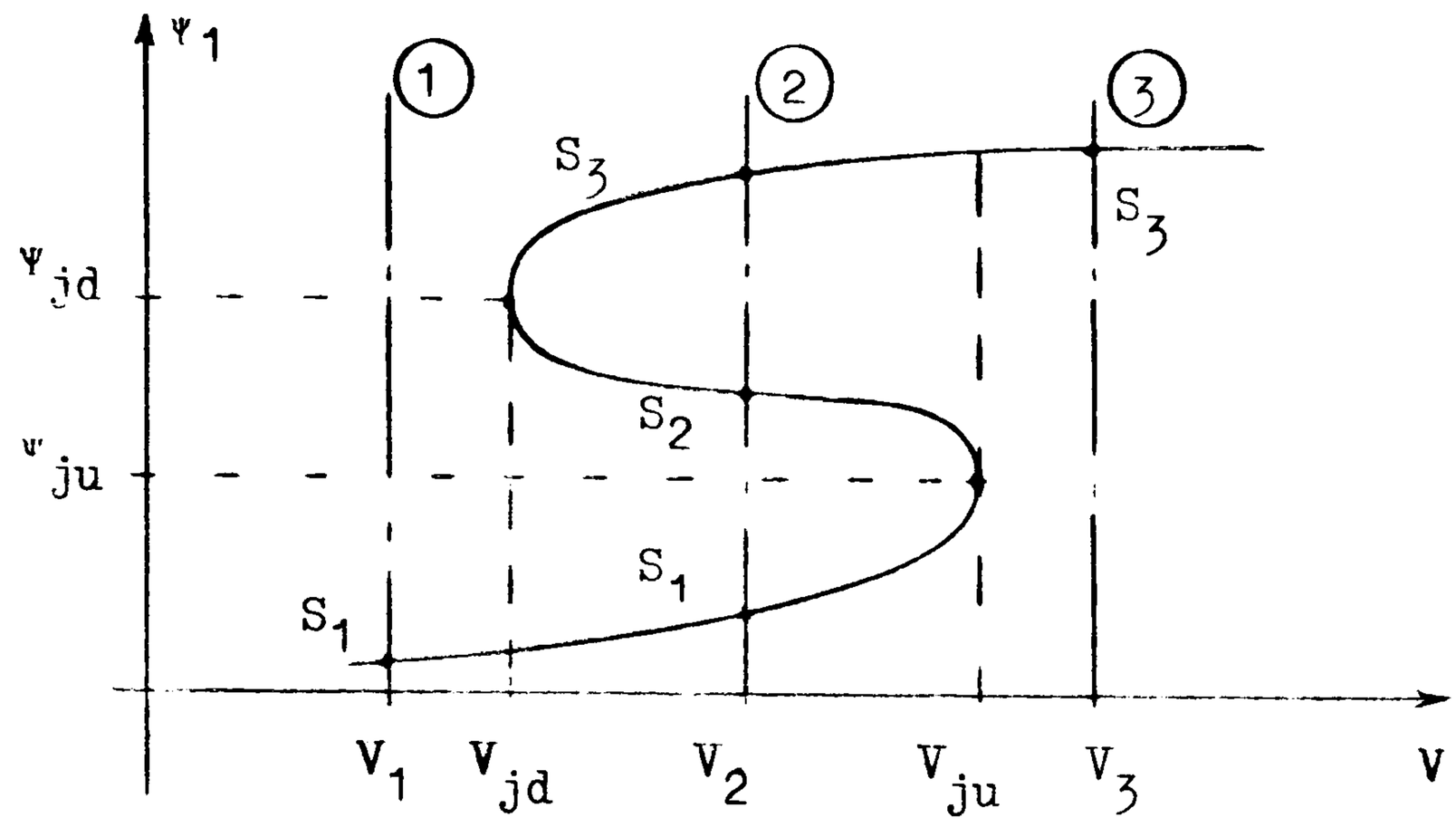

Figure 4.5

Now let us analyse the values of Ψ_1 corresponding to given values of V.

A) For $V = V_1$, i.e. on the vertical line (1)

$\Theta_1 < 0$ (inductive case), Ψ_1 has only one real root

B) For $V = V_3$, i.e. on the vertical line (3)

$\Theta > 0$ (capacitive case), Ψ_1 has only one real root

C) For $V = V_2$, i.e. on the vertical line (2)

at s_1 , $\Theta_1 < 0$ (inductive case)

s_3 , $\Theta_1 > 0$ (capacitive case)

s_2 , $\Theta_1 \gtrless 0$ (unstable case)

This last case corresponds to the transitional state which is an unstable state.

For $V = V_2$ Ψ_1 has three real roots.

Since at s_2 the slope $\frac{dV}{d\Psi_1}$ is negative this unstable point can easily be distinguished from the other points s_1 and s_3 which are on the same vertical line. Thus the slope $\frac{dV}{d\Psi}$ can be used as a stability criterion. That is:

a) $\frac{dV}{d\Psi} > 0$ corresponds to the stable state

b) $\frac{dV}{d\Psi} < 0$ corresponds to the unstable state

c) $\frac{dV}{d\Psi} = 0$ corresponds to the critical state

On the other hand, using the transformation

$$Y = \Psi_1^2$$

the above polynomial can be reduced to

$$AY^3 + BY^2 + CY + D = 0 \quad .. \quad 4.11$$

and the stability criterion $\frac{dV}{d\Psi} \gtrless 0$ now becomes

$$\frac{dD}{dY} \gtrless 0$$

For the purpose of using the standard graphs we will introduce the following transformations[52].

$$X = Y + \frac{B}{3A}$$

$$P = \frac{3AC - B^2}{9A^2}$$

$$Q = \frac{2B^3}{54A^3} - \frac{BC}{6A^2} + \frac{D}{2A}$$

Thus the equation 4.11 is brought into the standard cubic form

$$X^3 + 3PX + 2Q = 0$$

or

$$X^3 = -3PX - 2Q \quad .. \quad 4.12$$

This last equation implies that the solution points sought are the intersections of the standard cubic graph $z_1 = X^3$ by the straight line $z_2 = -3PX - 2Q$ as illustrated in Figure 4.6a. In fact, by

successive transformations we have converted the Figure 4.5 to the Figure 4.6a which does require only the slope of the straight line, i.e. $-3P$ to define the solution points.

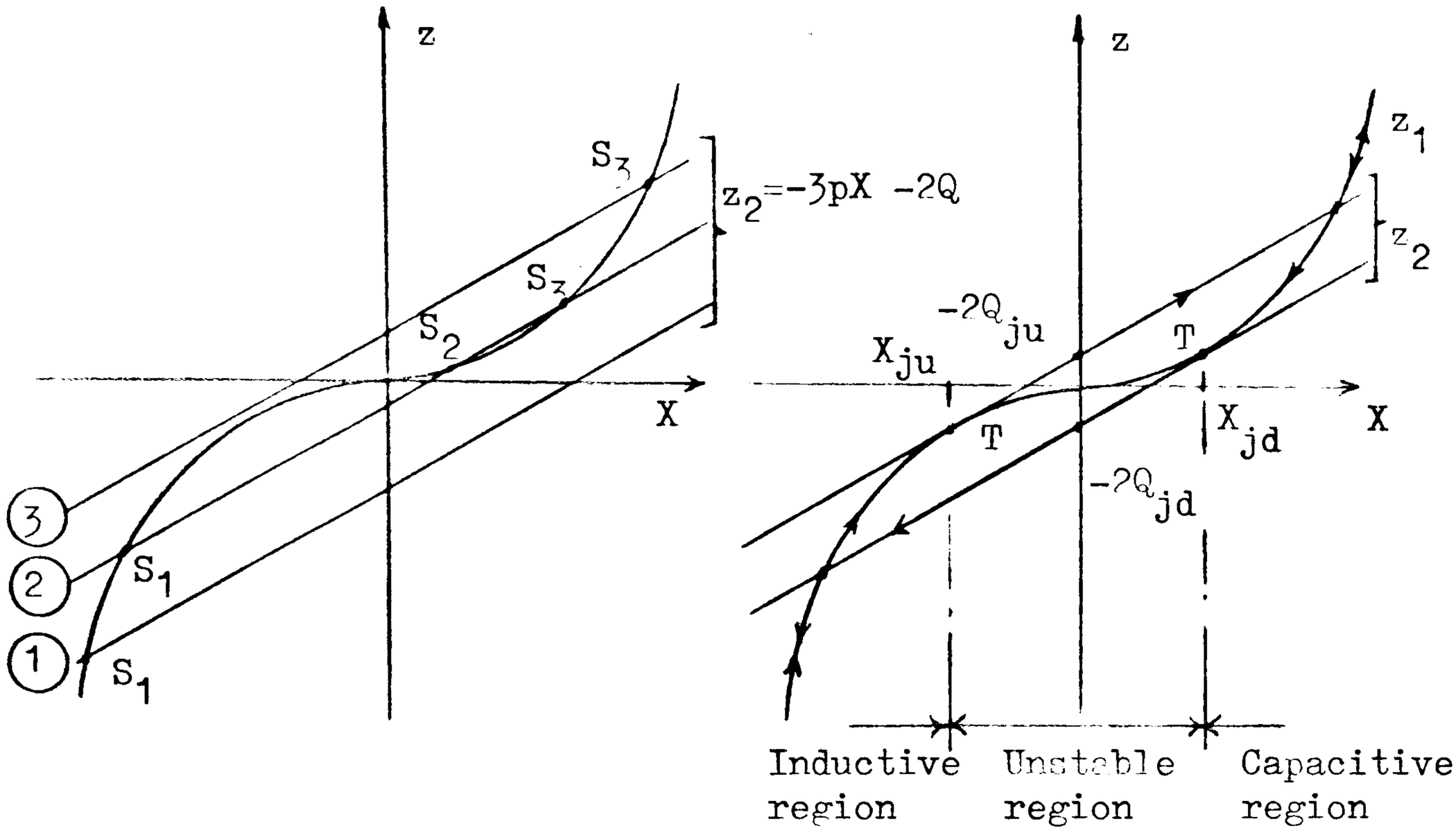

Figure 4.6

So, if P is known then drawing a straight line with a slope of $-3P$ and shifting it on the standard cubic graph we can find different solution points such as s_1, s_2, s_3.

The expression of the stability criterion $\frac{dD}{dY} \gtrless 0$ in terms of new variable X and new parameters P and Q is

$$X^2 + P \gtrless 0$$

i.e.

$$\frac{dz_1}{dX} + \frac{dz_2}{dX} \gtrless 0$$

So if at the solution point

a) $\frac{dz_1}{dX} > \frac{dz_2}{dX}$, this point corresponds to a stable state.

b) $\frac{dz_1}{dX} < \frac{dz_2}{dX}$, this point corresponds to an unstable state.

c) $\frac{dz_1}{dX} = \frac{dz_2}{dX}$, this point corresponds to the critical state.

By these criteria it is seen that the points s_1, s_3 on the Figure 4.6a give a stable solution, but s_2 corresponds to the transitional state, i.e. unstable state.

The points satisfying the criterion $\frac{dz_1}{dX} = \frac{dz_2}{dX}$ can easily be established just by drawing a straight line with a slope of -3P such that this straight line will be a tangent to the standard cubic function $z_1 = X^3$. Thus the points T, X_{ju}, X_{jd}, Q_{ju}, Q_{jd} are obtained as shown in Figure 4.6b (where ju and jd designate the jump-up and jump-down respectively).

These values can also be defined analytically so that

from $$\frac{dz_1}{dX} = \frac{dz_2}{dX}$$

$$X^2 = -P \quad .$$

Since P is assumed to be known

$$X_{jd} = + \sqrt{-P} \qquad .. \qquad 4.13$$

and

$$X_{ju} = - \sqrt{-P} \qquad .. \qquad 4.14$$

Since Ψ is a real value X_{jd} and X_{ju} must be real. In other words, P must always be negative.

Thus
$$Q_{ju} = - \frac{(X_{ju}^3 + 3P\, X_{ju})}{2} \qquad .. \qquad 4.15$$

and
$$Q_{jd} = - \frac{(X_{jd}^3 + 3P\, X_{jd})}{2} \qquad .. \qquad 4.16$$

By an inverse transformation the critical value of flux linkages corresponding to jumping points can be calculated

from $$Y_{jd} = X_{jd} - \frac{B}{3A} \qquad .. \qquad 4.17$$

and
$$Y_{ju} = X_{ju} - \frac{B}{3A} \qquad .. \qquad 4.18$$

Hence the corresponding flux linkages

$$\Psi_{ju} = \sqrt{Y_{ju}} \quad .. \quad 4.19$$

$$\Psi_{jd} = \sqrt{Y_{jd}} \quad .. \quad 4.20$$

The critical RMS values of the applied voltage corresponding jump-up and jump-down points can either be calculated from the expressions of Q_{ju} and Q_{jd} or from

$$V_{ju} = \sqrt{-A.\ Y_{ju}^3 \ -B.\ Y_{ju}^2 \ -C\ Y_{ju}} \quad .. \quad 4.21$$

and

$$V_{jd} = \sqrt{-A.\ Y_{jd}^3 \ -B.\ Y_{jd}^2 \ -C\ Y_{jd}} \quad .. \quad 4.22$$

In order to calculate the phase angle of the flux linkages corresponding to the critical points we will substitute Ψ_{ju}, Ψ_{jd}, V_{ju} and V_{jd} into the real part of equation 4.6 Hence

$$\theta_{ju} = -\zeta_1 + \text{arc cos}\left[\frac{D_1.\ \Psi_{ju} + F_1.\Psi_{ju}^3}{V_{ju}}\right] \quad .. \quad 4.23$$

and

$$\theta_{jd} = -\zeta_1 + \text{arc cos}\left[\frac{D_1.\ \Psi_{jd} + F_1.\ \Psi_{jd}^3}{V_{jd}}\right] \quad .. \quad 4.24$$

Thus at the jump-up point

$$\Psi(t) = \sqrt{2}\ \ \Psi_{ju}\ .\ \ \sin\ (\omega t + \theta_{ju}) \quad .. \quad 4.25$$

$$\Psi_m = \sqrt{2}\ \ \Psi_{ju}$$

and at the jump-down point

$$\Psi(t) = \sqrt{2}\ \ \Psi_{jd}.\ \ \sin\ \ (\omega t + \theta_{jd}) \quad .. \quad 4.26$$

$$\Psi_m = \sqrt{2}\ \ \Psi_{jd}$$

where Ψ_m designates the magnitude of the resultant flux linkages.

If the third harmonic is not neglected then

$$\Psi(t) = \sqrt{2}\ [\Psi_1 \sin\ (\omega t + \theta_1) + \Psi_3.\ \sin\ (3\omega t + \theta_3)\ ]$$

From inspection of Figure 4.4c

$$\Psi_m = \sqrt{2}\ (\Psi_1 + \Psi_3) \qquad .. \qquad 4.27$$

Since the current and flux linkages achieve their maximum values in the same time the peak value of current becomes equal to

$$I_p = c_1 \Psi_m + c_3 \Psi_m^3$$

or substituting the expression of Ψ_m above

$$I_p = \sqrt{2}\ [c_1 (\Psi_1 + \Psi_3) + 2.\ c_3.\ (\Psi_1 + \Psi_3)^3] \qquad 4.28$$

For single harmonic $(\Psi_3 = 0)$

$$I_p = \sqrt{2}\ (c_1 \Psi_1 + 2.\ c_3 \Psi_1^3) \qquad 4.29$$

Hence the peak values of current corresponding to jump-up and jump-down points can be obtained by the expressions for Ψ_{ju} and Ψ_{jd}.

4.6 Unsymmetrical Mode of Ferroresonance

After transition from inductive state to capacitive state further increases in the applied voltage constitute a strong, stable second harmonic in the current and flux waveform in addition to the first and third harmonic.

As mentioned before, the transition from the stable symmetrical capacitive state to this stable unsymmetrical capacitive state again occurs by a small jump-up phenomenon, and therefore a transient state is observed. We will discuss these in the analysis section of this chapter.

In this mode of fundamental ferroresonance the B/H loop includes an unusual portion of loop which is called 'Minor Loop'.

The minor loop is attributed to the history of the magnetisation of the core material during a cycle of its behaviour in that circuit[27]. This loop sometimes appears in the second quadrant, as shown in the following Figure 4.7a, and sometimes in the fourth quadrant as in the Figure 4.7b. The reason for this must be sought in the phase difference of the second harmonic because this harmonic creates this mode of ferroresonance.

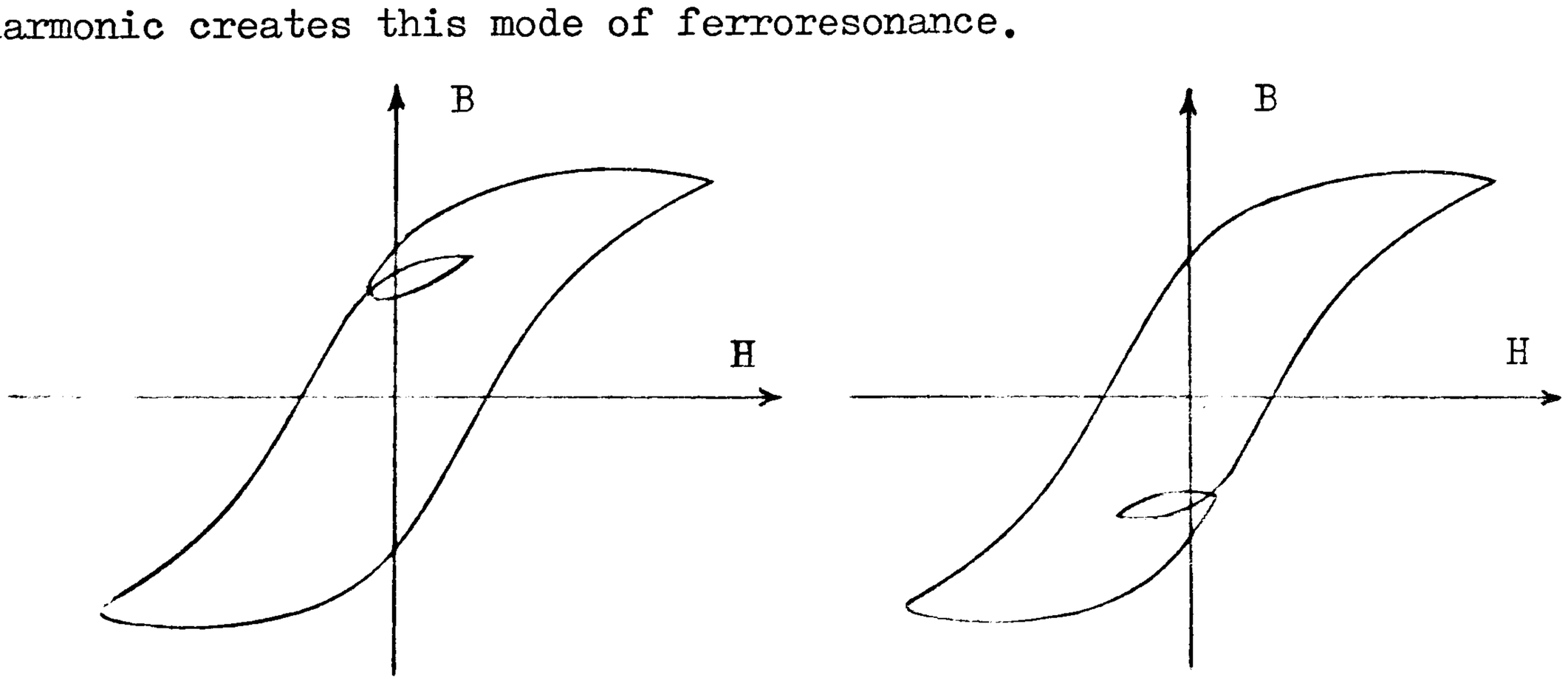

a b

Figure 4.7

The size of the minor loop depends on the voltage applied and the capacitance of the circuit.

Since this mode presents a significant second harmonic the analytical method developed in the foregoing section taking into account only the fundamental and third harmonic requires to be modified. But we will study this phenomenon by a numerical solution using both the Preisach representation and the generalized parametric method.

4.7 Analysis of the Results

Since the ammeters are able to give exact readings only at the rated frequency, they cannot be used to read rms values of the current which contains many harmonics. Therefore, in the experiments the peak values of the current are recorded at the various rms values of the applied voltage, various values of resistance and capacitance using an oscilloscope, and plotted against rms values of the voltage in Figures 4.8, 4.9, 4.10 and 4.11. From inspection of these Figures the following experimental conclusions can be drawn:

1) Any change in capacitance has a considerable effect on jump-up conditions but very slight effect on jump-down conditions at the small value of resistance. If the resistance of circuit is increased, this change becomes effective at jump-down conditions as well.

2) On the contrary, the jump-down conditions are affected by resistance very much while the jump-up conditions are only affected slightly.

3) The locus of jump-down and jump-up points is roughly an ellipse. This ellipse is inclined to the right hand side and becomes smaller in size with increases in the value of resistance.

The left hand side of this ellipse actually consists of two parts. The lower part has negative slope and the upper part has positive slope. So, during the jump-down from this upper side to inductive state sometimes subharmonic oscillations of orders $\frac{1}{2}$, $\frac{1}{3}$, $\frac{1}{5}$ have been observed. But, unfortunately, the same condition was not found to be possible in the numerical programme although attempts were made to include this.

4) There is such a value of resistance at which the transition from inductive state to capacitive state does not take place with a jump any longer, i.e. there is no discontinuity in the characteristic as in Figure 4.11. (for C = 40 μF).

For given circuit parameters R, ℓ, C, supply parameters ω, V, and magnetisation characteristic, the corresponding flux linkages can be calculated such that first P, Q in the equation 4.12 are calculated then this equation is solved for X. By the inverse transformation Ψ_1 and θ_1 are defined. The critical values of Ψ_1 and θ_1, the rms values of the applied voltage V corresponding to these critical values (i.e. Ψ_{Ju}, Ψ_{Jd}, θ_{Ju}, θ_{Jd}, V_{Ju}, V_{Jd}) are calculated through the equations 4.19, 4.20, 4.21, 4.22, 4.23 and 4.24. The Figure 4.12 and 4.13 show the function $\Psi_1 = f(V)$ and $\theta_1 = f(V)$ where Ψ_1 and V are the rms values of $\Psi_1(t)$ and v(t) respectively. All these quantities can also be calculated through the standard graph, as shown in Figure 4.14.

From inspection of the Figure 4.12 it is noticed that for the small value of the resistance the jump-down occurs at a very small value of the applied voltage. Increases in the value of resistance do not have an effect on the jump-up points practically but they considerably affect the jump-down points. Thus, this characteristic

feature confirms the experimental results given in Figures 4.7, 4.8, 4.9, 4.10 and 4.11.

As specified in the Figure 4.12 and mentioned before, there is such a value for resistance for which the characteristic $\Psi_1 = f(V)$ has no discontinuity. This value of resistance can be defined through the Figure 4.14. Before defining it, let us consider the following Figure 4.15.

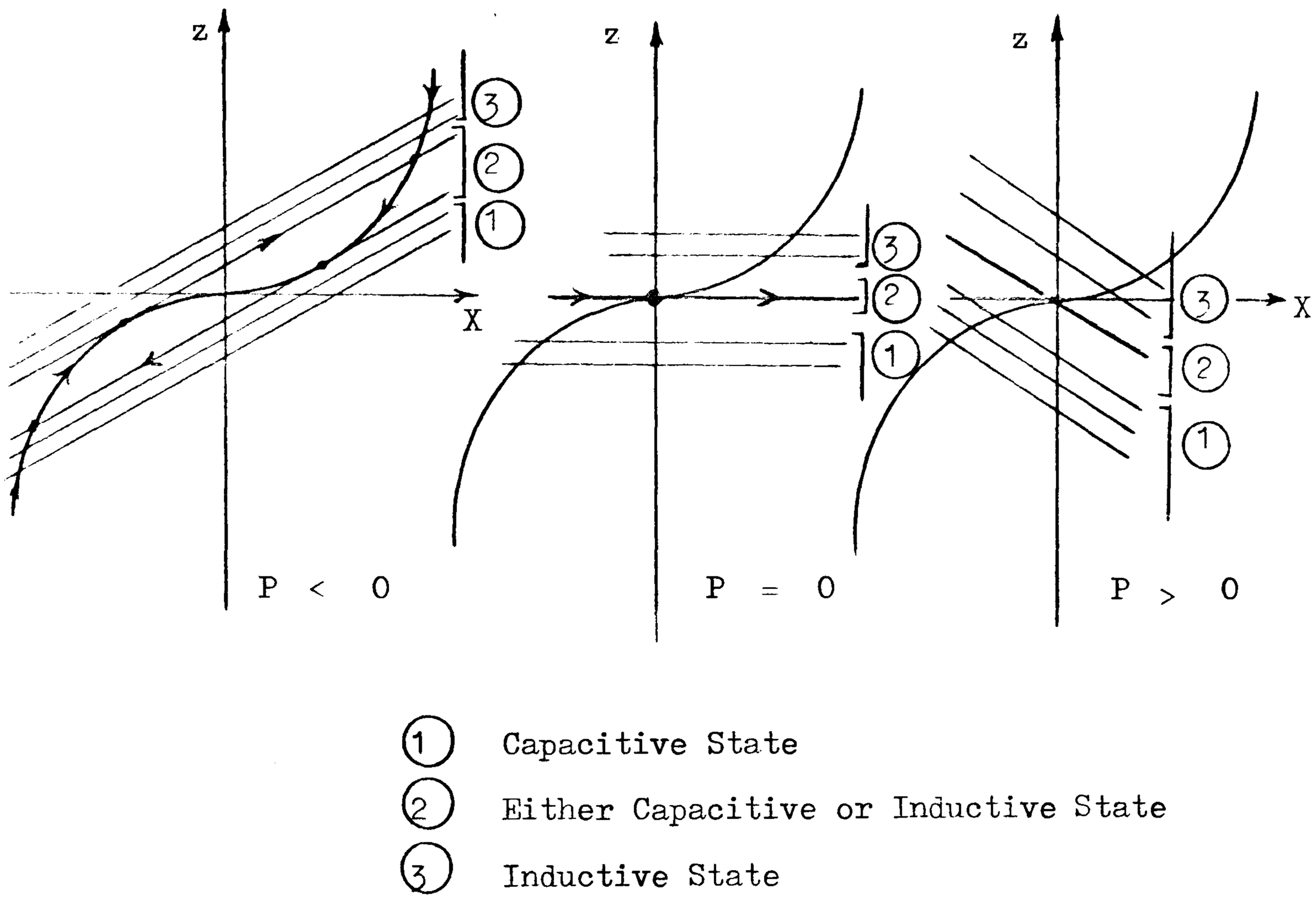

① Capacitive State

② Either Capacitive or Inductive State

③ Inductive State

Figure 4.15

So, from consideration of these figures it is clear that only when $P < 0$, $z_1 = X^3$ and $z_2 = -3PX - 2Q$ have the same tangent at two distinct points, one of which corresponds to the jump-up and the other one to the jump-down condition. When $P = 0$, z_1 and z_2 have

only one tangent point which is the origin ($X = 0$). This is the boundary condition because if P is now made positive then, as will be seen from the third figure above, there will not be any tangent point of z_1 and z_2. Therefore, from the second figure

$$\frac{dz_1}{dX} = \frac{dz_2}{dX} = 0$$

or

$$X^2 = -P = 0$$

hence

$$P = \frac{B^2 - 3AC}{9A^2} = 0$$

or

$$B^2 = 3AC$$

Substituting the expressions of A, B, C given in the section 4.5.3 of this chapter we obtain

$$D_1^2 - 3E_1^2 = 0$$

Taking the factor $D_1 + \sqrt{3}\, E_1 = 0$ of the above equation and using the expression of D_1 and E_1 we arrive at

$$c_1 Z_1 + \omega.\sin \xi_1 + \sqrt{3}\ (\omega.\cos \xi_1) = 0$$

Since $\sin \xi_1 = \frac{X_1}{Z_1}$

$$\cos \xi_1 = \frac{R}{Z_1}$$

$$X_1 = \omega.\ell - \frac{1}{\omega C}$$

$$Z_1 = \sqrt{R^2 + X_1^2}$$

The above equation becomes

$$c_1 R^2 + \sqrt{3}\ \omega R + c_1 X_1^2 + \omega X_1 = 0$$

Hence the value of resistance corresponding to $P = 0$ is

$$R_{cr} = \frac{-\sqrt{3}\ .\ \omega + \sqrt{3\omega^2 - 4c_1\ (c_1 X_1^2 + \omega X_1)}}{2\ c_1}$$

Thus, if the resistance of the circuit under consideration is

A) $R < R_{cr} \rightarrow P < 0$ the jump phenomena exist but depend on the value of the voltage applied.

B) $R = R_{cr} \rightarrow P = 0$ the boundary condition, i.e. the continuous transition starts.

C) $R > R_{cr} \rightarrow P > 0$ there are no jump phenomena at all value of the applied voltage.

For $\omega = 314$, $c_1 = 0.0248$, $c_3 = 1.212$, $\ell = 2.65$ mH, and $C = 30$ μF, R_{cr} is found to be 60Ω, i.e. in this case for $R > 60\Omega$ there is no jump. To compare this with the experimental result refer to Figure 4.11. For $R > R_{cr}$ if the applied voltage is increased the phase angle shifts from third quadrant to second quadrant, i.e. in a clockwise direction as illustrated in the following Figure 4.16.

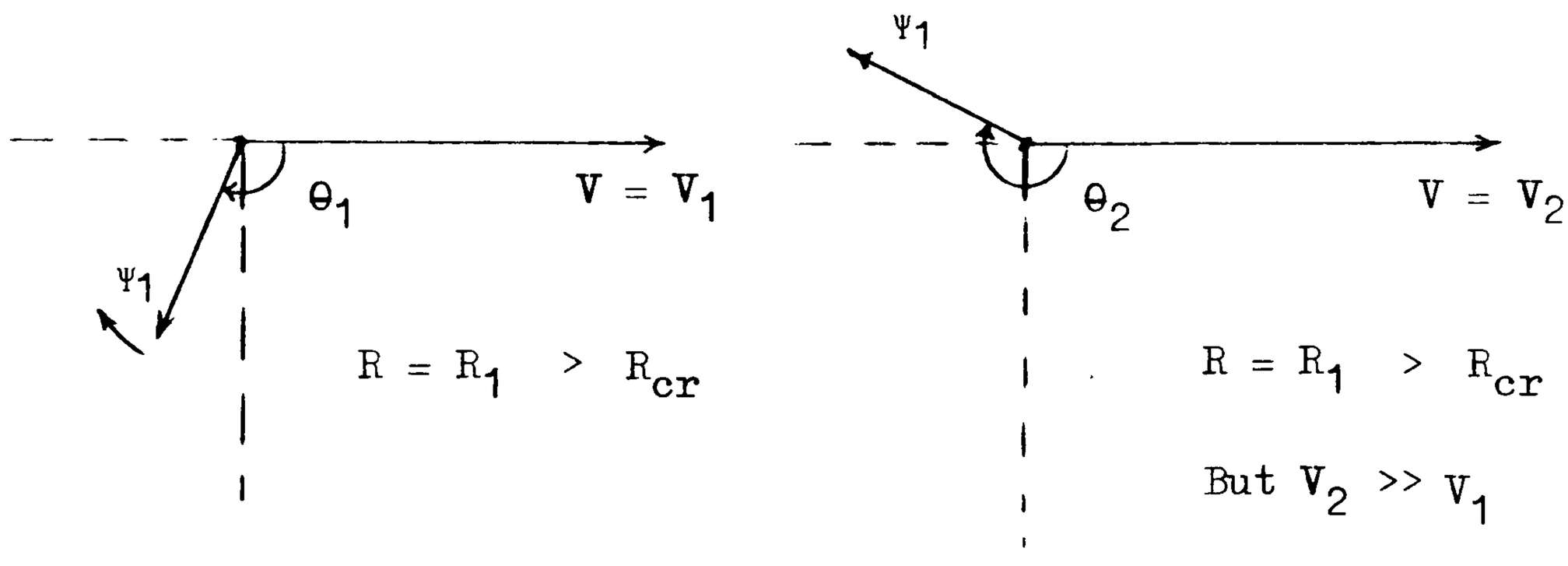

Figure 4.16

When the voltage is further increased, a value is reached for which the phase angle will be greater than -180°. That means, for higher values of voltage, the operation state moves from inductive state to capacitive state continually. The same results are observed from

Figure 4.12 as expected.

In order to observe the effect of third harmonic of flux linkages on the total flux linkages and on the peak value of the current the Table 4.1 and Table 4.2 below are introduced for

$$c_1 = 0.0248 \quad ,$$

$$c_3 = 1.212 \quad ,$$

$$R = 1.64\Omega \quad ,$$

$$\ell = 2.65 \text{ mH} \quad ,$$

$$C = 20 \ \mu F \quad .$$

For single harmonic:

$$\Psi_m = \sqrt{2} \ \Psi_1 \quad ,$$

$$I_p = \sqrt{2} \ (c_1 \ \Psi_1 + 2c_3 \ \Psi_1^3)$$

For two harmonics:

$$\Psi_m = \sqrt{2} \ (\Psi_1 + \Psi_3) \quad ,$$

$$I_p = \sqrt{2} \ [c_1 (\Psi_1 + \Psi_3) + 2 c_3 (\Psi_1 + \Psi_3)^3]$$

In capacitive state.

	Calculation			Experimental
V(V)	Ψ_1(Wb)	Ψ_m (Wb)	I_p(A)	I_p(A)
120	1.19	1.68	5.81	8.35
100	1.17	1.65	5.53	7.55
50	1.11	1.57	4.27	5.65
10	1.105	1.48	4.	0.06 *

Table 4.1

V(V)	Calculation				Experimental
	Ψ_1(Wb)	Ψ_3(Wb)	Ψ_m (Wb)	I_p(A)	I_p(A)
120	1.17	0.0688	1.76	6.65	8.35
100	1.16	0.0667	1.735	6.38	7.55
50	1.08	0.0538	1.61	5.11	5.65
10	1.04	0.0454	1.54	4.46	0.06 *

* While jump-down takes place in experiment it does not exist in the analytical solution at this value of resistance.

Table 4.2

By the comparison of these two tables it is seen that the contribution of the third harmonic to the current is more than to the total flux linkages.

Figure 4.17a shows the transient current pattern in fundamental ferroresonance. This transient corresponds to the transition from inductive state to capacitive state. The phase and value of the maximum peak in this transient does change with the phase angle between current and voltage. For instance, the maximum peak is negative at zero degree while it occurs on the positive side at 180 degrees. Of course, the phase angle has no effect on the peak. value of the current in ferroresonance circuit.

The other salient feature of this transient characteristic is the occurence of a small loop (minor loop) after a cycle is completed. In the numerical calculation this small loop causes the incorrect results, if we do not select appropriate step-length. For example, with a large step-length we may not use the appropriate B and μ functions. For instance, the use of μ_4 (H, HP) after μ_2 (H, HP) without using μ_3 (H,HP) may produce incorrect results.

Although there is only one small loop in the Figure 4.17a its existence depends on the applied voltage. With higher voltages it always occurs.

Employing the Preisach Theory to represent the B/H loop in the numerical calculation the B/H loop, i (t) and the voltage across the transformer terminals are plotted in Figure 4.18 with the corresponding experimental quantities.

We have also used the magnetisation curve representation to observe the hysteresis effect on the fundamental ferroresonance. For this purpose the procedure given before in this chapter must be followed to get the capacitive state. Thus we have four different solution methods (two numerical and two analytical) for the same problem. The results produced by these methods are shown in Figure 4.19. From inspection of this figure the following is observed.

1) The analytical methods give greater error for the higher values of the applied voltage. The only reason for this is the representation of the magnetisation curve because of the fact that the cubical polinomial used is not sufficient to represent the upper region of this characteristic accurately. Jump-down occurs only when the applied voltage is zero at the small value of resistance in the analytical solutions.

2) Although the numerical calculation involving the representation of the magnetisation curve yields more accurate results still the jump-down takes place only when the applied voltage is zero, as in the previous case, while the jump-down occurs before the applied voltage reaches zero value if the hysteresis effect is taken into account using the B/H loop representation in the numerical calculation. Thus it is proved that the hysteresis

losses only slightly affect the jump-up condition but have a significant effect on jump-down condition.

3) Since increase in the supply voltage causes the circuit to have ferroresonance conditions, in practice this voltage and jump-up condition are more important than the jump-down conditions. On the other hand, both of the analytical methods proposed are sufficient to predict the jump-up condition.

In Figure 4.8 the peak values of the current computed are plotted against the rms value of the supply voltage with the experimental results. Generally, the error between computed and experimental results is about 10% but the error between computed and experimental voltage at the jump-up points is less than 4%.

Since about twenty minutes are required to compute one I_p/V loop with the 1904S ICL Computer, the computed results corresponding to the experimental results given in Figures 4.9, 4.10 and 4.11 were not produced.

Since the Preisach model is also capable of producing the minor loops it can be applied to study the unsymmetrical mode of ferroresonance as well. In fact, if the supply voltage is increased in the computer programme after obtaining the symmetrical mode we get into the unsymmetrical mode of ferroresonance as in the experiments. The computed and experimental results produced are shown in Figure 4.20. The computed B/H loop is narrower than the experimental one. It may be due to the effect of eddy currents, because they are not included in the computation. At high voltage and small capacitance the size of the minor loop is large but at high voltage and high capacitance the size is getting smaller.

It is important to notice that at the high voltage the

resistance and leakage inductance of the circuit increase. Therefore, the values of these quantities used in the calculation of the symmetrical ferroresonance cannot be used, i.e. these must be remeasured.

To see the accuracy of the generalized parametric method proposed to study the ferroresonance phenomena we will change the applied voltage at the fixed values of capacitance, resistance and leakage inductance, then calculate the corresponding generalized parameters. Thus, the value of each parameter also changes in keeping with the voltage.

Hence for

$$R = 1.64\Omega \ , \qquad \ell = 2.65 \ \text{mH} \ , \qquad C = 20 \ \mu\text{F}$$

jump-up takes place at

$$V \cong 110 \ \text{V} \ , \quad P_1 = 8.57 \ \text{E} -04$$

$$P_2 = 4.35 \ \text{E} -04$$

$$P_3 = 2.56$$

$$P_4 = 0.166$$

and the corresponding peak value of the current is

$$I_p = 7.87 \ \text{A}$$

Now, for the same condition jump-down takes place at

$$V \cong 21.5 \ \text{V} \ , \quad P_1 = 4.1 \ \text{E} -03$$

$$P_2 = 2.08 \ \text{E} -03$$

$$P_3 = 12.3$$

$$P_4 = 0.797$$

and the peak value of current is

$$I_p \simeq 1.1 \ \text{A}$$

The comparison of these results with those given in Figure 4.19 reveals that the accuracy of this method is not as good as the

accuracy of the normal numerical methods. In spite of this disadvantage,using this method we can draw some general conclusions and we can have a compact solution. Therefore, in the Figures 4.21, 4.22, 4.23, 4.24, 4.25 and 4.26 the absolute values of the peak of h_p (see Chapter 2) are plotted against P_3 retaining the other parameters P_1, P_2, P_4 constant.

Two modes of the fundamental ferroresonance can clearly be seen from these figures. For example, in Figure 4.21 for

$$3.25 \leq P_3 \leq 5$$

the operation state is inductive. At $P_3 = 3.1$ the jump-up takes place. For

$$3.1 \leq P_3 \leq 0.9$$

the operation state is capacitive. Within this region the fundamental ferroresonance current, or h has a symmetrical waveform but at

$$P_3 = 0.9$$

by a small jump the unsymmetrical mode starts.

Increasing the generalized parameter P_3 from zero the third jump, i.e. jump-down from capacitive state to inductive state, can also be observed but due to the problem of computing time, instead, different plots similar to Figure 4.21 have been obtained to observe the jump-up condition at the various values of the parameters. So, from the analysis of these figures, we conclude the following.

A) An increase of 100% in P_4 results in a decrease of 54% in the average value of $|h_p|$ and causes the jump-up point to shift towards the higher values of P_3. For the small value of P_4, $|h_p|$ has a more stable nature.

B) An increase of 100% in P_1 results in a decrease of 11.3% in the average value of $|h_p|$ and causes the jump-up point to

shift backwards to the lower values of P_3.

C) In general, for the distinct values of P_1, P_2, P_4 the jump-up takes place in the region

$$0.3 \leq P_3 \leq 0.35$$

4.8 Comparisons

Odessey et al[12] suggests a method semi-graphical, semi-analytical to define the critical conditions (jump conditions). So, a solution follows from two independent relationships for the voltage V_T across the transformer terminals on the primary side, when the secondary size is on open circuit. These are the volt-ampere characteristic of the transformer

$$V_T = f(I)$$

and the circuit equation

$$V_T = \sqrt{V^2 - (IR)^2} + \frac{I}{\omega C}$$

Where

V : rms value of the applied voltage

I : rms value of the current

In these two relations they assume that V_T and I are sinusoidal quantities; in other words, they take only the fundamental harmonic (which has the same frequency as the supply) of the current into consideration and neglect the other harmonics.

Since they do not use the B/H characteristic of the core the analytical expressions given do not contain the leakage inductance and the construction parameters, such as cross-sectional area and average length of the core and number of turns. Therefore, the effects of these quantities on critical conditions cannot be studied by this method. They deal with only the jump-up condition, not jump-down condition.

Thomson[13] also treats the problem vectorially and expresses the reactance and apparent resistance in terms of effective current. Thus, he does not use any graphs. But he still assumes the current to be sinusoidal and therefore the leakage inductance and the construction parameters do not appear in the expressions.

Rudenberg[14] also describes the jump-up condition by a purely graphical solution using the two distinct expressions of V_T given above. From the practical point of view this is a relatively simple and accurate method.

Hayashi[17,18,19,20] investigates the same problem purely mathematically. In reference 20 he uses an ellipse to represent the B/H loop, but it is only applicable to the symmetrical modes.

In reference 23,24,25 the flux linkages ψ is assumed to be in the form

$$\Psi = A \cos(\omega t + \alpha) + B \cos \omega t$$

In other words, Ψ has not any harmonic except the fundamental harmonic. This assumption may be valid for the lower region of the capacitive state, but at the higher values of voltage ψ has a third harmonic as well as the first (fundamental) harmonic. In the unsymmetrical mode of ferroresonance the second harmonic also becomes effective.

In this present investigation two different expressions are proposed to use for Ψ. These are

$$\Psi = \Psi_1 \sin(\omega t + \theta_1)$$

$$\Psi = \Psi_1 \sin(\omega t + \theta_1) + \Psi_3 \sin(3\omega t + \theta_3)$$

Applying the former one enables us to use a standard graph by which both the jump-up and jump-down conditions can be visualized and determined easily. Using the latter one, we can produce more

accurate results compared to the former case. In both cases the leakage inductance and the construction parameters are included in the calculation.

Generally, the methods in which the B/H characteristic is used instead of volt-ampere characteristic allow us to take more parameters associated with the system into consideration, and therefore they are more flexible but require more mathematics, while graphical and semigraphical methods are more practical.

There is no doubt that by the numerical solution more accurate results are produced because less assumptions are made, and more accurate representations of the B/H characteristic are used. Therefore, numerical solutions are also carried out. In order to exhibit the accuracy of the numerical method as compared to analytical method, Figure 4.19 has been constructed.

Teape[37] studied the ferroresonance phenomena numerically but not in detail. On the other hand, Germay et al[39] also analyses these phenomena numerically using the Preisach model, but they use numerical values for the distribution function γ rather than an analytical expression. Since the new parameters H_1 and H_2 are established, the calculation of these brings additional difficulties and requires more computing time.

The generalized parametric method is not so accurate but, as mentioned before, it provides a general knowledge about jump-up conditions and modes of ferroresonance.

CHAPTER 5

SUBHARMONIC FERRORESONANCE

In a circuit as in Figure 1.4 the current could have two sustained values for the same value of the applied voltage and the same circuit parameters if certain initial conditions were fulfilled.

The higher value of the current thus obtained has a frequency which is a submultiple of the supply frequency. Such a phenomena is called "Subharmonic Ferroresonance". The current achieves its higher value by a jump-up but this jump-up takes place only when the circuit is switched on under certain conditions; in other words the initiation of the subharmonic resonance depends on the switching conditions, which are:

1. The initial flux linkages of the transformer
2. The initial capacitor charge
3. The switching angle (i.e. the applied voltage at the instant of energizing the circuit)

Once the sustained subharmonic resonance is initiated then the continuation of this phenomenon depends on the value of the circuit parameters. As illustrated in the following Figure 5.1 there are two limiting conditions at which the subharmonic resonance disappears, and the current returns to its normal value by jumping down.

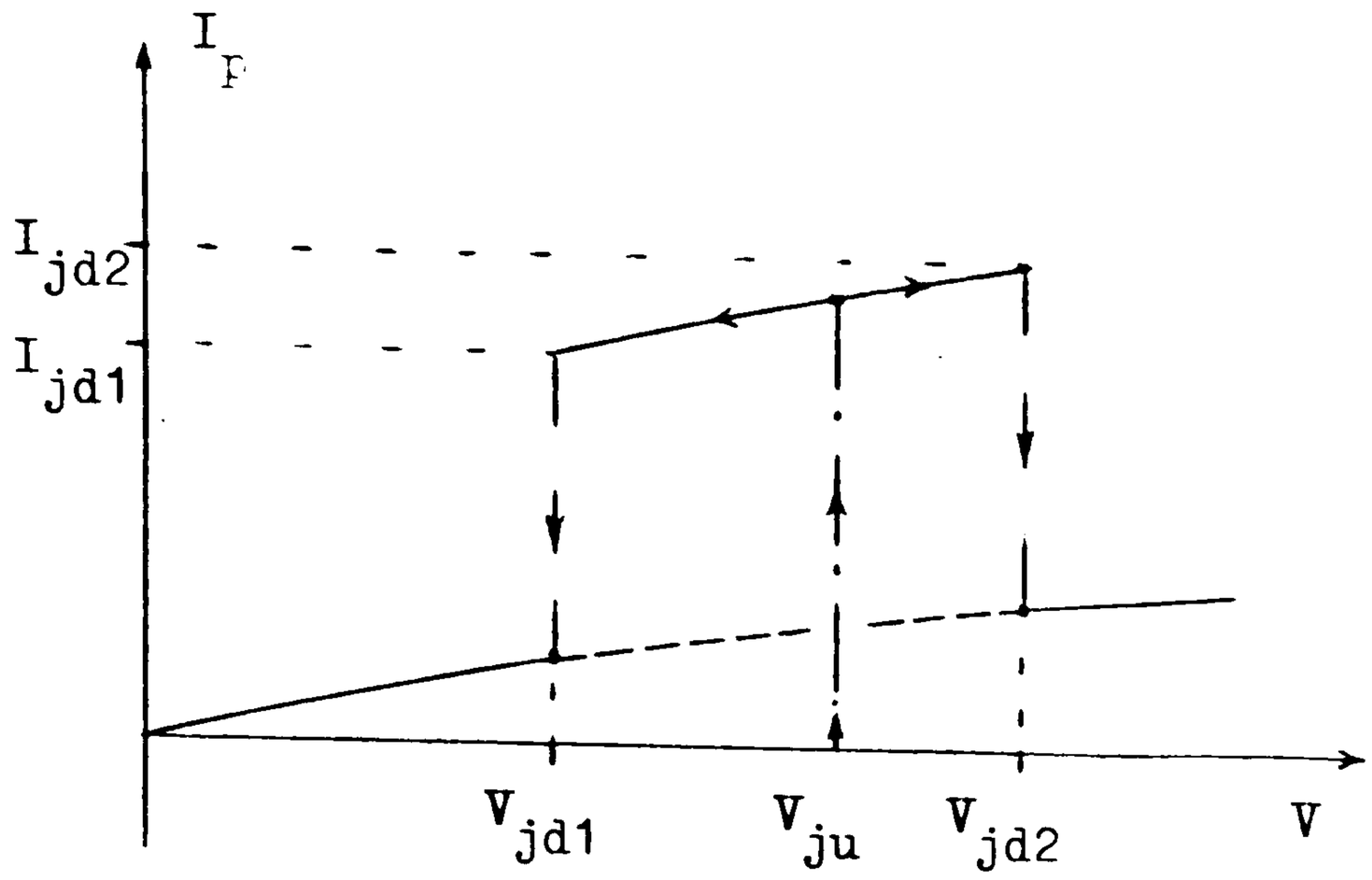

Fig. 5.1

Although subharmonic resonance is an experimentally known phenomenon since early years [10,29] the recently increasing use of series capacitors to overcome the inductive voltage drop and to improve the power factor in distribution systems has revived interest in the phenomenon. Therefore, a number of investigations which have been reviewed in Chapter 1 have been carried out.

In this chapter we will deal mainly with the $\frac{1}{3}$ order of subharmonic resonance presenting three different methods. These are:

1. The analytical method which allows study of sustained subharmonic resonance. This enables us to take into account all the parameters of the circuit except hysteresis and eddy current effects because the magnetisation curve is considered in the calculation.
2. The numerical method in which the exponential series is employed for the representation of the magnetisation curve.

3. The numerical method involving the Preisach model to represent the B/H loop.

In the case of the second and third methods we can observe the effect of hysteresis losses on subharmonic resonance.

In the third method, apart from eddy current losses, all the other parameters related with the system under the consideration are included, i.e. there is no simplifying assumption.

The procedure to be followed for the numerical solution and experiments is the same as for fundamental ferroresonance. Therefore, by an alteration in the initial conditions, the computer programme designed for the numerical calculation of the fundamental ferroresonance can be utilized for the subharmonic case. The result produced by these two numerical methods will be analysed at the end of this chapter.

For the relevant computer programme refer to the Appendix A4.

5.1 Analytical Solution for Sustained Subharmonic Ferroresonance

The waveform of the flux linkages in the sustained subharmonic case is as in the following Figure 5.2a.

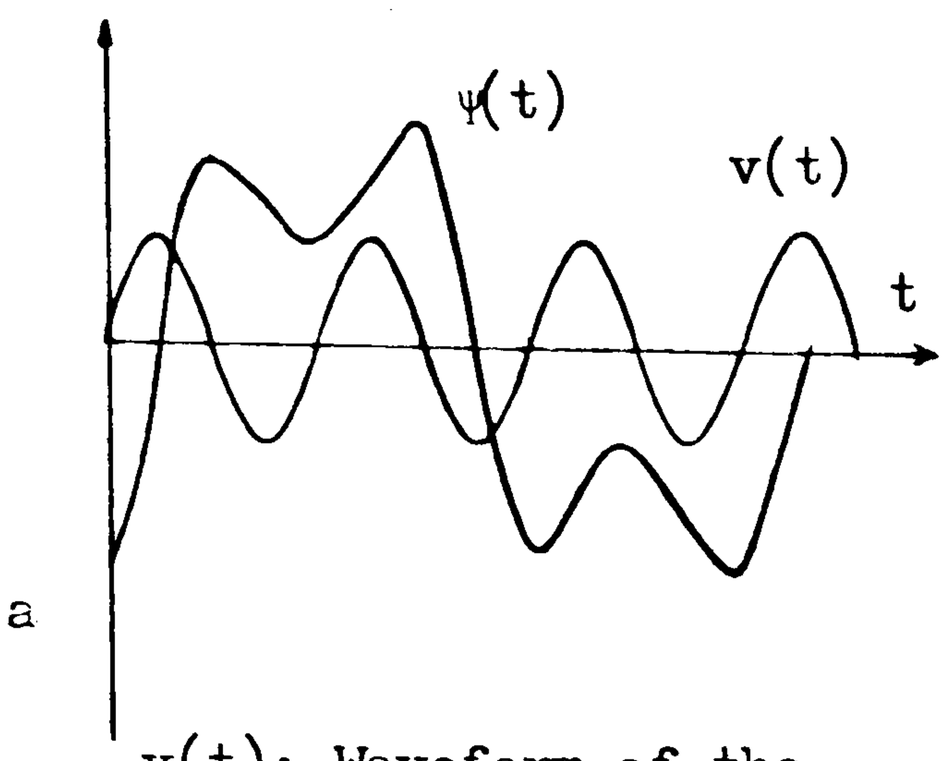

v(t): Waveform of the applied voltage

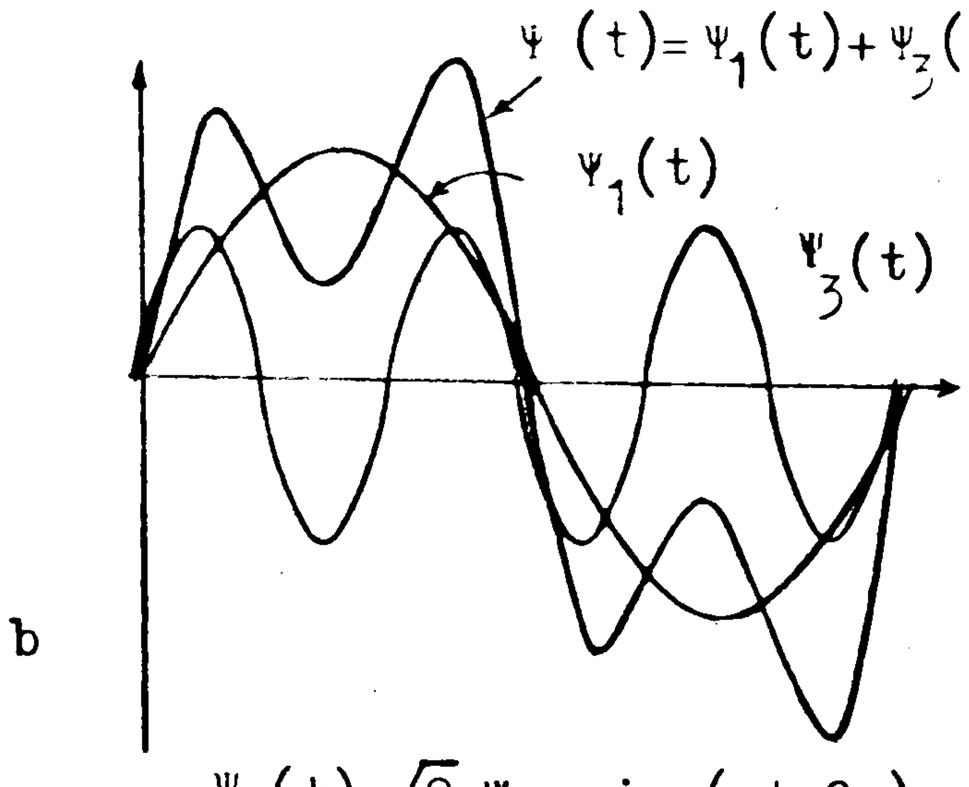

$\Psi_1(t) = \sqrt{2}\ \Psi_1 \sin(\omega t + \theta_1)$

$\Psi_3(t) = \sqrt{2}\ \Psi_3 \sin(3\omega t + \theta_3)$

Fig. 5.2

This waveform can be composed of two distinct forms, as shown in Figure 5.2b. One of them has the same frequency as the supply voltage and the other one only one third fraction of the first. Thus the equations 4.1, 4.2, 4.3 and 4.5 given in Chapter 4 can be employed in this case as well; but this time the voltage waveform v(t) must be expressed by

$$v(t) = \sqrt{2} \cdot V \sin(3\omega t)$$

So, as detailed in Appendix A5, we arrive at the following system of equations with complex coefficients for sustained subharmonic resonance.

$$0 = \bar{Z}_1 \bar{I}_1 + j\omega \bar{\Psi}_1 \qquad 5.1$$

$$\bar{V} = \bar{Z}_3 \bar{I}_3 + j3\omega \bar{\Psi}_3 \qquad 5.2$$

These two nonlinear equations will be solved by the method proposed in Chapter 4 but $\bar{F}$ and $\bar{G}$ are, in this case,

$$\bar{F} = \bar{Z}_1 \bar{I}_1 + j\omega \bar{\Psi}_1$$
$$\bar{G} = \bar{Z}_3 \bar{I}_3 + j3\omega \bar{\Psi}_3 - \bar{V}$$

5.1.1 Establishment of the Initial Conditions

From examination of Figure 5.2a there are two maxima and one minimum of Ψ in each side of the time axis. These are strictly functions of the phase angles θ_1 and θ_3. For instance, if $\theta_1 = \theta_3$ these two maxima become equal to each other. On the other hand, θ_1 and θ_3 are functions of the applied voltage as are Ψ_1 and Ψ_3. So, for the convergent solution of Ψ_1, Ψ_3, θ_1 and θ_3 from equations 5.1 and 5.2 we must establish some approximate values for these unknown variables. For that we will refer to the equations 5.1 and 5.2 such that if

$$\bar{I}_1 = c_1 \bar{\Psi}_1 + \frac{c_3}{2} (3 \bar{\Psi}_1^2 - 3(\bar{\Psi}_1^*)^2 \bar{\Psi}_3 + 6 \bar{\Psi}_1 \bar{\Psi}_3 \bar{\Psi}_3^*)$$

is substituted in the equation 5.1 and then divided into the real and imaginary parts (see Appendix A5 for detail) we find

$$\Psi_1^2 = \frac{-(3\Psi_3^2 + 2D_1) \mp \sqrt{\Delta_1}}{2} \qquad 5.3$$

where

$$\Delta_1 = (3\Psi_3^2 + 2D_1)^2 - 4F_1 \qquad 5.4$$

$$F_1 = 4\Psi_3^4 + 4\Psi_3^2 D_1 + D_1^2 + E_1^2$$

$$D_1 = [c_1 + \frac{\omega}{Z_1} \sin \xi_1] \frac{2}{3c_3}$$

$$E_1 = \frac{2\omega}{3c_3 Z_1} \cos \xi_1$$

From the imaginary part of equation 5.1 we also have

$$\sin(\theta_3 - 3\theta_1) = \frac{3\omega}{3c_3 Z_1 \Psi_1 \Psi_3} \cos \xi_1 \qquad 5.5$$

On the other hand, by the same manner, substituting the expression

$$\bar{I}_3 = c_1 \bar{\Psi}_3 + \frac{c_3}{2} (3 \bar{\Psi}_3^2 \bar{\Psi}_3^* + 6 \bar{\Psi}_1 \bar{\Psi}_1^* \bar{\Psi}_3 - \bar{\Psi}_1^3)$$

into the equation 5.2, then dividing it into real and imaginary parts we obtained the relation

$$\cos(3\theta_1 + \xi_3) = \frac{A_1^2 + A_4^2 - (A_2^2 + A_3^2)}{2 A_2 A_3} \qquad 5.6$$

where

$$A_1 = D_3 + 3\Psi_3^2 + 6\Psi_1^2$$

$$A_2 = \frac{\Psi_1^3}{\Psi_3}$$

$$A_3 = \frac{2V}{c_3 Z_3 \Psi_3}$$

$$A_4 = E_3$$

$$D_3 = \left(c_1 + \frac{3\omega}{Z_3} \sin \xi_3\right) \frac{2}{c_3}$$

$$E_3 = \frac{6\omega}{c_3 Z_3} \cos \xi_3$$

Since θ_1 and θ_3 are always negative and the impedance due to the circuit capacitance is greater than the impedance due to the leakage inductance

$$\xi_1 , \quad \xi_3 < 0$$

Therefore

$$(3\theta_1 + \xi_3) < 0$$

That means the cosine ratio must be between zero and minus one, i.e.

$$0 \geq \left[\frac{A_1^2 + A_4^2 - (A_2^2 + A_3^2)}{2 A_2 A_3}\right] \geq -1 \qquad 5.7$$

Now, for given values of $\bar{Z}_1$, $\bar{Z}_3$, c_1, c_3, ω and $\bar{V}_3$ if we take

$$\Psi_3 = F M \left(\frac{V}{3\omega}\right)$$

we can calculate Ψ_1 from equation 5.3 and check the condition 5.7.

In case 5.7 is not satisfied then by changing the multiplier FM starting with FM = 1 this procedure is repeated. When the iteration is

completed FM, Ψ_1, Ψ_3 are then known. Now, only θ_1 and θ_3 are required. But from equation 5.6

$$\theta_1 = -\frac{1}{3}\left[\cos^{-1}\left(\frac{A_1^2 + A_4^2 - (A_2^2 + A_3^2}{2\,A_2\,A_3}\right) + \xi_3\right] \qquad 5.8$$

and from equation 5.5

$$\theta_3 = \sin^{-1}\left[\frac{2\omega}{3c_3 Z_1 \Psi_1 \Psi_3}\cos\xi_1\right] + 3\theta_1 \qquad 5.9$$

So, θ_1 and θ_3 are finally known.

Thus, knowing only V and given values of $\bar{Z}_1$, $\bar{Z}_3$, c_1, c_3 and ω we can calculate the appropriate initial values for Ψ_1, Ψ_3, θ_1 and θ_3. With these initial values the solution of equations 5.1 and 5.2 is convergent. But there are such values of Ψ_3 for which Δ_1 is negative and consequently Ψ_1 has complex conjugate roots. Since such roots do not physically exist, this condition corresponds to the unstable state. Therefore, in the next stage we will deal with the stability of subharmonic resonance.

5.1.2 The Stability Analysis of the Subharmonic Oscillation

From consideration of equation 5.3 it is seen that the character of Ψ_1 depends strictly on Δ_1. Therefore, we will first study this equation for different values of Δ_1.

I - Δ_1 = 0, The Critical Condition

When Δ_1 is equal to zero (Ψ_1^2) becomes

$$(\Psi_1)^2 = -\frac{(3\Psi_3^2 + 2D_1)}{2}$$

or

$$\Psi_1^2 + \frac{3}{2}\Psi_3^2 + D_1 = 0 \qquad 5.10$$

For a selected value of D_1 the equation above gives an ellipse on the (Ψ_1, Ψ_3) plane as in Figure 5.3a. But the parts of this ellipse on the second, third and fourth quadrant do not physically exist because

Ψ_1 and Ψ_3 are always positive and real. So our solution domain will be only the first quadrant. In Figures 5.3a and 5.3b the shaded area indicates the physical boundaries.

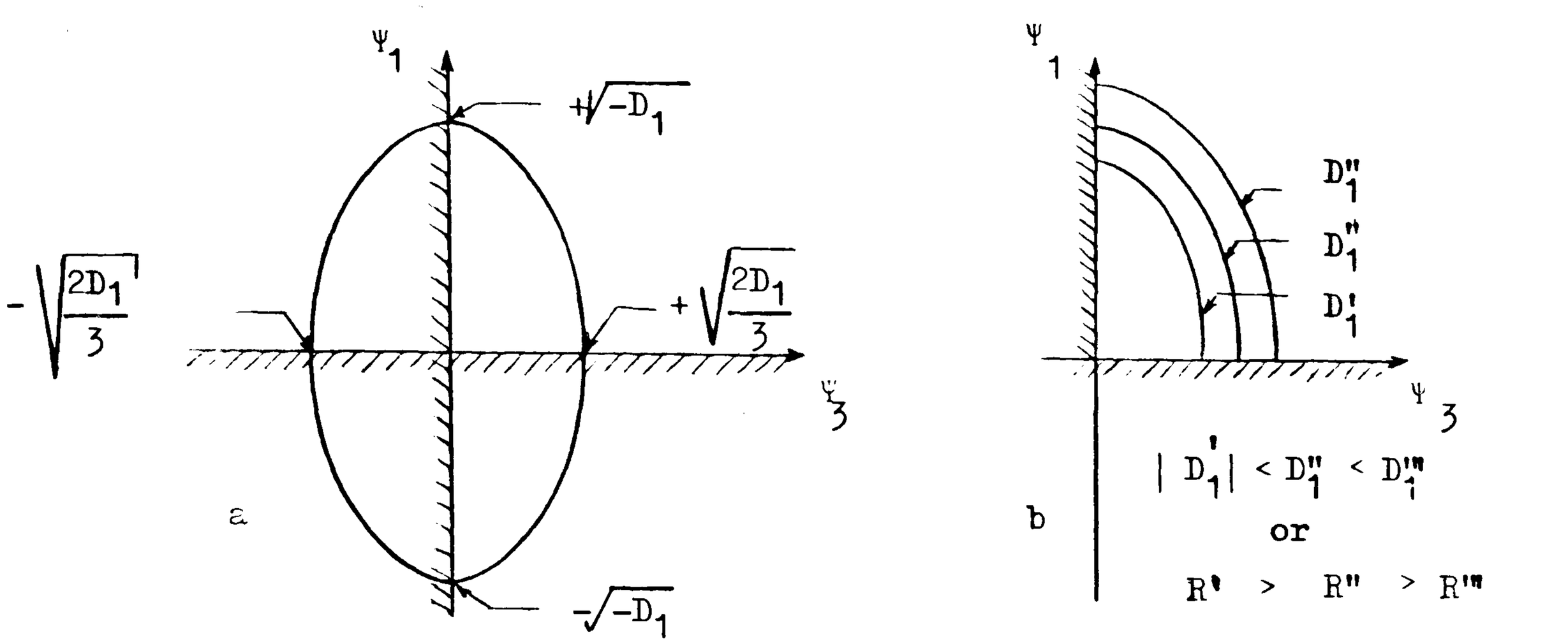

Fig. 5.3

For the various values of D_1 we get a family of ellipses as shown in Figure 5.3b. So that ψ_1 and ψ_3 are positive and real, D_1 must be negative, as will be seen from Figure 5.3a, i.e.

$$D_1 = [c_1 + \frac{\omega}{Z_1} \sin \xi_1] \frac{2}{3c_3} \leqslant 0 \qquad 5.11$$

Hence, if c_1 and c_3 are positive then the two conditions

1. $\xi_1 \leqslant 0$,
2. $c_1 \leqslant \frac{\omega}{Z_1} \sin |\xi_1|$

must be satisfied.

Since

$$\tan \xi_1 = \frac{(\ell\omega - \frac{1}{\omega C})}{R}$$

for the first condition

$$\frac{1}{\omega C} \geqslant \ell\omega$$

or

$$\frac{1}{\sqrt{\ell.C}} \geq \omega$$

Now, the question is at which conditions will Δ_1 become zero. In order to establish this we will examine the expression for Δ_1. Equating Δ_1 to zero we have

$$(\Psi_3^2)_{1,2} = \frac{-4D_1 \mp \sqrt{\Delta_2}}{14} \qquad 5.12$$

where

$$\Delta_2 = 16D_1^2 - 112\,E_1^2 \qquad 5.13$$

For various values of Δ_2, Ψ_3 has different characteristics. Therefore we will discuss the roots of Ψ_3 for various values of Δ_2

<u>a - $\Delta_2 = 0$</u>

If equation 5.13 is equated to zero we obtain

$$16\,D_1^2 - 112\,E_1^2 = 0$$

or

$$D_1 + \sqrt{7}\,E_1 = 0 \qquad 5.14$$

Substituting the expression of D_1 and E_1 into the above equation and rearranging it we arrive at

$$c_1 + \frac{\omega}{Z_1} \sin \xi_1 + \sqrt{7}\,\frac{\omega}{Z_1} \cos \xi_1 = 0$$

Since

$$Z_1 = \sqrt{R^2 + X_1^2}$$

$$X_1 = \omega \ell - \frac{1}{\omega C}$$

$$\sin \xi_1 = \frac{X_1}{Z_1}$$

$$\cos \xi_1 = \frac{R}{Z_1}$$

We can express the resistance R in terms of X_1 by the above equation but we will denote this resistance by R_c (critical resistance) to

distinguish it from other values of resistance. Thus R_c, from the following equation

$$c_1 R_c^2 + c_1 X_1^2 + \omega X_1 + \sqrt{7}\ \omega R_c = 0$$

is

$$R_c = \frac{-\sqrt{7}\ \omega + \sqrt{7\ \omega^2 - 4\ c_1\ (c_1 X_1^2 + \omega X_1)}}{2\ c_1} \qquad 5.15$$

Now we can examine the effect of the circuit resistance on Ψ_1 and Ψ_3. For instance, if $R = R_c$ then $\Delta_2 = 0$, and consequently

$$\Psi_{3c}^2 = -\frac{2D_1}{7}\ , \qquad 5.16$$

$$\Delta_1 = 0\ ,$$

and

$$\Psi_{1c}^2 = -\frac{4D_1}{7}\ . \qquad 5.17$$

So, in a circuit having critical resistance R_c if Ψ_3 has a value greater or less than Ψ_{3c} the unstable state occurs. That means, in this case we have only one solution point on the solution domain, as shown in Figure 5.4.

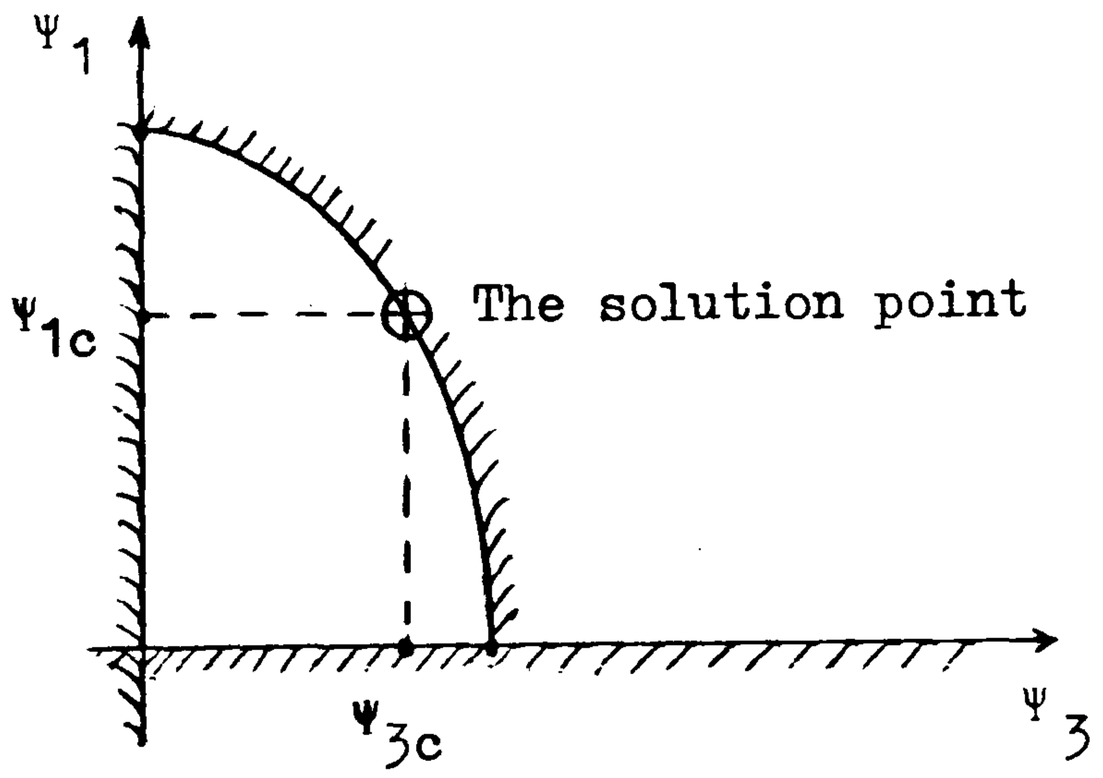

Shaded area shows the unstable region

Fig. 5.4

b - $\Delta_2 < 0$

If the value of the circuit resistance is greater than the

critical resistance then Δ_2 becomes negative, and therefore Ψ_3 has complex conjugate roots, no real roots. That means subharmonic resonance does not exist.

$\underline{c} - \Delta_2 > 0$

If the value of the circuit resistance is less than the critical resistance then Δ_2 becomes positive, and correspondingly Ψ_3^2 has two distinct roots so that

$$(\Psi_3^2)_{min} = \frac{-4D_1 - \sqrt{\Delta_2}}{14} \qquad 5.18$$

$$(\Psi_3^2)_{max} = \frac{-4D_1 + \sqrt{\Delta_2}}{14} \qquad 5.19$$

Since from either $(\Psi_3^2)_{min}$ or $(\Psi_3^2)_{max}$ Δ_1 will be zero, from equation 5.10

$$(\Psi_1^2)_{max} = -\frac{3}{2}(\Psi_3^2)_{min} - D_1 \qquad 5.20$$

$$(\Psi_1^2)_{min} = -\frac{3}{2}(\Psi_3^2)_{max} - D_1 \qquad 5.21$$

So the limiting values of Ψ_1 and Ψ_3 which correspond to the jump-down points, have been found. It should be remembered that these points are on the ellipse defined by the equation 5.10.

After producing sustained subharmonic resonance if we increase the applied voltage, Ψ_3 will also increase until the upper limit Ψ_{3max} is reached. At this point Ψ_1 has its minimum value, i.e. Ψ_{1min}. Now, if we increase the voltage a little more then Ψ_3 becomes greater than Ψ_{3max} and consequently

$$\Delta_1 < 0$$

Similarly, Ψ_3 can get its minimum value $(\Psi_3)_{min}$ by decreasing the applied voltage. A little further decrease in the voltage results

in

$$\Psi_3 < \Psi_{3min} \quad \text{and} \quad \Delta_1 < 0.$$

In figure 5.5 the limit points have been shown on the Ψ_1/Ψ_3 plane.

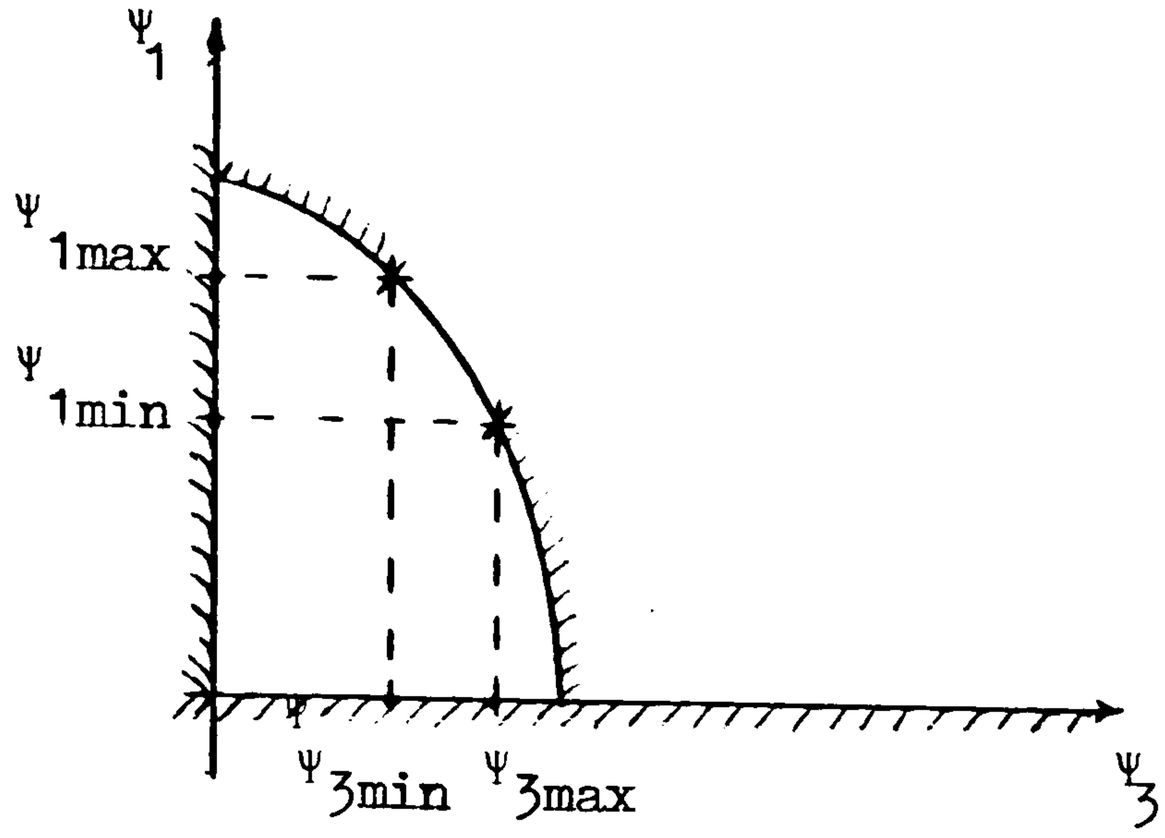

Shaded area shows the unstable region

Fig. 5.5

II - $\Delta_1 < 0$

We have already seen that for $\Psi_3 < \Psi_{3min}$ and $\Psi_3 > \Psi_{3max}$ Δ_1 becomes negative and Ψ_1 has complex conjugate roots. In other words subharmonic resonance again does not exist.

III - $\Delta_1 > 0$

In this case, so long as $\Delta_2 \geq 0$ subharmonic resonance exists and the relationship between Ψ_1 and Ψ_3 is expressed by equation 5.3 which is in a general polynomial form. We will call this curve "the solution curve". The following figures 5.6a and 5.6b show the function $\Psi_1 = f(\Psi_3)$ and $\Delta_1 = f(\Psi_3)$.

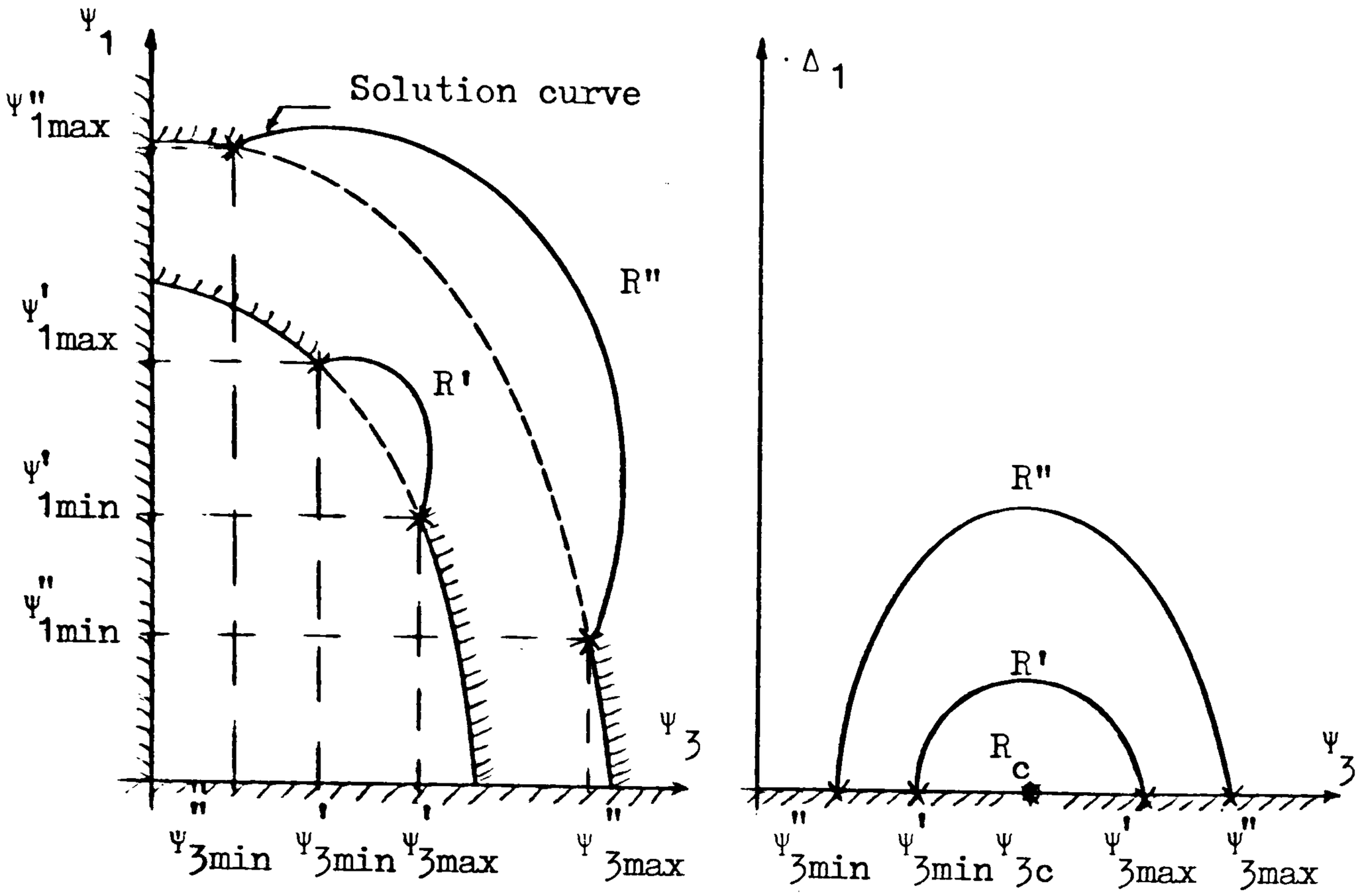

$R_c > R' > R''$

Shaded area shows the unstable region

a. b

Fig. 5.6

5.1.3 The Approximate Calculation of the Voltages Corresponding to the Critical Resistance R_c and Limit Points

From the practical standpoint having some knowledge about the applied voltage corresponding to the critical resistance R_c and limit points (jump-down points) is more important than knowing the critical and limit values of flux linkages Ψ_1 and Ψ_3. Therefore, here we will try to establish relationships for these particular supply voltages.

For various values of voltage the computational results obtained from the solution of equations 5.1 and 5.2 give a value

between -0.97 and -0.99 for the limits given by 5.7. Therefore we can equate approximately this value to -1. That is

$$\frac{A_1^2 + A_4^2 - (A_2^2 + A_3^2)}{2 A_2 A_3} = -1$$

Rearranging this we have

$$A_3 = A_2 + \sqrt{A_1^2 + A_4^2}$$

or substituting the expressions of A_1, A_2, A_3 and A_4

$$V = \frac{Z_3 \Psi_3 c_3}{2} \left[\frac{\Psi_1^3}{\Psi_3} + \sqrt{(D_3 + 3\Psi_3^2 + 6\Psi_1^2)^2 + E_3} \right] \qquad 5.22$$

From this expression the voltages corresponding to the critical resistance and limit points are found.

<u>Example</u> For

$c_1 = 0.0248$

$c_3 = 1.212$

$\omega = 314/3$

$C = 22\ \mu F$

$\ell = 2.65$ mH

From Equation 5.15 $R_c = 145\Omega$

Hence the critical values of flux linkages

$\Psi_{1c} = 0.274$ Wb

$\Psi_{3c} = 0.182$ Wb

and from equation 5.22 the critical voltage

$V_c = 51.2$ V.

Now, for a chosen value $R = 100\Omega < R_c$

$\Psi_{3max} = 0.235$ Wb $\qquad \Psi_{3min} = 0.07$ Wb

$\Psi_{1min} = 0.19$ Wb $\qquad \Psi_{1max} = 0.335$ Wb

$V_{max} = 67$ V $\qquad V_{min} = 24$ V

Either for (Ψ_{3max}, Ψ_{1min}) or for (Ψ_{3min}, Ψ_{1max}) Δ_1 is zero but for a value such as

$$\Psi_3 > \Psi_{3max} \quad \text{or} \quad \Psi_3 < \Psi_{3min}$$

Δ_1 becomes negative, i.e. the subharmonic ferroresonance does not exist.

5.2 Analysis of the Results

The analytical method has been based on the assumption of constant circuit resistance, i.e. the resistance of the circuit does not vary with the current. In the physical system it is the function of the current due to the iron losses. Therefore, when point B in Figure 5.7a below moves along CA on the current-voltage plane the corresponding point B on the Ψ_1/Ψ_3 plane in Figure 5.7b

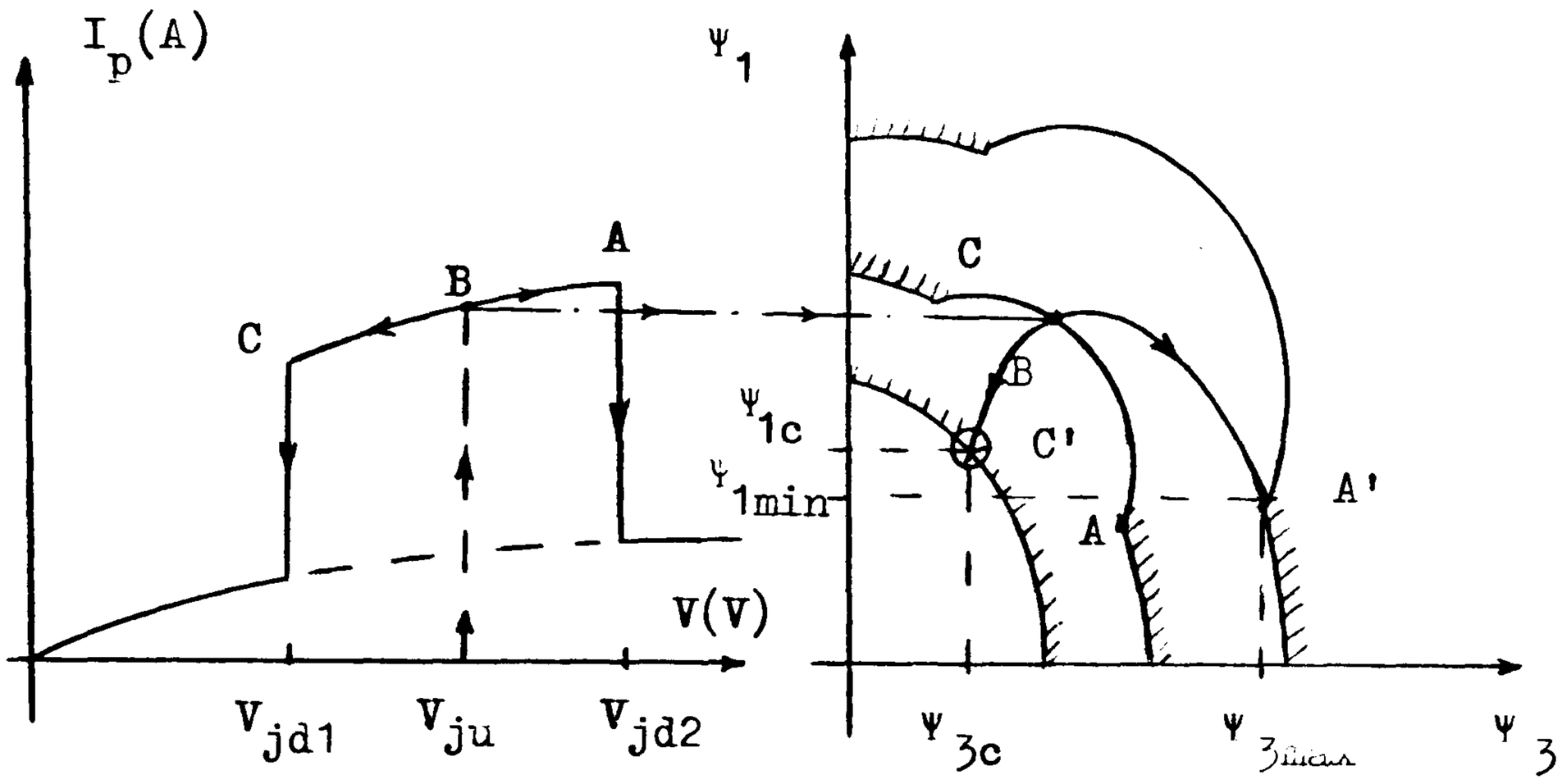

Shaded area shows the unstable region.

Fig. 5.7

will move along C'A' instead of CA. Thus, even if there is no actual resistance, due to the iron losses the physical system has an "apparent resistance"[13]. This resistance becomes bigger when the supply voltage is decreased and it is defined by the ratio

$$R \triangleq \frac{P\ (W)}{I_{rms}^2\ (A)}$$

That is, if the active power drawn from the supply, and the rms value of the current are measured by moving-iron type instruments, the apparent resistance can be calculated. For the capacitance $C = 22\,\mu F$ the sustained subharmonic ferroresonance disappears when

V = 53V. Just before jump-down takes place the measured values are

$$P = 4.8\ W, \quad I = 0.18\ A.$$

Hence the apparent resistance R = 148.15Ω . On the other hand, the calculated critical resistance and voltage were

$$R_c = 145\Omega \quad \text{and} \quad V_c = 51.2\ V$$

which correspond to the point C' on Figure 5.7b.

In addition to the effect of iron losses on the lower jump-down point these losses also affect the waveform of the current whereas they do not have a considerable effect in the case of fundamental ferroresonance. To demonstrate this we solve the equations 1.8 numerically employing two computer programmes as mentioned at the beginning of this chapter. The results produced are shown in Figure 5.8 together with the corresponding experimental results. As will be seen from this figure the Preisach model gives very small errors. The current waveform in Figure 5.8c certainly contains a subharmonic component. It is also seen, however, that the cyclic pattern does not repeat itself accurately since it is impossible to stabilise the prolonged computation while highly accurate B/H representation is used.

In Figure 5.9 computed and experimental B/H patterns are presented. The computed pattern in this figure is narrower then the experimental one. The only reason for this discrepancy is the eddy current effect which is not included in numerical calculations.

As in the fundamental ferroresonance phenomenon, in this case the voltage across the transformer terminals is also higher than the applied voltage. The computed and experimental transformer voltage waveforms are shown in Figure 5.9.

In order to confirm the results reached in the analytical

method proposed $\Psi_1 = f(\Psi_3)$ and $\Delta_1 = f(\Psi_3)$ are plotted in Figure 5.10 and 5.11 for the different values of the resistance for the sample transformer.

As is clearly seen from Figure 5.12, 5.13 and 5.14 by increasing the voltage the main harmonic flux Ψ_3 increases linearly while the third harmonic Ψ_1 decreases nonlinearly. Therefore, in the estimation of the initial value of Ψ_3

$$\Psi_3 = FM. \quad (\frac{V}{3\omega})$$

was used.

The current waveform in Figure 5.12 produced by the analytical method is not similar to the experimental one given in Figure 5.8. This is not an unexpected result under the assumptions made in the method.

As illustrated in Figure 5.15 the subharmonic ferroresonance is initiated at the conditions

$$C = 22\,\mu F, \quad V = 65\ V \text{ and } V_c = 10\ V$$

Then, if the capacitance is changed around 22 μF the sustained subharmonic ferroresonance is stable but if the capacitance is changed considerably, in either direction, from 22 μF the resonance disappears.

5.3 Comparisons

The analytical method developed and used is very helpful in the explanation of the stability, and the effect of the iron losses on the continuation of the sustained subharmonic ferroresonance. On the other hand, its accuracy is not as high as that of the numerical methods. In fact, the accuracy of the analytical method is a function of the coefficients c_1, c_3 used in the representation of the magnetisation curve. So, in order to see how the accuracy

depends on these coefficients, the following table is given.

c_3	c_1	I_{pmax}^{*}(A)
	0	0.453
	0.1	0.442
0.1	0.15	0.437
	0.2	0.432
	0.25	0.426

c_3	c_1	I_{pmax}^{*}(A)
	0	0.25
	0.1	0.238
1.0	0.15	0.233
	0.2	0.228
	0.25	0.219

* I_{pmax} indicates the maximum peak value of the current and its experimental value is 0.52 A.

TABLE 5.1

In the analytical calculation in this chapter the coefficients employed are the same as those used in the case of fundamental ferroresonance.

To compare the results obtained from analytical and two numerical methods I_{pmax} is plotted against the rms value of the applied voltage as in Figure 5.16 together with the experimental results. An interesting result observed from this figure is that I_{pmax} has a maximum. This figure also reveals the accuracy of the Preisach model.

In his analytical calculation Travis[30] assumes that there is no current flowing until the saturation point is reached and then the magnetisation characteristic is a straight line, as Specht[4] and Holcomb[5] do in their analytical calculation of the transient current. He treats the circuit as a nondissipative system. Both these assumptions are not valid because it is proved by numerical and analytical methods in this chapter that the iron losses and circuit resistance affects phenomenon critically.

Hayashi[19], Wright[33] and Shenkman[34] give similar method for the analytical calculation of the sustained subharmonic resonance. But, in all these works, the leakage inductance is not included in the calculation which leads to simplifications but either for high value of leakage inductance or high value of capacitance the impedance due to this leakage inductance can not be neglected. Also, in the reference 19 and 34 there is no experimental verification made.

Teape[37] introduced a few characteristic features of the phenomenon numerically but did not make any attempt at either an analytical solution or a detailed numerical analysis. However, the results produced by his own B/H representation method are in good agreement with the experimental results.

Germay et al[39] studies the subharmonic ferroresonance applying the Preisach model but, as mentioned before, they use numerical distribution function which may cause some problem of computing time.

CHAPTER 6

GENERAL CONCLUSIONS AND SUGGESTIONS FOR FURTHER WORK

6.1 General Conclusions

In the analytical method developes in Chapter 3 by the modification of the Frohlich formula the various residual conditions of the iron core are represented in the analytical calculations of the first peak value of the transient current.

By this method neither the saturation current[4,5,6] nor the residual conditions of the core[7] are neglected. Besides this, the nonlinear differential equation of the system under consideration is reduced to a nonlinear ordinary equation which can either be solved by a numerical method or by a graphical construction.

The results produced by this method for the range of the switching angle

$$0^{\circ} \leqslant \alpha \leqslant \alpha_s$$

are very accurate, the error between experimental and these results being less than 3% (see Table 3.7).

Since α_s is a function of the residual flux densities (see Table 3.6) the accuracy is also a function of the residual flux densities. But for

$$\alpha > \alpha_s$$

the agreement is not as good as before.

In addition to the representation of the B/H loop the Preisach model can be employed to represent the magnetisation curve as well. But, for the magnetisation curve this method is not as accurate as the exponential series representation method. (refer to pages 22, 23, 25-28 and Table 6.1).

		$H=c_1 B+c_3 B^3$		Frohlich Form		Exponential Seri.		Preisach Model	
		Trans.	Ferro	Trans.	Ferro	Trans.	Ferro	Trans.	Ferro.
B/H Curve Representation	Analytical Calculations	P	S	E	P	I	I	I	I
	Numerical Calculation	P	S	E	P	E	S	S	I
B/H Loop Representation	Analytical Calculation	P	P	P	P	I	I	I	I
	Numerical Calculation	P	P	P	P	S	S	E	E

In the table: E : Excellent , S : Satisfactory

P : Poor , I : Impossible

Trans : Transient, Ferro : Ferroresonance

Table 6.1

So the Preisach model for the B/H loop, the exponential series method for the magnetisation curve have been used in the numerical calculations of the transient current and ferroresonance phenomena. Thus, comparing the produced results it is possible to observe the hysteresis effect on these phenomena and the accuracy of the Preisach model.

The results obtained for the transient current reveal that the effect of the hysteresis losses is not perceptible (see table 3.5). Therefore, if the computer facilities are available the exponential series representation method is preferable because less computing time is required. But, as is in many cases in practice, suitable computer facilities are not always available and analytical formula is preferable. The analytical method is, therefore, the only satisfactory way for the calculation of the transient current.

In the case of ferroresonance phenomena (both fundamental and subharmonic ferroresonance) the hysteresis losses become more important because they not only affect the peak values but also the waveforms and jump points, and hence the stability of the phenomenon (see Figures 4.19, 5.8, 5.16). So in order to observe this effect it is essential to represent the B/H loop in the numerical calculations. But, even if the hysteresis losses are taken into consideration, there is some discrepancy between experimental and computed results. For instance, the computed B/H loops in Figures 4.20 and 5.9 are narrower than the experimental ones. The only likely reason for this is the eddy current losses which are not included in the calculations.

Again, since it is more practical, an analytical method

is developed for the ferroresonance phenomena. In the application of this method to the fundamental ferroresonance (in Chapter 4) it is divided into two parts. In the first part only the fundamental harmonic Ψ_1 of the flux linkages, and in the second part both the fundamental Ψ_1 and third harmonic Ψ_3 are considered. The first part leads to more practical results and a graphical solution which is a very useful tool to visualize the jump phenomena and to predict the jump-up and jump-down points (see Figure 4.14). The second part produces more accurate results but is relatively complicated. Using the complex variable techniques four equations are reduced to two equations with complex coefficients.

The accuracy of the analytical method depends on the applied voltage and the coefficients used in the representation of the magnetisation curve ($H = c_1 B + c_3 B^3$). For the comparison refer to Fig. 4.19.

The transient state in fundamental ferroresonance and unsymmetrical state of ferroresonance have been investigated using numerical computing techniques.

Using the same analytical technique given in Chapter 4, the stability of the sustained subharmonic ferroresonance has been investigated in Chapter 5. It is observed that, although this analytical method is very good in explaining the stability of the phenomenon (see Figures 5.4, 5.5, 5.6 and 5.14) and the effect of the circuit resistance (see Figures 5.6, 5.10, 5.14), it does not produce very accurate results (see Figure 5.16). The reason for this lies in the estimation of the coefficients c_1 and c_3. Since they are obtained by selecting two points on the experimental magnetisation curve their values depend on the selection of these

two points. Table 5.1 shows how the variations in the coefficients affect the accuracy of the method.

The generalized parametric method established in Chapter 2 is applied to the transient and fundamental ferroresonance phenomena. But it has been noticed that the accuracy in the case of transient current calculation is better than that in the case of fundamental ferroresonance. For instance, in the calculation of the first few peak values of the transient current (see Table 3.5) the error between computed and experimental results is about 1%. But the error in fundamental ferroresonance calculation is about 30% (refer to page 76 and Figure 4.19), the reason being that the normalized B/H loop in Chapter 2 does not fit accurately the actual B/H loop. In spite of these disadvantages it provides us with a compact solution to the circuit and it makes it possible to draw a general conclusion about the response of the circuit to the change in parameters of the circuit (see Figures 3.23, 3.24, 4.21, 4.22).

6.2 Suggestions for Further Work

The analytical method for the calculation of the first peak value of the transient current established in Chapter 3 can be used to calculate further peak values at the various circuit and residual conditions. It can also be applied to three phase transformers. Thus, much computing time may be saved and more practical formulae may be obtained.

A computer programme for the Preisach model has been designed for the numerical calculations in the single phase system. By a little modification to this programme three phase systems could be investigated. Since it is possible to establish the

previous conditions of the iron core by Preisach model, the problem of initiating the subharmonic ferroresonance can be also investigated in detail.

The analytical method established for the fundamental and subharmonic ferroresonance is a general method. Therefore, this method of calculation can be used as a basis for the analytical calculations in three phase systems.

By the generalized parametric method the transient current, especially the first few peaks, can be predicted accurately. So, if there were ready-made tables or graphs the peak values of the transient current may be calculated without requiring any computer. The same purpose can be carried out for the ferroresonance phenomena.

All the calculations in this investigation require an experimental magnetisation curve and outermost loop. There is no problem in obtaining these characteristics in the case of small and medium size transformers. But in the case of large size transformer it may be impossible to get them. Therefore, if a relationship between the B/H characteristics of the material used in the construction of the transformer and the B/H characteristics of the transformer can be established then the problem mentioned above may be solved.

REFERENCES

1. Turner, H.M.: "Transient currents in transformers", Journal of the Franklin Institute, Jan. 1931, Vol.211, No.1, pp.1-33.

2. Blume, L.F., Camilli G., Farnham, S.B., Peterson, H.A.: "Transformer Magnetizing Inrush Currents and Influence on System Operation", AIEE Trans., 1944, Vol.63, pp.366-374.

3. Blume, L.F.: "Transformer Engineering", Wiley, New York, 2nd Edition,1951, pp.32-34.

4. Specht, T.R.: "Transformer Magnetizing Inrush Current", AIEE Trans., 1951, Vol.70, pp.323-327.

5. Holcomb, J.E.: "Distribution Transformer Magnetizing Inrush Current", AIEE Trans.,1961, Vol.80, pp.697-702.

6. Drozdov, A.D., et al "Methods of calculating the kick of Magnetizing Current of Large Transformers in Power Systems", 1968, Elektrichestvo, No.10, pp.72-76.

7. Malyshev, V.I.: "Determining the Maximum Inrush Current in the No-load Closure of a Transformer", 1968, Elektrichestvo, No.6, pp.16-18.

8. Sarkar, B.K. et al: "The Transient Analysis of the Single Phase Core Type Transformer", June 1976, The Matrix and Tensor Quarterly, pp.115-125.

9. Martienssen, O.: "Uber Neue Resonanzerscheinungen in Wechselstromkreisen", 1910, Phys.Zeit, Vol.11, pp.448-460.

10. Rouelle, E.: "Contribution à l'étude experimentale de la Ferrorésonance", Revue Generale de l'Electricité.

Part I, November 24, 1934 pp.715-741

December 1, 1934 pp.763-780

Part II, December 8, 1934 pp.785-819

December 15, 1934 pp.841-858

11. Duffing, G.: "Erzwungene Schwingungen bei veranderlicher Eigenfrequenzund ihne technisch Bedeuting", Sammlung Vieweg, Braunschweig, 1918.

12. Odessey, P.H., Weber, E,: "Critical Conditions in Ferroresonance", AIEE Trans.,1938, Vol.57, pp.444-452.

13. Thomson, W.T.: "Resonant Nonlinear Control Circuit", AIEE Trans., 1938, Vol.57, pp.469-477.

14. Rudenberg, R.: "Transient Performance of Electric Power Systems", 1950, McGraw-Hill, New York, pp.642-656.

15. Keller, E.G.: "Analytical Methods of Solving Discrete Nonlinear Problems in Electrical Engineering", AIEE Trans., 1941, Vol. 60, pp.1194-1199.

16. Keller, E.G.: "Resonance Theory of Series Non-linear Control Circuits", Journal of the Franklin Institute, May, 1938, Vol. 225, No.1349, pp.561-577.

17. Hayashi, C.: "Forced Oscillations with Nonlinear Restoring Force", Journal of Applied Physics, 1953, Vol.24, No.2, pp.198-207.

18. Hayashi, C.: "Stability Investigation of the Nonlinear Periodic Oscillations", Journal of Applied Physics, 1953, Vol. 24, No.3, pp.344-348.

19. Hayashi, C.: "Subharmonic Oscillations in Nonlinear Systems", Journal of Applied Physics, 1953, Vol.24, No.5, pp.521-528.

20. Hayashi, C.: "The Influence of Hysteresis on Nonlinear Resonance", Journal of the Franklin Institute, 1966, Vol.281, No.5, pp.379-386.

21. Ku,Y.H.: "Analysis of Nonlinear Coupled Circuits", AIEE Trans., January,1955, pp.626-631.

22. Ku, Y.H.: "Acceleration Plane Method for Analysis of a Circuit with Nonlinear Inductance and Nonlinear Capacitance", AIEE Trans., January,1955, pp.619-626.

23. Huey, R.M. et al: "Extension of the Duel-input Describing-function Technique to Systems containing Reactive Non-linearity", IEE Monograph No.383M, June,1960, pp.334-341.

24. Swift, G.W.: "An Analytical Approach to Ferroresonance", IEEE Trans., 1969, Vol. PAS-88, No.1, pp.42-45.

25. Swift, G.W.: "Transformer Core Simulation in Ferroresonance Studies", Ph.D.Thesis, Illinois Institute of Technology, June, 1968.

26. Kumar, A. et al: "Approach to the Problem of Ferroresonance in e.h.v. Systems", IEE Proc. 1972, Vol.119, No.6, pp.672-676.

27. Baycura, O.M., Donovan, J.C.: "An Unsymmetrical Mode of Ferroresonance", IEEE Trans.,1971, Vol.Mag-7, No.4, pp.890-895.

28. Pipes, L.A.: "The Reversion Method for Solving Nonlinear Differential Equations", Journal of Applied Physics, 1952, Vol. 23, No.2, pp.202-207.

29. Fallow, J.: "Sur un Demultiplicateur de Frequency Statique", Revue Generale de l'Electricité , 1926, No.19, pp.987-991.

30. Travis,I, Weygandt, C.N.: "Subharmonics in Circuits Containing Iron-cored Reactors", AIEE Trans.,1938, Vol.57, pp.423-431.

31. Angello, S.J.: "The Effect of Initial Conditions on Subharmonic Currents in a Nonlinear Series Circuit", AIEE Trans., 1962, Vol.61, pp.625-627.

32. Spitzer, C.F.: "Sustained Subharmonic Response in Nonlinear Series Circuits", Journal of Applied Physics,1945, Vol. 16, pp.105-111.

33. Wright, I.A., Morsztyn, K.: "Subharmonic Oscillations in Power Systems - Theory and Practice", IEEE Trans. 1970, Vol. PAS-89, pp.1805-1815.

34. Shenkman, L.Z.: "Subharmonic Oscillations in a Circuit with an Essentially Non-linear Inductance", Elektrichestvo,1967, No.10, pp.23-28.

35. Norimatsu, T.T., Uyeda, H.: "Subharmonic Ferroresonance in Coupling-capacitor Potential Device and Method of Prevention", AIEE Trans., June,1960, pp.264-271.

36. MacFadyen, W.K.: "Transient Currents in Nonlinear Electromagnetic Devices", Ph.D.Thesis, The University of Strathclyde, 1973.

37. Teape, J.W.: "Hysteresis Effects in Transformers", Ph.D.Thesis, The University of Strathclyde, 1976.

38. Yamashita, H. et al: "A Program to Analyse Transient Phenomena of Circuits including Precisely Represented Transformers", IEEE Trans., April, 1975, pp.1-9.

39. Germay, N. et al: "Review of Ferroresonance Phenomena in High Voltage Power System and Presentation of a Voltage Transformer Model for Predetermining Them", CIGRE, Paris, 1974, pp.33-

40. Chikazumi, S.: "Physics of Magnetism", J.Wiley & Sons, 1964.

41. Weiss Journal de Physique 6, 1907, pp.667.

42. Preisach, F.: "On Magnetic After Effect", Zeitschrift fur Physik, 1935, 94, No.5-6, pp.277.

43. Feldtkeller, R. et al: " Hysteresis in Soft Magnetic Materials", Etz-A, 1956, Vol.77, No.13, pp.497-502.

44. Girke, H. et al: "The Measurement of the Probability Distribution of Barkhausen jumps in a Ferromagnetic Material", Zeitschrift fur angewandte Physik, Vol.XI, No.9, 1957, pp.339-342.

45. Biorci, G., Pescetti, D.: "Analytical Theory of the Behaviour of Ferromagnetic Materials", II Nuovo Cimento, 1958, Vol.VII, No.6, pp.829-842.

46. Germay, N. et al: "A Study of Magnetic Hysteresis Cycles and their Application to Ferroresonance", Laborelec Report, IRSIA Convention, 1956, (1973 - 1974).

47. Coulson, M.A., Slater, R.D., Simpson, R.R.S.: "Representation of Magnetic Characteristic, including Hysteresis, using Preisach's Theory", IEE Proc., Oct.1977, Vol.124, No.6, pp.136-142.

48. Dunker, S.: "An Approximate Graphical Analysis of the Steady State Response of Nonlinear Networks", Philips Res. Rep.8, 1953, pp.133-147.

49. Cunningham, W.J.: "Introduction to Nonlinear Analysis", McGraw-Hill, New York, 1958.

50. Williams, P.W.: "Numerical Computation, 1972.

51. Brown, K.M.: "Approximate Solution of the Nonlinear Equations", Communications of the ACM, Vol.10, No.11, Nov.1967, p.728.

52. Hildebrand, B.F.: "Advanced Calculus for Applications", 1968.

ACKNOWLEDGMENTS

The author wishes to express his thanks to Professor D.J.Tedford for providing the facilities for undertaking the work.

Thanks are due to Dr.R.D.Slater and Dr.R.R.S.Simpson for their invaluable advice and criticism.

Thanks are gratefully expressed to Dr.W.S.Wood for his encouragement, supervision and kindness.

Thanks are also expressed to Dr.F.P.Flynn for help in trying to solve financial problems.

Appreciation is expressed to my colleagues in the department for help in computer programming.

The help of Miss J.Baird in typing the thesis is gratefully acknowledged.

The author is also grateful to staff of the Cumbernauld Town Centre Library for permission to use their library facilities during preparation of the manuscript of this work.

Special thanks to my wife for her continued patience, encouragement and understanding.

APPENDICES

APPENDIX A1

TRANSFORMER DESIGN DETAIL

Nominal Rating	:	500 V.A.
Voltage Ratio	:	240/125
Rated Frequency	:	50 Hz
Primary Turns	:	446
Secondary Turns	:	240
Stacking Factor	:	0.96

In Fig. 1.1

L_1	:	13.96 cm
L_2	:	7.605 cm
L_3	:	2.54 cm
L_4	:	5.08 cm
L_5	:	17.75 cm
L_6	:	16.5 cm
$L = 2 (L_1 + L_2)$	:	0.4059 m
A	:	24.774 cm^2
A_1	:	12.387 cm^2

MEASURED PARAMETERS

For 250 V winding:

Winding resistance	:	1.63Ω
Leakage inductance	:	4.4 mH

For 125 V winding:

Winding resistance	:	1.03Ω
Leakage inductance	:	1.27 mH
External primary resistance	:	0.58Ω
External primary inductance	:	1.38 mH
Impedance of switching angle selector	:	$0.03 + \frac{0.89}{\lvert i \rvert}$ Ω

COEFFICIENTS FOR THE REPRESENTATIONS

From experimental B/H characteristic

B_r = 0.958 T

B_s = 2.08 T

H_s = 14000 (A.T)/m

H_c = 45 (A.T)/m

μ_o = 7.5 E - 06

Coefficients for the exponential series representation

C_1 = 0.692 E + 00

C_2 = 0.210 E - 01

C_3 = 0.767 E + 00

C_4 = 0.358 E - 02

C_5 = 0.536 E + 00

C_6 = 0.233 E - 03

C_7 = 0.149 E - 01

C_8 = 0.752 E - 03

C_9 = 0.201 E + 01

Coefficients for the loop representation

C_1 =	0.311	C_4 =	0.00296	C_7 =	0.0543	C_{10} =	0.26
C_2 =	C_1	C_5 =	0.0296	C_8 =	0.00543	C_{11} =	0.000267
C_3 =	0.619	C_6 =	0.320	C_9 =	0.513	C_{12} =	0.532

Coefficients for the cubical polynomial i = f (Ψ)

C_1 = 0.0248 C_3 = 1.212

APPENDIX 2

DETERMINATION OF THE COEFFICIENTS FOR THE EXPONENTIAL SERIES REPRESENTATION

In order to evaluate the coefficients in Equation 1.17 the iteration method is employed.

Since each term has two coefficients there are altogether six unknown coefficients for three terms exponential series. So it is necessary to select six points from the experimental curve.

Now, let two points (B_1,H_1) and (B_2,H_2) be considered. Subtracting the contribution of the linear term $(\mu_o H)$ from each point so that

$$B_{m1} = B_1 - \mu_o.H_1$$

$$B_{m2} = B_2 - \mu_o.H_2$$

and equating these modified Bs to the first term of the series

$$B_{m1} = c_1 (1 - \exp(-c_2.H_1))$$

$$B_{m2} = c_2 (1 - \exp(-c_3.H_2))$$

the following ratio is found

$$Y = \frac{B_{m1}}{B_{m2}} = \frac{(1 - \exp(-c_2.H_1))}{(1 - \exp(-c_2.H_2))}$$

Since the value of Y is known we can find the coefficient c_2 using the Newton-Raphson's method. Then, substituting c_2 into the expression of B_{m1} or B_{m2} c_1 is calculated. Thus, the first term is defined but it satisfies only the points (B_1,H_1) as shown in Fig.3.1.

To improve the fitting a second exponential term is added to the first one. Therefore, another two points (B_3, H_3) and (B_4, H_4) on the experimental curve are selected.

Hence, the modified B's

$$B_{m3} = B_3 - \mu_o.H_3$$

$$B_{m4} = B_4 - \mu_o.H_4$$

Let the equations

$$DB_{m3} = B_{m3} - c_1.\ (1 - \exp(-c_2.H_3))$$

$$DB_{m4} = B_{m4} - c_1.\ (1 - \exp(-c_2.H_4))$$

equate to

$$DB_{m3} = c_3.\ (1 - \exp(-c_4.\ H_3))$$

$$DB_{m4} = c_3.\ (1 - \exp(-c_4.\ H_4))$$

So the ratio function is

$$Y = \frac{DB_{m3}}{DB_{m4}} = \frac{(1 - \exp(-c_4.H_3))}{(1 - \exp(-c_4.H_4))}$$

Since c_1, c_2 are already known, B_{m3}, B_{m4}, DB_{m3}, DB_{m4} and Y can easily be calculated. Then from the last relation c_4 is solved and substituting this into the expression of DB_{m3} or DB_{m4} c_3 is found.

It is seen that the fitted curve obtained using two exponential series satisfies the points (B_3,H_3) and (B_4,H_4) perfectly but lies below the points (B_5,H_5), (B_6,H_6) and above the points (B_1,H_1), (B_2,H_2) as shown in the second figure of Figure 3.1.

The addition of the third exponential term also requires two experimental points for the definition of its coefficients c_5, c_6. So, selecting the points (B_5,H_5) and (B_6,H_6), following the above procedure

$$Y = \frac{(1 - \exp(-c_6.H_5))}{(1 - \exp(-c_6.H_6))}$$

Thus c_6 and c_5 are found. But this time, this series composed of three terms perfectly fits at the points (B_5,H_5) and (B_6,H_6) but lies above the other points. In order to get an accurate representation an iteration loop consisting of three steps is constructed.

A. <u>First step</u>

From the above initial approximation c_3, c_4, c_5 and c_6

are known. So, an improved estimation for c_1, c_2 can be made in this step so that

$$DB_{m1} = B_{m1} - c_3.(1 - \exp(-c_4.H_1)) - c_5.(1 - \exp(-c_6.H_1))$$

$$DB_{m2} = B_{m2} - c_3.(1 - \exp(-c_4.H_2)) - c_5.(1 - \exp(-c_6.H_2))$$

also

$$DB_{m1} = c_1.(1 - \exp(-c_2.H_1))$$

$$DB_{m2} = c_1.(1 - \exp(-c_2.H_2))$$

hence

$$Y = \frac{DB_{m1}}{DB_{m2}} = \frac{(1 - \exp(-c_2.H_1))}{(1 - \exp(-c_2.H_2))} .$$

Thus new values of c_1 and c_2 are defined.

B. Second step

Using new c_1, c_2 and approximate values of c_5, c_6

$$DB_{m3} = B_{m3} - c_1.(1 - \exp(-c_2.H_3)) - c_5.(1 - \exp(-c_6.H_3))$$

$$DB_{m4} = B_{m4} - c_1.(1 - \exp(-c_2.H_4)) - c_5.(1 - \exp(-c_6.H_4))$$

and equating these to

$$DB_{m3} = c_3.(1 - \exp(-c_4.H_3))$$

$$DB_{m4} = c_3.(1 - \exp(-c_4.H_4))$$

and solving the ratio function

$$Y = \frac{DB_{m3}}{DB_{m4}} = \frac{(1 - \exp(-c_4.H_3))}{(1 - \exp(-c_4.H_4))}$$

The improved values of c_3 and c_4 are obtained.

C. Third step

For the improved values of c_5, c_6 the new values of c_1, c_2, c_3, and c_4 are substituted in the following equations.

$$DB_{m5} = B_{m5} - c_1.(1 - \exp(-c_2.H_5)) - c_3.(1 - \exp(-c_4.H_5))$$

$$DB_{m6} = B_{m6} - c_1.(1 - \exp(-c_2.H_6)) - c_3.(1 - \exp(-c_4.H_6))$$

$$DB_{m5} = c_5 . (1 - \exp(-c_6 . H_5))$$

$$DB_{m6} = c_5 . (1 - \exp(-c_6 . H_6))$$

$$Y = \frac{DB_{m5}}{DB_{m6}} = \frac{(1 - \exp(-c_6 . H_5))}{(1 - \exp(-c_6 . H_6))}$$

If these relations are solved for c_5 and c_6 the first iteration loop is completed.

The iteration is repeated over these three steps until the error on the six points reaches an acceptable level.

It is very important to point out that under certain circumstances the initial approximations to the coefficients could result in the expression of DB_m being negative and this causes an unstable solution, but this is overcome by using the absolute values of DB_m's.

The other important points which must be observed when a program is made are:

A) The first point to be selected must be the point (H_1, B_1) defined as in Figure 3.2.a. Otherwise, if it is selected arbitrarily the difference curve may have the form as in Figure 3.2.b which is difficult to represent.

B) The sixth point to be selected must be the real saturation point (B_s, H_s) at which the straight line section of the B/H characteristic starts. If the point below the saturation point is selected, the fitted curve will always be below the experimental curve.

C) Since the Newton-Raphson method is used to solve nonlinear equations the initial values must exist. It is observed by trial and error that

$$C_{20} = \frac{5}{H_2} \quad , \qquad C_{40} = \frac{5}{H_4} \quad , \qquad C_{60} = \frac{5}{H_6}$$

give a reasonable result (where H_2, H_4 and H_6 are the abscissa of the selected points). These are the maximum values for these coefficients. If the solution in any iteration section is divergent then the initial value of the section is made small. So a convergent solution is approached.

D) If the solution is still divergent the selected points for this section should be made closer to each other.

In order to define the coefficients of Equation 1.18 the difference curve $\Delta B(H)$ in Figure 3.3 is analysed. As it is noticed, this curve has a maxima at $H = H_m$, it is zero at the origin and tends to zero at $H = H_1$. Using these facts we derive the relation

$$\left.\frac{d\ (\Delta B)}{dH}\right|_{H = H_m} = 0$$

hence

$$c_8 = \frac{1}{c_9 \cdot H_m c_9} \quad .$$

Taking two points from the difference - data points substituting into the expression of ΔB, c_7, c_8 and c_9 are evaluated.

APPENDIX A3

PREISACH THEORY FUNDAMENTALS

According to the general magnetic material theory the induction (the magnetic flux density) in the magnetic material is expressed by

$$\vec{B} = \mu \vec{H}$$

This expression is extended in terms of magnetic polarization (or magnetisation) so that

$$\vec{B} = \mu_o \vec{H} + \mu_o \vec{I}$$

where μ_o is the permeability of the air.

If either the relative permeability μ_r or differential permeability μ is known the magnetisation is

$$\vec{I} = (\mu_r - 1). \vec{H}$$

where

$$\mu = \mu_o . \mu_r .$$

This additional induction $\mu_o \vec{I}$ is just due to all the small magnetic dipoles supposed to exist in the magnetic material[40]. In practice neither $\vec{I}$ nor μ are known because both of them are the function of the field strength H. Therefore a number of theories have been developed to explain the behaviour of the dipoles under the field applied and to establish an analytical relation between $\vec{I}$ and $\vec{H}$.

In 1907 Weiss[41] suggested that each magnetic material consists of elementary domains in which $\vec{I}$ is uniform in direction and size, its absolute value being equal everywhere to an upper limit called the saturating magnetisation I_s. The direction of the

magnetisation is different from one domain to the next but it is distributed statistically as illustrated in the following figure.

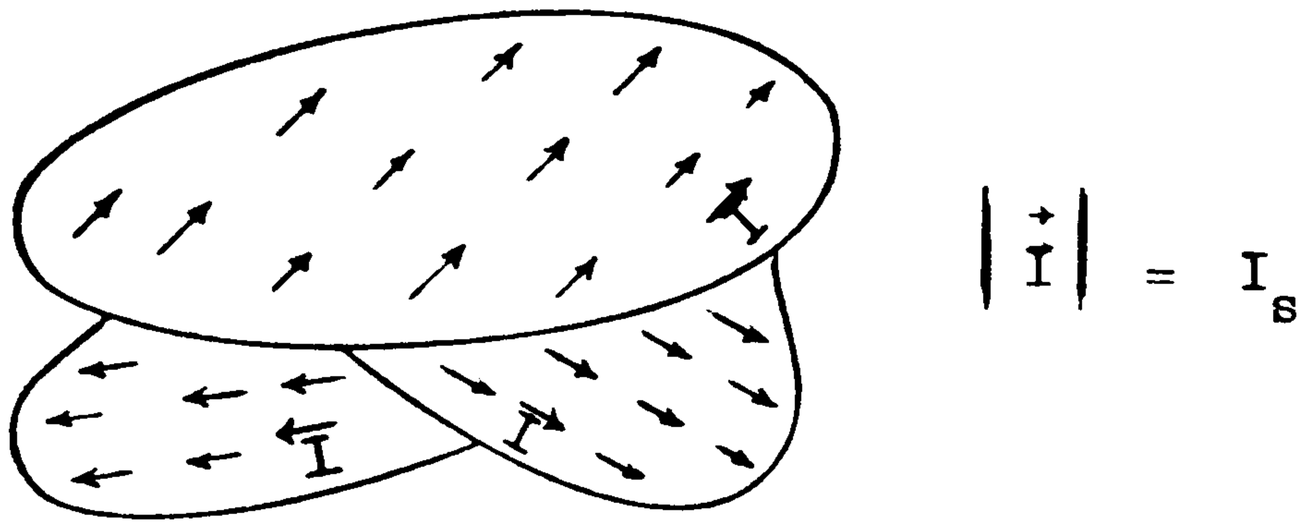

Fig. A3.1

If there is no external field ($\vec{H} = 0$) applied to the material, the resultant magnetisation will be zero. Figure A3.2 shows two adjacent Weiss domains taken from a uniform medium.

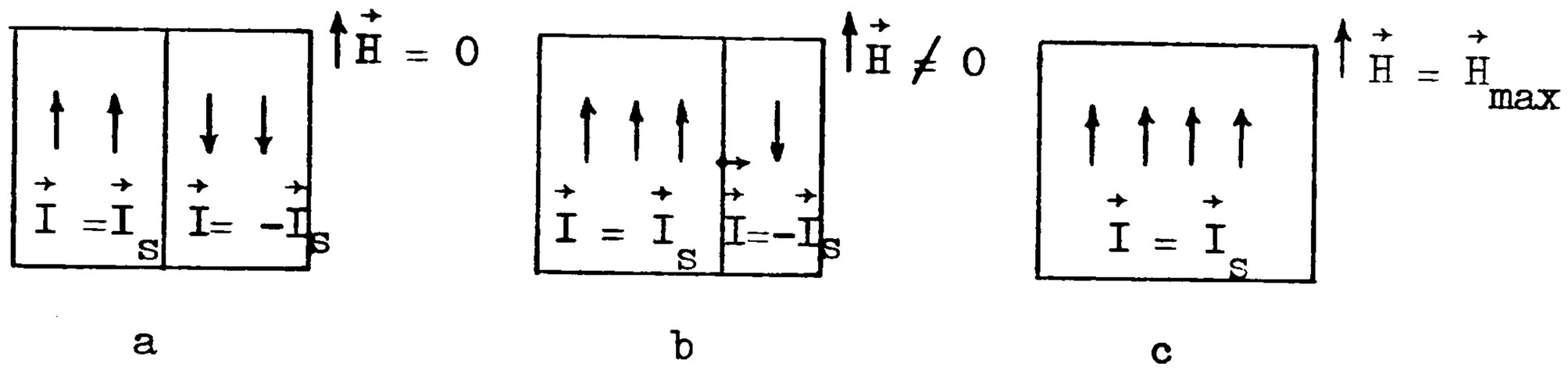

Fig. A3.2

Now, if a field H is applied to this sample the wall between two domains will move and if H is continually increased a value will be reached at which the material completely consists of a monodomain containing only unique directed dipoles as in Figure A3.2c.

The displacement of the wall changes direction when $\vec{H}$ decreases and reverses, i.e. it is possible to recreate the inverse Weiss domains but, according to this theory, the inverse field must be greater than a critical threshold H_t to change the direction of $\vec{I}$.

This characteristic thus gives the "Remanent Magnetisation" (see the figure below).

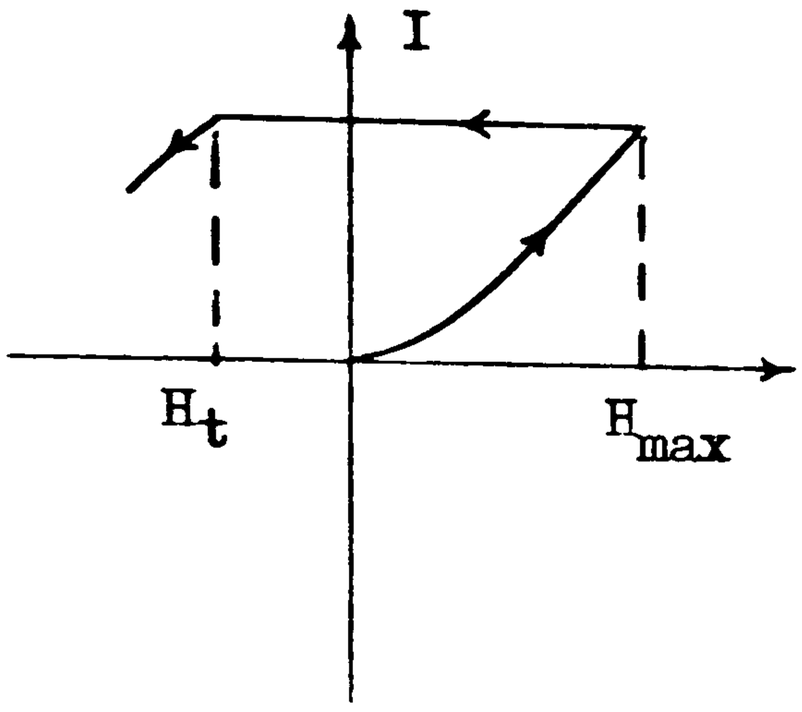

Fig. A3.3

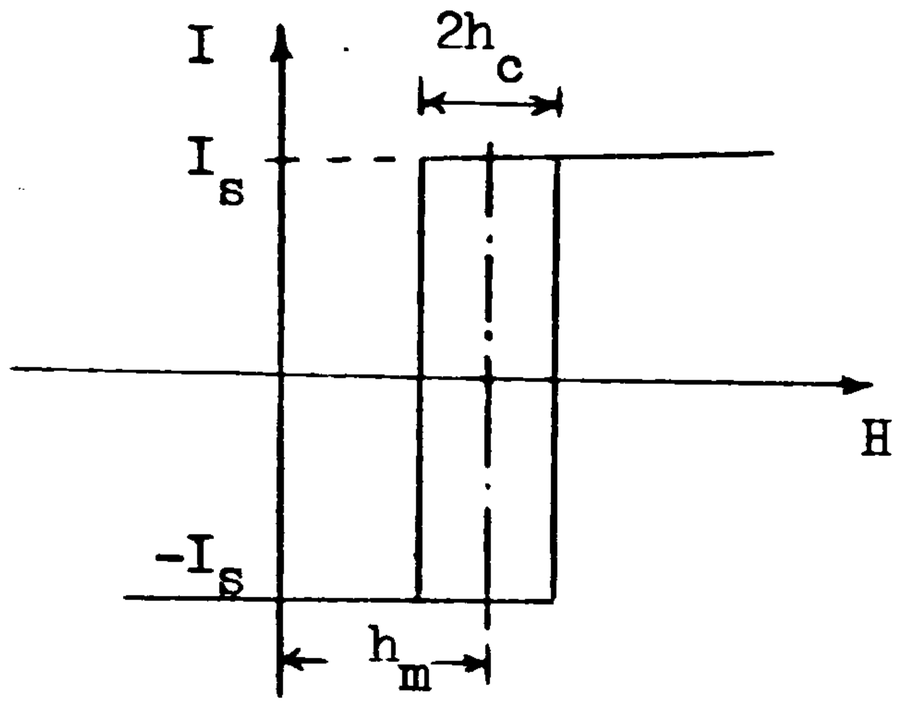

Fig. A3.4

Preisach[42] studied the interaction of the two elementary adjacent dipoles and gave a model representing the effects of all other dipoles, and of the external field on the given dipole.

In this model Preisach assumed that each dipole corresponds to one rectangular hysteresis loop as shown in Figure A3.4, having two parameters, one of which, h_c, represents coercivity and the other, h_m, represnts the field of neighbouring dipoles. So, from Figure A3.4 it is easily seen that the applied field H must be greater than the threshold value $(h_m + h_c)$ to be in state of positive magnetisation + I_s or must be less than the other threshold value $(h_m - h_c)$. For a value of H between $(h_m - h_c)$ and $(h_m + h_c)$ the dipole is either in the state of + I_s or - I_s, i.e. the state of dipole depends on its initial state. For this reason Preisach made another assumption to make clear the initial state of the dipoles so that all the dipoles characterized by $h_m > H$ have been left in the state (- I_s) and all the dipoles $h_m < H$ have been left in the state (+ I_s) by demagnetisation. By this assumption, in the h_m/h_c plane

(Preisach Diagram) all the dipoles having + I_s lie on the quadrant $h_c > 0$, $h_m > 0$ and all the other dipoles having - I_s on the quadrant $h_c > 0$, $h_m > 0$ as in Figure A3.5.

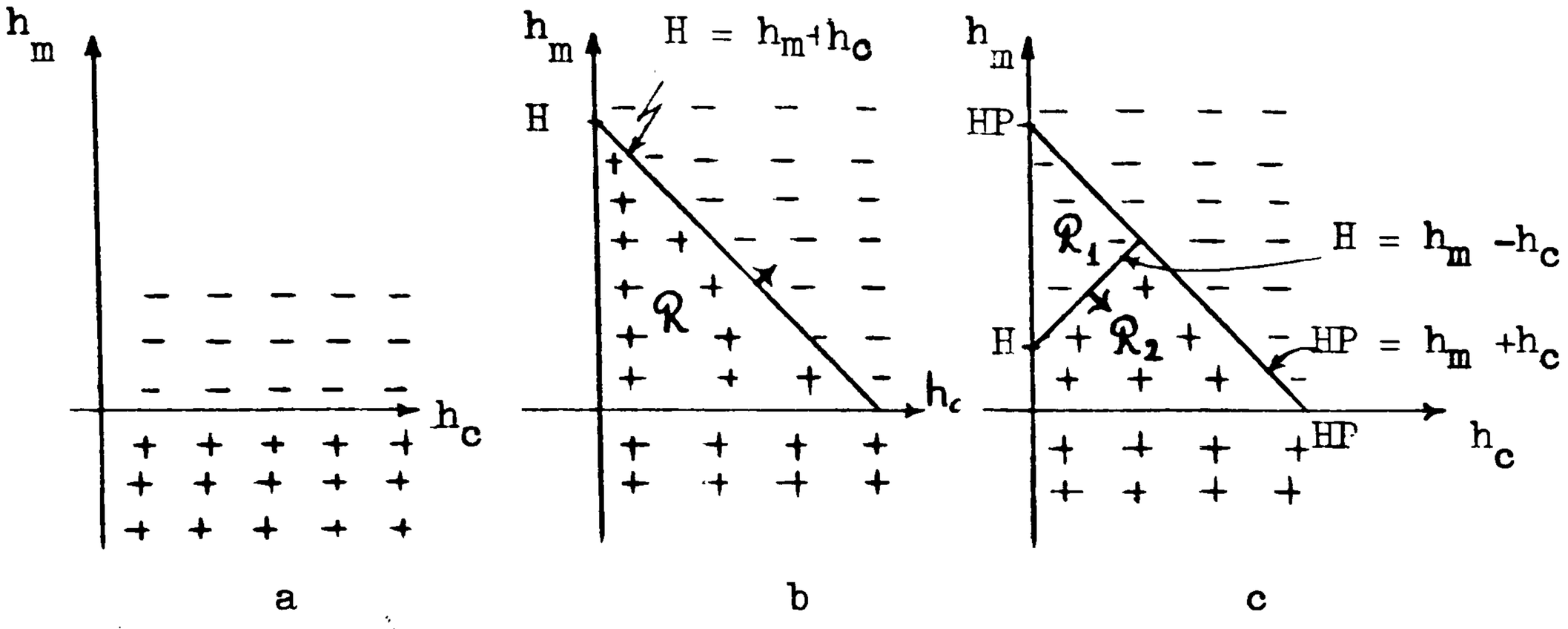

Fig. A3.5

Now, application of an increasing field to this sample will cause a change in the state of the dipoles in the first quadrant. At this point, a question arises. How many dipoles have changed their state? So, to find out the number of dipoles changing state under the field

$$H = h_m + h_c$$

Preisach gives the following definition for the number of dipoles

$$dn = \gamma (h_m, h_c)\, dh_m\, dh_c$$

Hence the individual magnetisation

$$I = \int_R I_s \cdot dn = I_s \int_R \gamma (h_m, h_c)\, dh_m\, dh_c$$

But the resultant magnetisation (under the field there are two dipoles having the same direction)

$$I = 2\, I_s \int_R \gamma (h_m, h_c)\, dh_m\, dh_c \qquad \text{A3.1}$$

Where

dn: number of dipoles per unit volume of material

$\gamma\ (h_m, h_c)$: distribution function of dipoles

R : Integration region (in this case the area of the triangle in Figure A3.5b)

If H reverses there will be a decrease in the number of dipoles which are in '+' and in the first quadrant.

Since we are concerned with the number of dipoles whose states differ from their original states, the region R_2 in Figure A3.5c is taken for the integration. However, as will be explained later, R_1 will be taken for the sake of the simplicity in calculation.

In the application of this theory to power engineering studies the magnetisation I is not very meaningful so without affecting the principal idea Equation A3.1 may be written in terms of induction so that

$$B_s = \mu_o I_s$$

Hence

$$B = \mu_o H + \mu_o I$$

becomes

$$B = \mu_o H + 2 B_s \int_R \gamma\ (h_m, h_c)\ dh_c\ dh_m \qquad A3.2$$

Some Characteristic Features of the Preisach Theory

Although the Preisach theory is more complicated than other methods used to represent the B/H characteristic, it gives a number of important properties of hysteresis cycles. These are:

A. Occurence of the Cross-Overs in the B/H Plane

As it apparently occurs in inrush current cases, sometimes the B/H trajectory crosses the previous trajectory. Whereas the other methods of the representation are not able to give an explanation of this fact, the Preisach model explains it.

In order to present this explanation, let us consider the B/H characteristic and corresponding Preisach diagram shown in the following Figure A3.6.

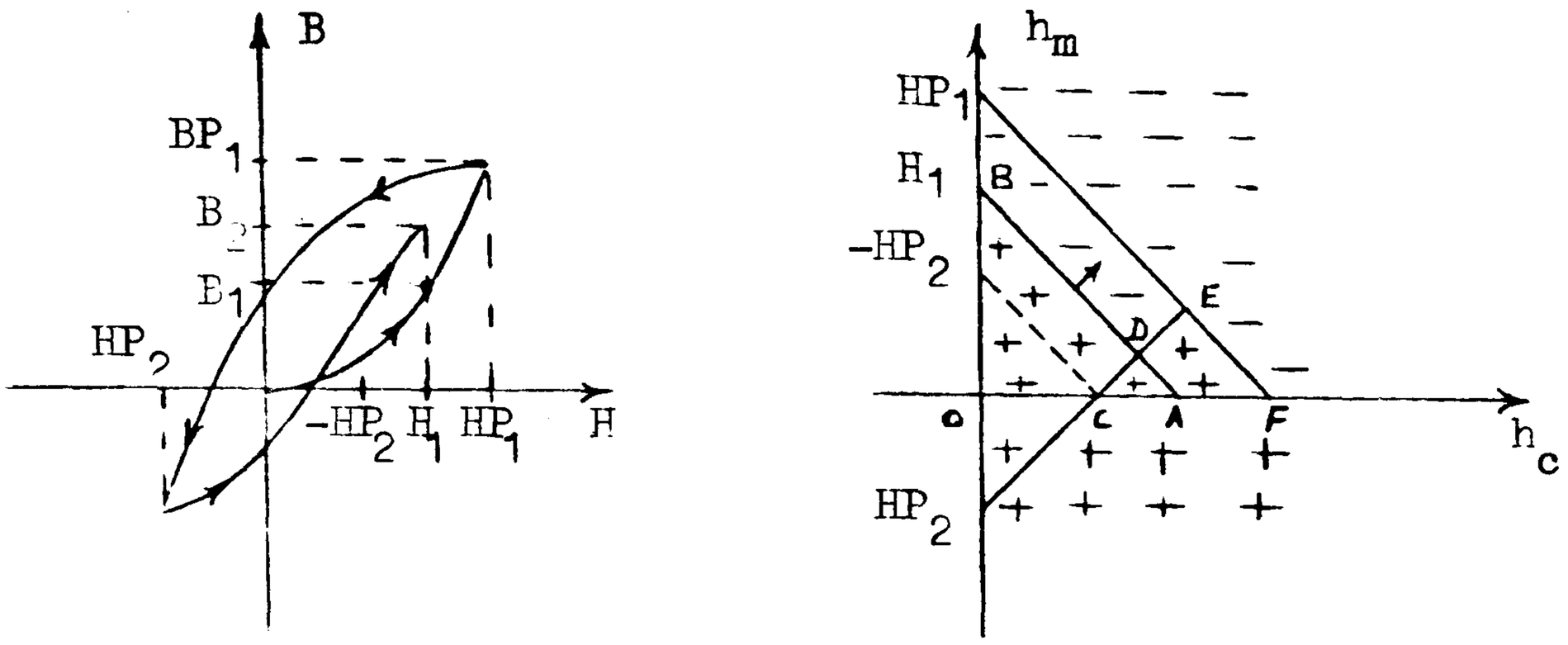

Fig. A3.6

For the point $H = H_1$, as will be seen from B/H plane, the value of the induction B_2 is greater than the previous one, B_1. That means the trajectory now being considered crosses over the previous trajectory. Now if the corresponding Preisach diagram is examined it is noticed that at $H = H_1$, the integration region of the distribution function is BOAB for B_1 and BOAB plus ADEFA for B_2. That means the integration region for B_2 is greater than that for B_1. Consequently the integration of the distribution function over the greater region yields a greater value, greater induction.

B. Minor Loops

In the case of steady-state subharmonic resonance and unsymmetrical ferroresonance phenomenon, some minor loops appear. The figure A3.7 shows such a loop and corresponding Preisach diagram.

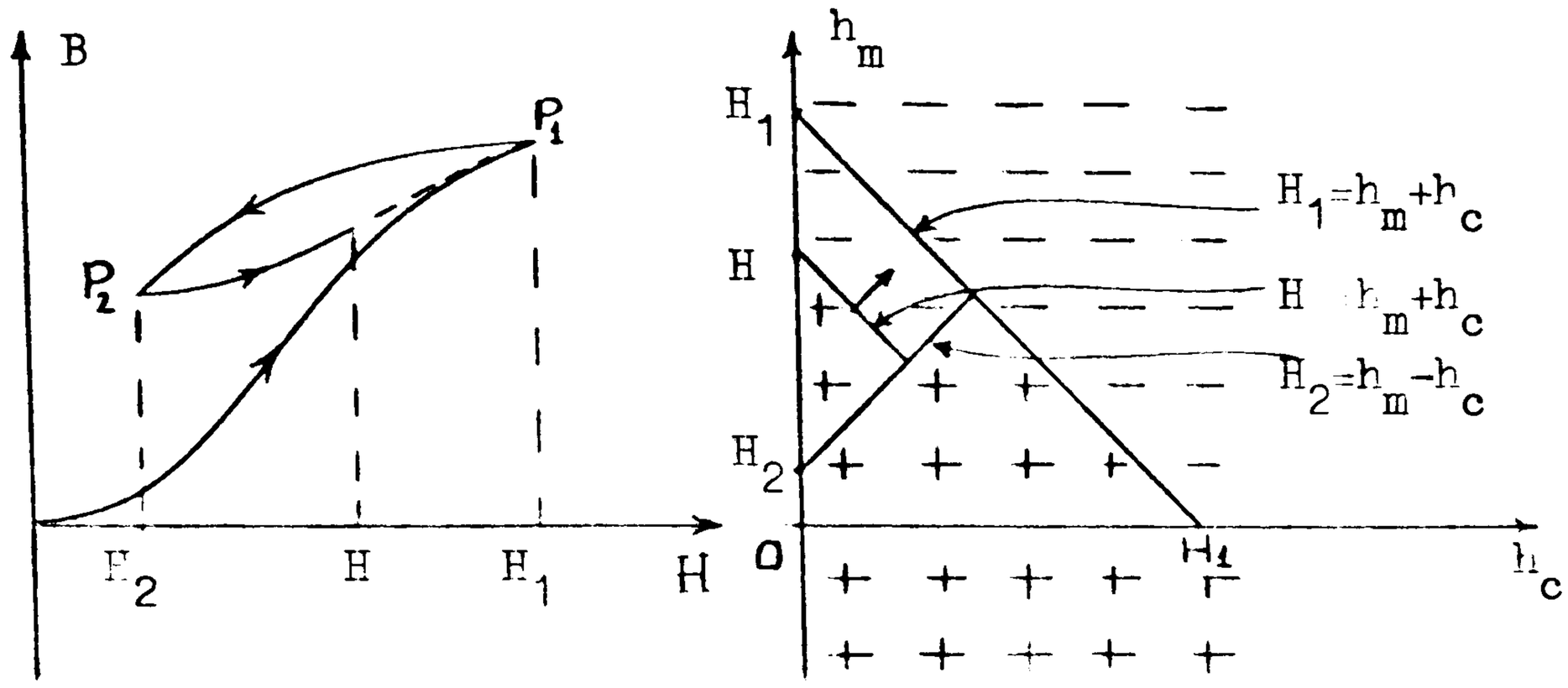

Fig. A3.7

If H is increased starting from P_2 the trajectory returns to the point P_1 when $H = H_1$. On the Preisach diagram it is also observed that when $H = H_1$ the line $H = h_m + h_c$ coincides with the line $H_1 = h_m + h_c$. That is to say, the inner diagram (see the Figure above) corresponding to the minor loop, closes.

If H is still rising the line $H = h_m + h_c$ continues moving up.

C. Return to the Magnetisation Curve

At the jumping condition, after a transient state, the current takes its steady-state value. During this transient the second peak of the current is much bigger than the first peak which is the largest previous peak and corresponding B, H are on the magnetisation curve. It is possible to prove this situation by constructing the Preisach diagrams given in Figure A3.8

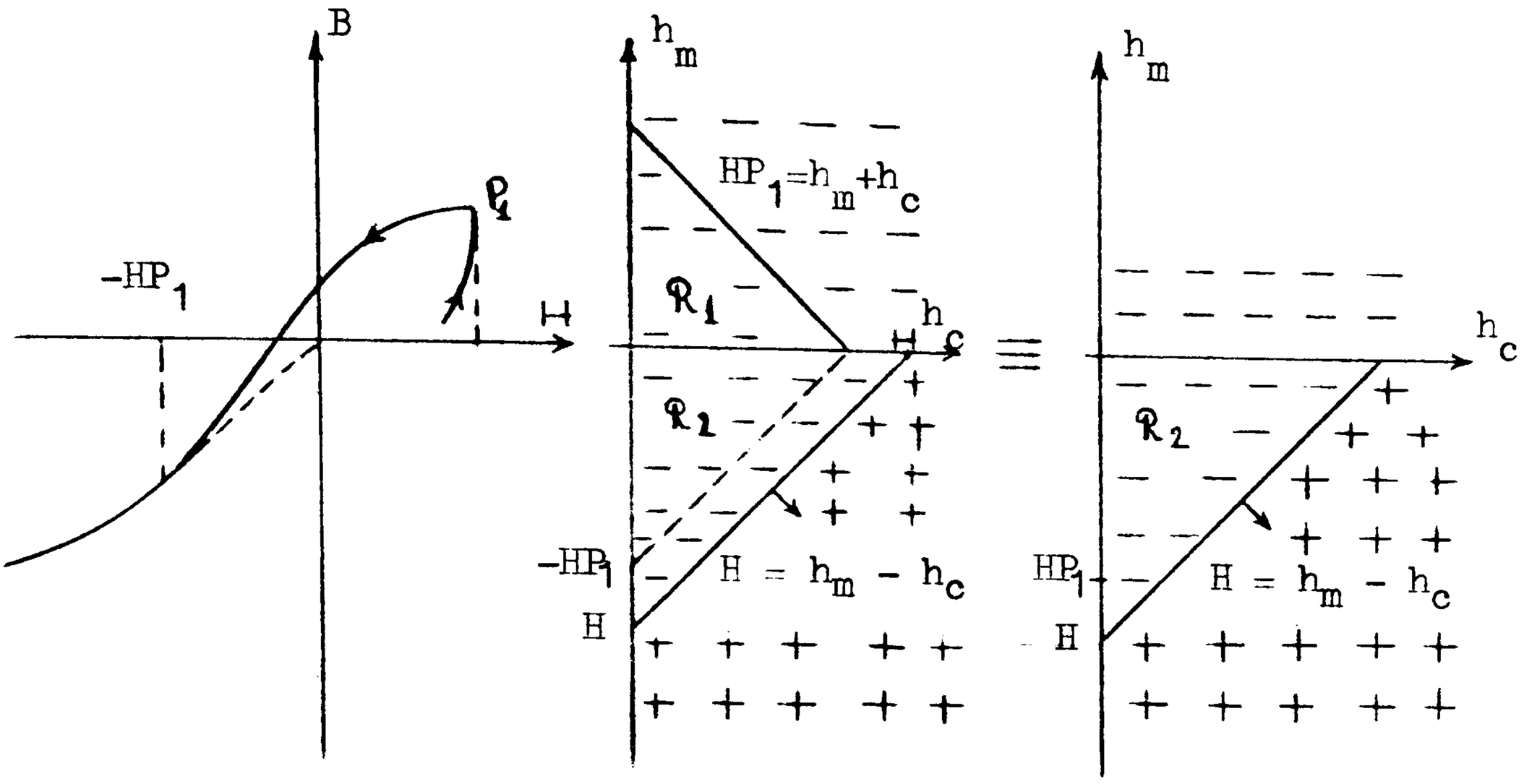

Fig. A3.8

Since for $H = -HP_1$ (HP_1 is the largest previous peak) all the dipoles lying on the region R_1 under the line $HP_1 = h_m + h_c$ will return to their original state (to -'ve state) and all the dipoles lying on the region R_2 above the line $H = h_m - h_c$ will change state (to -'ve state from + 've). The diagram, then, is equivalent to the third in Figure A3.8, which is given for the magnetisation characteristic.

1.3.5.2 Representation of The Distribution Function

The basic problem in the Preisach theory is to find out a proper distribution function γ which characterizes the magnetic material.

Felltkeller et al[43] used the analytical expression.

$$\gamma(h_m, h_c) = \exp\left(-\left(\left(\frac{h_m}{a}\right)^2 + \left(\frac{h_c}{b}\right)^2\right)\right)$$

where a, b are constants to be determined.

They noticed that this expression has two maxima for the soft material. But Girke et al[44] experimentally showed that some

soft material has one or two maxima.

Introducing new variables

$$H_1 = h_m - h_c \quad .$$

$$H_2 = h_m + h_c$$

which are independent from each other, a new distribution function

$$\bar{\gamma}\ (H_1, H_2) \;=\; \gamma\ (\frac{H_1 + H_2}{2} \;,\; \frac{H - H_1}{2})$$

is obtained. Biorci and Pescetti[45] separate this new function into independent functions with one variable so that

$$\bar{\gamma} \quad (H_1, H_2) \;=\; \bar{\gamma}_1\ (H_1)\ .\ \bar{\gamma}_2\ (H_2)$$

So, for the magnetisation curve

$$\frac{d\ B_2}{d\ H_2} \;=\; \bar{\gamma}_2\ (H_2)\ .\ \int_{H_{1max}}^{H_{1min}} \bar{\gamma}_1\ (H_1)\ .\ dH_1$$

and for the branch of the outermost loop descending from H_s to $-H_s$ (see following Figure 1.17)

$$\frac{d\ B_1}{d\ H_1} \;=\; \bar{\gamma}_1\ (H_1) \int_{H_{2min}}^{H_s} \bar{\gamma}_2\ (H_2)\ d\ H_2$$

By the small variations ΔH_1, ΔH_2, ΔB_1, ΔB_2 the above integro-differential equations are replaced by sums since $\bar{\gamma}_1$ and $\bar{\gamma}_2$ are assumed to be constant within each interval.

Germay et al[46] solve these integro-differential equations for $\bar{\gamma}_1$ and $\bar{\gamma}_2$ by substituting ΔH_1, ΔH_2, ΔB_1 and ΔB_2 obtained from the experimental outermost loop as illustrated in Figure A3.9.

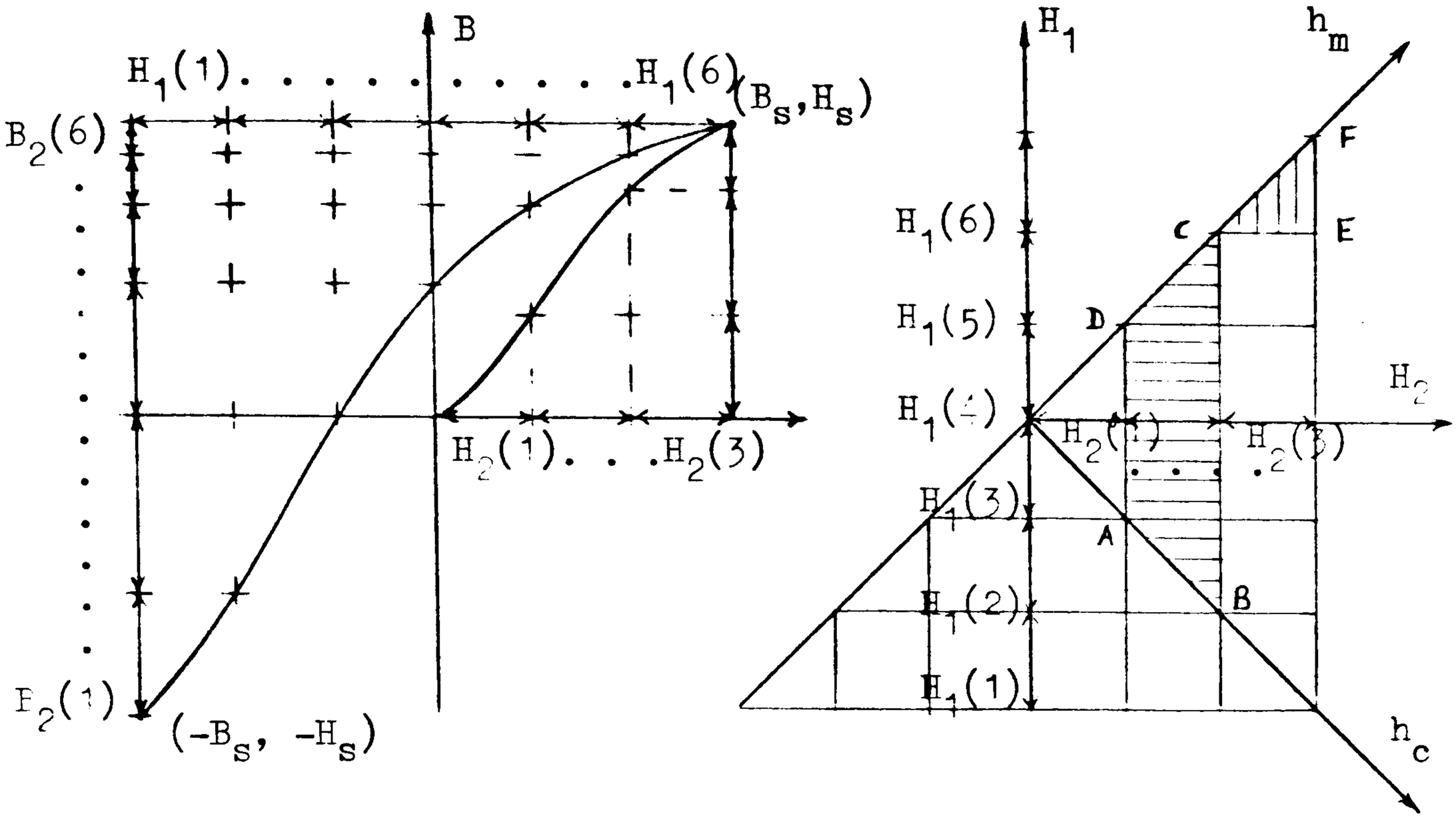

Fig. A3.9

For the example in Figure A3.9 in the shaded area ABCDA H_2 and corresponding $\bar{\gamma}_2$ do not change. Thus, the corresponding incremental induction

$$\Delta B_2(2) = \Delta H_2(2)\bar{\gamma}_2(2)\left[\frac{1}{2}\Delta H_1(2)\bar{\gamma}_1(2)+\Delta H_1(3)\bar{\gamma}_1(3)+\Delta H_1(4)\bar{\gamma}_1(4)+\frac{1}{2}\Delta H_1(5)\bar{\gamma}_1(5)\right]$$

and in the shaded area CDFC ΔH_1, $\bar{\gamma}_1$ are constant, so

$$\Delta B_1(6) = \Delta H_1(6).\ \bar{\gamma}_1(6)\ \ (\tfrac{1}{2}\ \Delta H_2(3)\ \ \bar{\gamma}_2\ (3))$$

Thus, numerical γ functions are derived directly from the magnetisation curve and descending branch of the loop. By the γ functions, curve and loop are reconstructed.

Coulson[47] has given the following expression for γ

$$2B_s.\gamma(h_m,h_c) = \sum_{i=1}^{m} c_{1i}c_{2i}c_{3i}\ \frac{(c_{1i}h_c)^n}{n!}\ .\ \exp(-c_{1i}.h_c).\exp(-c_{2i}\,|h_m|)$$

where m : number of terms to be used

n, c_{1i}, c_{2i}, c_{3i}: coefficients

In this present investigation the first four terms of Coulson's expression have been employed to calculate the flux density and differential permeability by Preisach theory.

The terms are:

<u>First Term (n = 12)</u>: In this term $c_1 = c_2$ is taken to simplify the estimation of the coefficients. So the first term

$$c_1^{\,2}\, c_3\, \frac{(c_1 h_c)^{12}}{12!}\, \exp(-c_1 h_c)\, \exp(-c_1 . |h_m|)$$

<u>Second Term (n = 0)</u>:

$$c_4\, c_5\, c_6\, \exp(-c_4 h_c).\, \exp(-c_5 |h_m|)$$

<u>Third Term (n = 0)</u>

$$c_7\, c_8\, c_9\, \exp(-c_7 h_c).\, \exp(-c_8 |h_m|)$$

<u>Fourth Term (n = 0)</u>

$$c_{10}\, c_{11}\, c_{12}\, \exp(-c_{10} h_c)\, .\, \exp(-c_{11} |h_m|)$$

The Calculation of the Flux Density and Differential Permeability by Preisach Theory

Analysis of the Preisach diagrams in Figure 3.4 suggests that there are mainly two types of diagrams. But, since Coulson[47] uses the absolute value of h_m he gives three types of diagram as shown in Figure 3.5

In the case of transient current or occurrence of minor loops there are another two abnormal B/H characteristics, so another two Preisach diagrams,as in Figure 3.6.

All the available Preisach diagrams are given in Figure 3.7

An interesting property of this theory is that there is no need to take very complicated forms of integration region such as R in the first figure of Figure 3.8, so long as the values of H and

B corresponding to the Preisach diagrams already completed, are stored. In fact, this is the reason for dividing the actual Preisach diagrams into the subdiagrams. For instance, in the first figure of Figure 3.8 the flux density B corresponds to the integration of the distribution function over the region R. But, if B_1 is stored, B is equal to

$$B = B_1 - \Delta B$$

where ΔB will be called the "Complementary function" because the corresponding region R_2 is the complement of R. So the integration region R_2, which has a considerably simple form compared to R, is taken.

Generalizing the idea of subdividing the diagrams, the general form of complementary function becomes

$$\Delta B = 2.B_s \int_{R_n} \gamma(h_c, h_m) \cdot dh_c \, dh_m$$

and resultant induction

$$B = \mu_o H + \sum_{i=1}^{n} (DIR \cdot B_i) + DIR. \Delta B$$

where

n: Number of previous peak

DIR: Direction of the trajectory which is + 've for the rising trajectory and - 've for the descending trajectory.

B_i: Already stored values being measured from peak to peak.

ΔB: Present value of B being measured from last peak to the point being calculated

R_n's have the form of one of those given in Figure 3.7

This formulation will be used in the programme for the calculation of the flux density.

Derivation of the First Function - ΔB_1 (H)

If the magnetic material to be used previously has no residual flux density when a field is applied, the Preisach diagrams will be as in Figure 3.5a and the complementary function required can be derived taking the integration over the shaded area. So within the limits

$$0 \leq h_m \leq H - h_c$$

$$0 \leq h_c \leq H$$

by the integration of the distribution function for the first term

$$(n = 12, \quad c_1 = c_2)$$

$$\Delta B_{11} = c_3 \, f_{n+1} \, (c_1 . H)$$

where

$$f_n (X) = (1 - \exp(-X) . \sum_{i=1}^{n} \frac{X^i}{i!})$$

and for the second term (n = 0)

$$\Delta B_{12} = c_6 \left[1 + \frac{c_5}{c_4 - c_5} \exp(-c_4 . H) - \frac{c_4}{c_4 - c_5} \exp(-c_5 . H)\right]$$

The third and fourth terms are similar to ΔB_{12} but only the coefficients are different. So the resultant complementary function

$$\Delta B_1(H) = \Delta B_{11} + \Delta B_{12} + \Delta B_{13} + \Delta B_{14}$$

Derivation of the Second Function - ΔB_2 (H,HP)

Figure 3.5b shows a portion of the B-H trajectory which is rising from a previous peak point (HP, BP), and the corresponding Preisach diagram. As specified in the figure, the boundaries of the integration are

$$HP + h_c \leq h_m \leq H - h_c$$

$$0 \leq h_c \leq \frac{H - HP}{2}$$

Hence

$$\Delta B_{21} = \frac{c_3}{2^{n+1}} \cdot \exp(c_1 H) \cdot f_{n+1}(c_1 \cdot (H - HP))$$

for the first term (n=12) and

$$\Delta B_{22} = c_6 \left[\frac{c_4}{c_4+c_5} \cdot \exp(c_5 H) - \frac{c_4}{c_4-c_5} \cdot \exp(c_5 HP) + \frac{2\, c_4 c_5}{c_4^2-c_5^2} \cdot \exp\left((c_4+c_5) \cdot \frac{HP}{2} - (c_4-c_5) \frac{H}{2} \right) \right]$$

for the second term.

Since the third and fourth terms are similar to the second term, the resultant function

$$\Delta B_2 (H, HP) = \Delta B_{21} + \Delta B_{22} + \Delta B_{23} + \Delta B_{24}$$

It must be remembered that this function is valid for only

$$HP \leq H \leq 0$$

Derivation of the Third Function - $\Delta B_3 (H, HP)$

This function also has a previous peak value and the integration region is the same as B_2, but it is valid, as shown in Figure 3.5c, for only

$$HP \leq 0$$

$$0 \leq H \leq -HP$$

Thus, the first term (n = 12)

$$\Delta B_{31} = c_3 \left[2 \cdot f_n (c_1 H) - \frac{(c_1 H)^{n+1}}{(n+1)!} \cdot \exp(-c_1 H) + \frac{\exp(c_1 H)}{2^{n+1}} \left(f_{n+1}(c_1 (H-HP)) - f_n (2 c_1 H) \right) \right]$$

and the second term (n=0)

$$\Delta B_{32} = c_6 \left[2 + \frac{2\, c_5^2}{c_4^2 - c_5^2} \exp(-c_4 H) - \frac{c_4}{c_4 - c_5} (\exp(-c_5 H) + \exp(c_5 HP)) + \frac{2\, c_4 c_5}{c_4^2 - c_5^2} \exp\left((c_4+c_5) \frac{HP}{2} - (c_4 - c_5) \frac{H}{2} \right) \right]$$

The resultant function becomes

$$\Delta B_3 (H, HP) = \Delta B_{31} + \Delta B_{32} + \Delta B_{33} + \Delta B_{34}$$

Derivation of the Subfunctions of Differential Permeability - μ

So far as the current in the circuit is concerned, it is not necessary to use B - functions, but essentially the slope (differential permeability) functions are required. These functions are available either by taking the derivatives of the B - functions already obtained with respect to H or taking the integration of the γ - function only with respect of h_c. Of course, both must give the same result.

A) Derivation of the First Function - $\mu_1(H)$

By taking the derivative of $B_1(H)$ so that

$$\mu_{11} = \frac{d(\Delta B_{11})}{dH} = \frac{c_1 c_3 (c_1 H)^{n+1}}{(n+1)!} \exp(-c_1 H)$$

and $$\mu_{12} = \frac{d(\Delta B_{12})}{dH} = \frac{c_4 c_5 c_6}{c_4 - c_5} (\exp(-c_5 H) - \exp(-c_4 H))$$

hence $$\mu_1(H) = \frac{d(\Delta B_{11})}{dH} + \frac{d(\Delta B_{12})}{dH} + \frac{d(\Delta B_{13})}{dH} + \frac{d(\Delta B_{14})}{dH} + \mu_o$$

or $$\mu_1(H) = \mu_{11} + \mu_{12} + \mu_{13} + \mu_{14} + \mu_o$$

B) Derivation of the Second Function - $\mu_2(H,HP)$

Derivative of the second B - functions yields

$$\mu_{21} = \frac{d(\Delta B21)}{dH} = \frac{c_1 c_3 \exp(c_1 H) \cdot f_n(c_1 (H - HP))}{2^{n+1}}$$

$$\mu_{22} = \frac{d}{dH} (\Delta B_{22}) = \frac{c_4 c_5 c_6}{c_4 + c_5} [\exp(c_5 H) - \exp((c_4 + c_5)\frac{HP}{2} - (c_4 - c_5)\frac{H}{2})]$$

and resultant slope

$$\mu_2(H,HP) = \mu_o + \mu_{21} + \mu_{22} + \mu_{23} + \mu_{24}$$

C) Derivation of the Third Function - $\mu_3(H, HP)$

By a similar manner

$$\mu_{31} = \frac{d}{dH}(\Delta B_{31}) = c_1 c_3 \left[\frac{(c_1 H)^{n+1}}{(n+1)!} \exp(-c_1 H) + \frac{\exp(c_1 H)}{2^{n+1}} (f_n(c_1 (H - HP)) - f_n(2c_1 H)) \right]$$

$$\mu_{32} = \frac{d}{dH}(\Delta B_{32}) = c_4 c_5 c_6 \left[\frac{-2c_5}{c_4^2 - c_5^2} \exp(-c_4 H) + \frac{1}{c_4 - c_5} \exp(-c_5 H) - \frac{1}{c_4 + c_5} \exp\left((c_4 + c_5)\frac{HP}{2} - (c_4 - c_5)\frac{H}{2}\right) \right]$$

and

$$\mu_3(H, HP) = \mu_o + \mu_{31} + \mu_{32} + \mu_{33} + \mu_{34}$$

Derivation of the Subfunctions of the Abnormal B/H Characteristic

The expressions given so far are for the B/H characteristics which are only encountered in the steady-state operation. But, in the case of transient or occurrence of minor loops, there are another two types of subfunction to be expressed.

Now, let us consider the first B/H characteristic in Figure 3.6. For $0 \leq H \leq -HP$ the required B and μ cannot be found using the expressions in the foregoing sections because the integration limits are different. In this case the integration limits are

$$HP + h_c \leq h_m \leq H - h_c$$

$$0 \leq h_c \leq \frac{H - HP}{2}$$

but

$$HP \leq 0 \quad \text{and} \quad H \geq -HP$$

So, taking account of these conditions, the result of the integration

$$\Delta B = 2 B_s \int_{HP+H_c}^{HP-H_c} \int_{0}^{\frac{H-HP}{2}} \gamma(h_m, h_c) \, dh_m \, dh_c$$

is exactly the same as $\Delta B_3 (-HP, -H_3)$ and the slope function for this new case

$$\mu_4 = 2 B_s \int_{0}^{\frac{H-HP}{2}} \gamma(H - h_c, h_c) \, dh_c$$

Hence, for the first term (n = 12)

$$\mu_{41} = \frac{c_1 c_3 \left(c_1 \left(\frac{H-HP}{2}\right)\right)^{n+1}}{(n+1)!} \cdot \exp(-c_1 H)$$

and for the second term (n = 0)

$$\mu_{42} = \frac{c_4 c_5 c_6}{c_4 - c_5} \left[\exp(-c_4 H) - \exp\left((c_4 - c_5)\frac{HP}{2} - (c_4 + c_5)\frac{H}{2}\right) \right]$$

and thus the resultant slope function is

$$\mu_4 (H, HP) = \mu_o + \mu_{41} + \mu_{42} + \mu_{43} + \mu_{44} \cdot$$

If the second characteristic in the Figure 3.6 is analysed in the same manner, it is found that

$$\Delta B = \Delta B_2 (-HP, -H)$$

and

$$\mu = \mu_4 (H, HP)$$

These are valid for only the region

$$0 < HP < H$$

Determination of The Coefficients

In the analysis of the transient currents and ferroresonance there is no need for the more accurate representation of B/H loop. Therefore, in the estimation of the coefficients the third and fourth terms have been taken in the following forms:

$$B_3 = c_9 (1 - \exp(-c_8 . H))$$

$$B_4 = c_{12}(1 - \exp(-c_{11} H))$$

Since a soft magnetic characteristic is considered the B/H loop appears very narrow. Therefore, the region of B/H characteristic above B_r in the first figure of Figure 3.9 could be represented by

$$B = B_r + B_3 + B_4 + \mu_o H.$$

On the other hand, c_{12} can be estimated by drawing. If we draw an asymptotic line to the B/H curve from (B_s, H_s) we find the point A, B, C on the second figure of Figure 3.9. Hence

$$BC = \mu_o H_s$$

$$BA = c_{12} = 0.532$$

At the point $(B = B_s, H = H_s)$ the above relation becomes

$$B_s = B_r + c_9 + c_{12} + \mu_o . H_s .$$

So for $B_r = 0.94$, $B_s = 2.08$, $H_s = 14000$, $\mu_o = 0.75$ E -05 and $c_{12} = 0.532$ this equation gives

$$c_9 = 0.513$$

For the region $B \geq B_r$ the representing function is now

$$B = 0.94 + 0.513 (1 - \exp(-c_8 . H)) + 0.532(1 - \exp(-c_{11} . H)).$$

Using points obtained from the experimental characteristic this equation is solved for c_{11} and c_8 by least-square method.

The above expressions given for B_3 and B_4 are valid as long as $c_7 >> c_8$ and $c_{10} >> c_{11}$. So c_7 and c_{10} can be any number satisfying these inequalities. However, the error may be minimized by changing c_7 and c_{10}.

For the region below B_r the sums of the saturation values of representing functions should be equal to B_r, i.e.

$$B_r = c_3 + c_6.$$

The first term of the expression of B has high saturation. For this, 0.619, which corresponds to the "knee" point (H = 60), is taken for c_3. Then

$$c_6 = B_r - c_3 = 0.320.$$

Since we now know the third and fourth terms, we can find the differences between the experimental points and the fitted curve so that

$$DB_1 = B_{exper.} - (\mu_o.H + \text{third term} + \text{fourth term})$$

If the attempt of fitting a curve using only the first term for DB_1's is made, the coefficient c (for the sake of simplicity c_2 is taken equal to c_1) can be evaluated by least-square method. Of course, again there will be differences between fitted and experimental points. For example, only the first term will give a loop as in the third figure of Figure 3.9. It is seen that we get the point B^1 instead of B. So, in order to overcome this difficulty, a second term is fitted to the points.

$$DB_2 = B_{exper.} - (\mu_o H + \text{first term} + \text{second term} + \text{fourth term})$$

Taking $c_5 >> c_4$ and using least-square technique c_4 is estimated. By changing c_5 the error is minimized.

APPENDIX A4

COMPUTER PROGRAMME FOR THE NUMERICAL SOLUTIONS

As will be seen from Figure 1.3 and Figure 1.4 the only difference between these two circuit configurations is the capacitance. Therefore, a computer programme designed for the study of ferro-resonance can be employed to investigate the transient phenomenon as well just by omitting the capacitance. But a small section of programme must be added to take into account the effect of initial (residual) flux density on the transient current. Therefore we have two computer programmes which are slightly different from each other. These are

TRANS 12

and

FER 12

In the following sections these programmes are presented in detail.

I - "TRANS 12"

This programme mainly consists of three sections as follows:

1. Data Section: In this section the data such as coefficients for the representation of B/H loop or magnetisation curve, total resistance and leakage inductance of the system used are given (see Flow charts at the end of this Appendix).

2. Establishment of the Residual Flux Densities: Since there are only two possible residual conditions such as $B_r > 0$ and $B_r < 0$ this section contains two subsections.

2.1 Establishment of the Positive Residual Flux Density:

The procedure of establishing the initial residual flux densities in the programme is performed exactly as in the experimental procedure.

In the experimental establishment first the transformer core is demagnetised (see Chapter 3) then by means of the system in Figure 3.10 the current flowing through the transformer primary side is increased such that a positive flux density will be produced, so after reaching the saturation flux density B_s the current is reversed and decreased till it takes zero value. Thus a maximum positive residual flux density is obtained.

Now, to establish a positive residual flux density in the programme we first call the subroutine programme

BH LOOP (IT, H, B, DMU)

for

IT = 0

$H = H_s = 14000 \ \frac{A.T}{m}$

Thus this subroutine computes the value of $B = B_s$ and DMU $= \mu$ (Since this will be examined in detail very soon we will not deal with it in this section). By this subroutine we, in fact, build up the following diagrams and store $HP = H_s$, NPK = 2, DIR = 1 (where NPK is the number of peaks and DIR is the pointer showing the direction of the magnetic trajectory)

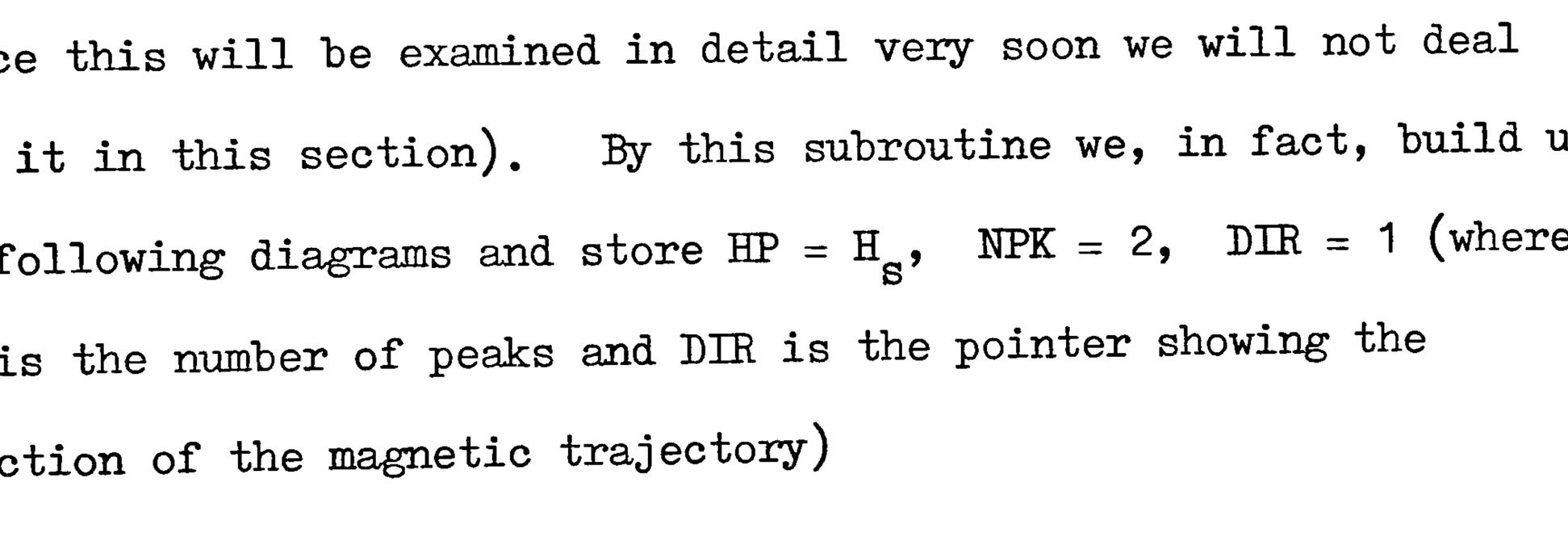

Fig. A4.1

Then by the subroutine programme, for

$$IT = 0$$

$$H = 0$$

we compute $B = B_r$ and $DMU = \mu$ and set up the following diagrams.

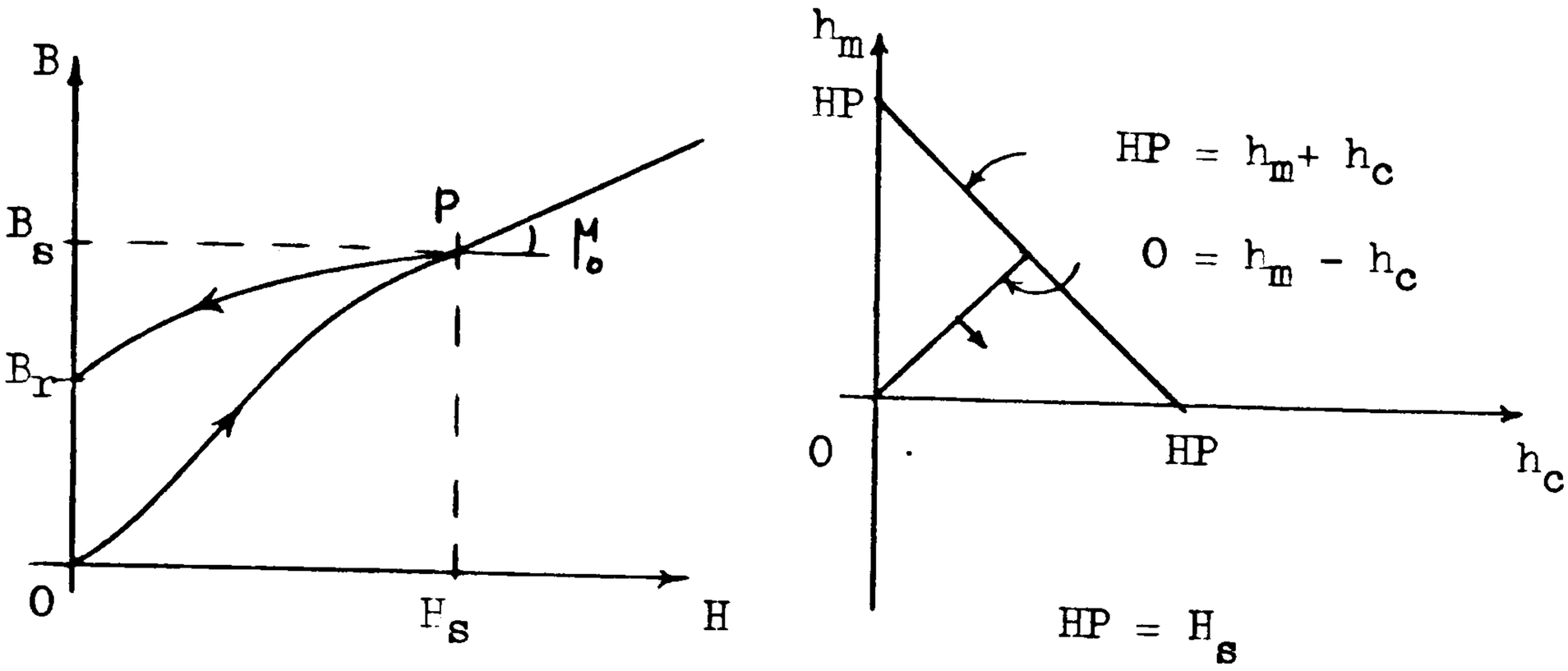

Fig. A1.2

But, now, since the magnetic trajectory changes the direction the conditions stored in memory become

$$HP = H_s$$

$$NPK = 3$$

$$DIR = -1$$

and the residual condition of the core is

$$B = +B_r \quad (H = 0)$$

2.2 Establishment of the Negative Residual Flux Density:

For a negative residual flux density an inverse procedure is performed, i.e. first the current is decreased till B reaches its negative saturation value $-B_s$, then current is reversed and increased up to zero. Thus the flux density will take its maximum negative value $-B_r$.

Similarly, if the subroutine programme

BHLOOP (IT, H, B, DMU)

is called for

$$IT = 0$$

$$H = -H_s = -14000 \quad \frac{A.T}{m}$$

it computes

$$B = -B_s$$

and $DMU = \mu$

In this case subroutine programme traces the diagrams in the following figure

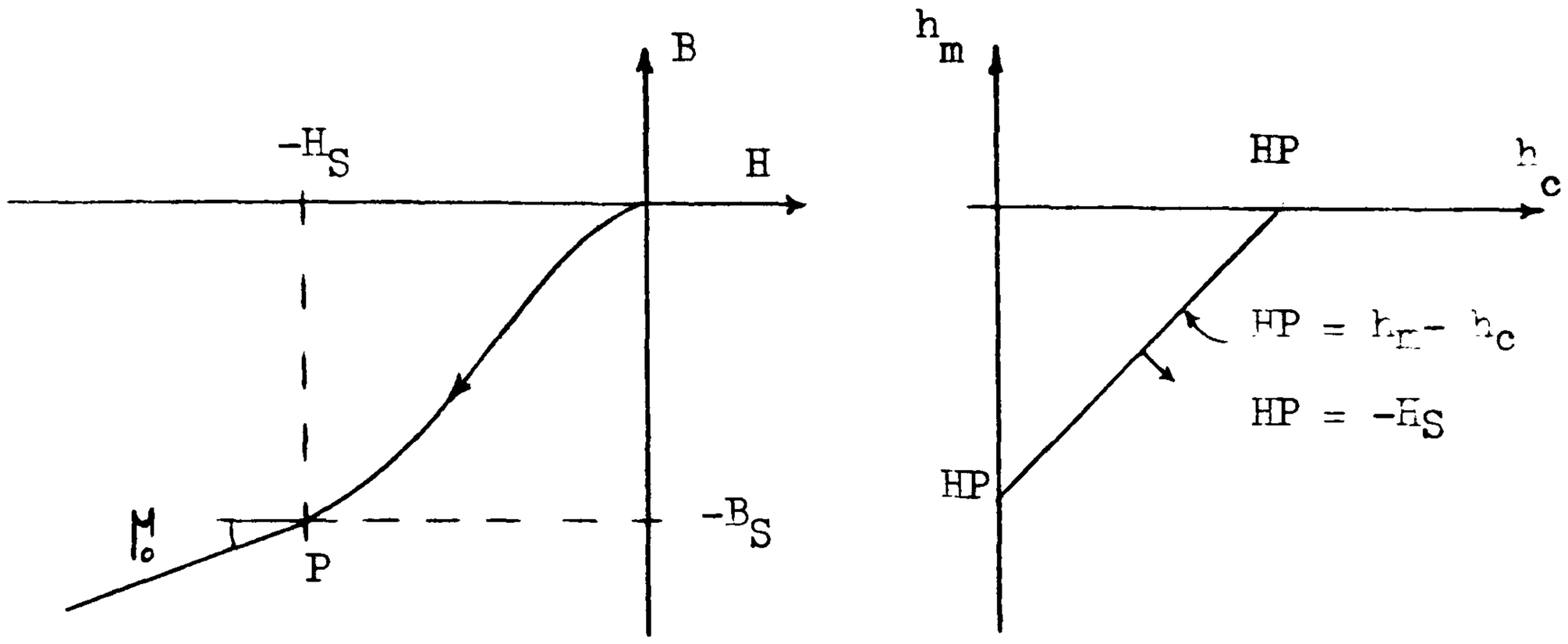

Fig. A4.3

and stores

$$HP = -H_s,$$

$$NPK = 2,$$

$$DIR = -1$$

Finally, if the same subroutine is called again but for

$$IT = 0$$

$$H = 0$$

the condition of magnetic trajectory becomes

$$HP = -H_s$$

$$NPK = 3$$

$$DIR = +1$$

$$BP = -B_s$$

$$B = -B_r \qquad (H = 0)$$

The diagrams corresponding to this final call are shown in Fig. A4.4.

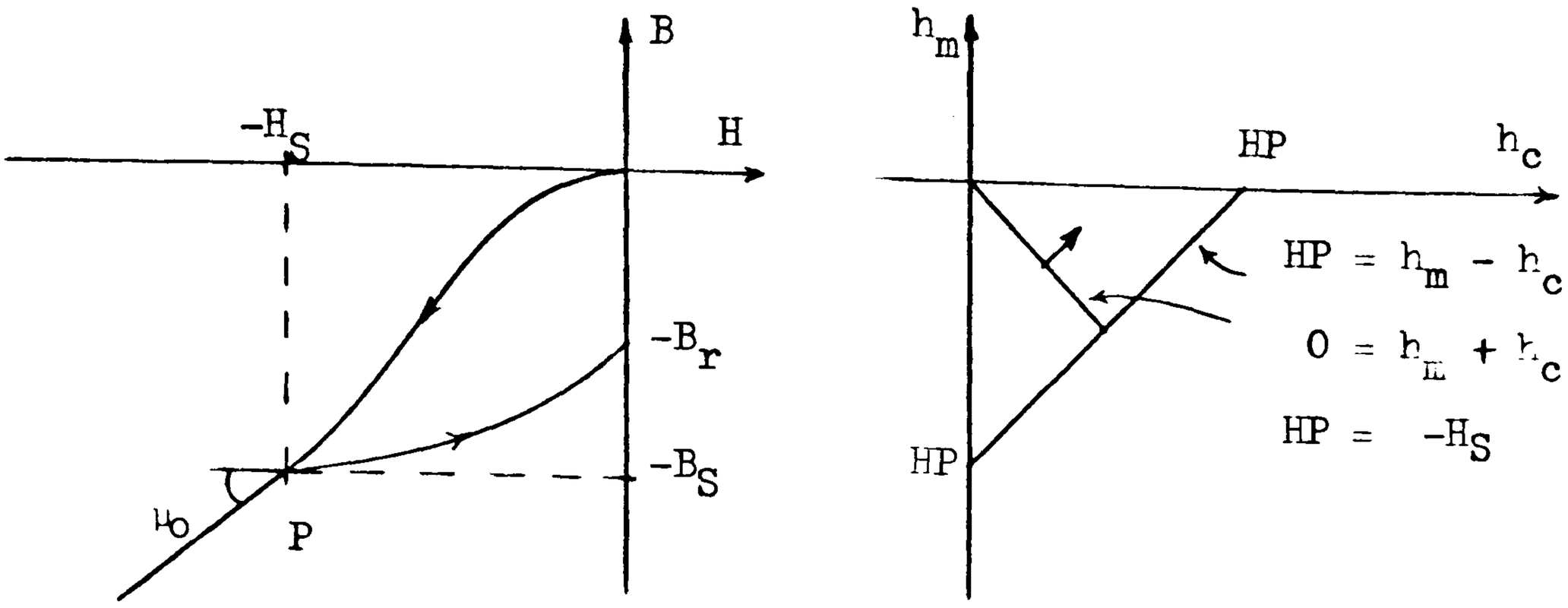

Fig. A4.4

If the effect of residual flux densities on transient current are not required this second section of TRANS 12 should be skipped over.

3. <u>The Solution of the Differential Equations</u>: At the beginning of this section the initial values of the dependent and independent variables are given. Then system equations 1.7 are solved by four-steps Runge-Kutta method[49,50].

According to this method first the differential equations to be solved are rearranged so that the first order derivatives with respect to time T will be on the left hand side, i.e.

$$\left[\frac{dX\ (NM)}{dt}\right] = [FX\ (NM)\ ]$$

where [ ] and NM designates the matrix form of equations and number of first order differential equations (in other words, number of time-dependent variables X(NM) to be solved) respectively.

Thus the right hand side of this form, i.e. [FX(NM)] simply means some expressions involving X, T but not any first order derivative. For given time-step length dt and initial conditions $[X_o(NM)]$, To the state variables

$$[X(NM)] = [X_o(NM)]$$

$$T = T_o$$

are substituted in the expressions of [FX(NM)], i.e. [FX(NM)] is defined. Thus, at the first step of this method

$$[FA(NM)] = [FX(NM)]$$

is calculated. Similarly

For second step: The state variables are

$$[X(NM)] = [X_o(NM)] + \tfrac{1}{2}.\ dt.\ [FA(NM)]$$

$$T = T_o + \tfrac{1}{2}.\ dt$$

Hence calculating [FX(NM)]

$$[FB(NM)] = [FX(NM)]$$

is found.

For third step: The state variables are

$$[X(NM)] = [X_o(NM)] + \tfrac{1}{2}.\ dt.\ [FB(NM)]$$

$$T = T_o + \tfrac{1}{2}.\ dt$$

Substituting these into the expression of [FX(NM)]

$$[FC(NM)] = [FX(NM)]$$

is defined.

For fourth step: The state variables become

$$[X(NM)] = [X_o(NM)] + dt.\ [FC(NM)]$$

$$T = T_o + dt$$

and again, calculating [FX(NM)] corresponding to these state variables, we find

$$[FX(NM)] = [FX(NM)]$$

Thus the new values of time-dependent variables [X(t)] are

$$[XN(NM)] = [X_o(NM) + \frac{dt}{6} [\ [FA(NM) + 2\ FB(NM) + 2\ FC(NM) + FD(NM)]\ ]$$

and the corresponding time is

$$T_N = T_o + dt$$

For the next step of calculation we just repeat the processes given above by the initial conditions

$$[X_o(NM)] = [XN(NM)]$$

$$T_o = T_N$$

Now, the question is the calculation of [FX(NM)] for given state variables [X(NM)] and T. For this purpose a subroutine programme

FUNCT (IT, H, B)

and a common statement

COMMON FX(NM), X(NM), T

are employed. So, as soon as calling this subroutine programme the state variables

[X(NM)] , T

are sent to the subroutine programme and the value of

[FX(NM)]

are solved and withdrawn from the programme.

3.1 Subroutine "FUNCT":

The differential equations of the system in matrixal form are

$$[V_s(NM)] = [ZR(NM,NM)]\,[X(NM)] + [ZL(NM,NM)]\,[\frac{dX(NM)}{dt}]$$

where

$[V_s]$: matrix of supply voltages

$[ZR]$: matrix of resistances

$[ZL]$: matrix of inductances

$[X]$: matrix of state variables

$[\frac{dX}{dt}]$: matrix of first order derivatives.

Denoting

$$[V(NM)] = [V_s(NM)] - [ZR(NM,NM)]\,[X(NM)]$$

$$[FX(NM)] = [\frac{dX(NM)}{dt}]$$

and then rearranging this matrixal form we obtain

$$[V(NM)] = [ZL(NM,NM)]\ [FX(NM)]$$

Hence, using the Gauss-Sidel elimination method[49,50] [FX(NM)] is solved and sent back to the main programme through the common statement used.

Since [ZL] requires the differential permeability μ first H is calculated and then the subroutine programme

BH LOOP (IT, H, B, DMU)

is called at the beginning of this subroutine.

3.2 Subroutine "BH LOOP"

In the establishment of the residual flux densities and in the calculation of the differential permeability this subroutine programme is called. It is composed of several sections. We will study these in order.

3.2.1 Section of Logical Statements

As mentioned above there are four steps in Runge-Kutta method. During the calculation of the differential permeability required for these steps there must not be any change in magnetic history and trajectory, i.e. H, HP, NPK and DIR shown in the following figure must not change.

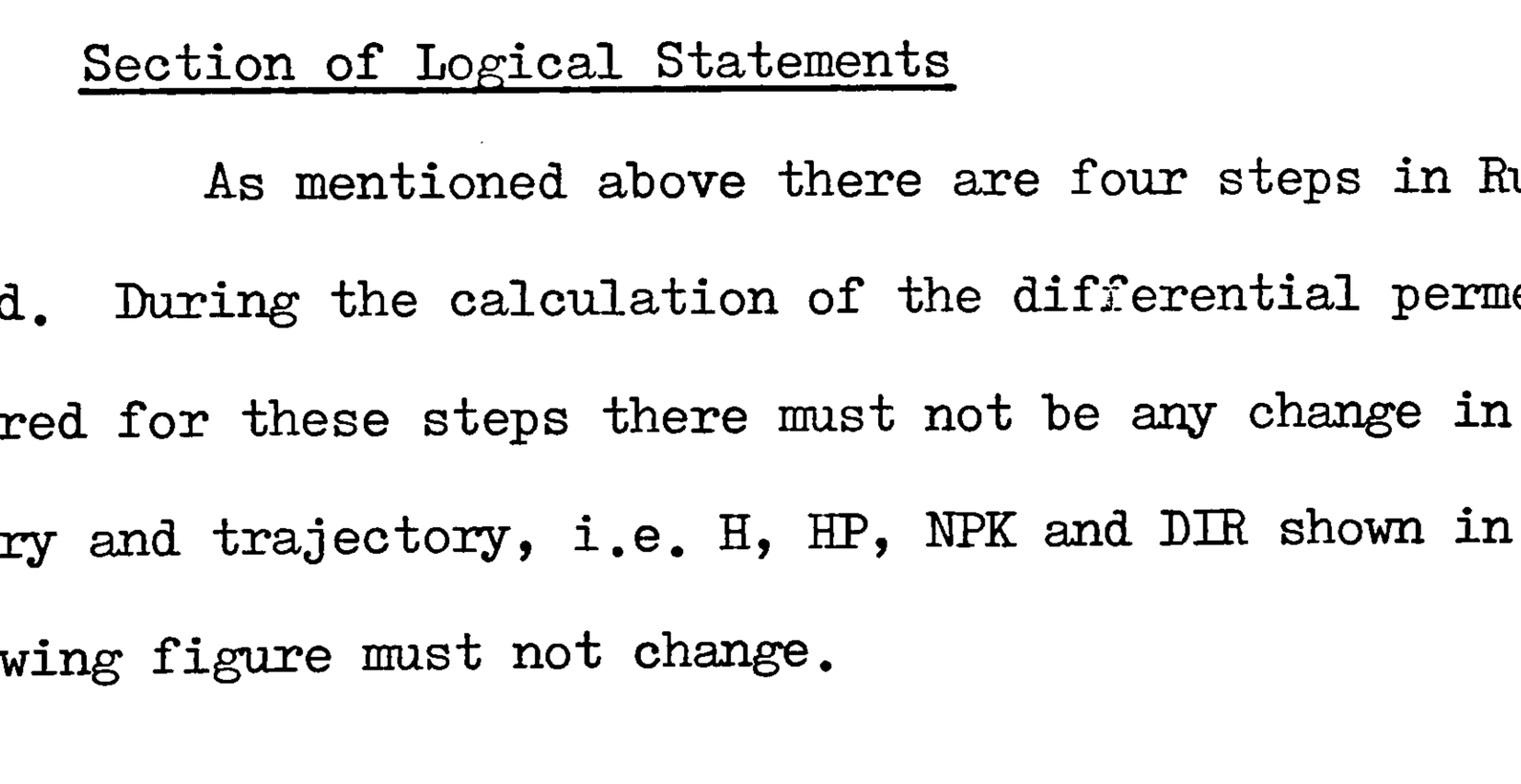

Fig. A4.5

So putting an iteration pointer IT at the beginning of each Runge-Kutta step we can detect these steps in the subroutine programme "BHLOOP" and using logical statement to check the value of IT we can retain the values of H, HP, NPK and DIR. The present values of these quantities may change only when the new value of H corresponding to X (1), which denotes the current is required. In order to distinguish this case IT = 0 is taken for the iteration pointer as in the establishment of the residual flux densities.

3.2.2 Generation of the New Peaks and Reduction of the Peak Number

Comparing the present value of H with its previous value the direction of the magnetic trajectory, i.e. DIR, can be defined as +1 or -1. DIR = +1 designates the rising trajectory, DIR = -1 the descending trajectory. By the comparison of the present value of DIR with its previous value enables us to generate a new peak and to detect it (see the Figure A4.6 below).

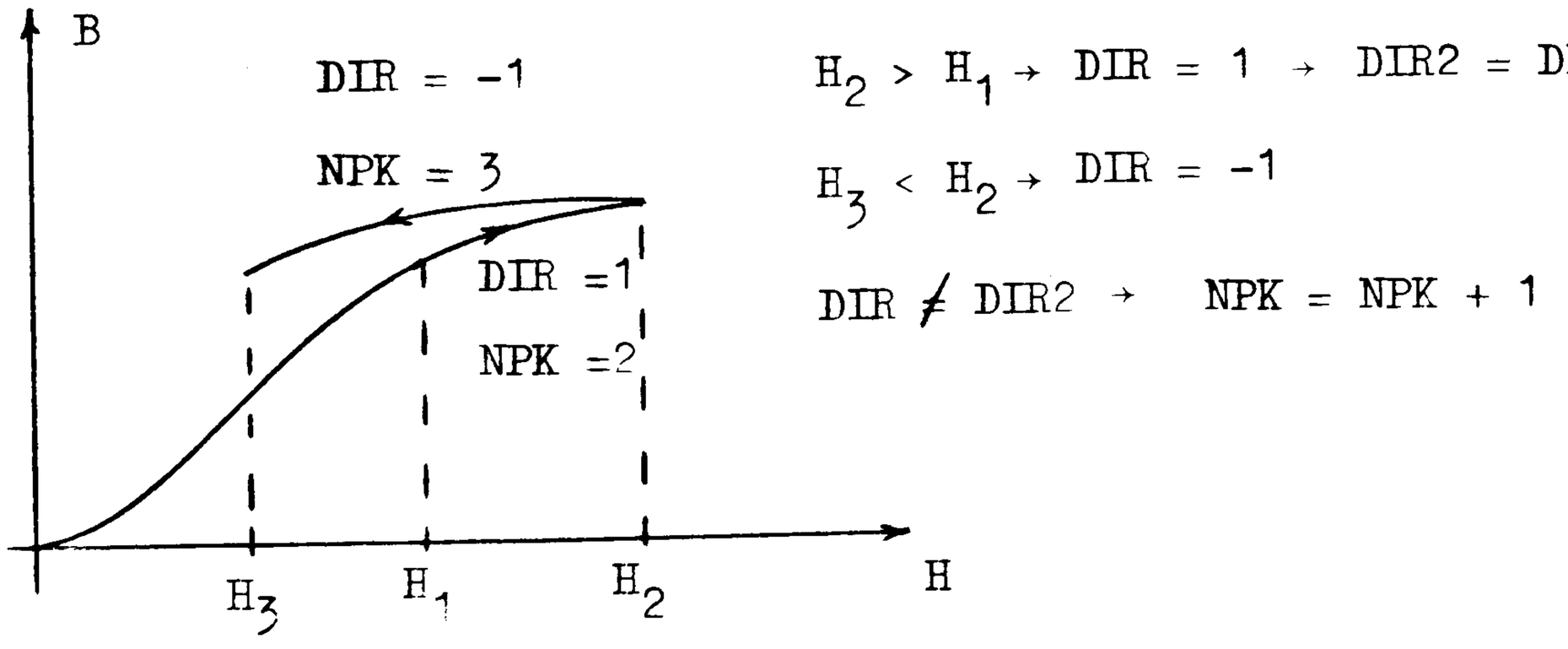

Fig. A4.6

To explain the reduction in the peak number let us consider the following B/H loops and corresponding Preisach diagram.

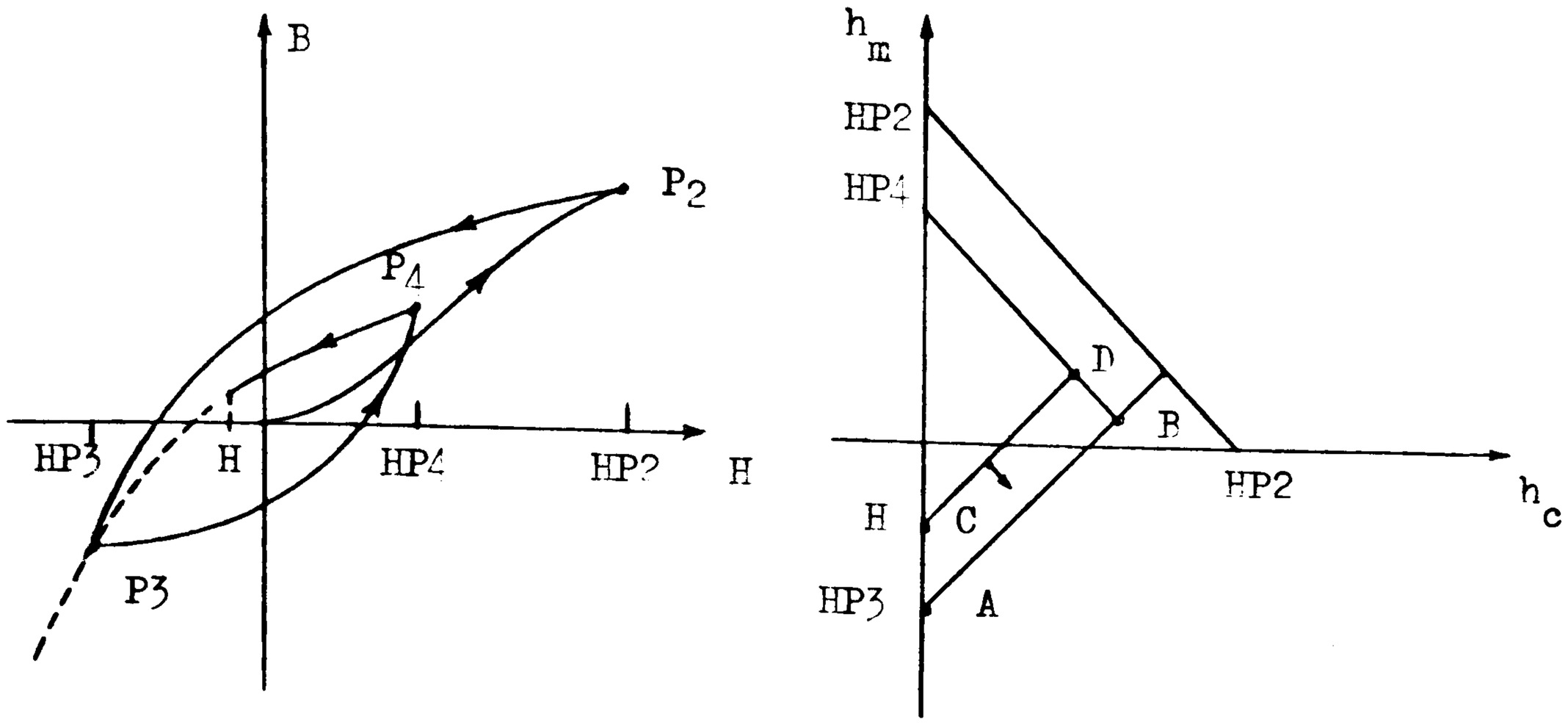

Fig. A4.7

When the present trajectory descending from P_4 coincides with P_3 the straight line $\overline{CD}$ on the Preisach diagram coincides with $\overline{AB}$. That means the loop P_3 P_4 P_3 is closed and corresponding triangle ECD becomes equal to ABE. Thus the previous peak value of H becomes HP2 instead of HP4.

If we formulate what we have said to generalize the idea it is seen that when the present value of H on the rising curve (DIR = 1) is greater than the (NPK - 2)th peak or the present value of H on the descending curve (DIR = -1) is less than the (NPK - 2)th peak, the new peak number becomes

$$NPK = NPK - 2$$

where NPK on the right hand side is the old one. It is important to point out that along the first trajectory (e.g. along $\overline{OP}_2$) and for the first peak NPK = 2 is taken for the number of peaks.

3.2.3 Selection of the Proper Function to Calculate B and μ

Since the B/H plane is divided into regions and different functions representing the B/H characteristic are used in each region

(see appendix A3 and Figure 3.7), it is essential to know all previous values of HP(NPK), and DIR, NPK as well as the present value of H to determine the region in which H falls. Thus, after determining the region the related functions are called, then B and μ are calculated.

Although Preisach theory can be employed to represent the magnetisation curve, the exponential series will be used for this purpose to achieve more accurate results, to observe the effect of hysteresis on transient current accurately. Therefore the subroutine

BH LOOP (IT, H, B, DMU)

is replaced with

BH CURVE (IT, H, B, DMU)

Of course, the coefficients related to this representation are placed in the data section.

This subroutine is very small compared to the subroutine for the loop because only one function is used.

At the end of this Appendix "Flow Charts" are given for "TRANS 12", subroutine "FUNCT" and subroutine "BH LOOP".

II - "FER 12"

In order to study the ferroresonance phenomena including subharmonic resonance this programme is utilized.

There are only two differences between this programme and "TRANS 12". The first is the number of the differential equation to be solved and, second, the matrix [ZL(NM,NM)] is different. Since the system contains two energy storing elements, two differential equations are required to represent the system mathematically. Therefore NM = 2 is taken for the number of differential equations in this case. The matrix [ZL(NM,NM)] is also different because

the capacitance of the system will be placed in this matrix.

The rest of this programme is exactly the same as the "TRANS 12".

III - The Programmes used for the Generalized Parametric Method

For the transient current studies

PARAM 1

and for the ferroresonance phenomena

PARAM 2

are used and these are simply reproduced from "TRANS 12" and "FER 12" respectively. But the standard coefficients (see Chapter 2) are placed in the data section and the matrices

[ZR(NM,NM)] , [ZL(NM,NM)]

are reconstructed using the generalized parameters.

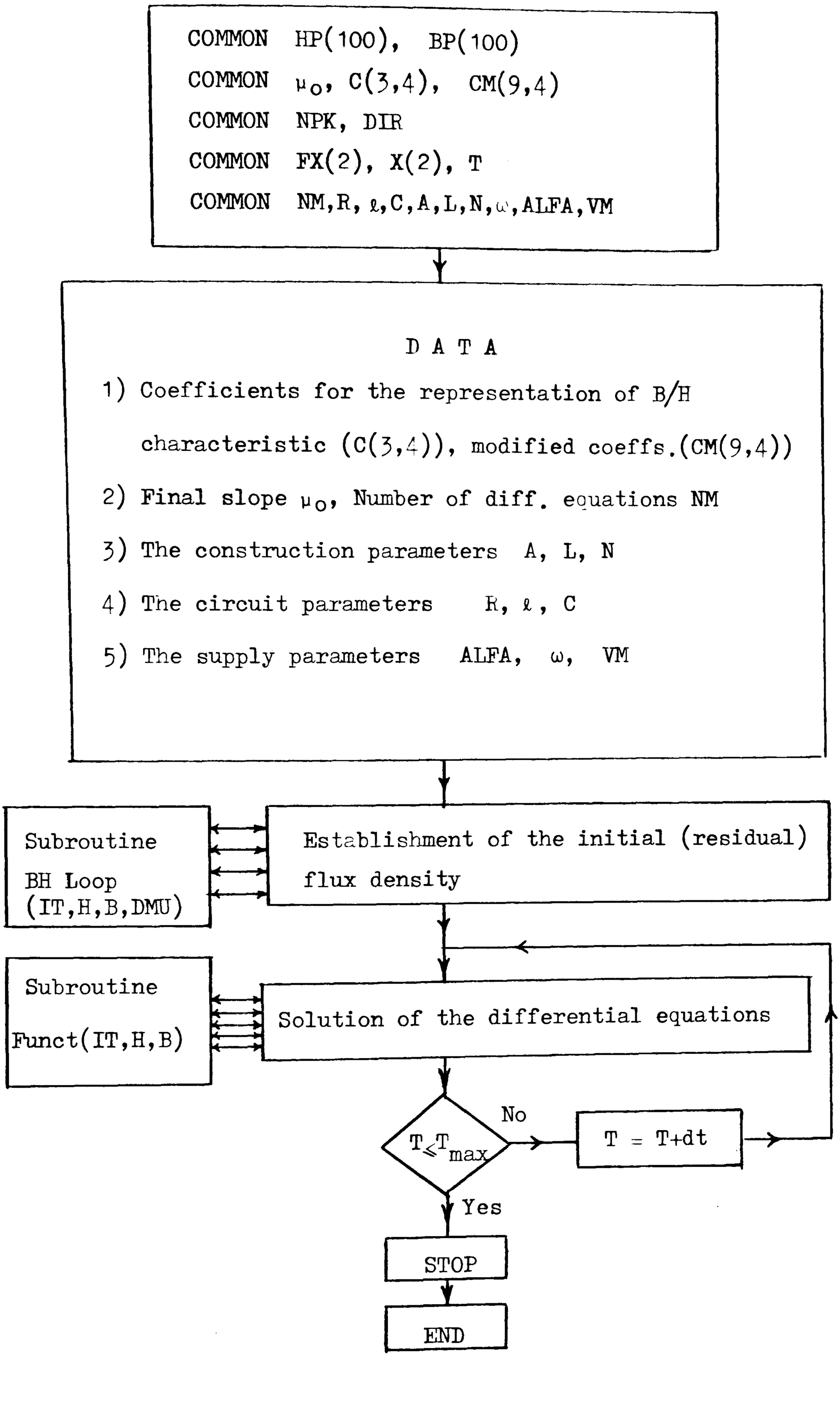

Fig. A4.8 Flow Chart of TRANS 12

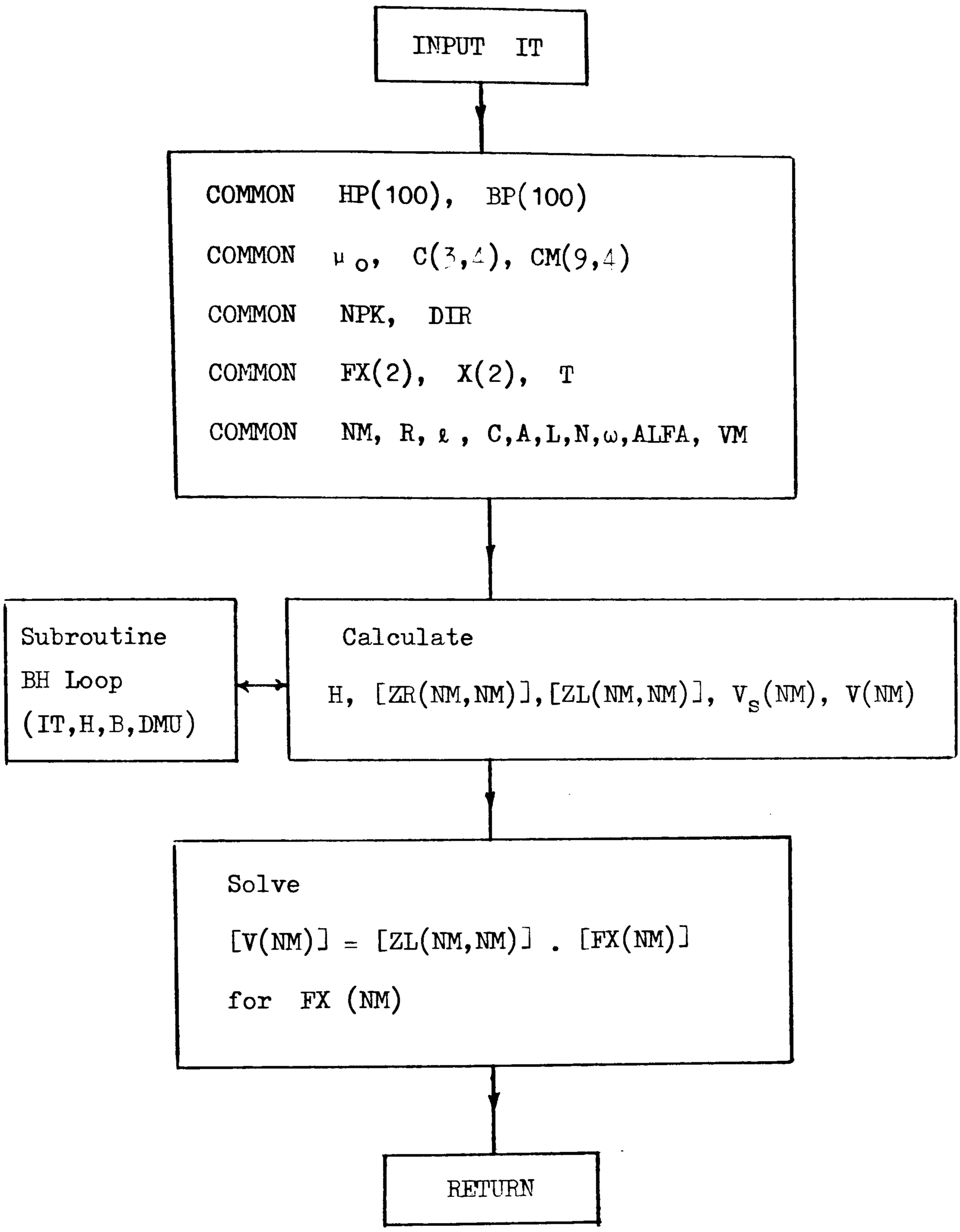

Fig. A4.9 Flow Chart of Subroutine FUNCT

BH LOOP

(4 pages)

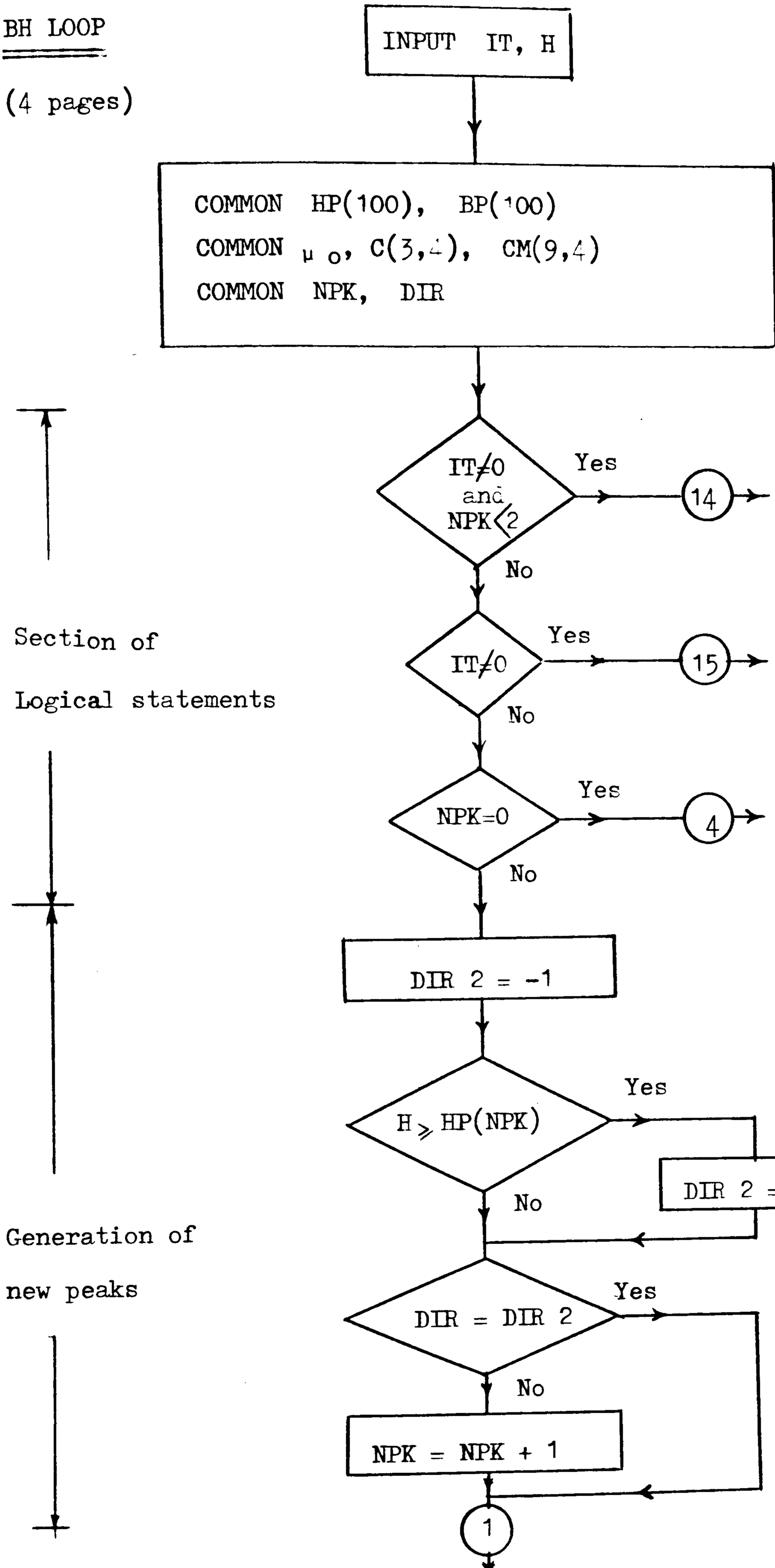

Section of

Logical statements

Generation of

new peaks

Reduction of peak number

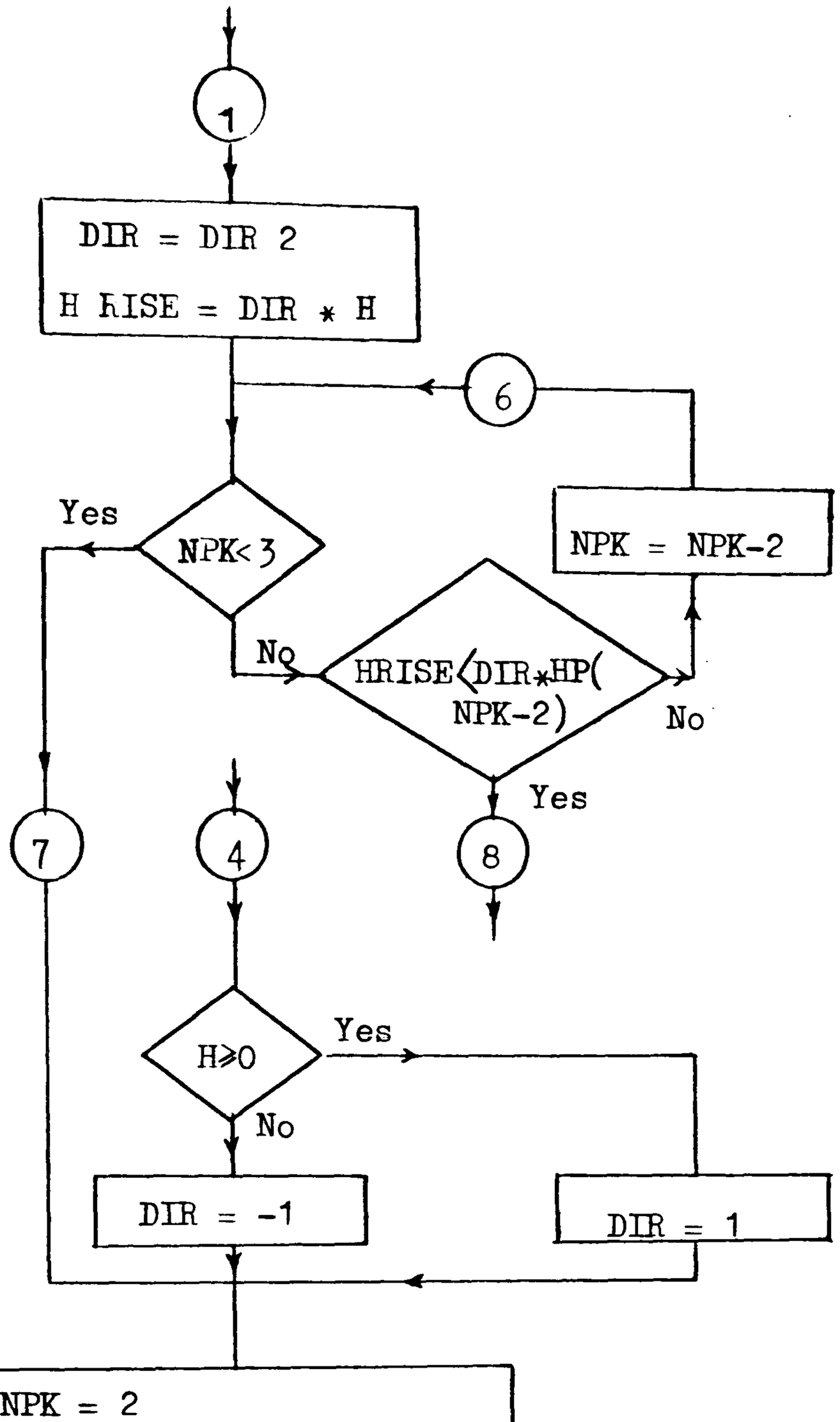

Selection of proper Functions

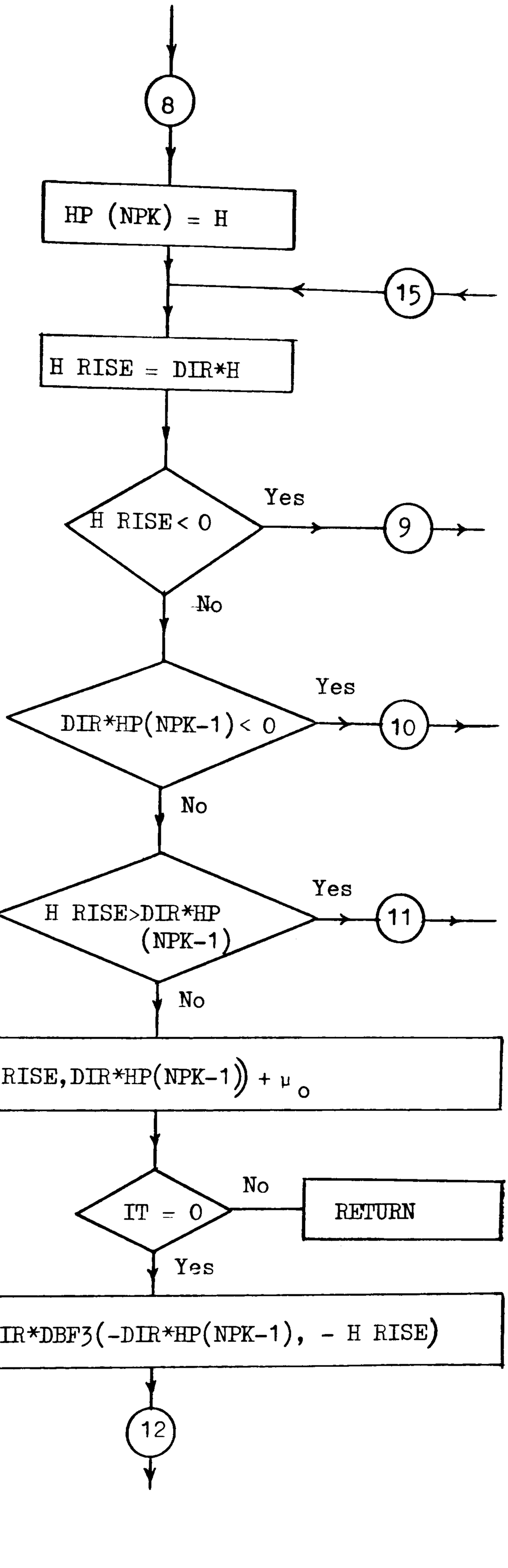
8
HP (NPK) = H
15
H RISE = DIR*H
H RISE < 0
Yes
9
No
DIR*HP(NPK-1) < 0
Yes
10
No
H RISE>DIR*HP (NPK-1)
Yes
11
No
DMU=DBDH4(H RISE, DIR*HP(NPK-1)) + μ o
IT = 0
No
RETURN
Yes
BP(NPK) = DIR*DBF3(-DIR*HP(NPK-1), - H RISE)
12

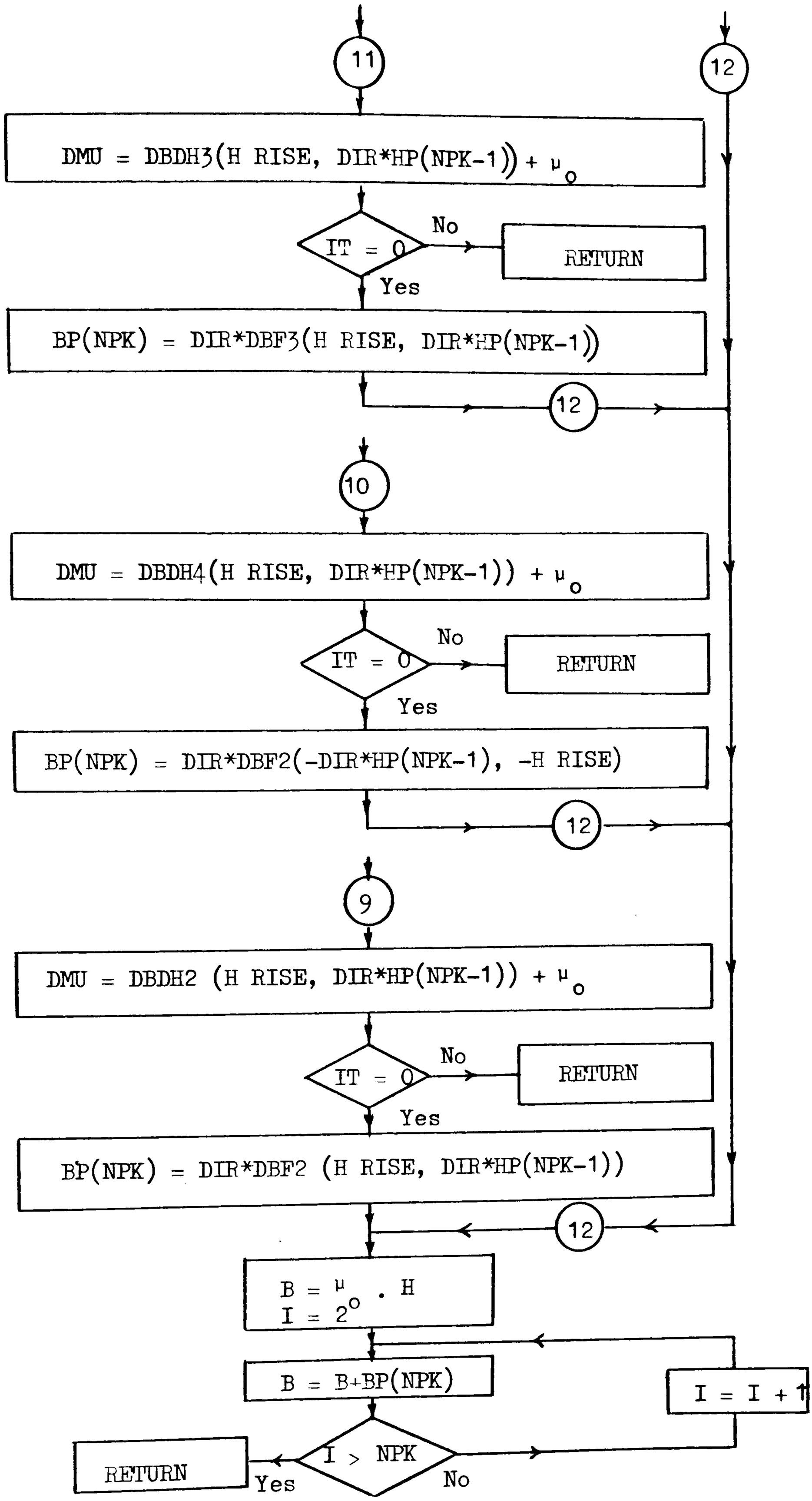

Fig. A4.10 Flow Chart of Subroutine BH LOOP

In the Flow Chart of Subroutine BH Loop

DIR : Direction of magnetic trajectory

DIR = 1 for rising curves

DIR = -1 for descending curves

NPK : Number of peak.

Subfunctions for the calculation of B

$DBF_1 = \Delta B_1 (H)$

$DBF_2 = \Delta B_2 (H, HP)$

$DBF_3 = \Delta B_3 (H, HP)$

(for the expression of ΔB's see the Appendix A3)

Subfunctions for the calculation of μ

μ_o : Final slope of B/H characteristic

$DBDH_1 = \mu_1 (H)$

$DBDH_2 = \mu_2 (H, HP)$

$DBDH_3 = \mu_3 (H, HP)$

$DBDH_4 = \mu_4 (H, HP)$

(Also for the expression of μ's, see the Appendix A3)

All these subfunctions are given immediately after subroutine BH Loop.

APPENDIX A5

THE DERIVATION OF THE EQUATIONS WITH COMPLEX COEFFICIENTS

In both the fundamental ferroresonance case and subharmonic resonance case we are dealing with the equation

$$v(t) = Ri(t) + \ell . \frac{di(t)}{dt} + \frac{1}{C}\int i(t)dt + \frac{d\Psi(t)}{dt} \quad \ldots \qquad A5.1$$

where

$$i(t) = c_1 \Psi(t) + c_3 \Psi^3(t)$$

$$\Psi(t) = \Psi_1(t) + \Psi_3(t)$$

$$\Psi_1(t) = \sqrt{2}\ \Psi_1 \sin(\omega t + \theta_1)$$

$$\Psi_3(t) = \sqrt{2}\ \Psi_3 \sin(3\omega t + \theta_3)$$

$$v(t) = \sqrt{2}\ V. \sin(\nu \omega t)$$

$$\nu = 1 \quad \text{(Fundamental Ferroresonance)}$$

$$\nu = 3 \quad \text{(Subharmonic Resonance)}$$

Using the mathematical fact that

$$\sin(\alpha) = \frac{1}{2j}(\exp(j\alpha) - \exp(-j\alpha))$$

The equation A5.1 can be transformed to a new equation with complex coefficients. In fact, by this transformation each time-dependent quantity is replaced with two vectors having the same modulus, revolving with the same angular velocity but in opposite directions as shown in Figure A5.1 below.

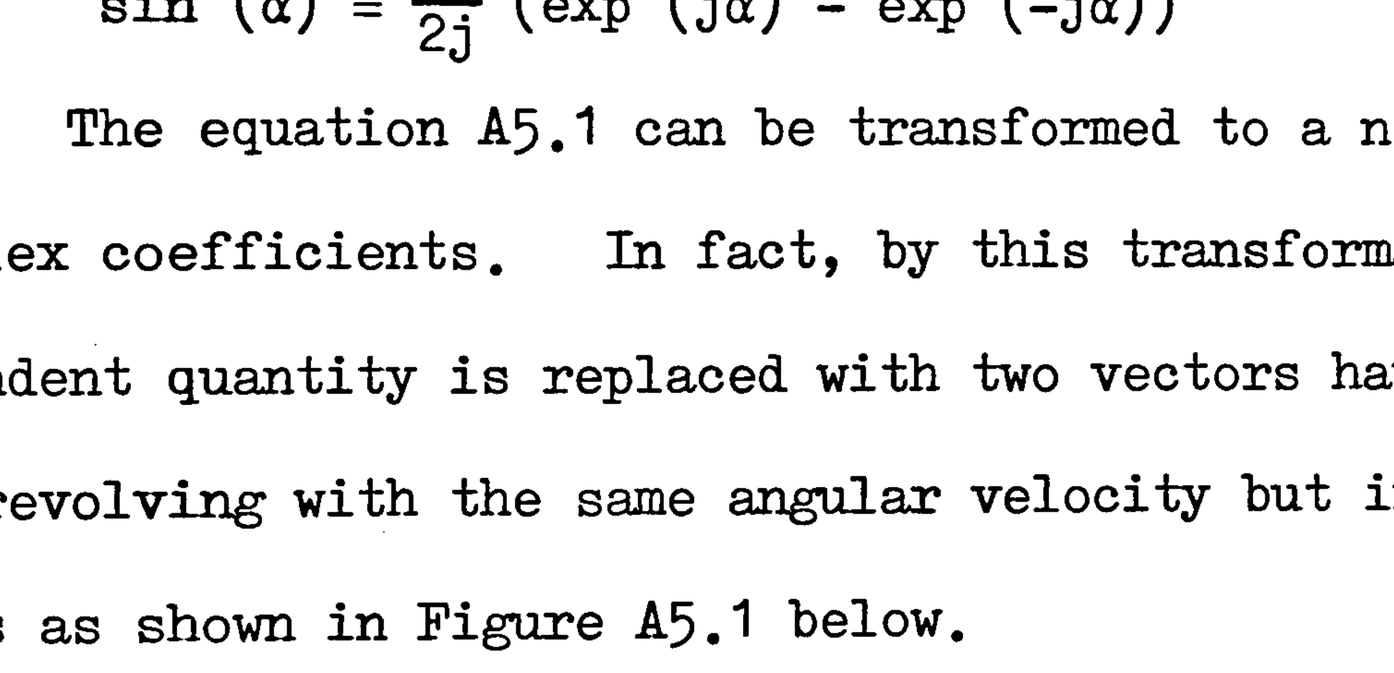

Fig. A5.1

Hence

$$\frac{di(t)}{dt} = \frac{\sqrt{2}}{2j} \left(j\omega \bar{I}_1 \exp(j\omega t) + j3\omega \bar{I}_3 \exp(j3\omega t)\right)$$

and

$$i(t)dt = \frac{\sqrt{2}}{2j} \left(\frac{1}{j\omega} \bar{I}_1 \exp(j\omega t) + \frac{1}{j3\omega} \bar{I}_3 \exp(j3\omega t)\right)$$

Now, if these relations are substituted into the Equation A5.1 we obtain

$$V.\exp(j\nu\omega t) = (\bar{Z}_1.\ \bar{I}_1 + j\omega \bar{\Psi}_1) \exp(j\omega t) + (\bar{Z}_3.\ \bar{I}_3 + j3\omega \bar{\Psi}_3) \exp(j3\omega t) \quad .. \quad A.5.2$$

where

$$\bar{Z}_1 = R + j\left(\omega\ell - \frac{1}{\omega C}\right)$$

$$\bar{Z}_3 = R + j\left(3\omega\ell - \frac{1}{3\omega C}\right)$$

or in the polar form

$$\bar{Z}_1 = Z_1 . \exp(j\zeta_1)$$

$$\bar{Z}_3 = Z_3 . \exp(j\zeta_3)$$

$$Z_1 = \sqrt{R^2 + \left(\omega\ell - \frac{1}{\omega C}\right)^2}$$

$$Z_3 = \sqrt{R^2 + \left(3\omega\ell - \frac{1}{3\omega C}\right)^2}$$

$$\tan\zeta_1 = \frac{\left(\omega\ell - \frac{1}{\omega C}\right)}{R}$$

$$\tan\zeta_3 = \frac{\left(3\omega\ell - \frac{1}{3\omega C}\right)}{R}$$

By the harmonic balance rule we can derive two distinct equations from the Equation A5.2 so that if $\nu = 1$ (fundamental ferroresonance case) the first term of the right hand side of this equation becomes equal to the left hand side and the second term to zero; if $\nu = 3$ (subharmonic resonance case) the first term becomes equal to zero and the second term equal to the left hand side.

Therefore, after applying the transformation, we have two equations which are exactly the same instead of Equation A5.1. One is due to the vectors rotating in the positive direction (counter clockwise) and the other due to the vectors rotating in the negative direction (clockwise). So that the latter one is rejected we use

$$v(t) = \frac{\sqrt{2}}{2j} (\bar{V}. \exp(\nu\, \omega t)) + \quad \ldots \quad \text{(the rejected term)}$$

$$\Psi(t) = \frac{\sqrt{2}}{2j} (\bar{\Psi}_1 . \exp(j\omega t) + \bar{\Psi}_3 . \exp(j3\omega t)) + \ldots \text{(the rejected term)}$$

where

$$\bar{V} = V. \exp(j.0)$$

$$\bar{\Psi}_1 = \Psi_1 . \exp(j.\theta_1)$$

$$\bar{\Psi}_3 = \Psi_3 . \exp(j.\theta_3)$$

Hence

$$\frac{d\,\Psi(t)}{dt} = \frac{\sqrt{2}}{2j} (j\omega\, \bar{\Psi}_1 . \exp(j\omega t) + j3\omega . \bar{\Psi}_3 . \exp(j3\omega t))$$

and

$$\Psi^3(t) = \frac{\sqrt{2}}{4j} (\bar{s}_1 \exp(j\omega t) + \bar{s}_3 \exp(j3\omega t))$$

where

$$\bar{s}_1 = 3 . \bar{\Psi}_1^2 \bar{\Psi}_1^* - 3(\bar{\Psi}_1^*)^2 \bar{\Psi}_3 + 6 \bar{\Psi}_1 \bar{\Psi}_3 \bar{\Psi}_3^*$$

$$\bar{s}_3 = 3 \bar{\Psi}_3^2 \bar{\Psi}_3^* + 6 \bar{\Psi}_1 \bar{\Psi}_1^* \bar{\Psi}_3 - \bar{\Psi}_1^3$$

Substituting the new expression of $\Psi(t)$ into the expression of $i(t)$ we get

$$i(t) = \frac{\sqrt{2}}{2j} (\bar{I}_1 . \exp(j\omega t) + \bar{I}_3 . \exp(j3\omega t))$$

where

$$\bar{I}_1 = c_1 \bar{\Psi}_1 + \frac{c_3 . \bar{s}_1}{2} ,$$

$$\bar{I}_3 = c_1 \bar{\Psi}_3 + \frac{c_3 . s_3}{2}$$

THE DERIVATION OF THE ANALYTICAL RELATIONS

In order to derive analytical relations for the sustained subharmonic resonance we will refer to the equation A5.2.

If $\nu = 3$ is taken in this equation by the harmonic balance rule we obtain the equations

$$0 = \bar{Z}_1 \bar{I}_1 + j\omega \bar{\Psi}_1 \qquad \text{A5.3}$$

$$\bar{V} = \bar{Z}_3 \bar{I}_3 + j 3\omega \bar{\Psi}_3 \qquad \text{A5.4}$$

Substituting the expression of $\bar{I}_1$ into the above equation A5.3 and dividing both sides by $\bar{Z}_1 \bar{\Psi}_1$ we have the equation

$$c_1 + \frac{c_3}{2}\left[3\Psi_1^2 - \frac{3(\bar{\Psi}_1^*)^2}{\bar{\Psi}_1}\bar{\Psi}_3 + 6\Psi_3^2\right] + \frac{j\omega}{\bar{Z}_1} = 0 \qquad \text{A5.5}$$

Splitting this into the real and imaginary part we get

$$c_1 + \frac{c_3}{2}\left(3\Psi_1^2 - 3\Psi_1\Psi_3\cos(\theta_3 - 3\theta_1) + 6\Psi_3^2\right) + \frac{\omega}{Z_1}\cos\left(\frac{\pi}{2} - \xi_1\right) = 0$$

$$\frac{c_3}{2}\left(-3\Psi_1\Psi_3\sin(\theta_3 - 3\theta_1)\right) + \frac{\omega}{Z_1}\sin\left(\frac{\pi}{2} - \xi_1\right) = 0$$

Rearranging these such that

$$\Psi_1\Psi_3\cos(\theta_3 - 3\theta_1) = \left(c_1 + \frac{\omega}{Z_1}\cos\left(\frac{\pi}{2} - \xi_1\right)\right)\frac{2}{3c_3} + \Psi_1^2 + 2\Psi_3^2$$

$$\Psi_1\Psi_3\sin(\theta_3 - 3\theta_1) = \frac{2\omega}{3c_3Z_1}\sin\left(\frac{\pi}{2} - \xi_1\right)$$

then squaring both sides and adding, finally we find

$$\Psi_1^4 + 3\Psi_1^2\Psi_3^2 + 2\Psi_1^2 D_1 + 4\Psi_3^4 + 4\Psi_3^2 D_1 + D_1^2 + E_1^2 = 0 \qquad \text{A5.6}$$

where

$$D_1 = \left(c_1 + \frac{\omega}{Z_1}\cos\left(\frac{\pi}{2} - \xi_1\right)\right)\frac{2}{3c_3}$$

$$E_1 = \frac{2\omega}{3c_3Z_1}\sin\left(\frac{\pi}{2} - \xi_1\right)$$

From equation A5.6 the roots of Ψ_1 are

$$(\Psi_1^2)_{1,2} = \frac{-(3\,\Psi_3^2 + 2D_1) + \sqrt{\Delta_1}}{2} \qquad \text{A5.7}$$

where
$$\Delta_1 = (3\,\Psi_3^2 + 2D_1)^2 - 4F_1 \qquad \text{A5.8}$$

$$F_1 = 4\,\Psi_3^4 + 4\,\Psi_3^2 D_1 + D_1^2 + E_1^2$$

And from the imaginary part of equation A5.5

$$\sin(\theta_3 - 3\theta_1) = \frac{2\omega}{3c_3 Z_1 \Psi_1 \Psi_3} \cos \xi_1 \qquad \text{A5.9}$$

By the same manner, substituting the expression of $\bar{I}_3$ into the equation A5.4 and dividing both sides by $\bar{Z}_3\,\bar{\Psi}_3$ we arrive at the equation

$$c_1 + \frac{c_3}{2}\left(3\,\bar{\Psi}_3\,\bar{\Psi}_3^* + 6\,\bar{\Psi}_1\,\bar{\Psi}_1^* - \frac{\bar{\Psi}_1^3}{\bar{\Psi}_3}\right) + j\,\frac{3\omega}{\bar{Z}3} - \frac{\bar{V}}{\bar{\Psi}_3\bar{Z}_3} = 0 \qquad \text{A5.10}$$

If this is split into the real and imaginary parts we find

$$A_1 = A_2 \cos(3\theta_1 - \theta_3) + A_3 \cos(\xi_3 + \theta_3)$$

and
$$A_4 = A_2 \sin(3\theta_1 - \theta_3) + A_3 \sin(\xi_3 + \theta_3) \qquad \text{A5.11}$$

where

$$A_1 = D_3 + 3\,\Psi_3^2 + 6\,\Psi_1^2$$

$$A_2 = \frac{\Psi_1^3}{\Psi_3}$$

$$A_3 = \frac{2V}{c_3 Z_3 \Psi_3}$$

$$A_4 = E_3$$

$$D_3 = \left(c_1 + \frac{3\omega}{Z_3} \sin \xi_3\right)\frac{2}{c_3}$$

$$E_3 = \frac{6\omega}{c_3 Z_3} \cos \xi_3$$

Squaring both sides of equations A5.11 then adding we obtain

$$\cos\,(3\theta_1 + \xi_3) = \frac{A_1^{\,2} + A_4^{\,2} - (A_2^{\,2} + A_3^{\,2})}{2\,A_2\,A_3} \qquad \text{A5.12}$$

DIAGRAMS

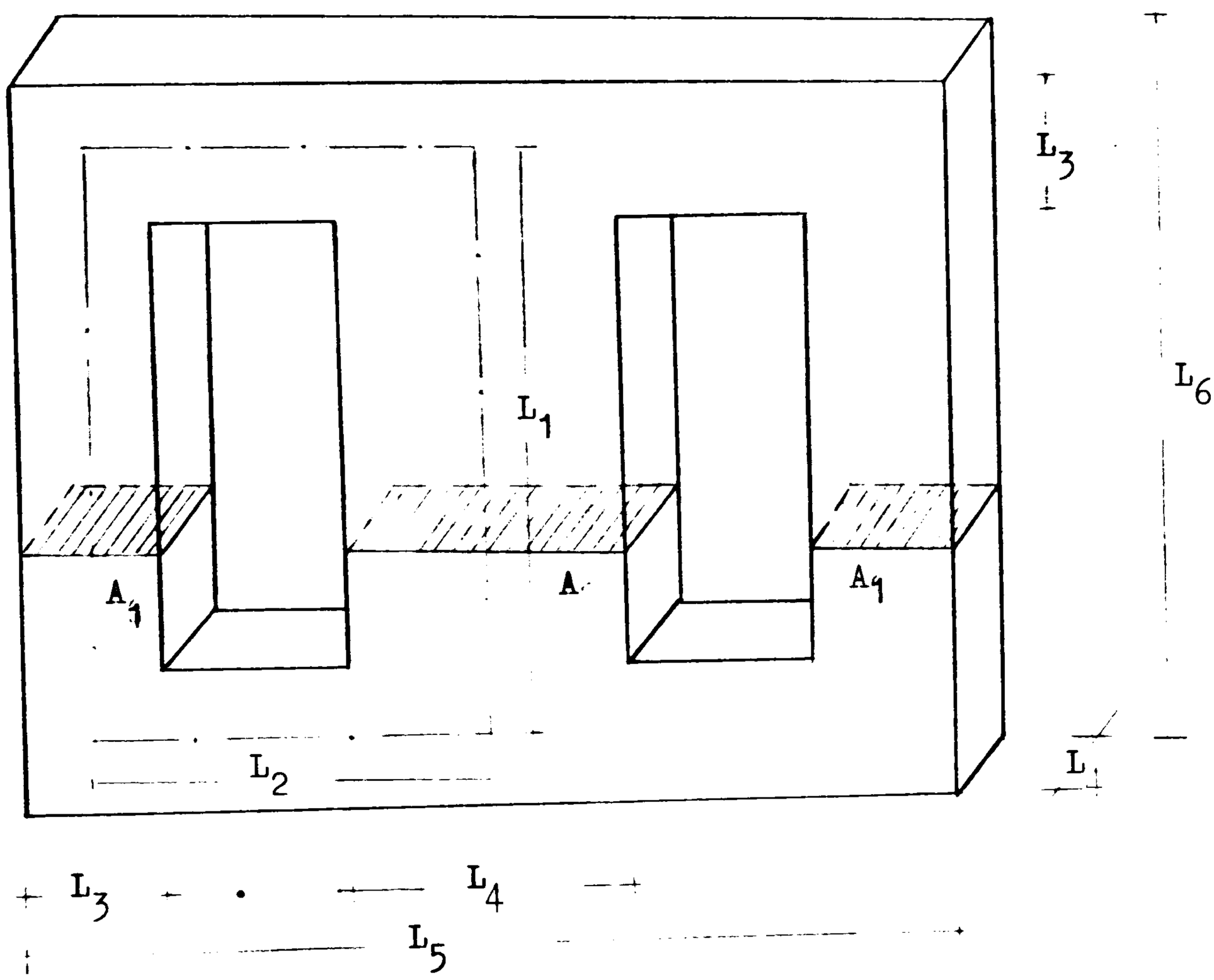

Fig. 1.1 Single phase shell type transformer construction

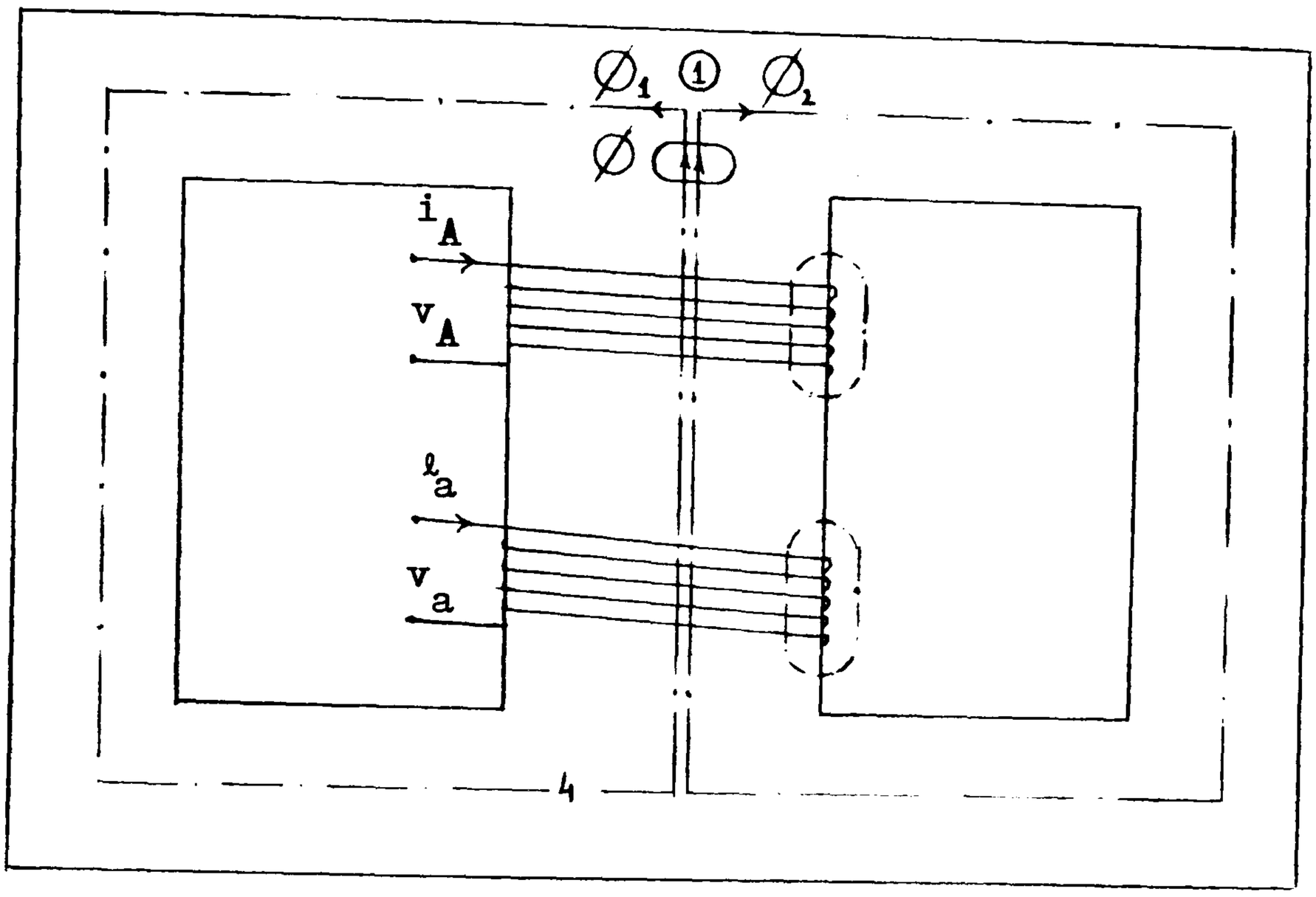

Fig. 1.2 Paths of fluxes in a concentric coil, shell type transformer

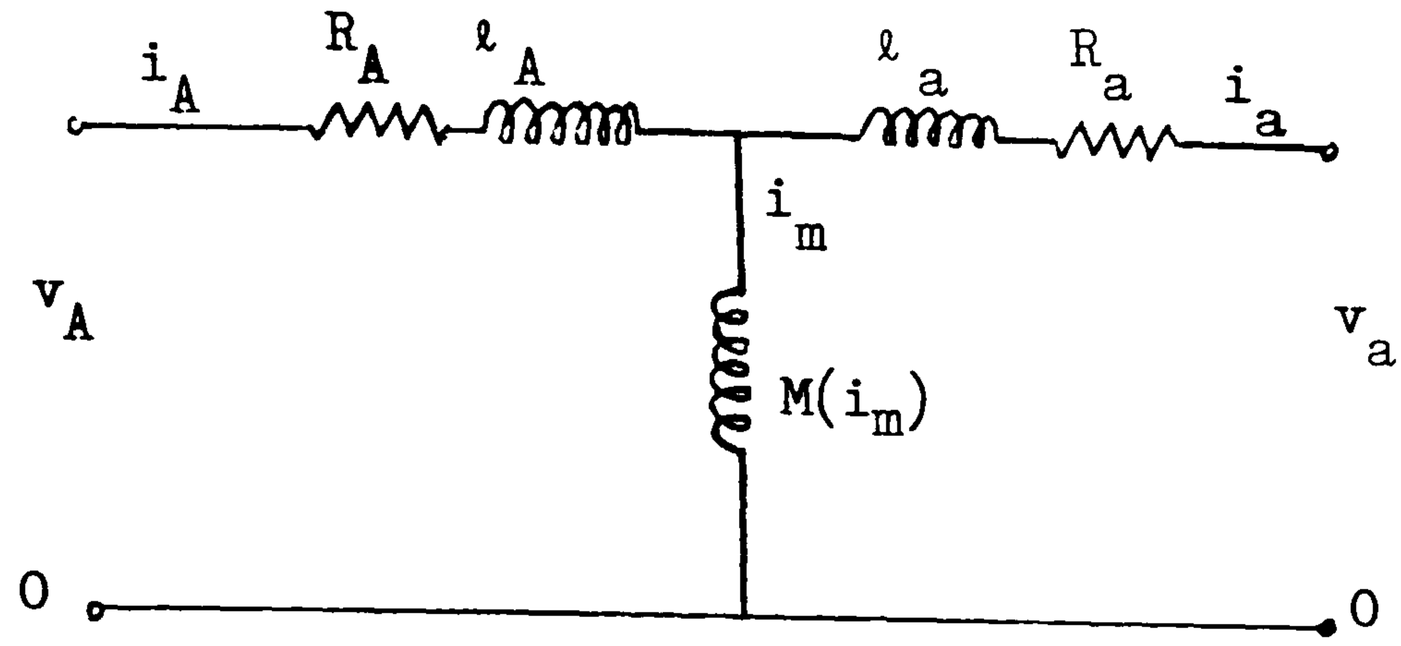

Fig. 1.3 Single phase transformer equivalent circuit

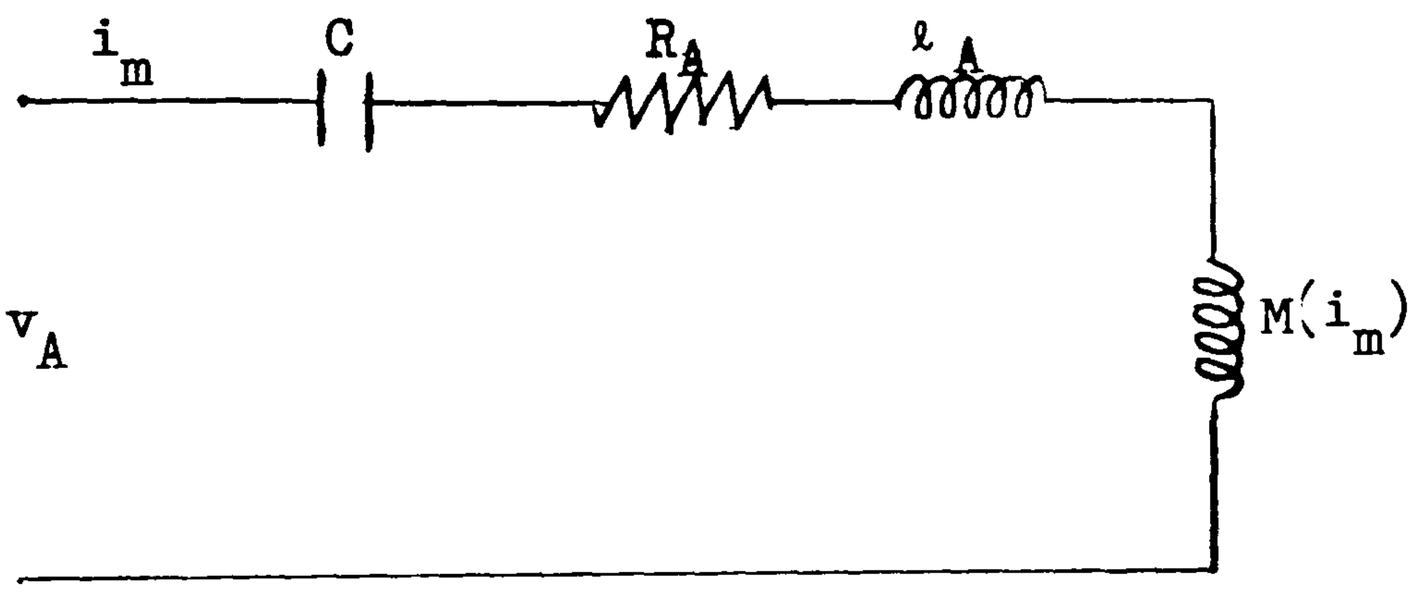

Fig. 1.4 Single phase series ferroresonance circuit

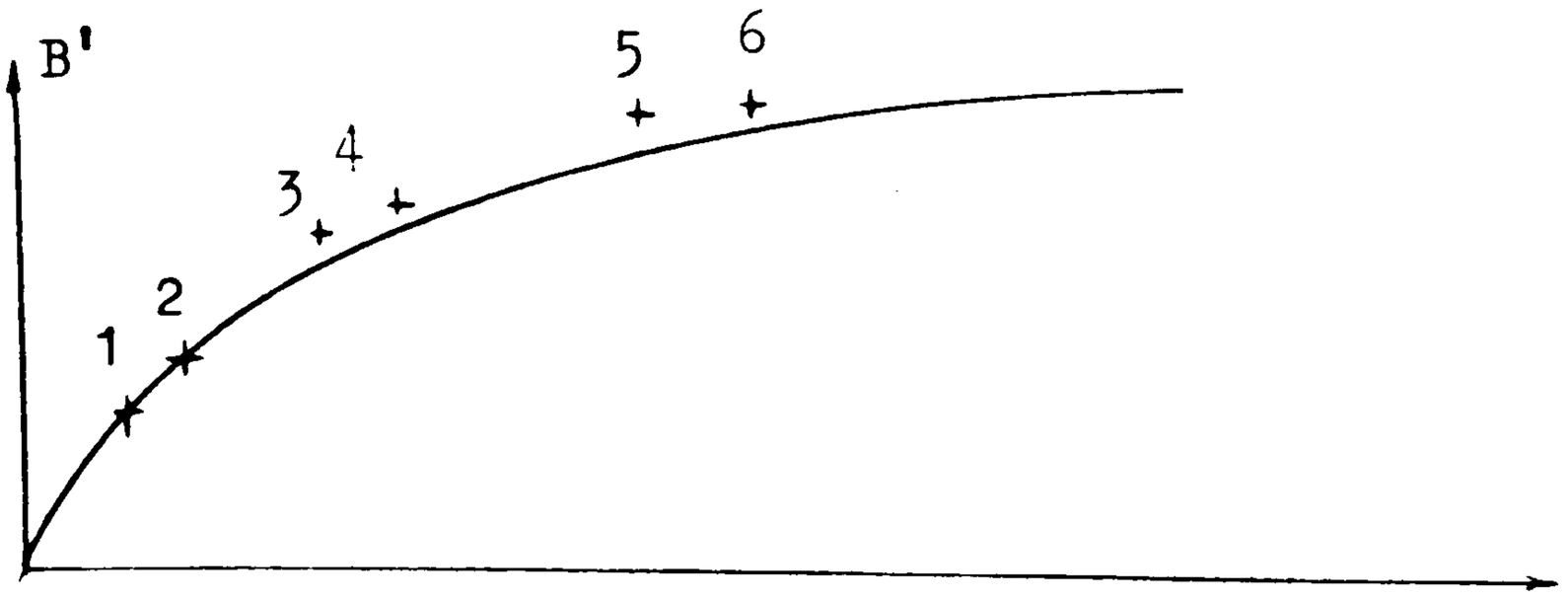

\+ Experimental points

— $B' = c_1 (1 - \exp(-c_2 H))$

Evaluation of coefficients c_1 and c_2

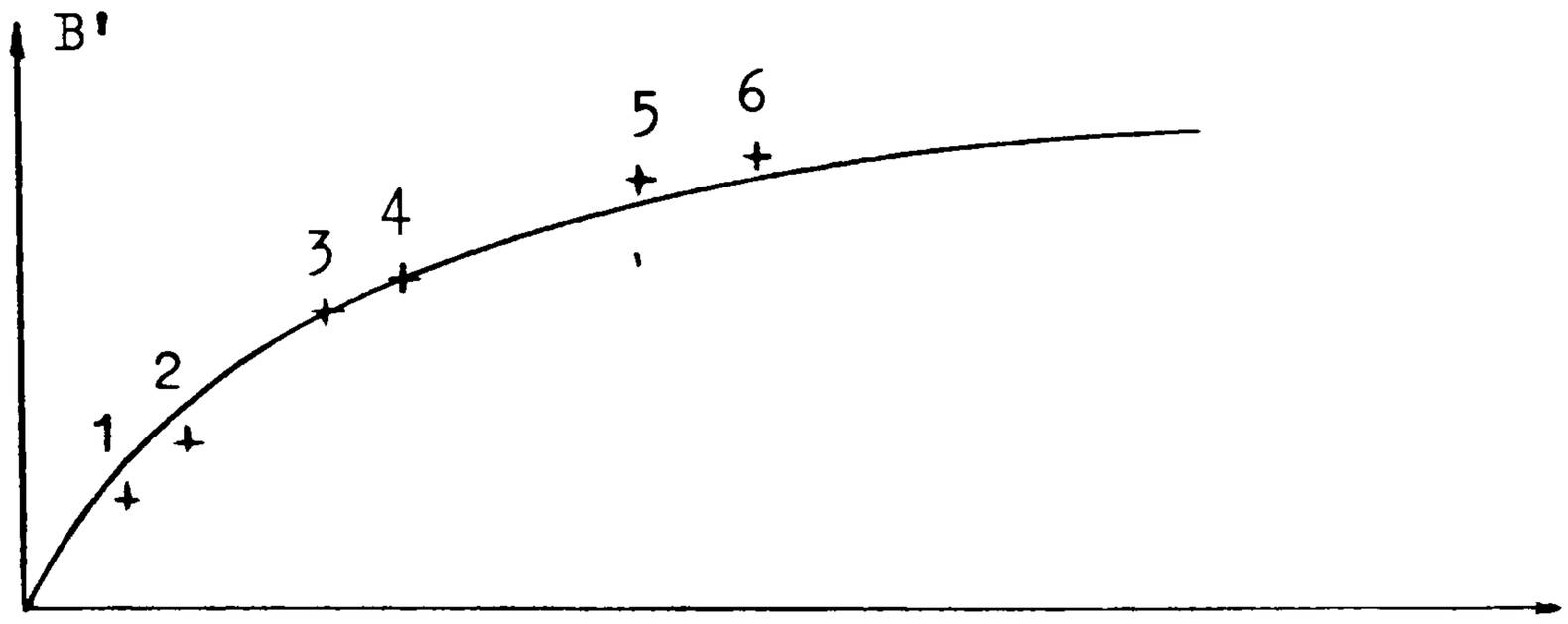

\+ Experimental points

— $B' = c_1 (1 - \exp(-c_2 H)) + c_3 (1 - \exp(-c_4 H))$

Evaluation of coefficients c_3 and c_4

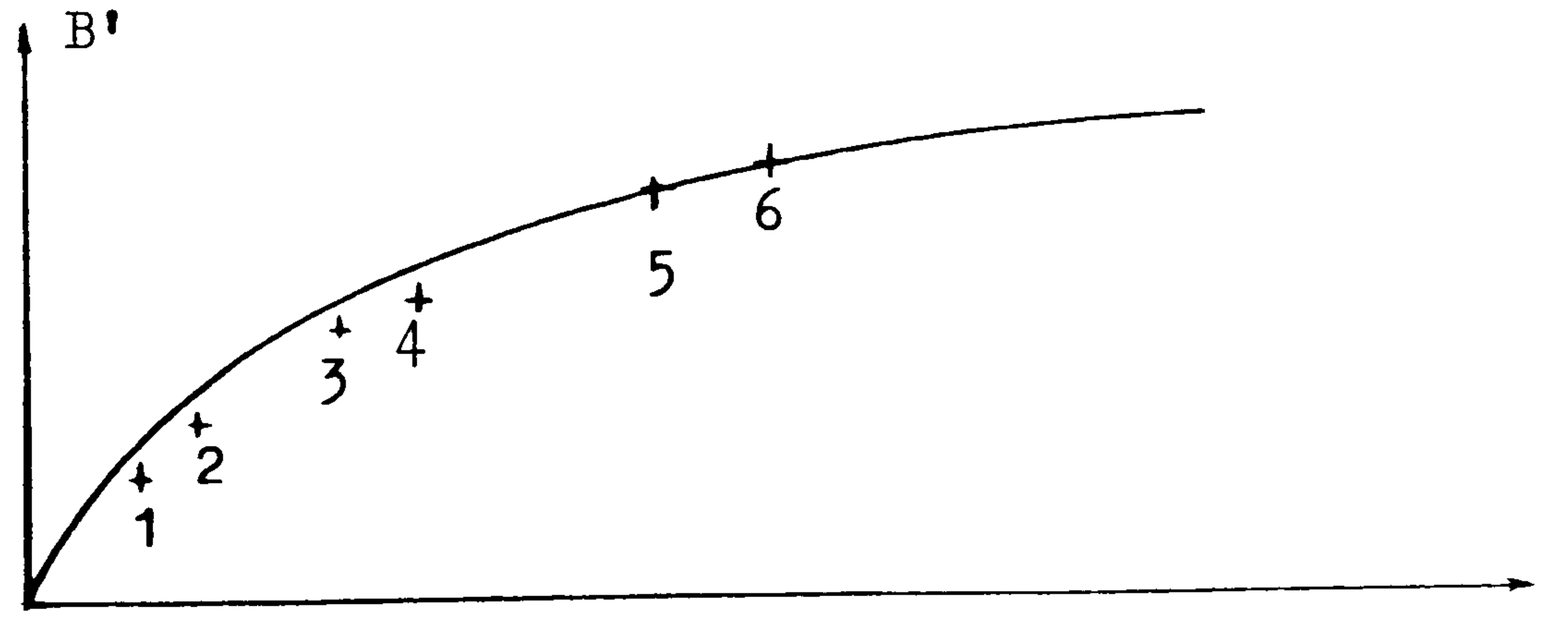

\+ Experimental points

$B' = c_1 (1 - \exp(-c_2 H)) + c_3 (1 - \exp(-c_4 H)) + c_5 (1 - \exp(-c_6 H))$

Evaluation of coefficients c_5 and c_6

Fig. 3.1

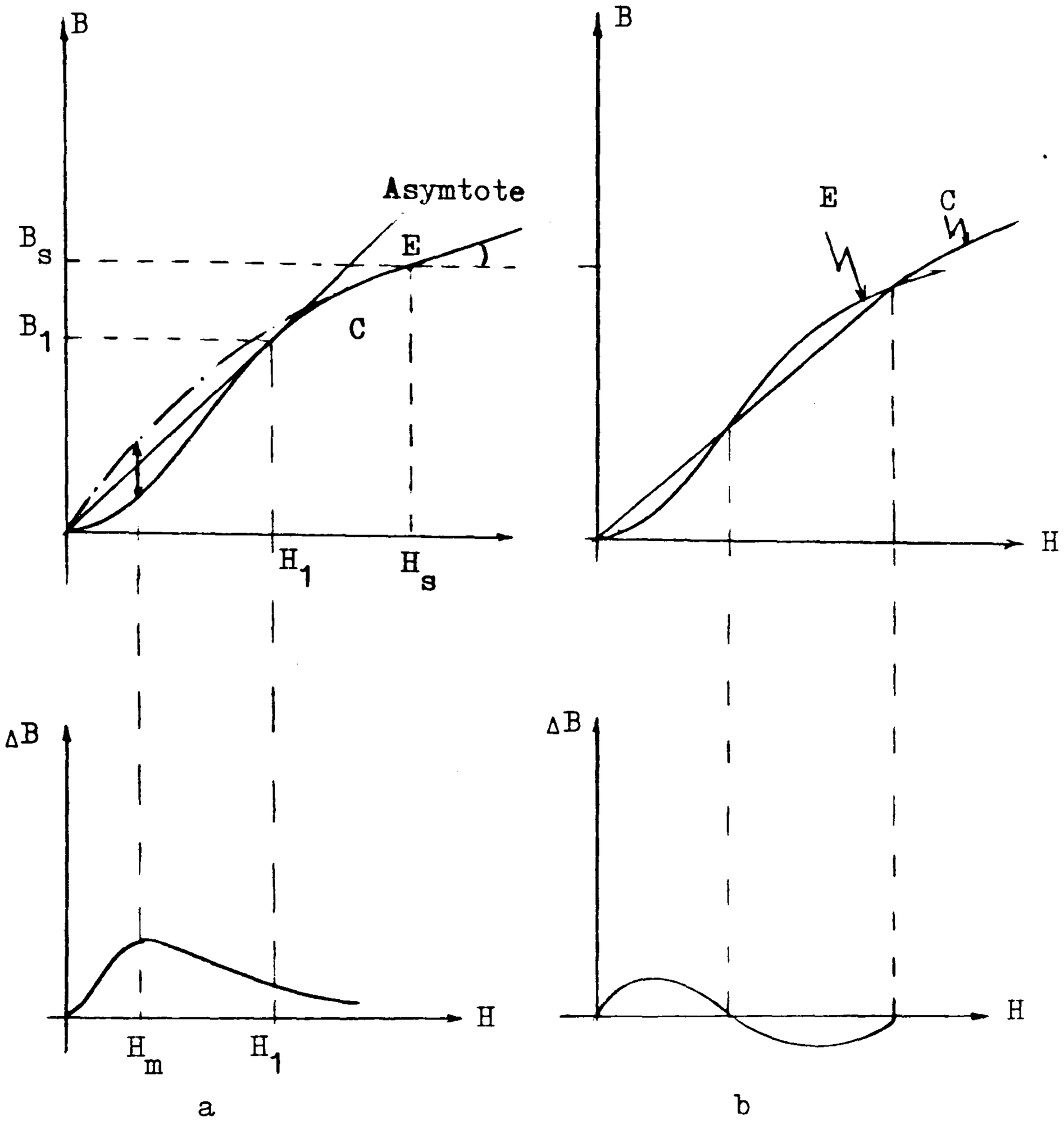

C : Computed curve

E : Experimental curve

ΔB : Difference curve

Fig. 3.2

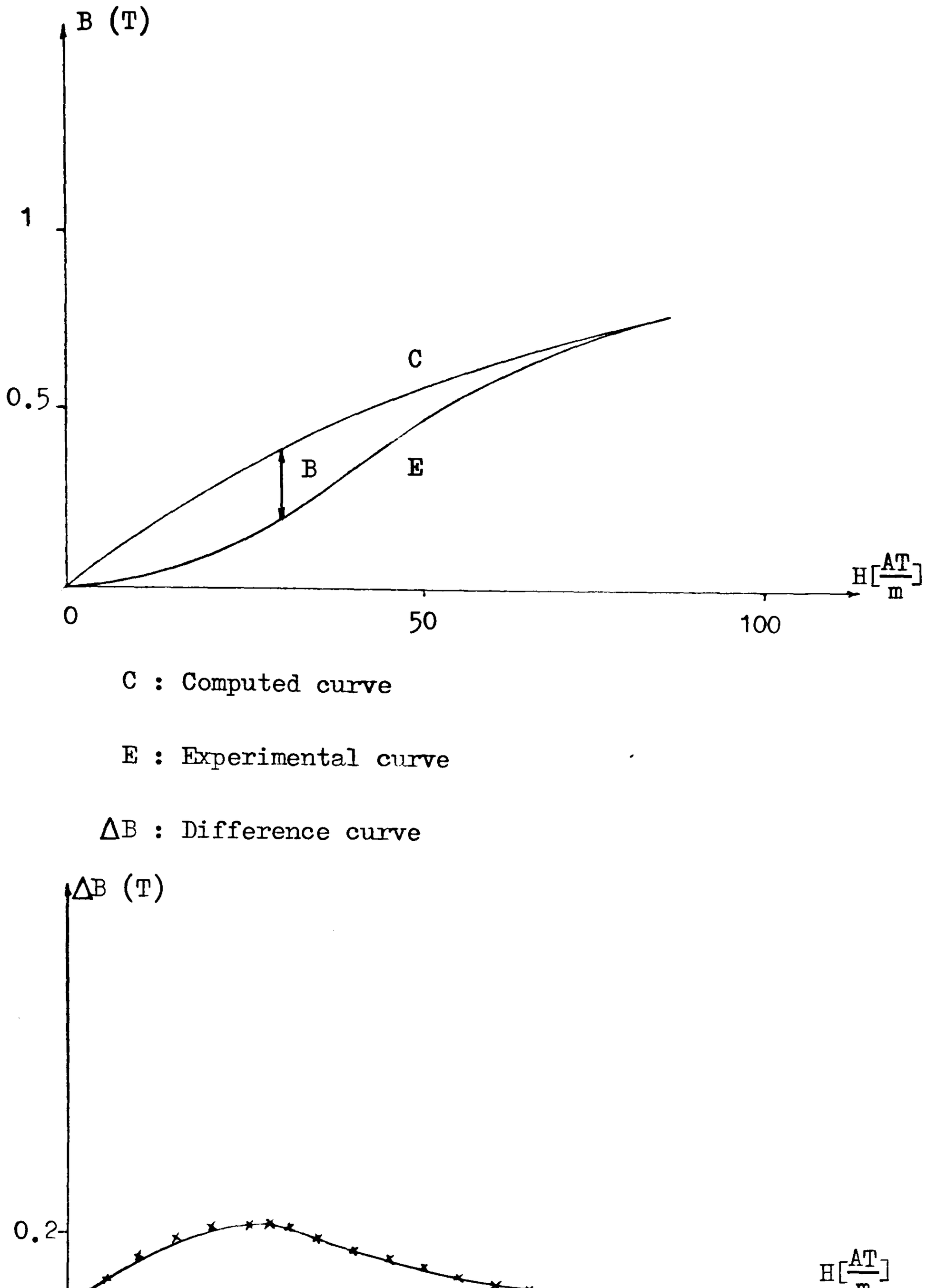

Fig. 3.3 Difference curve

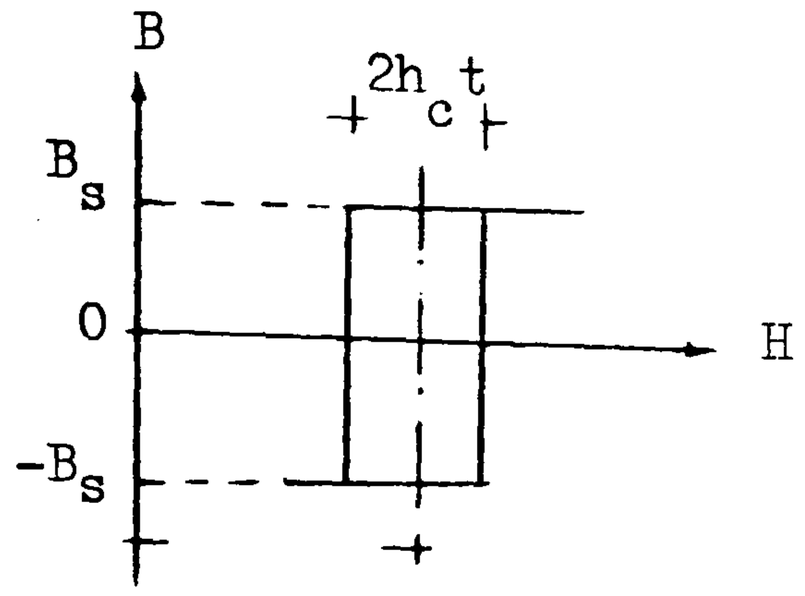

The characteristic of the elementary dipole

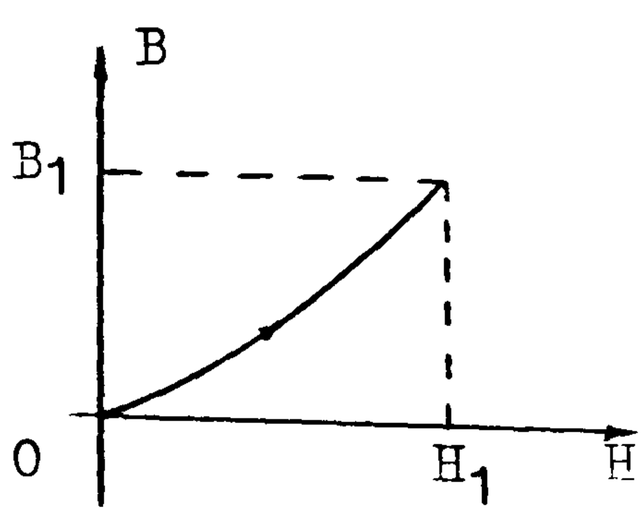

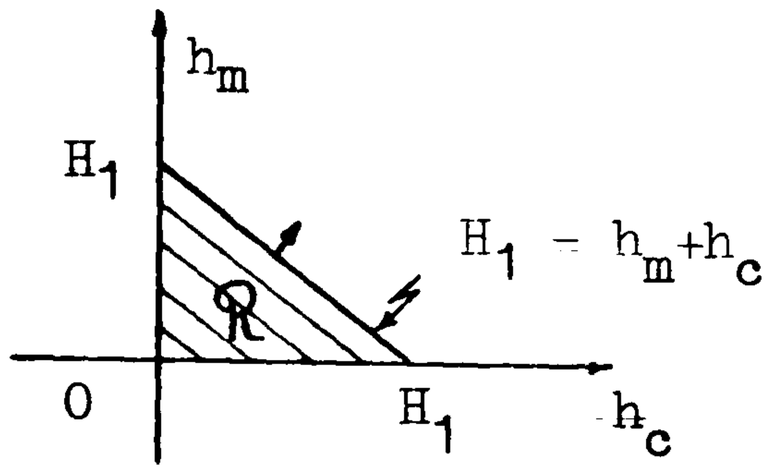

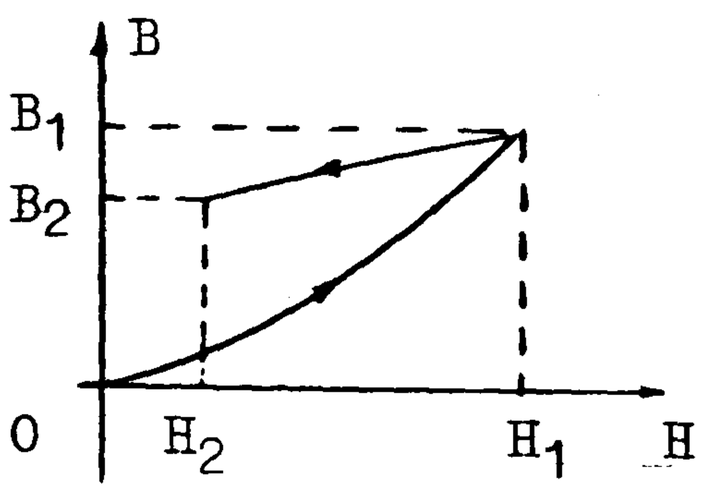

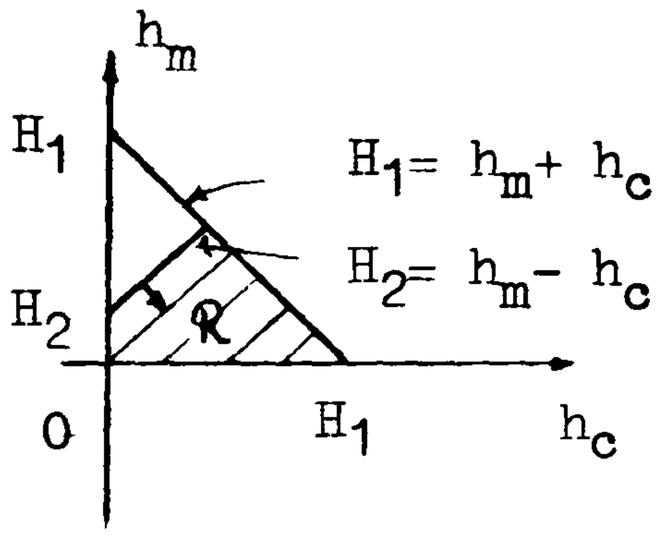

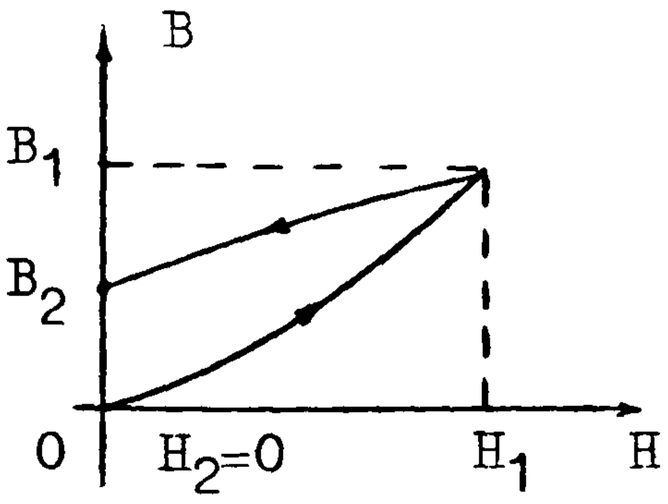

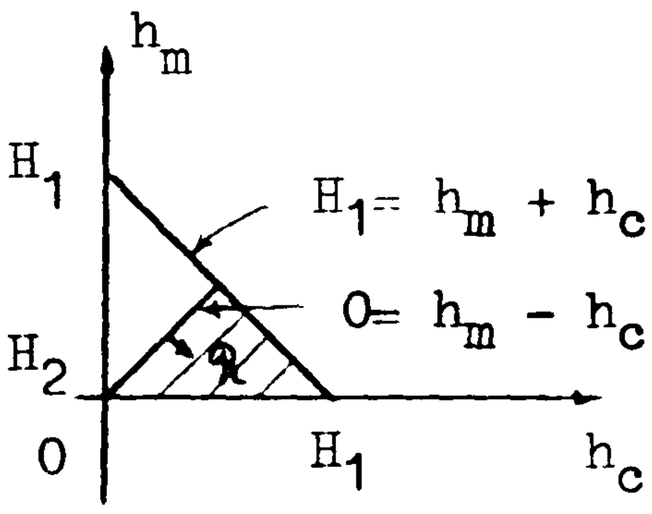

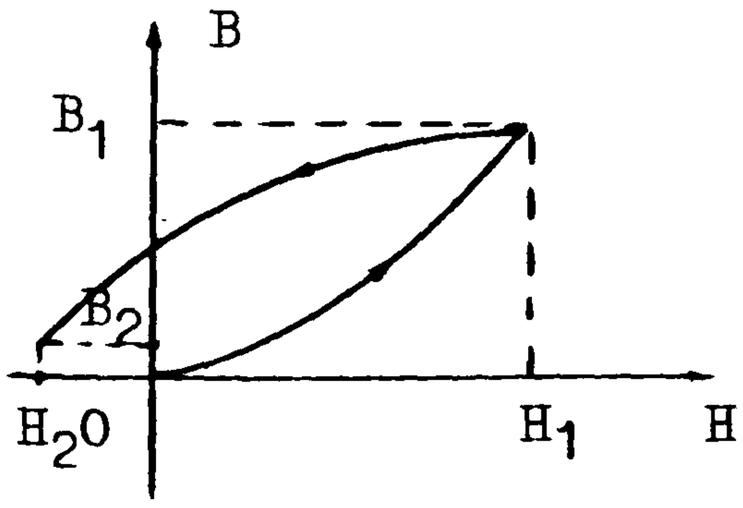

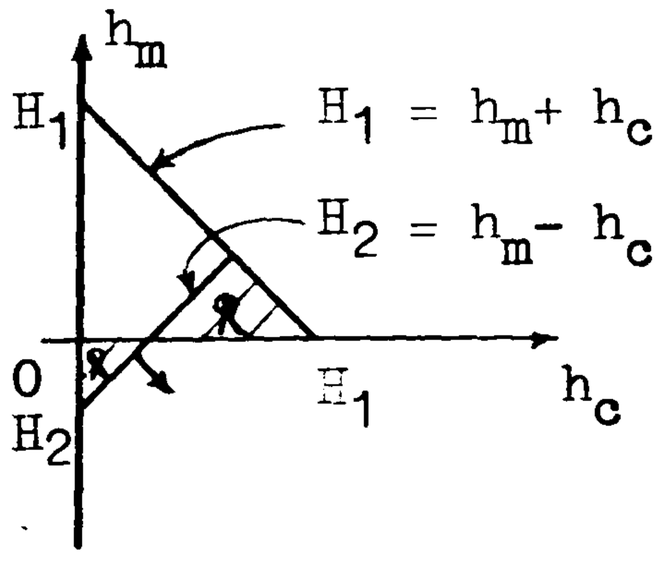

Fig. 3.4 Various B/H characteristics and corresponding Preisach diagrams

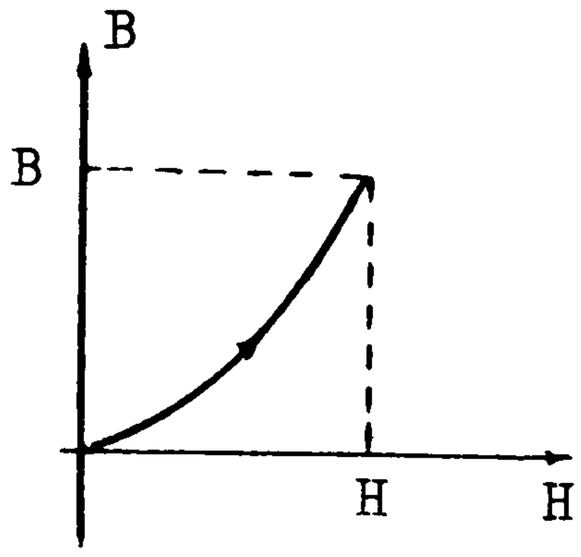

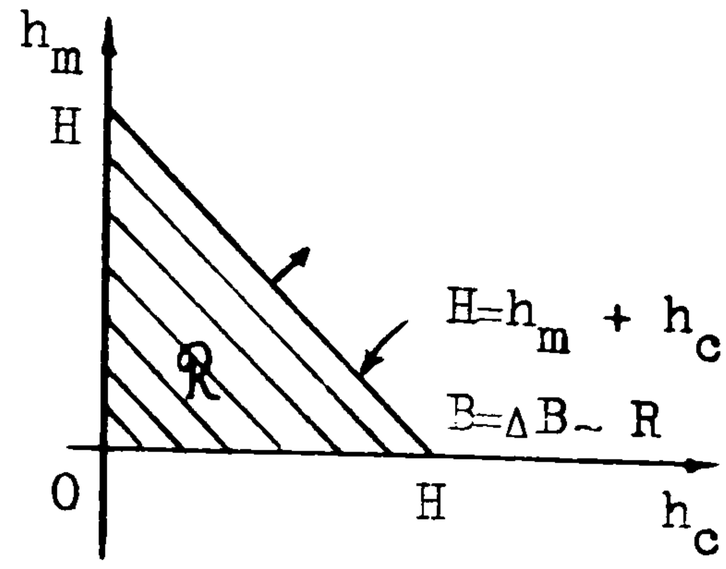

a. First type of B function ($\Delta B = B_1(H)$, $\mu = \mu_1 (H)$)

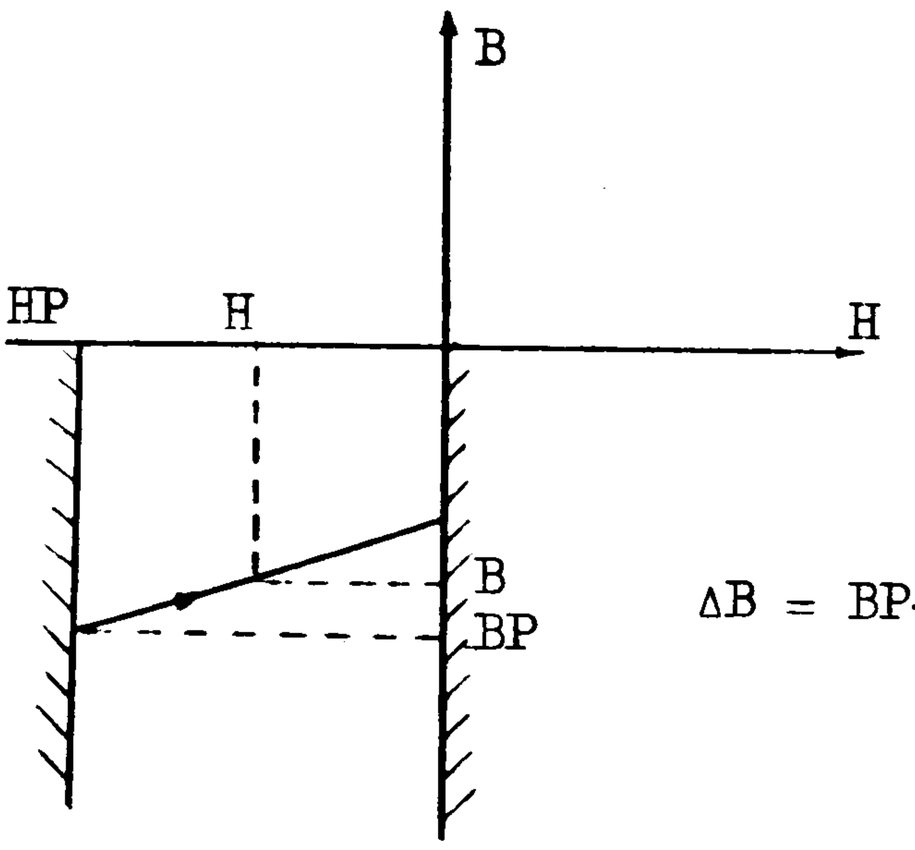

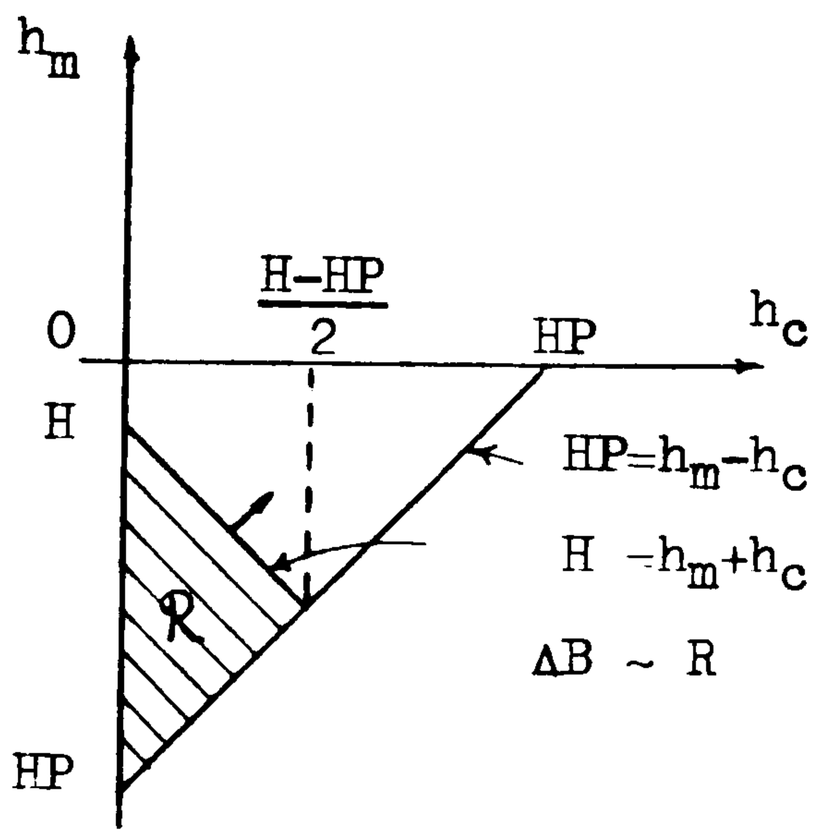

b. Second type of B function ($\Delta B = B_2(H,HP)$, $\mu = \mu_2 (H,HP)$)

c. Third type of B function ($\Delta B = B_3 (H,HP)$, $\mu = \mu_3 (H,HP)$)

Fig. 3.5

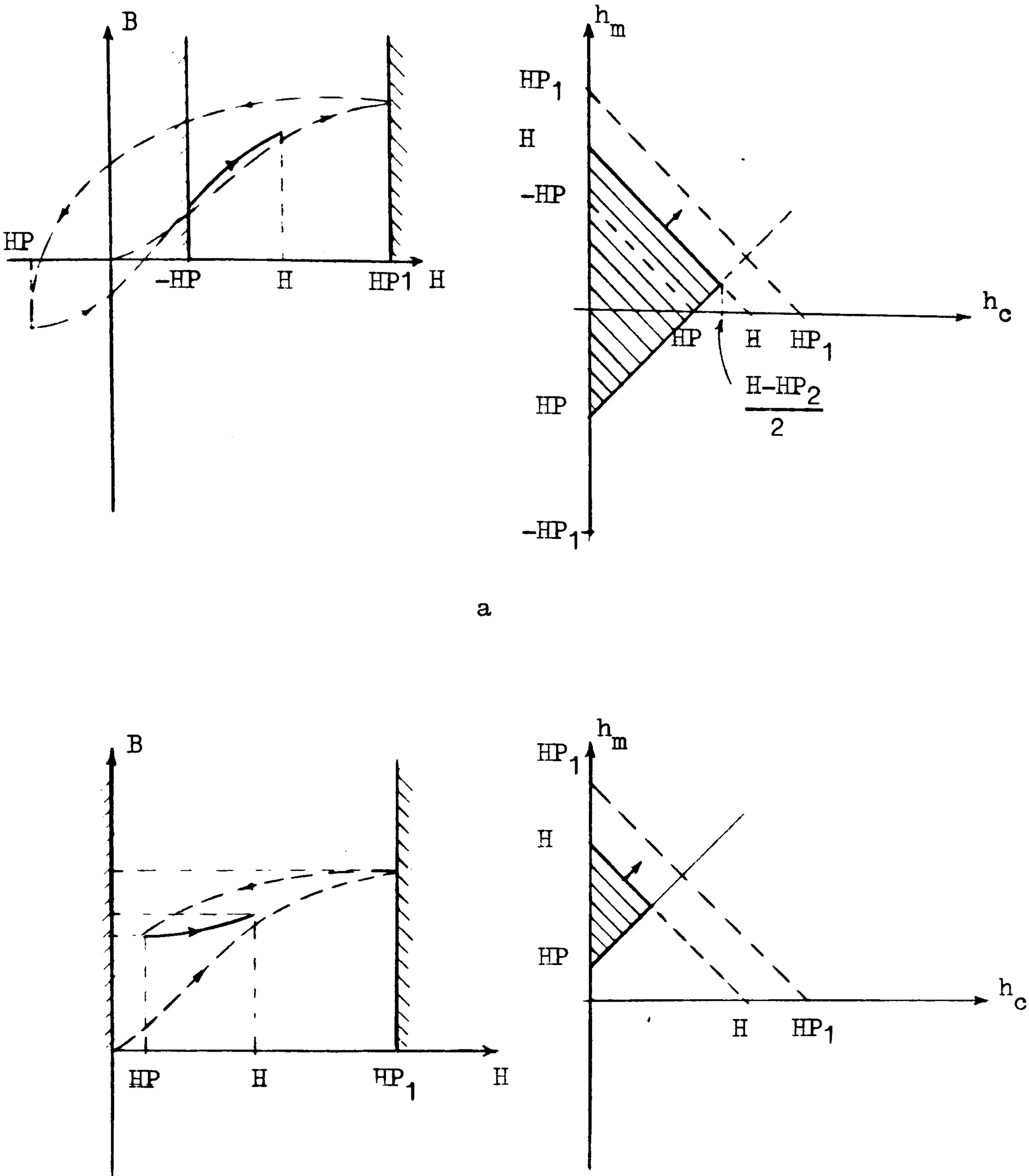

Fig. 3.6 Abnormal B/H characteristics and corresponding Preisach diagrams

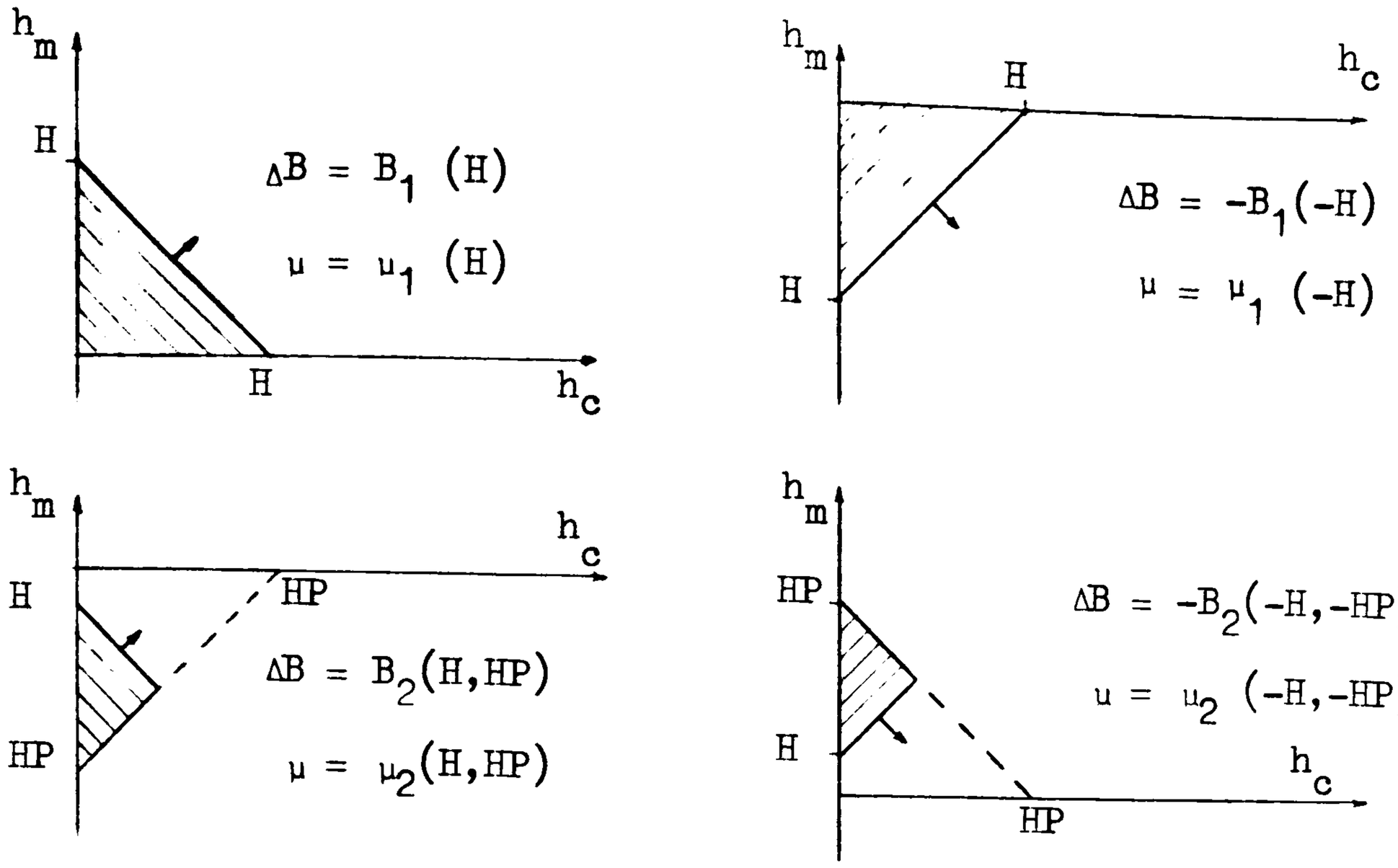

Fig. 3.7 Main and sub-divided Preisach diagrams

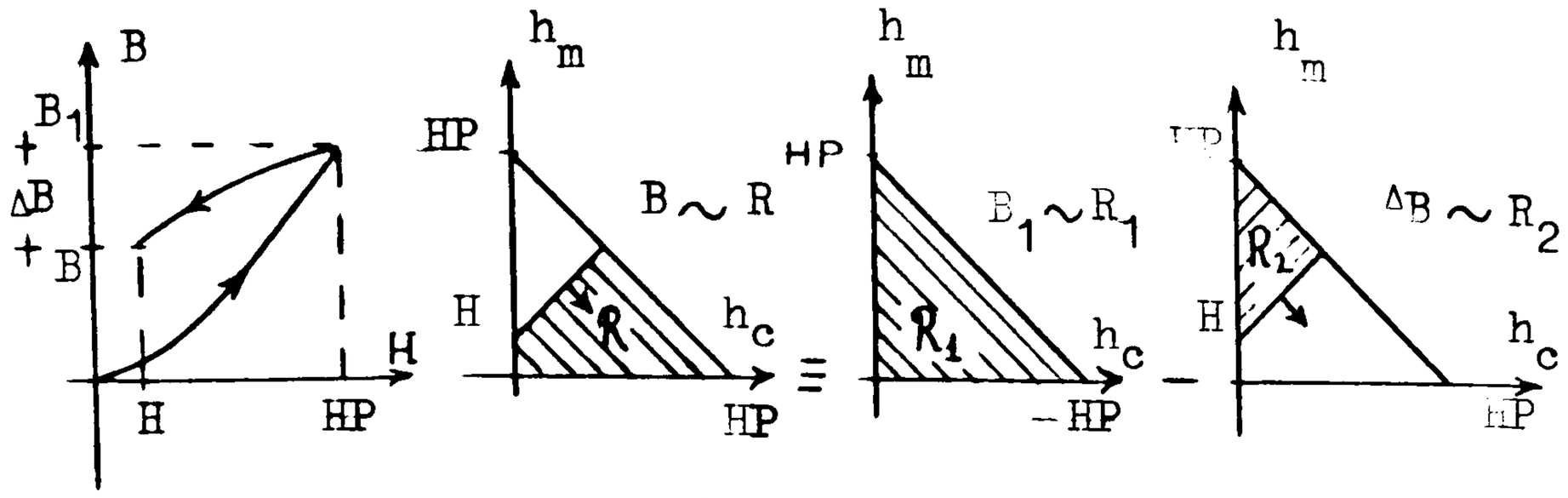

$$B = B_1 - \Delta B$$

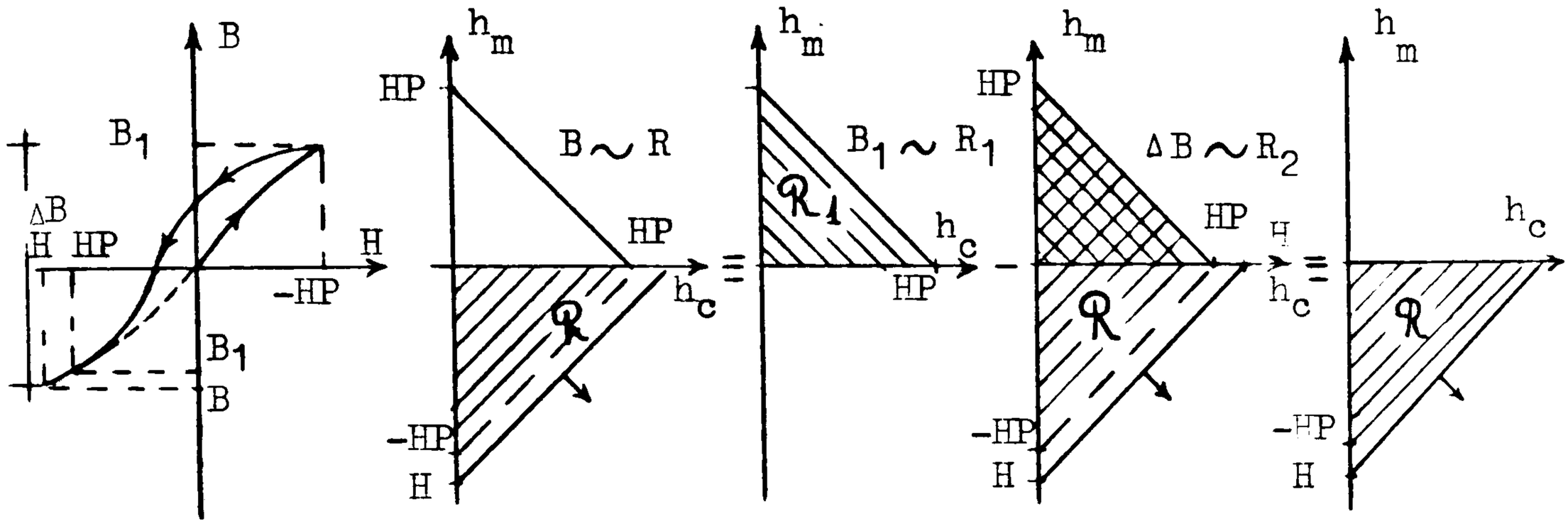

$$B \equiv B_1 - \Delta B \equiv B(-H)$$

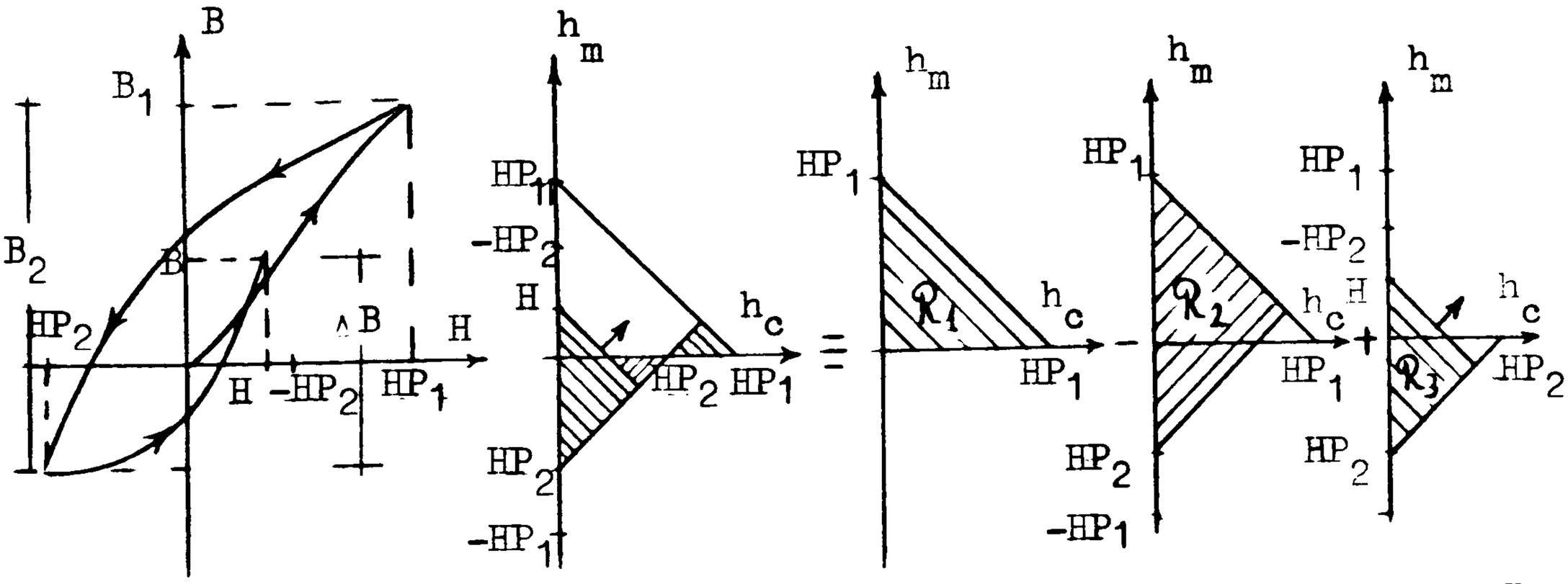

$$B \equiv B_1 - B_2 + \Delta B$$

Fig. 3.8 The calculation of flux density by Preisach theory.

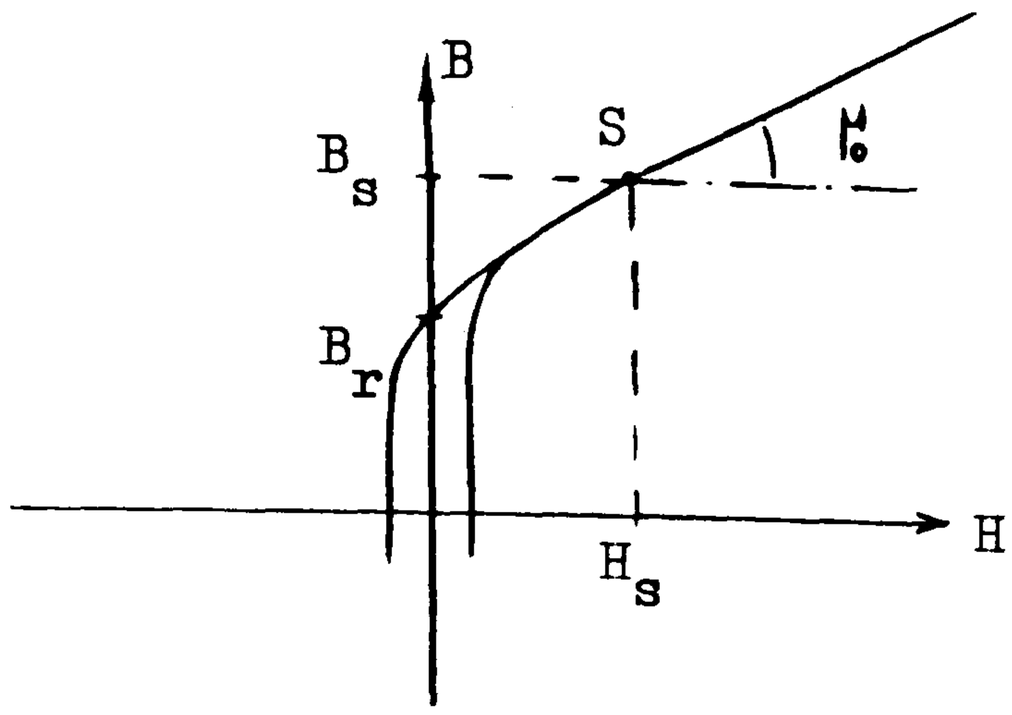

B-H Loop of soft material

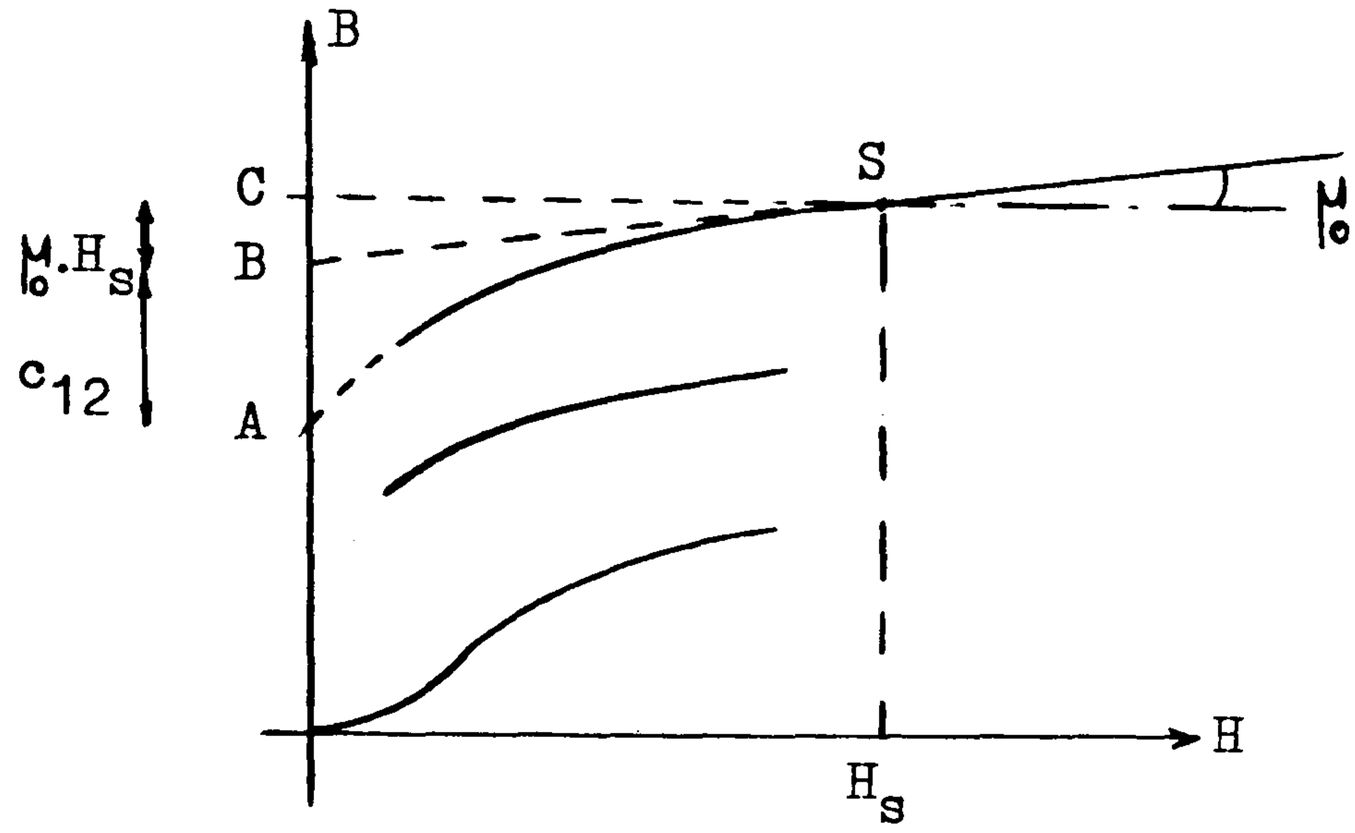

The estimation of c_{12} by drawing

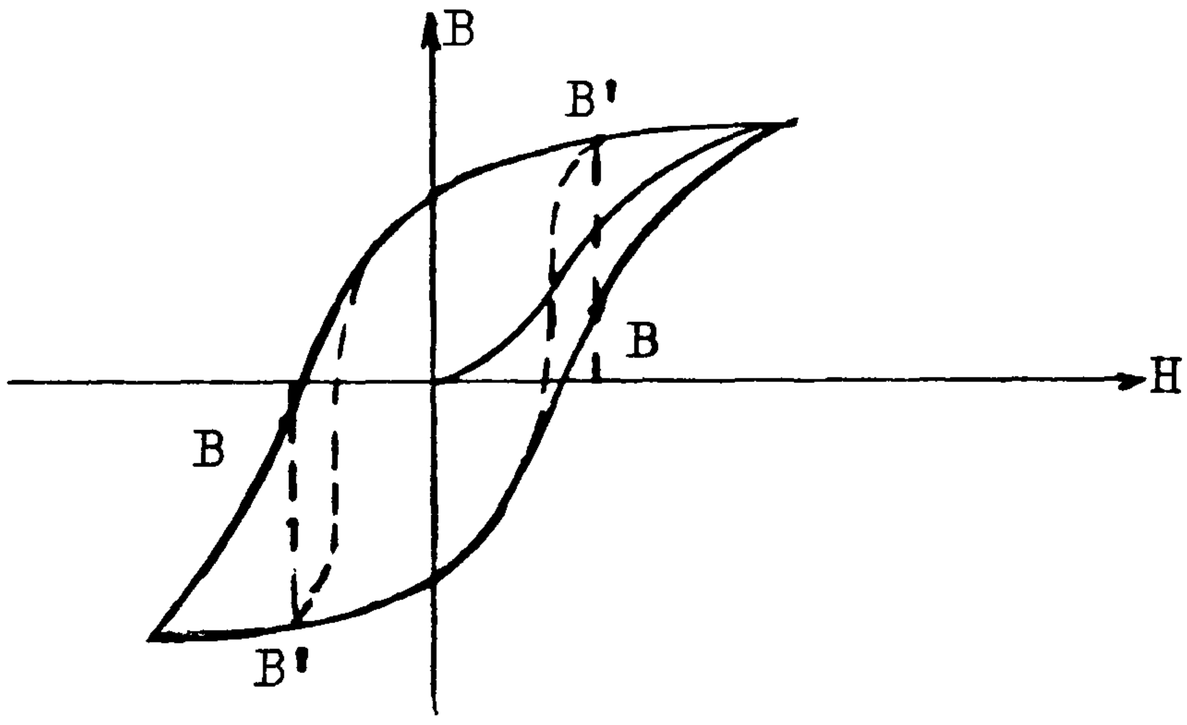

B-H Loop obtained from first term

Fig. 3.9

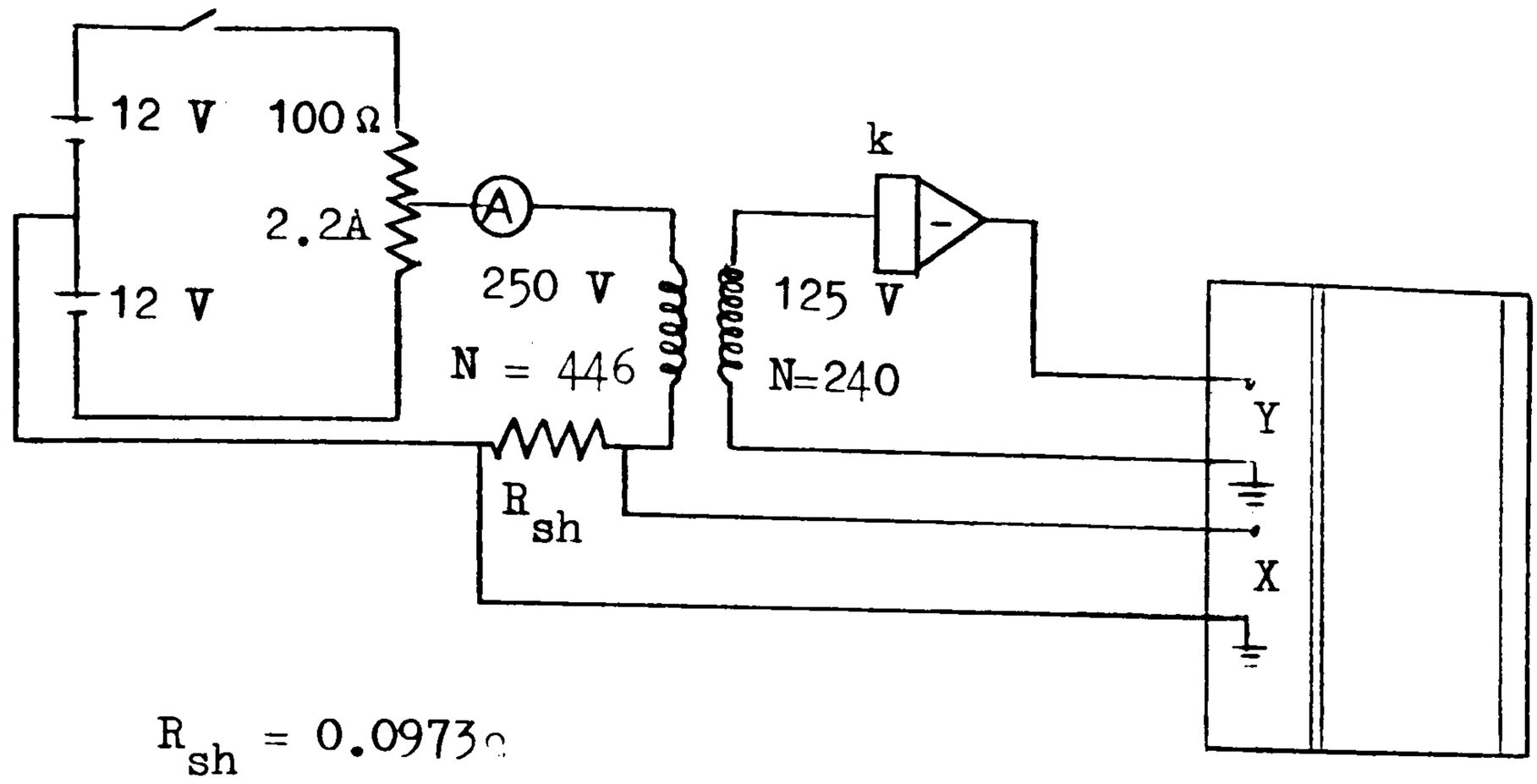

Fig. 3.10 System to measure the B/H characteristic

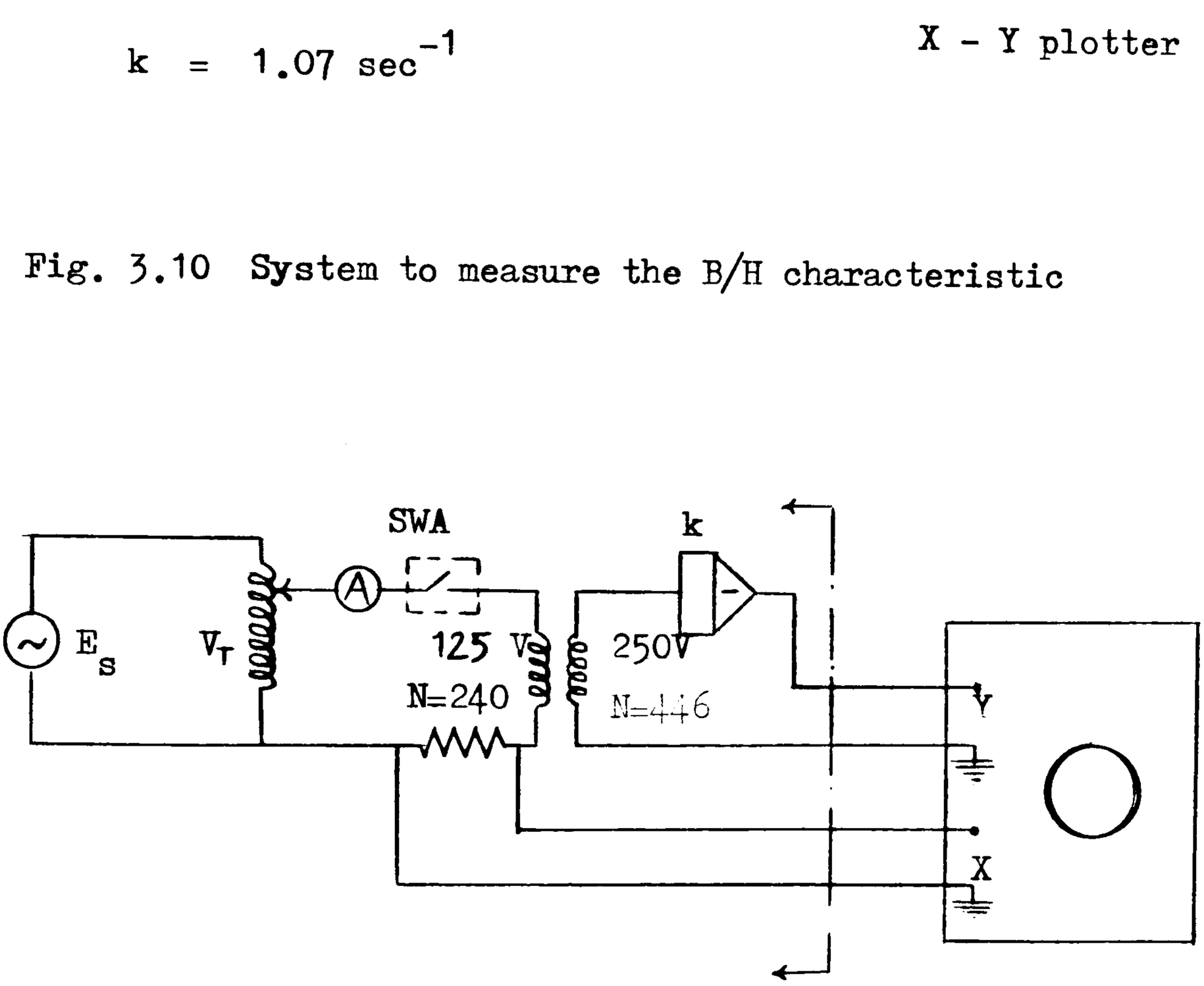

E_s : Supply voltage

V_T : Variable transformer

SWA: Switching angle selector

Fig. 3.11 Transient recording-circuit diagram

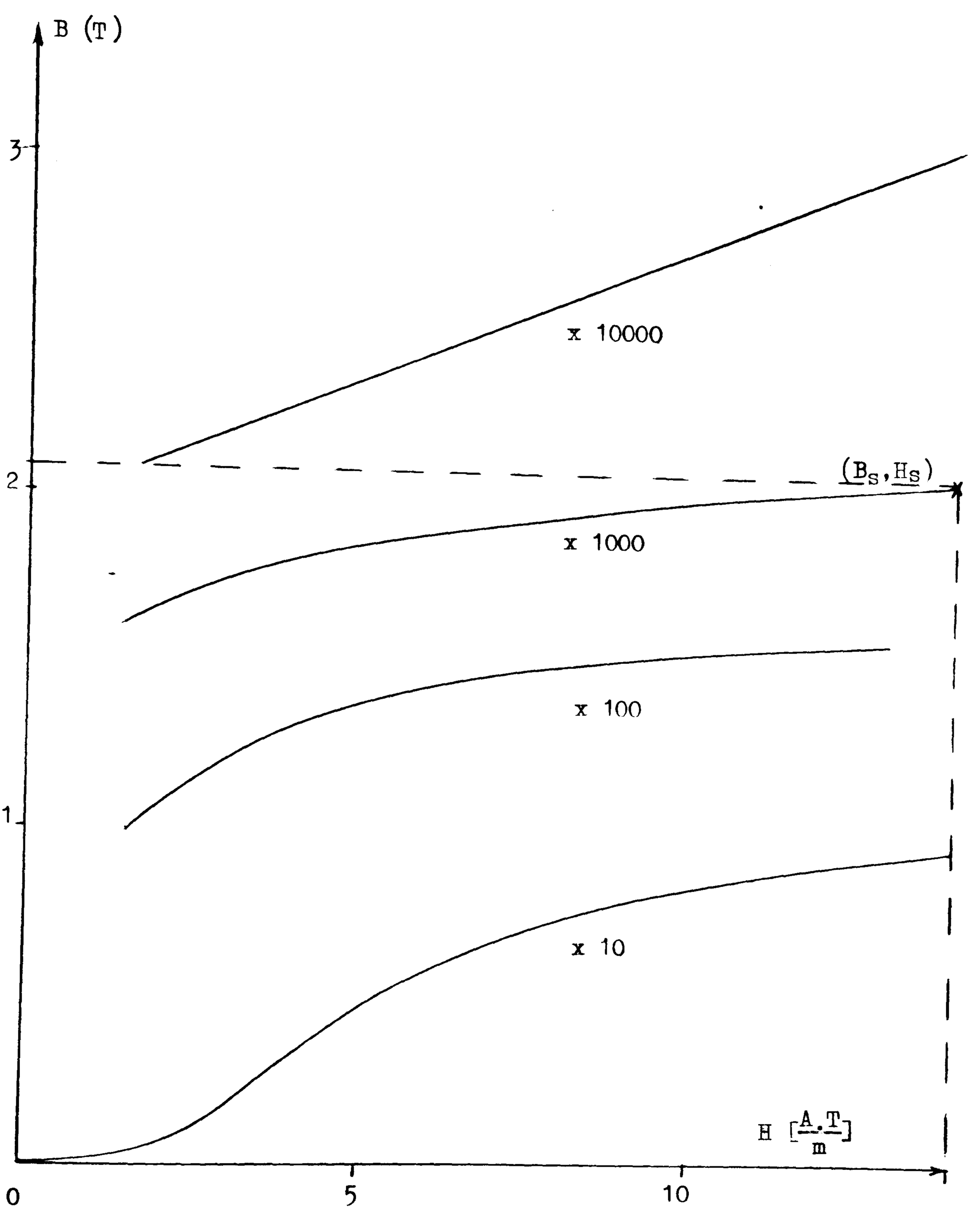

Fig. 3.12 Magnetisation characteristic of the sample transformer

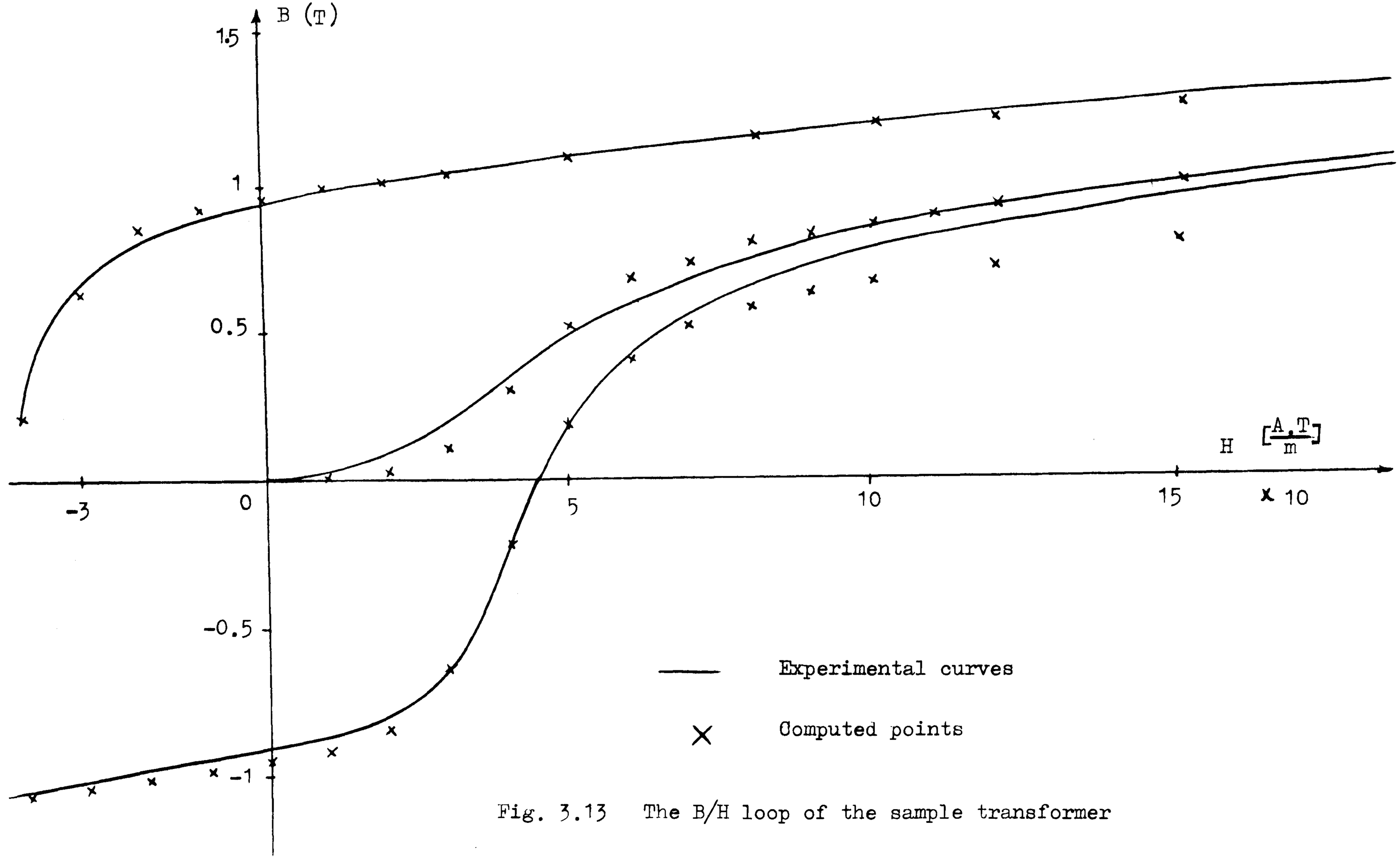

Experimental curves

× Computed points

Fig. 3.13 The B/H loop of the sample transformer

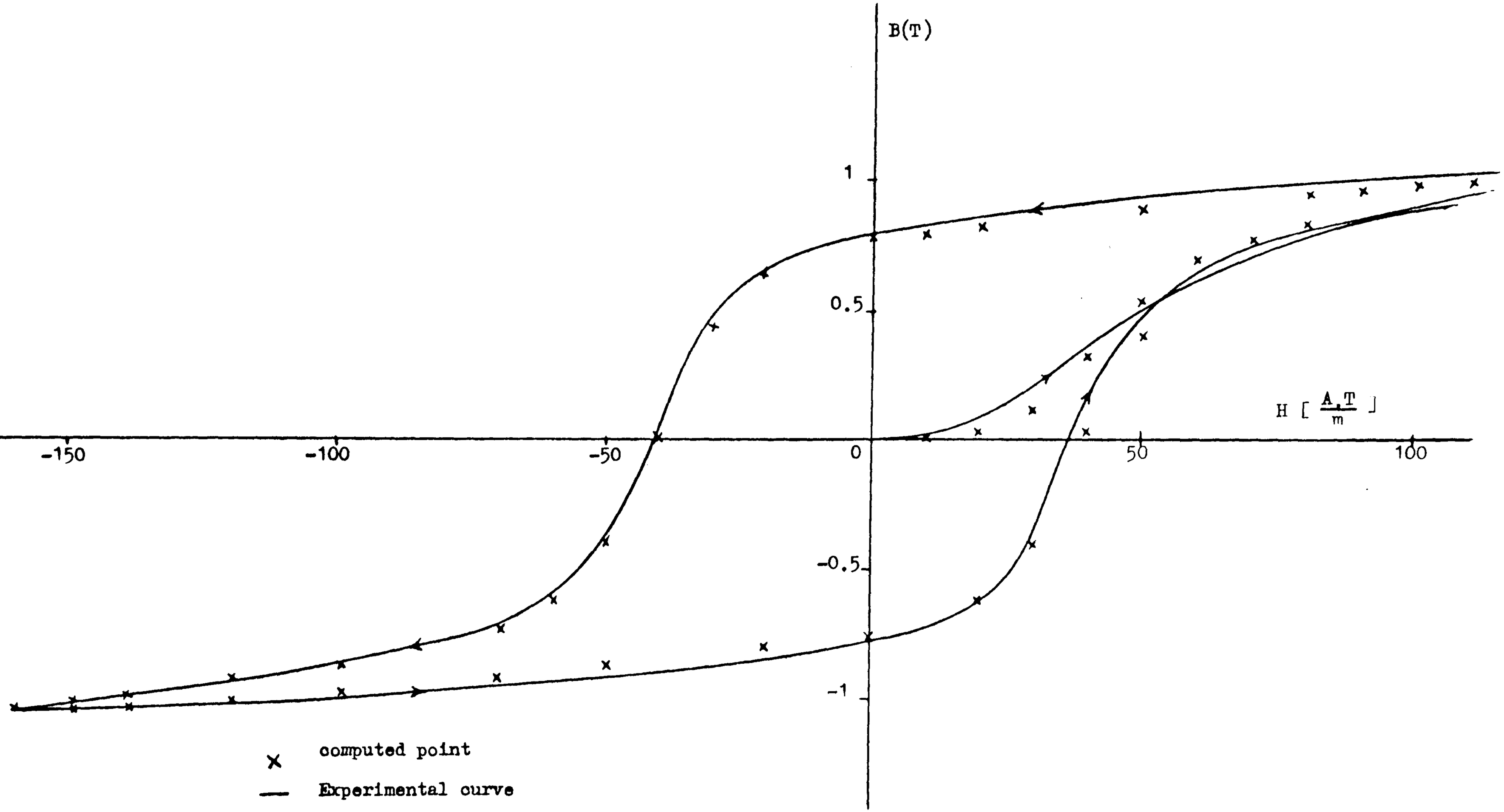

Fig. 3.14 A small loop of the sample transformer

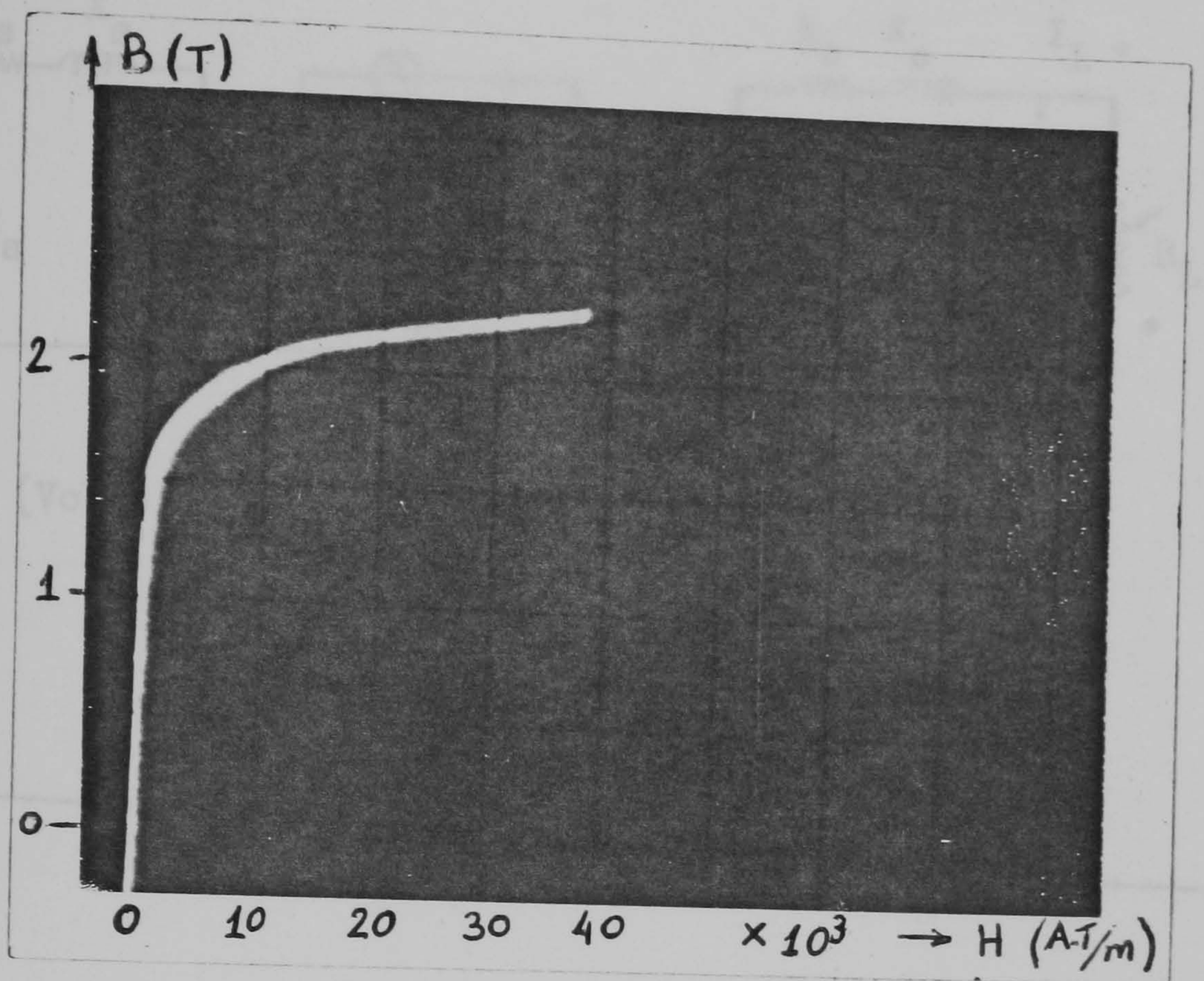

Fig. 3.15 Experimental B/H Characteristics

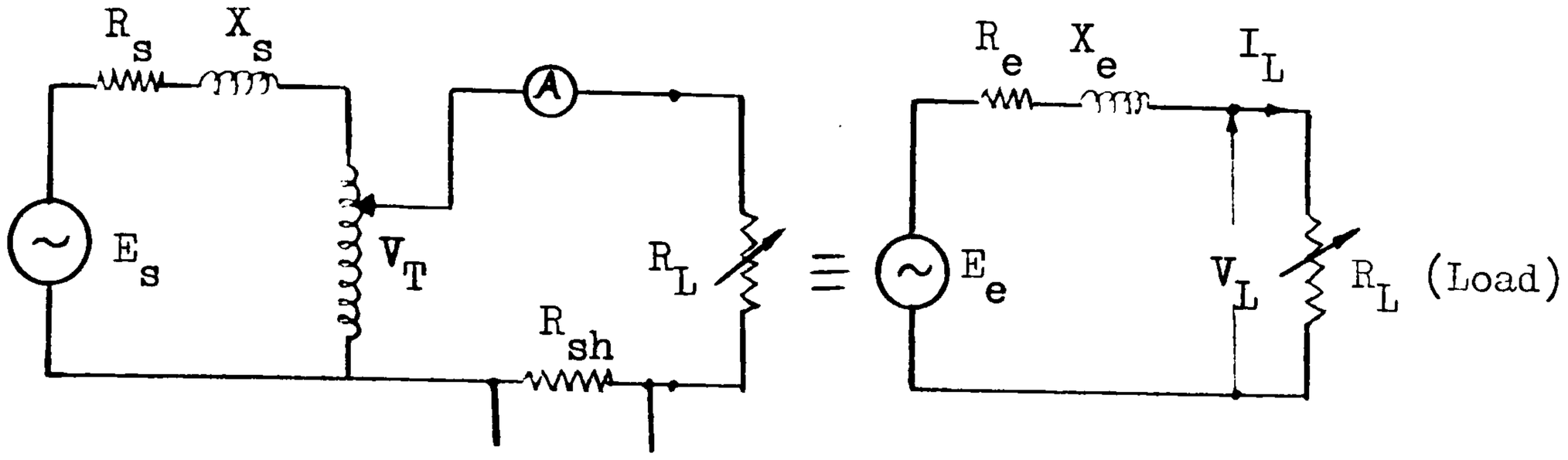

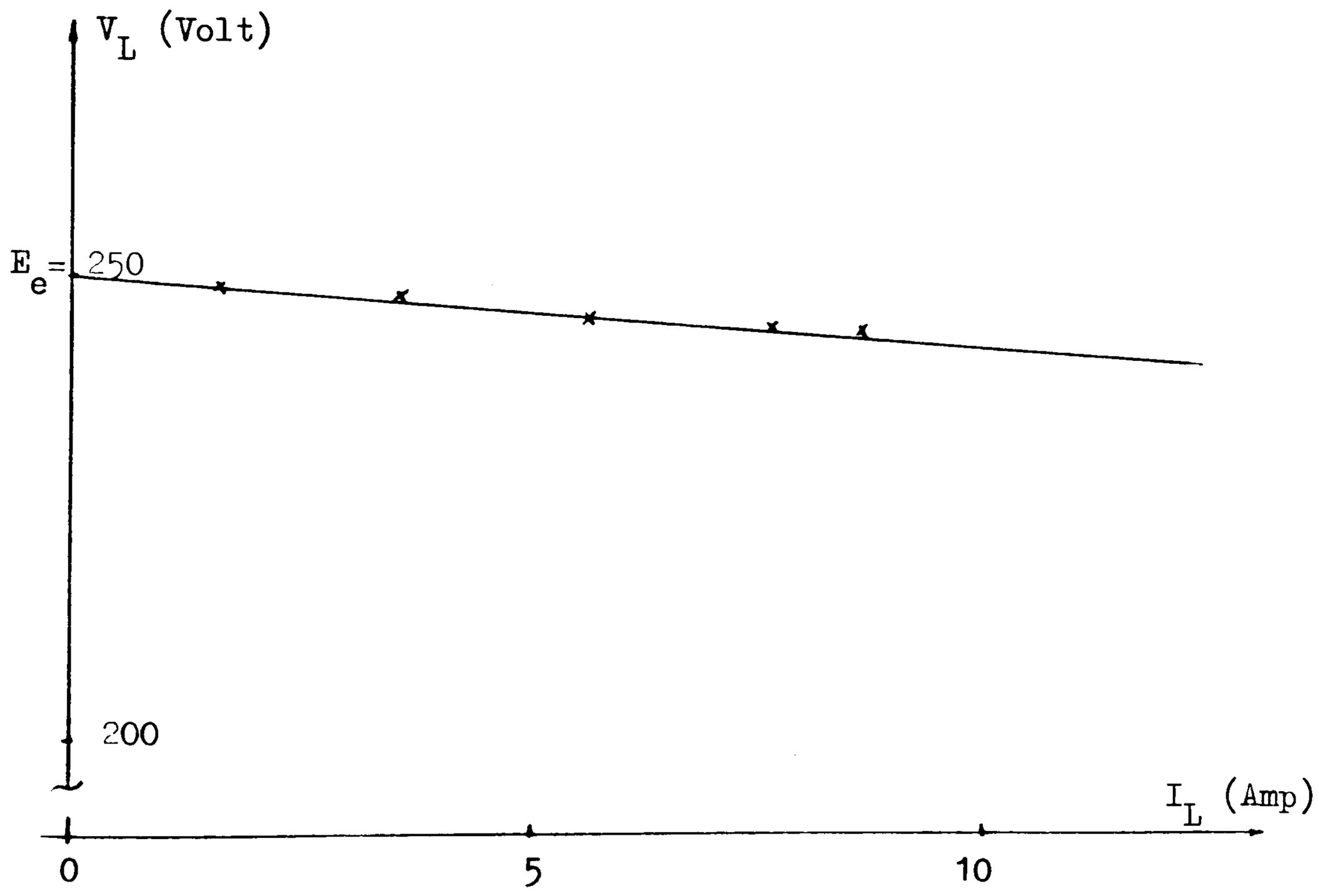

R_e : External Resistance
X_e : External Reactance
E_e : Open-Circuit Voltage
R_L : Variable Load
E_s : Supply Voltage
R_{sh}: Shunt Resistance
V_T : Variable Transformer

Fig. 3.18 External circuit, equivalent circuit and characteristic of $V_L(I_L)$

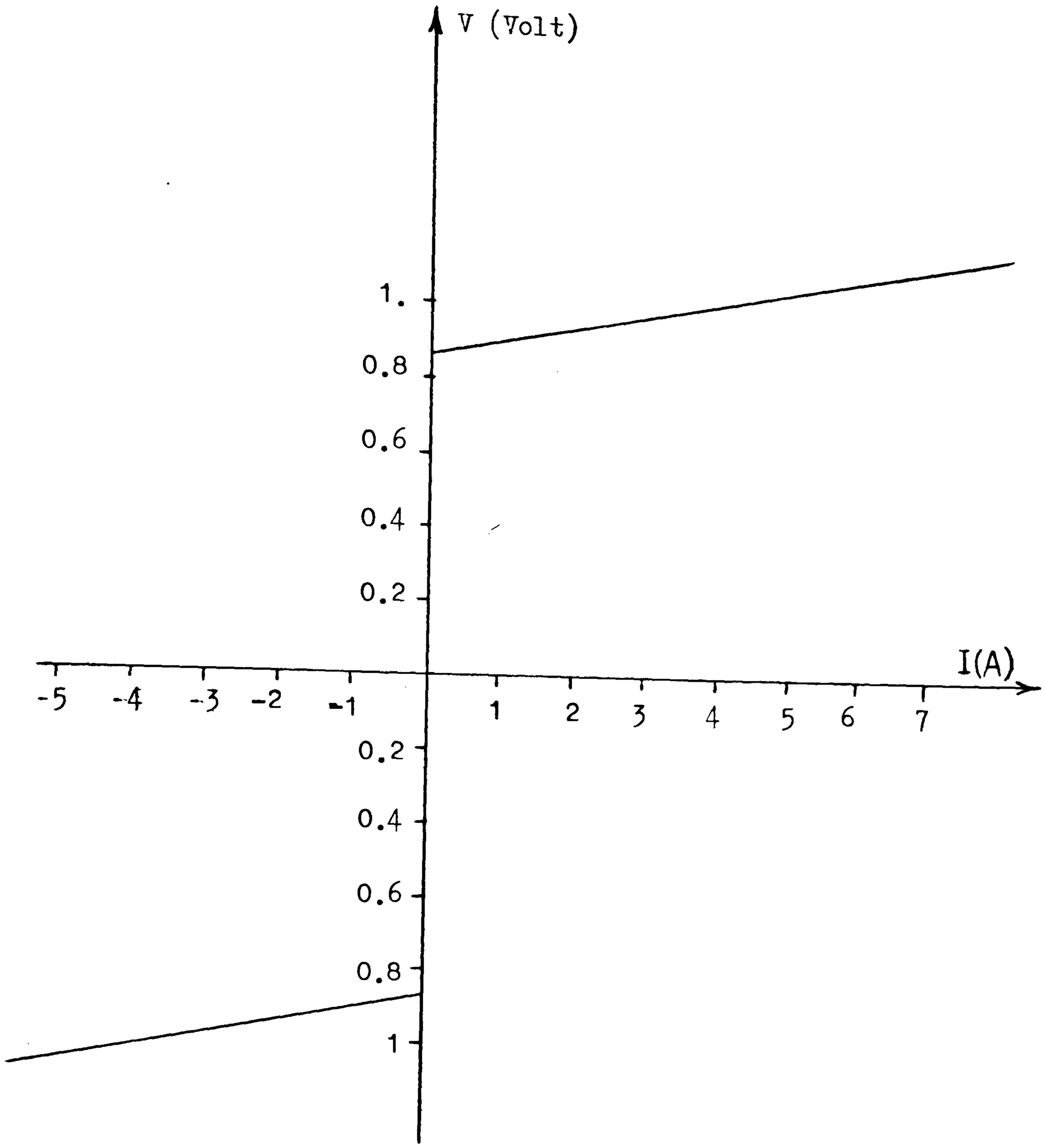

Fig. 3.19: Voltage/current characteristic of the switching-angle selector

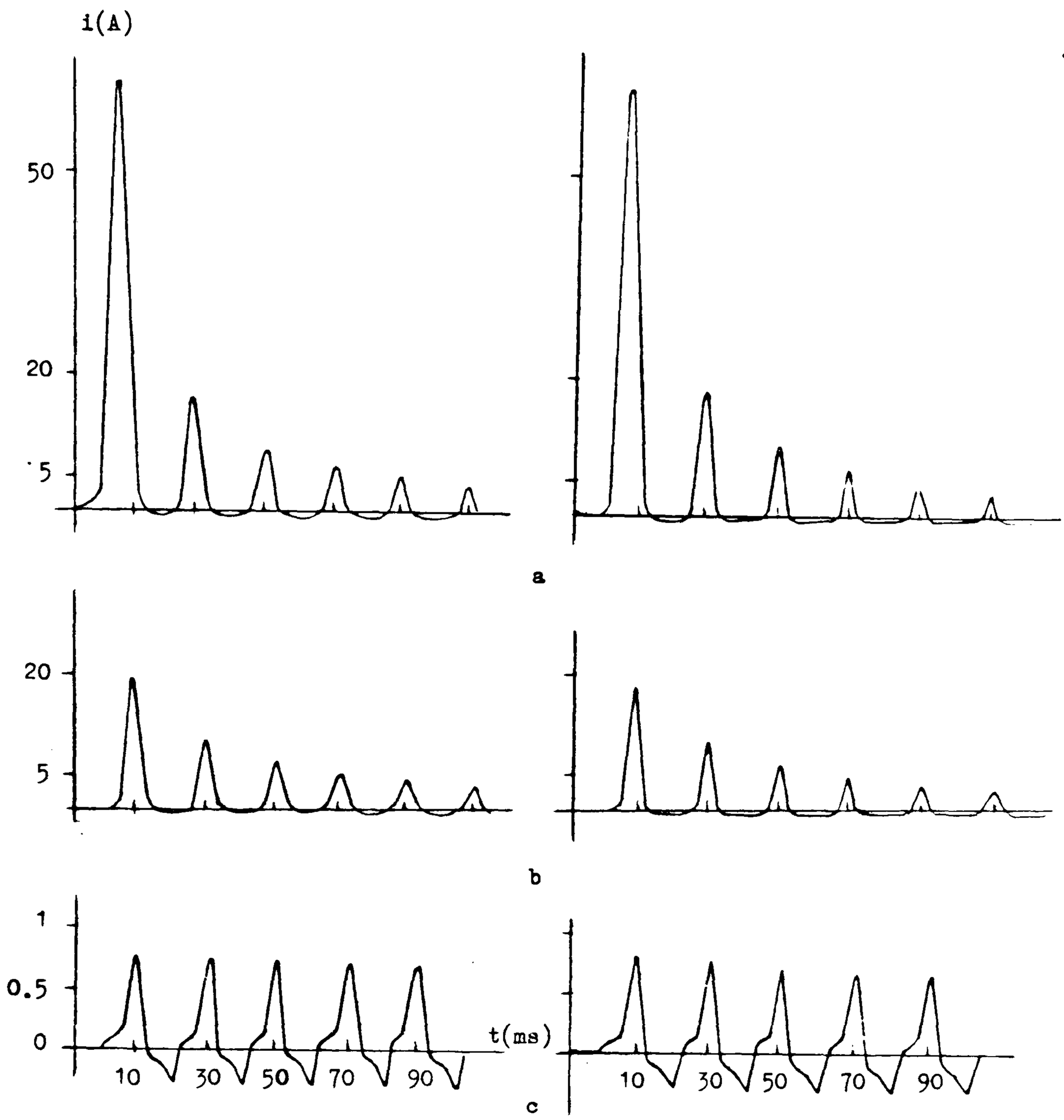

Fig. 3.20
Transient current patterns for 0.5 kVA, single-phase transformer, unloaded, 150 V supply, 0^{o} switching angle.

a. Maximum positive residual flux density (B_r = +0.958)

b. Zero residual residual flux density (B_r = 0)

c. Maximum negative residual flux density (B_r = -0.958)

Left hand side computed, Right hand side recorded.

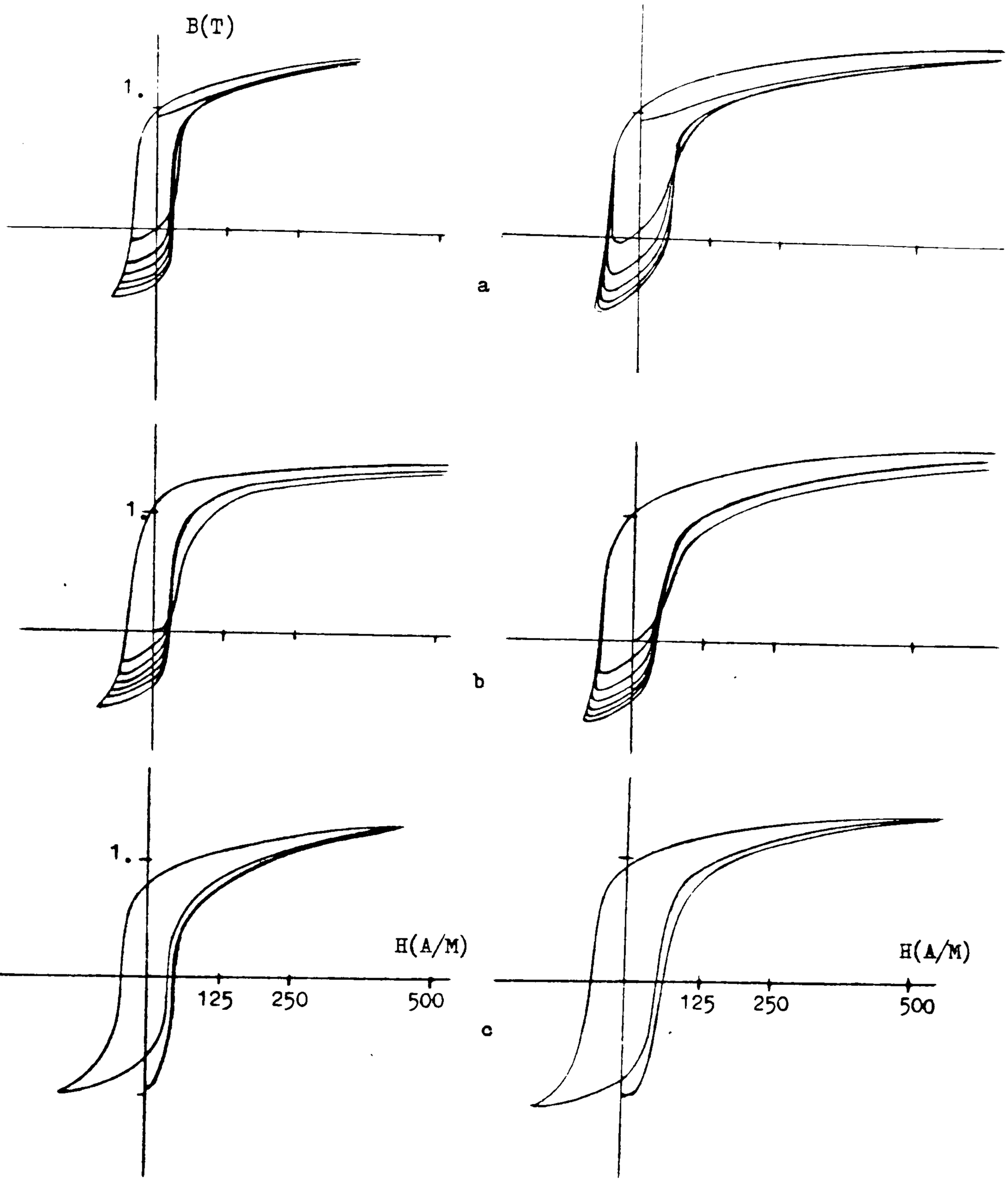

Fig. 3.21
Transient B/H patterns for the same transformer and conditions as Fig.

a. Maximum positive residual flux density (B_r = +0.958)

b. Zero residual flux density (B_r = 0.0)

c. Maximum negative residual flux density (B_r = -0.958)

Left hand side computed, Right hand side recorded.

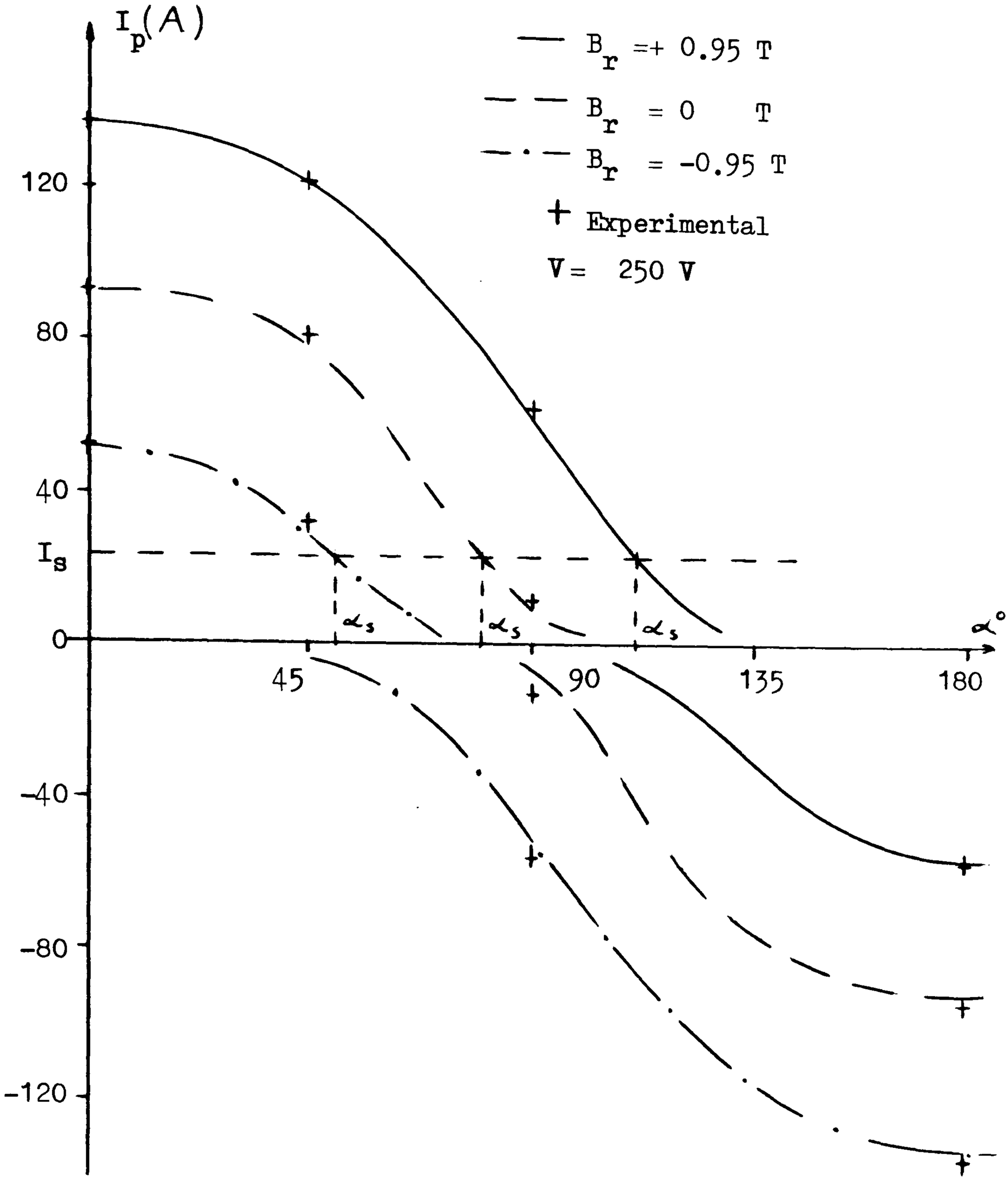

Fig. 3.22 : Effect of residual condition on peak transient current variation with switching angle α

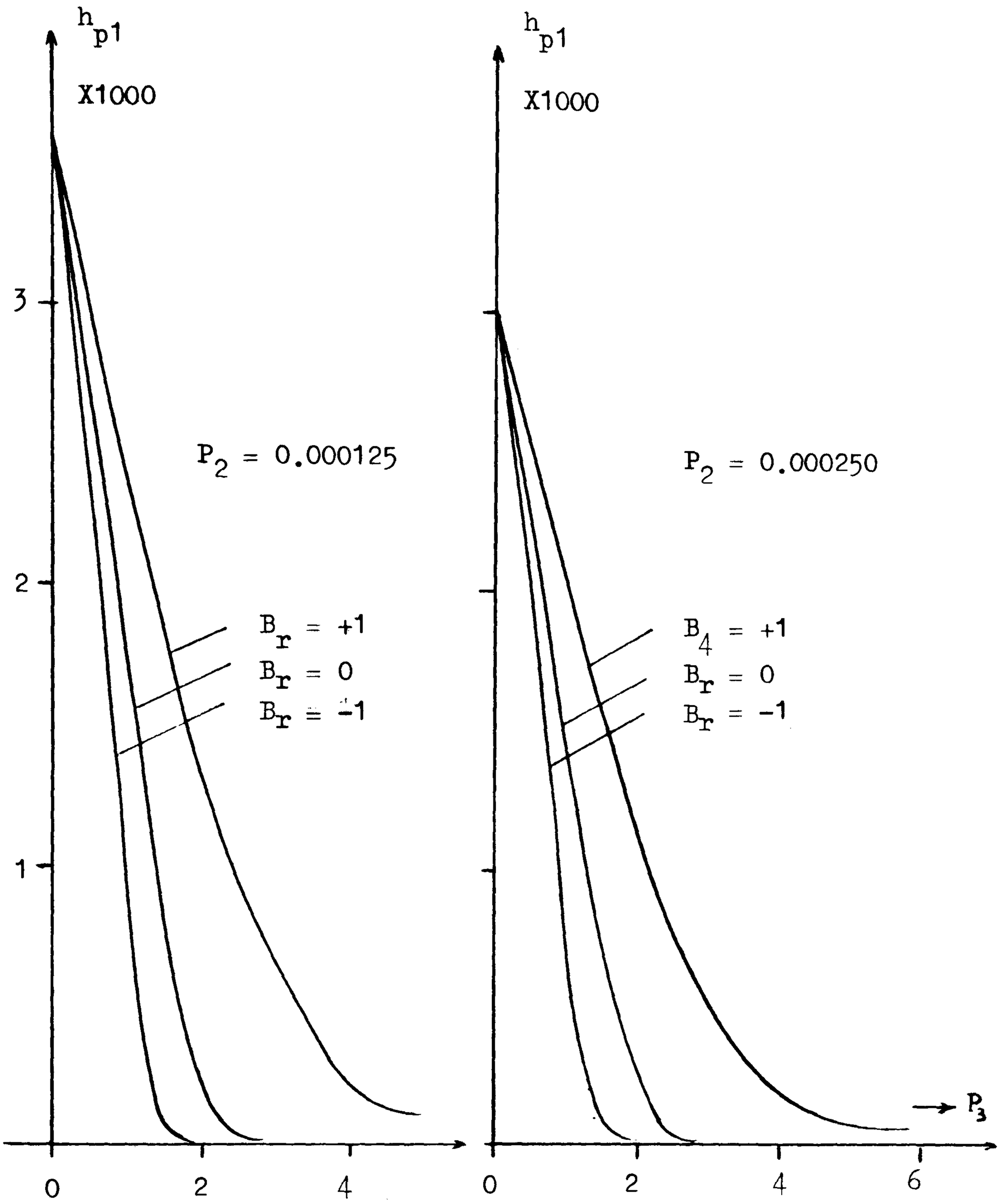

Figure 3.23 Variation of the first peak value of h with generalized parameters

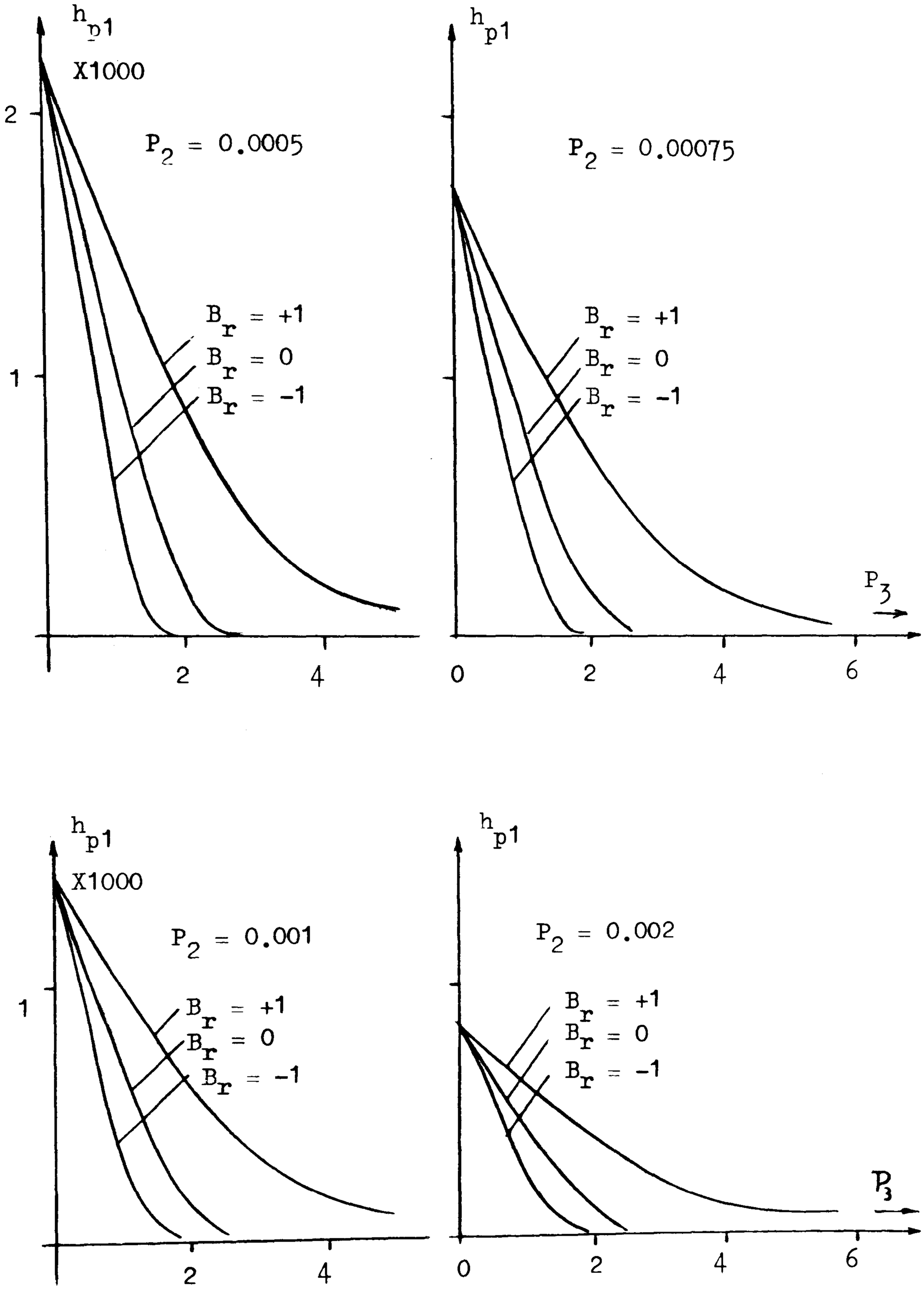

$\alpha = 0^{\circ}$ $P_1 = 0.00025$

Figure 3.24 Ibid

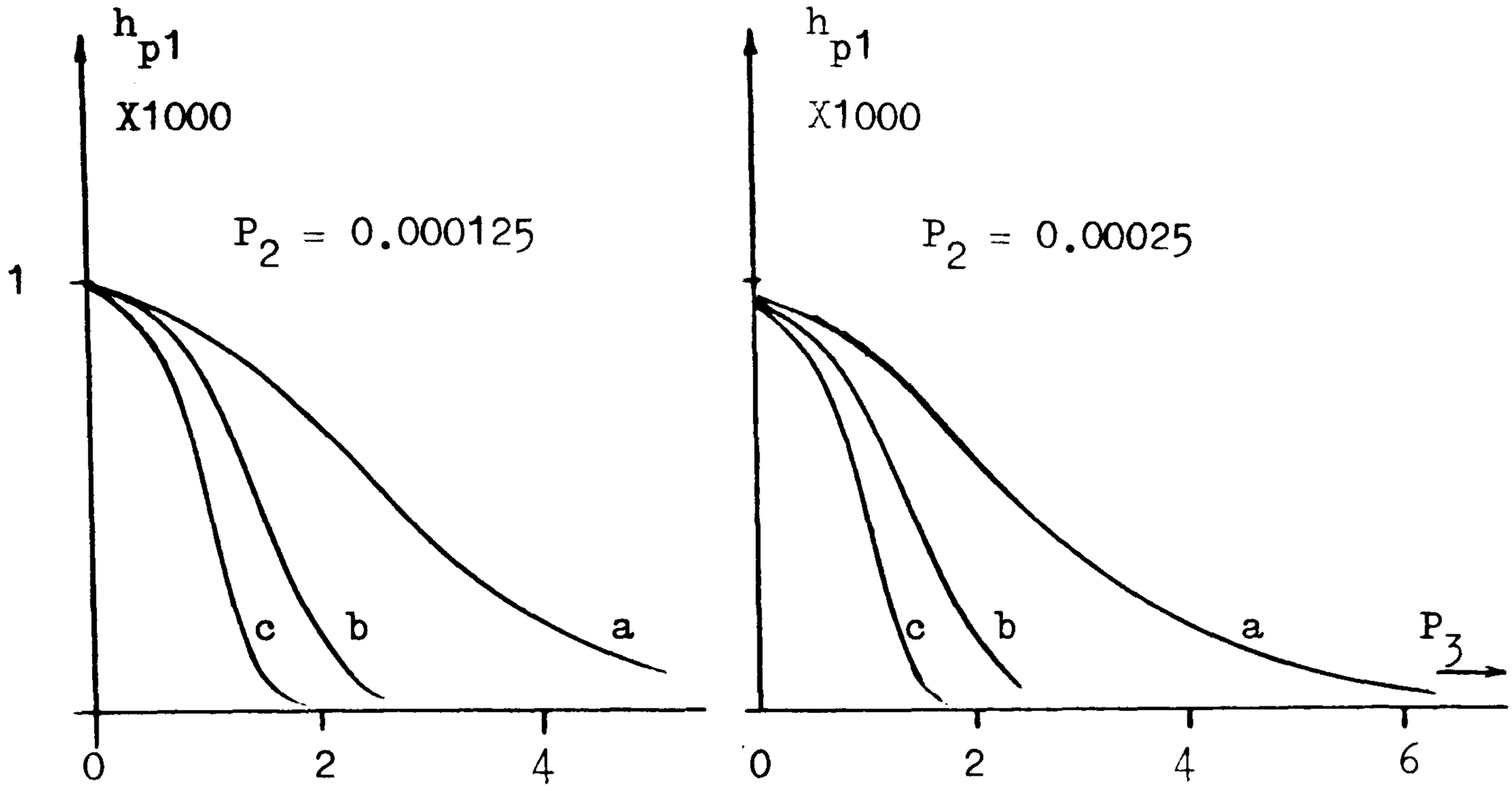

$\alpha = 0^{\bullet}$ $P_1 = 0.001$

a - $B_r = -1$ b - $B_r = 0$ c - $B_r = -1$

Figure 3.25 Ibid

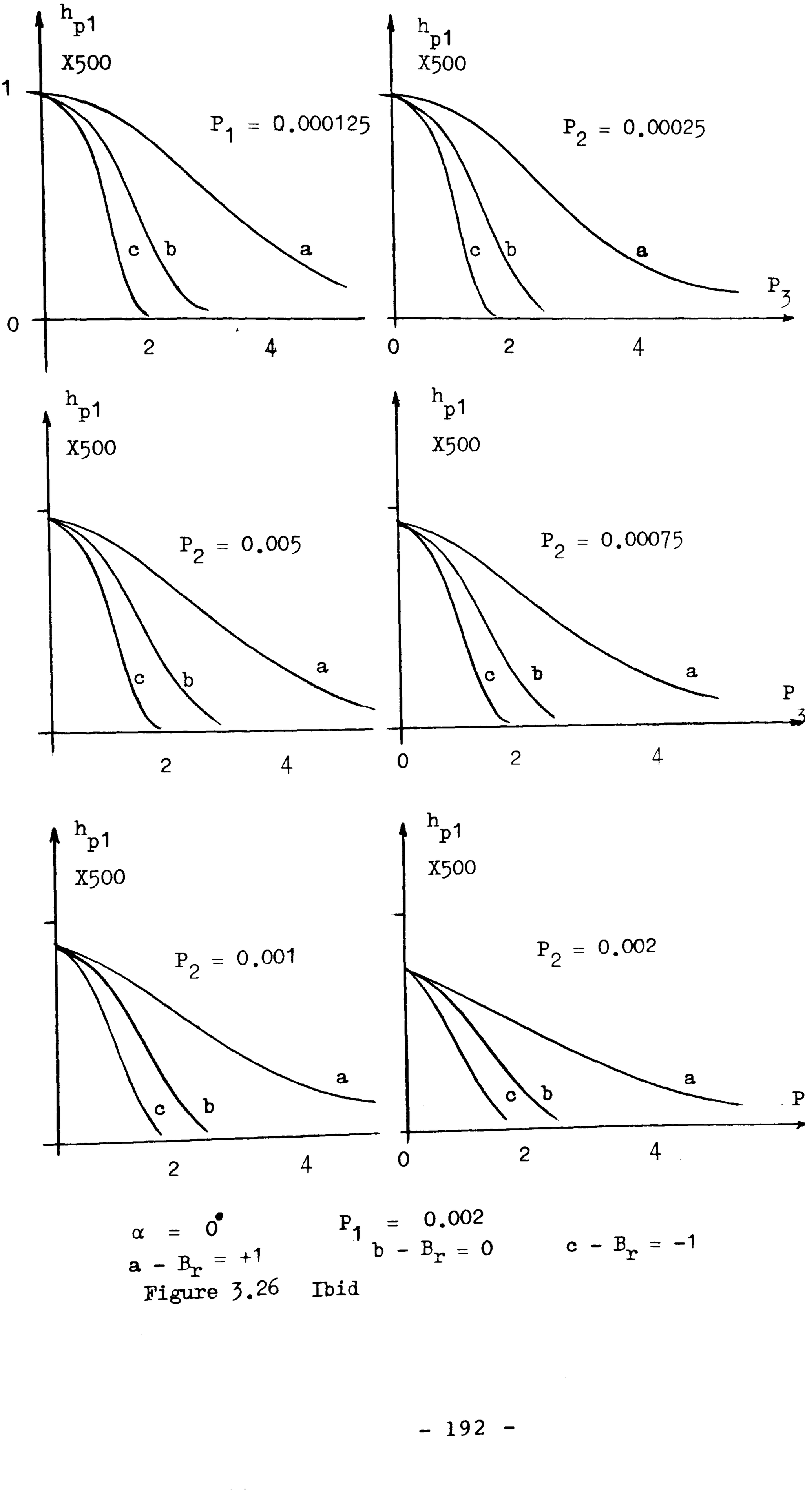

α = 0° P_1 = 0.002

a - B_r = +1 b - B_r = 0 c - B_r = -1

Figure 3.26 Ibid

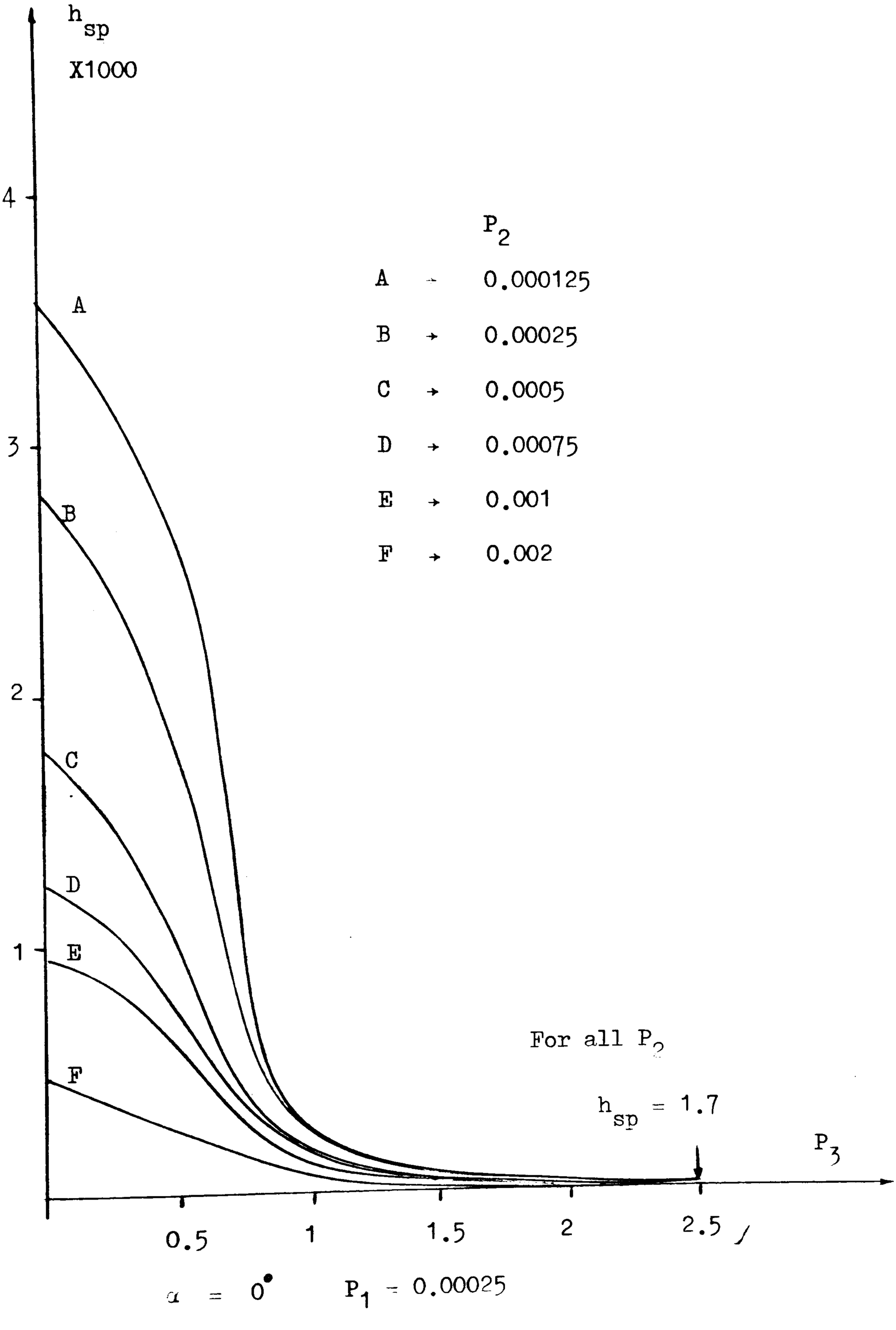

Figure 3.27 Variation of steady-state peak value of h with generalized parameters

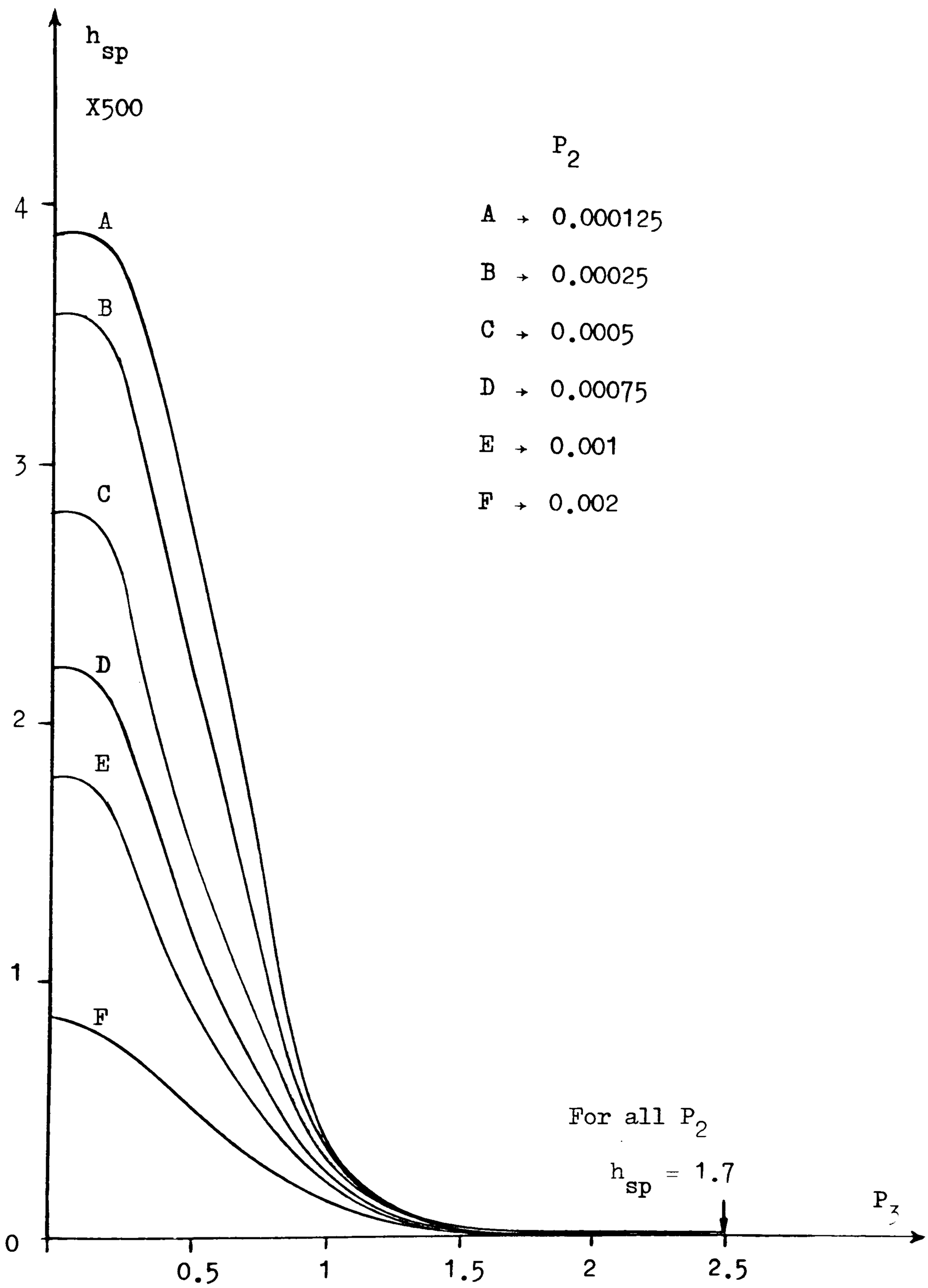

Figure 3.28 Ibid

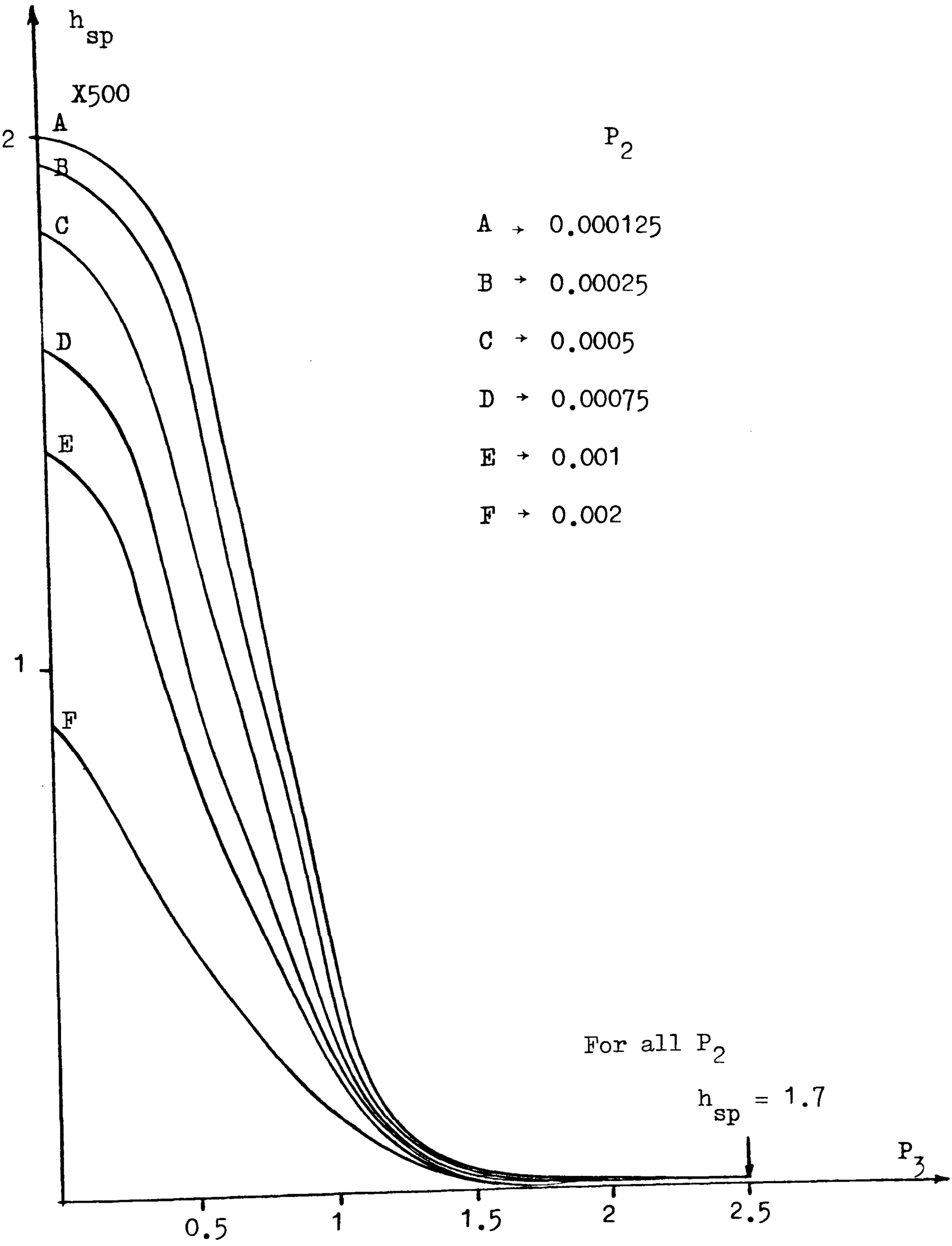

$\alpha = 0^{\circ}$ $P_1 = 0.001$

Figure 3.29 Ibid

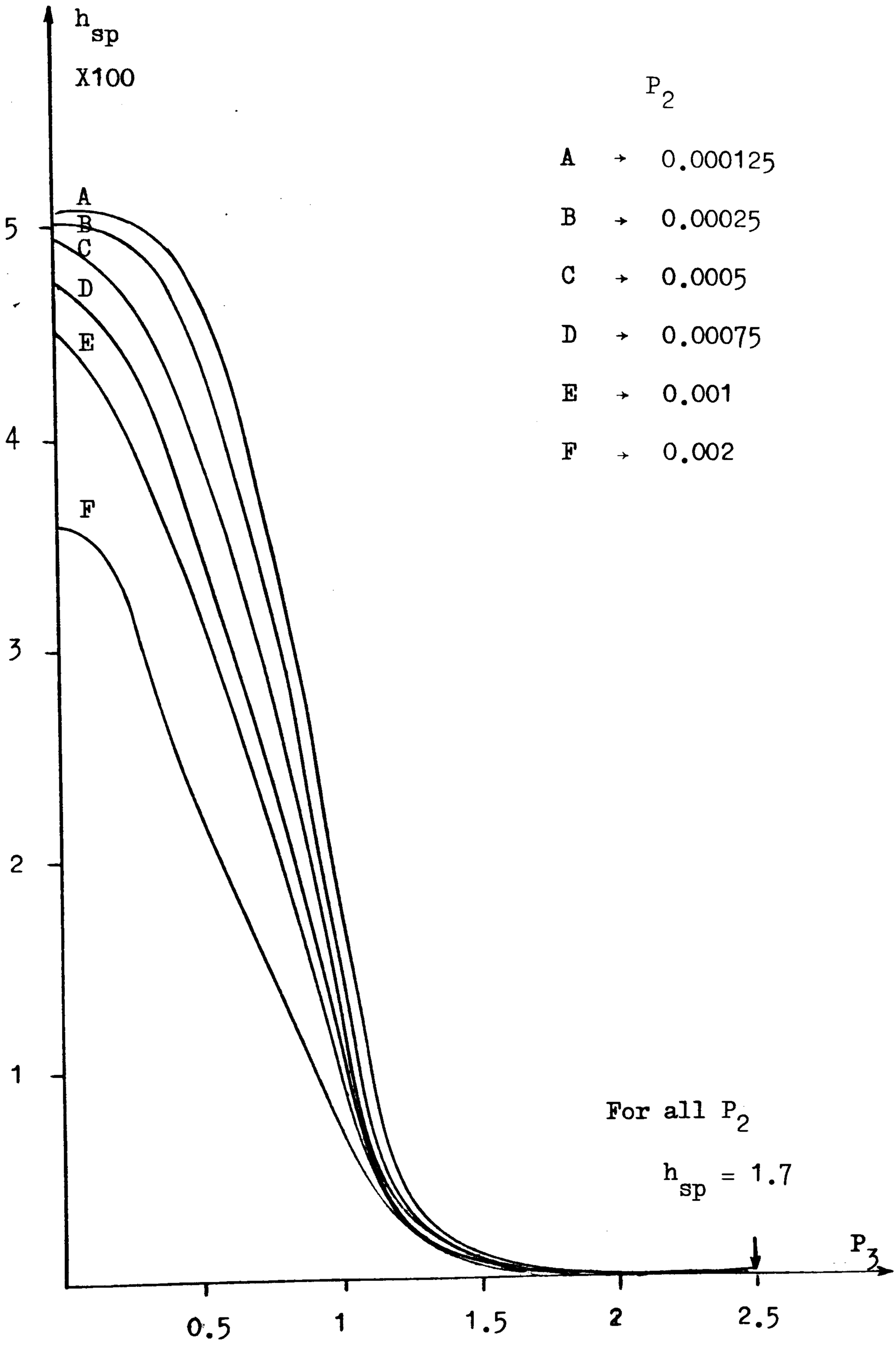

Figure 3.30 Ibid

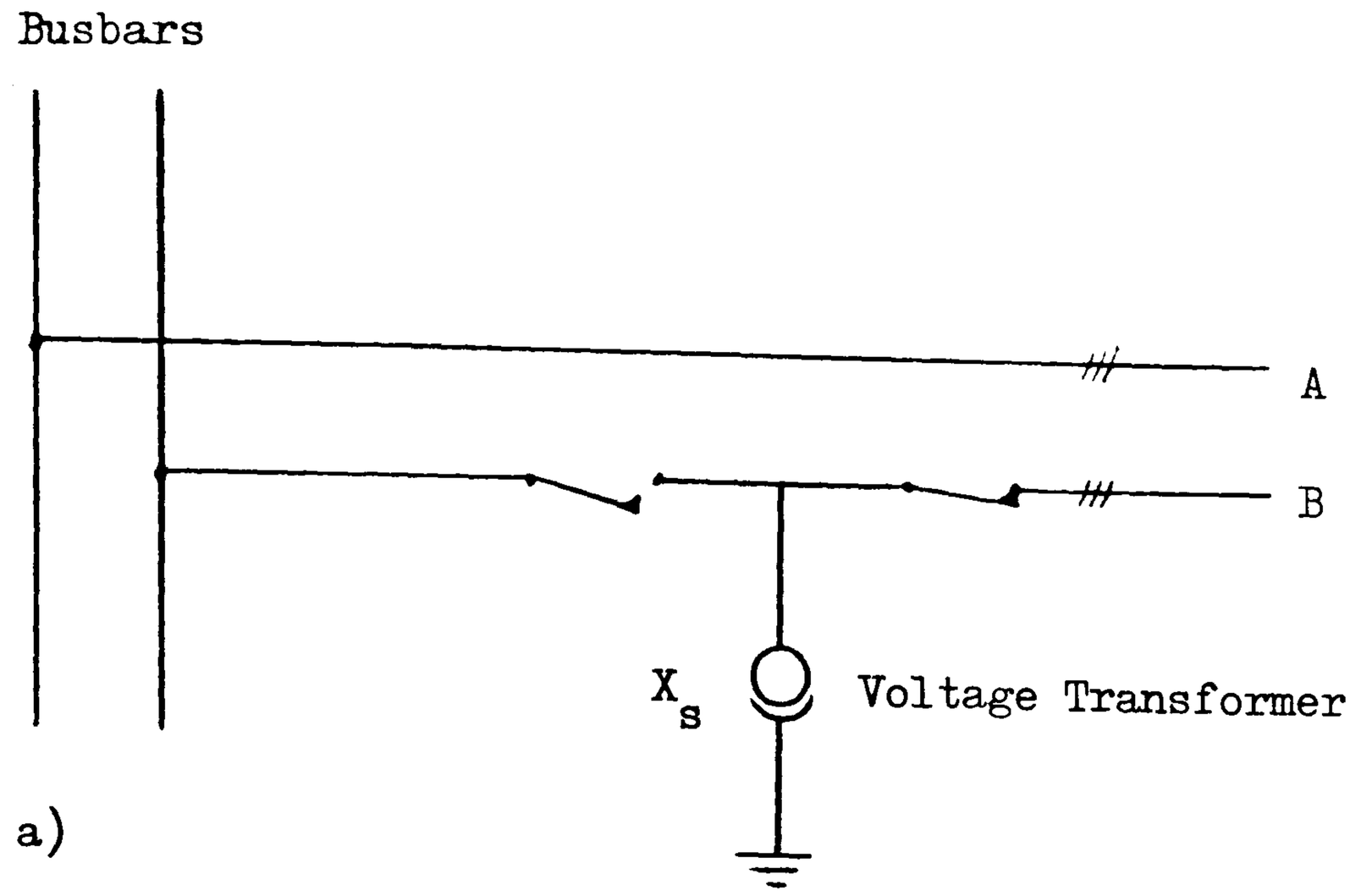

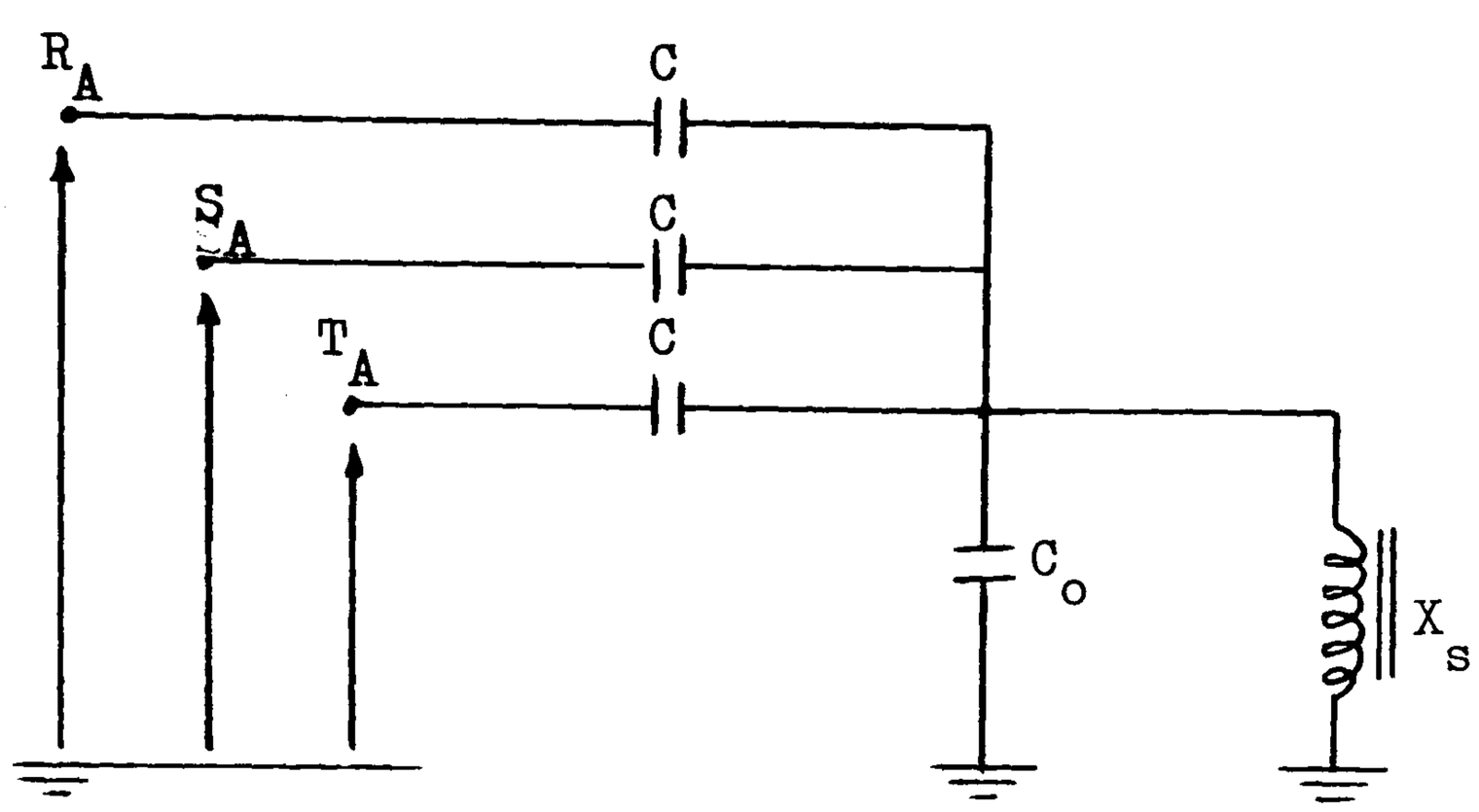

C_o Capacitance between line and earth.

C Capacitance between two lines.

a. : Actual system.

b. : Equivalent diagram for one phase.

Fig. 4.2 Single phase ferroresonance

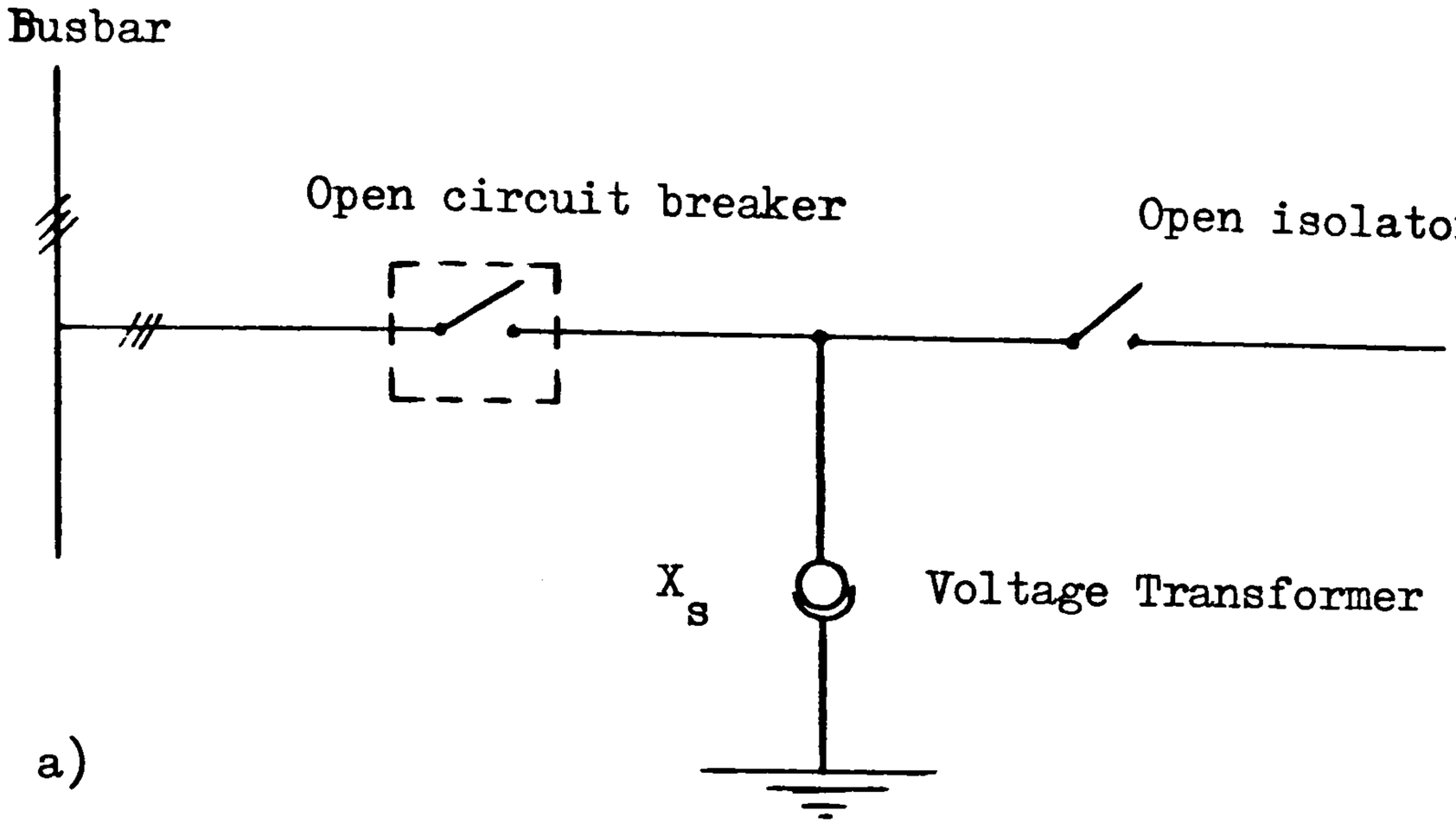

a)

Open circuit breaker

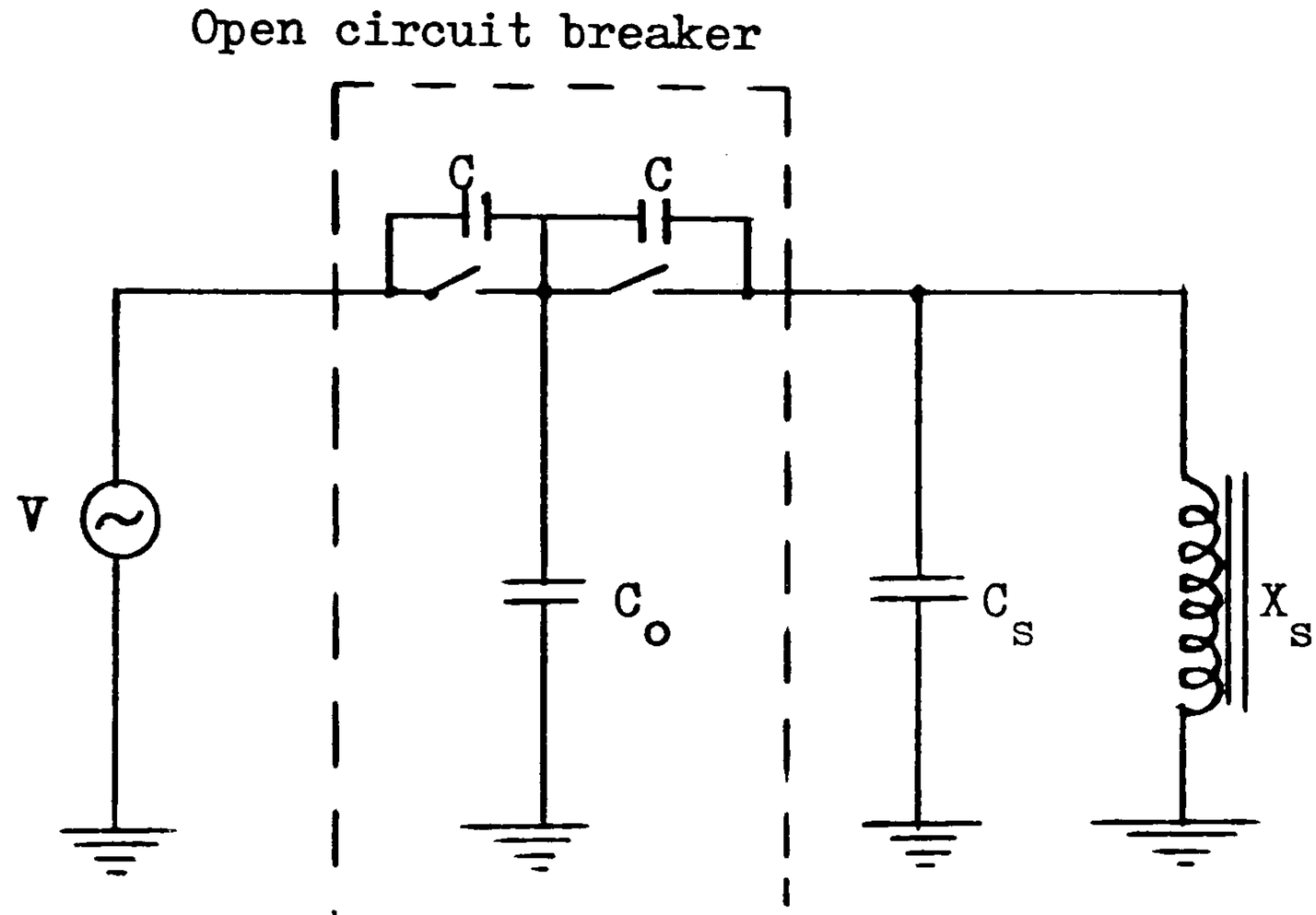

b)

V : Phase-earth voltage of system.

C : Capacitance between the interrupter head.

C_o,C_s : Capacitance to earth.

b: Equivalent diagram for one phase.

Fig. 4.3 Ibid

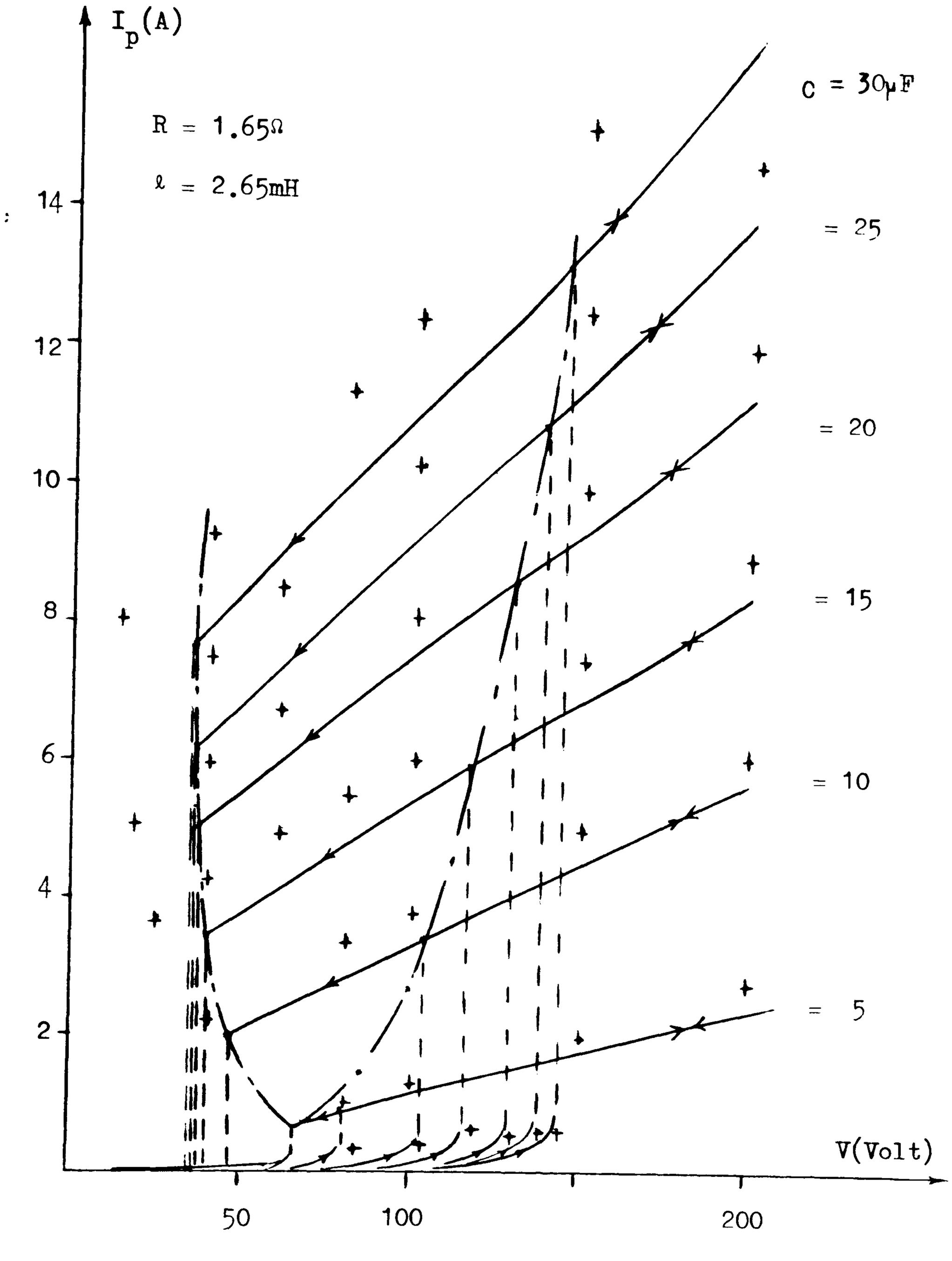

\+ computed points using Preisach model

\- experimental characteristics

Figure 4.8 I_p/V characteristics in Fundamental ferroresonance

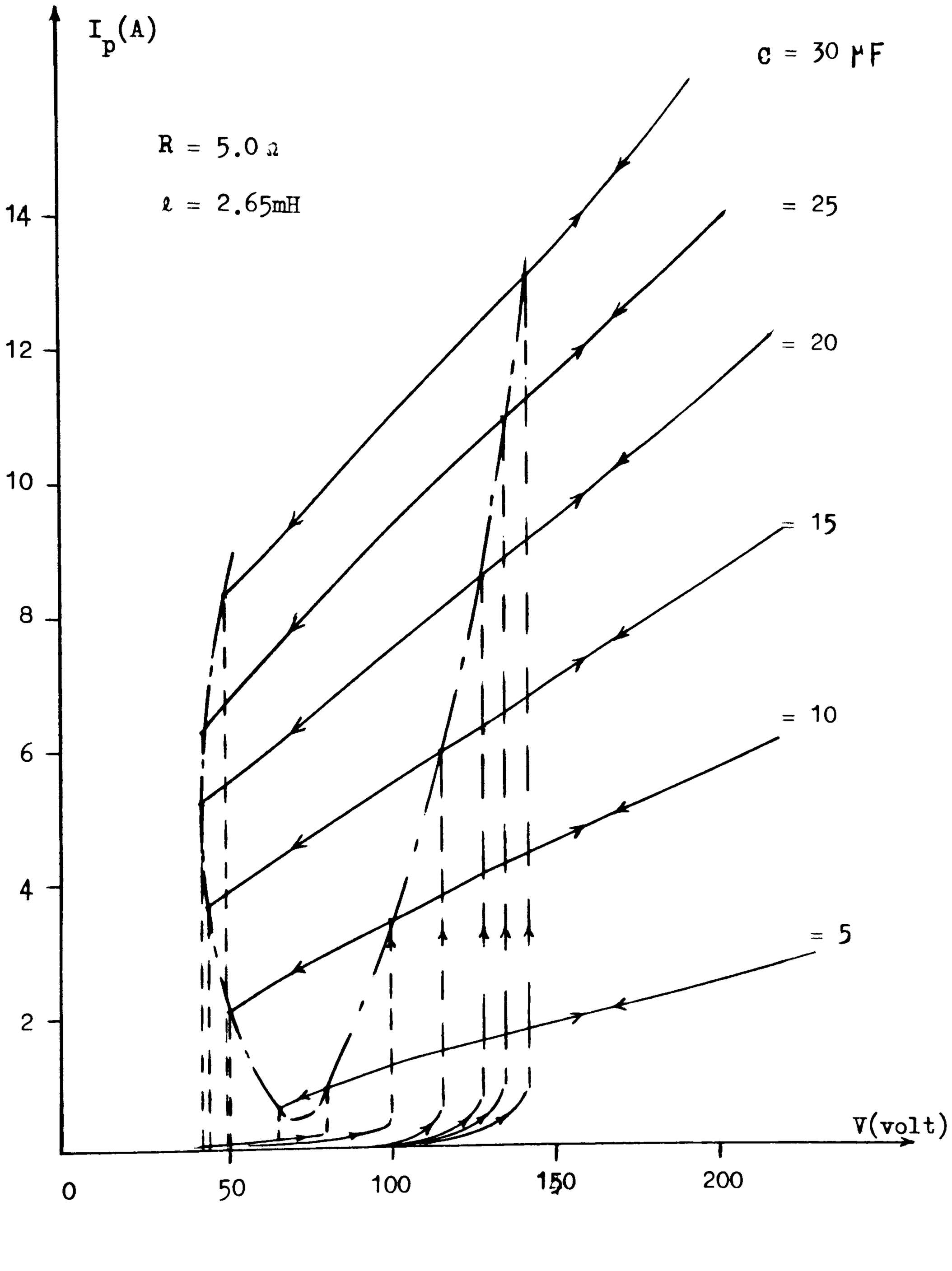

Figure 4.9 Ibid

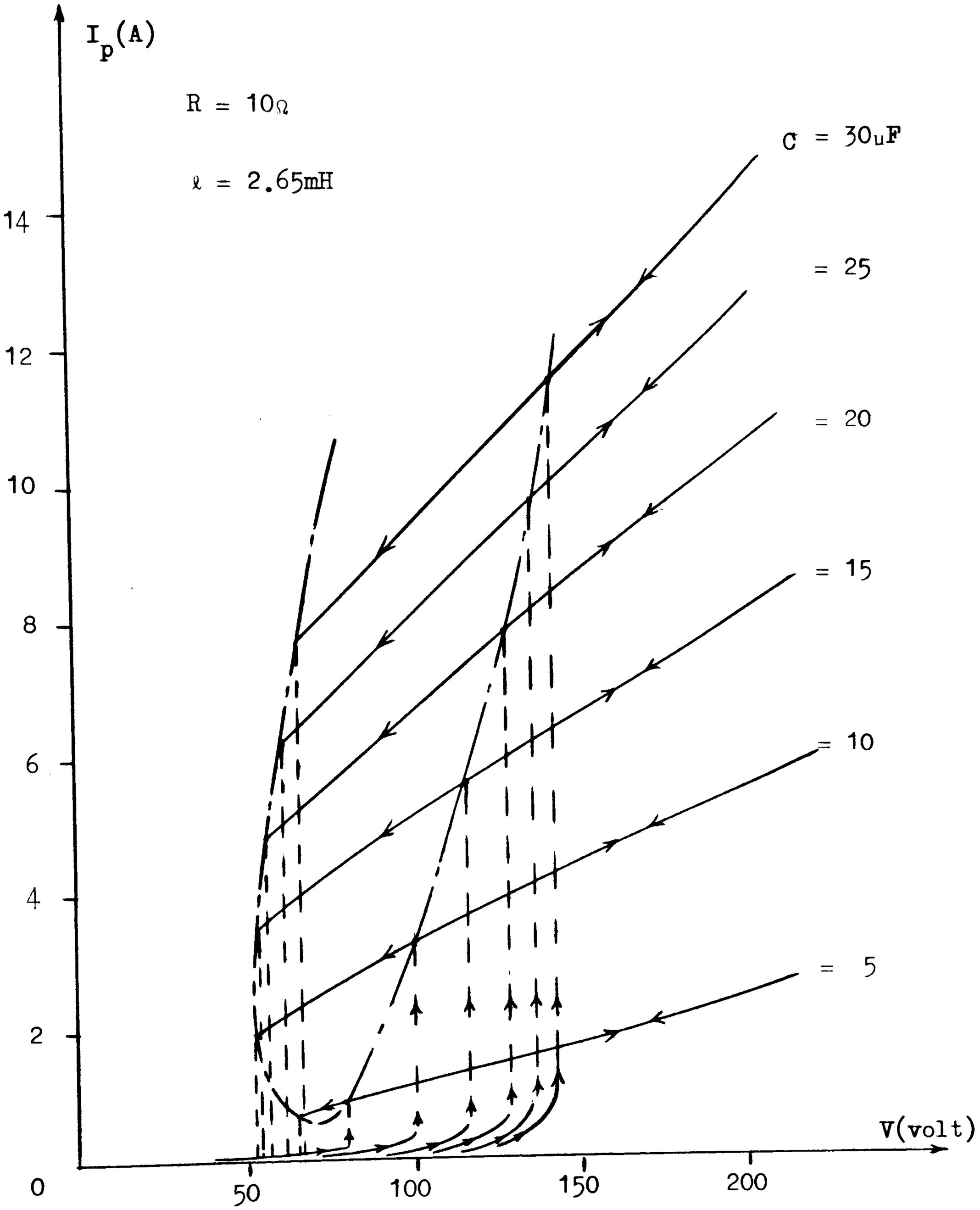

Figure 4.10 Ibid

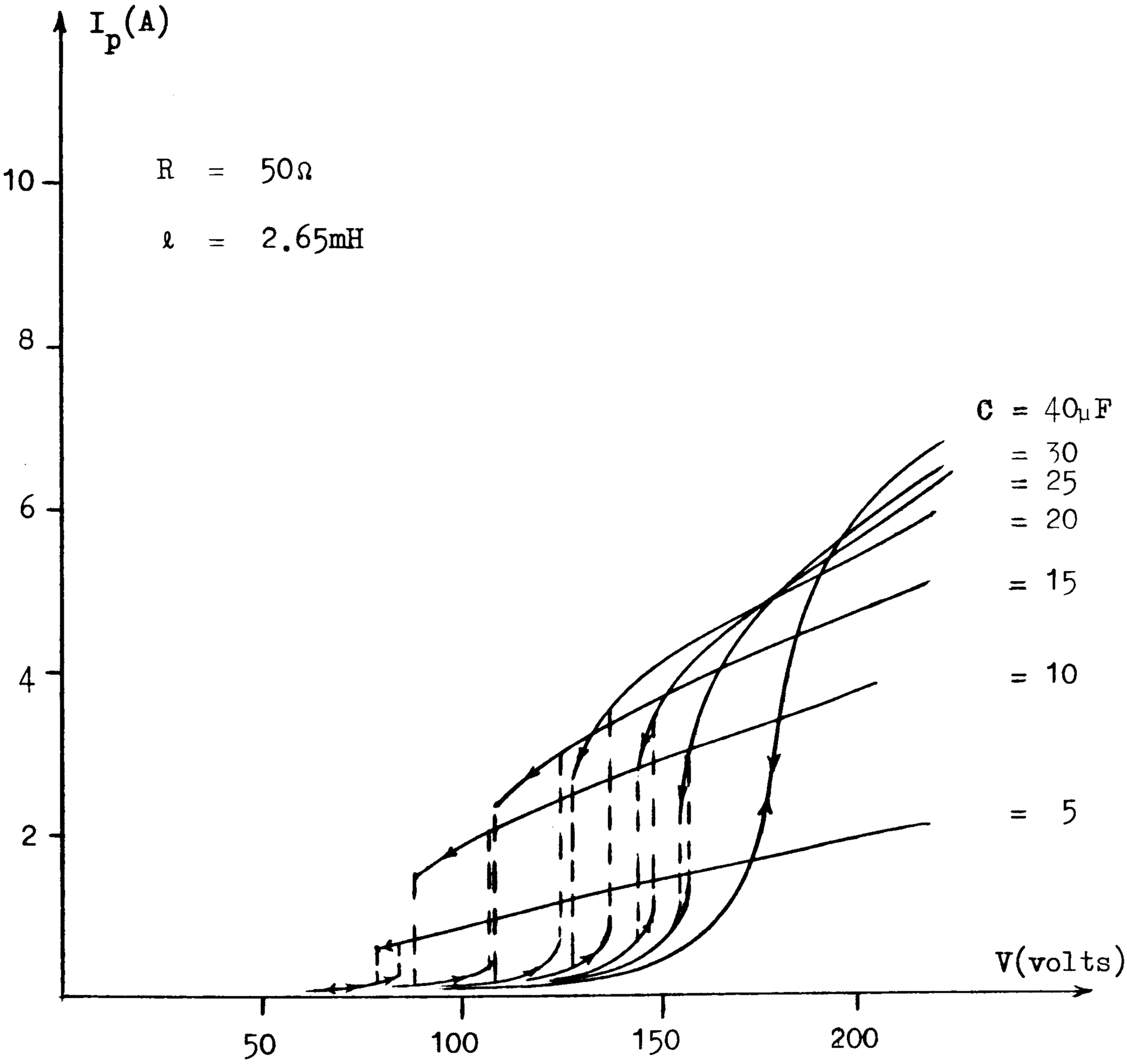

Figure 4.11 Ibid

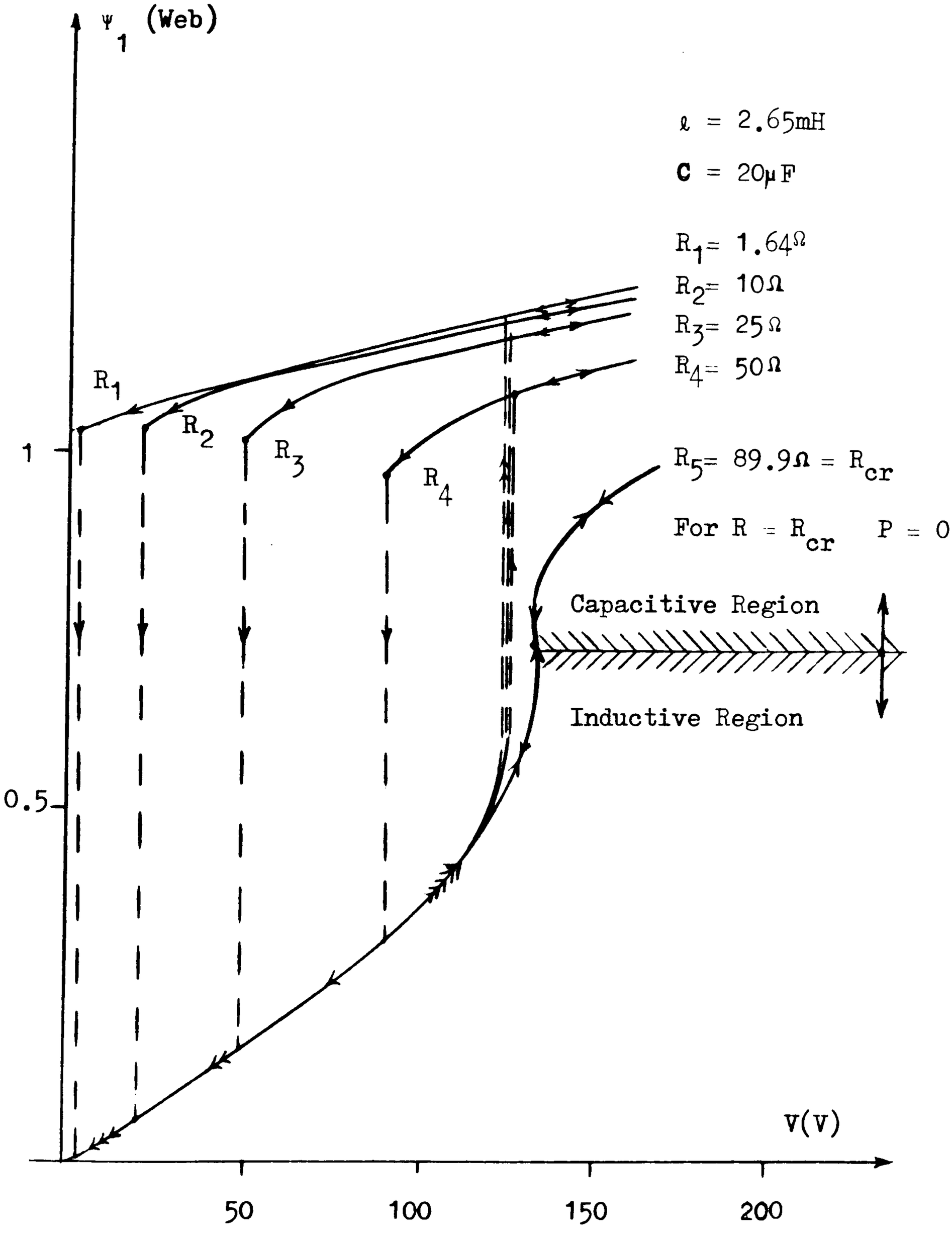

Figure 4.12 Flux - voltage characteristic of Fundamental Ferroresonance

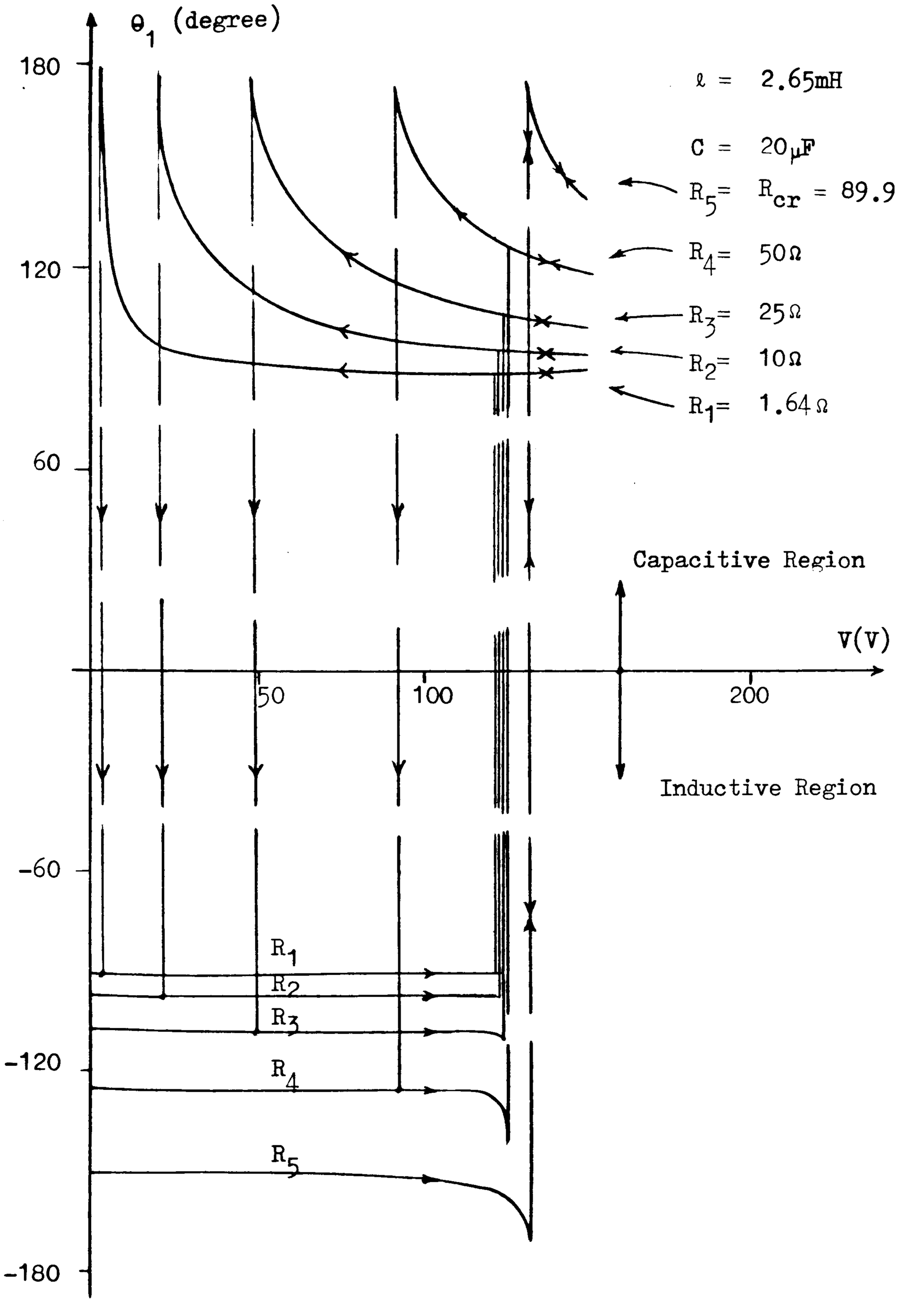

Figure 4.13 Phase Angle - voltage characteristic of Fundamental Ferroresonance

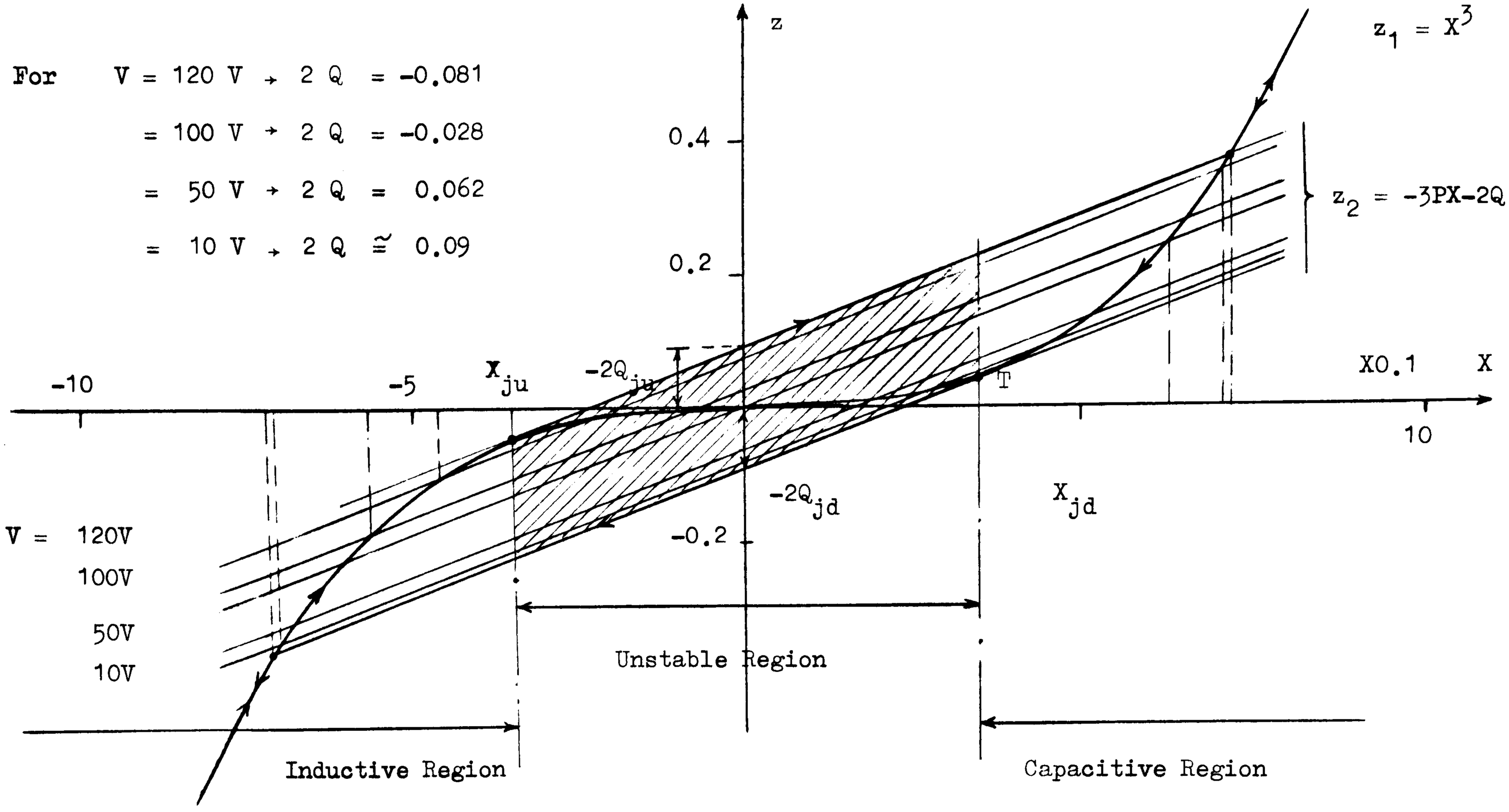

Figure 4.14 Graphical Solution and Determination of the jumping points

$R = 1.64\Omega$ $C = 20\mu F$ $\ell = 2.65mH$

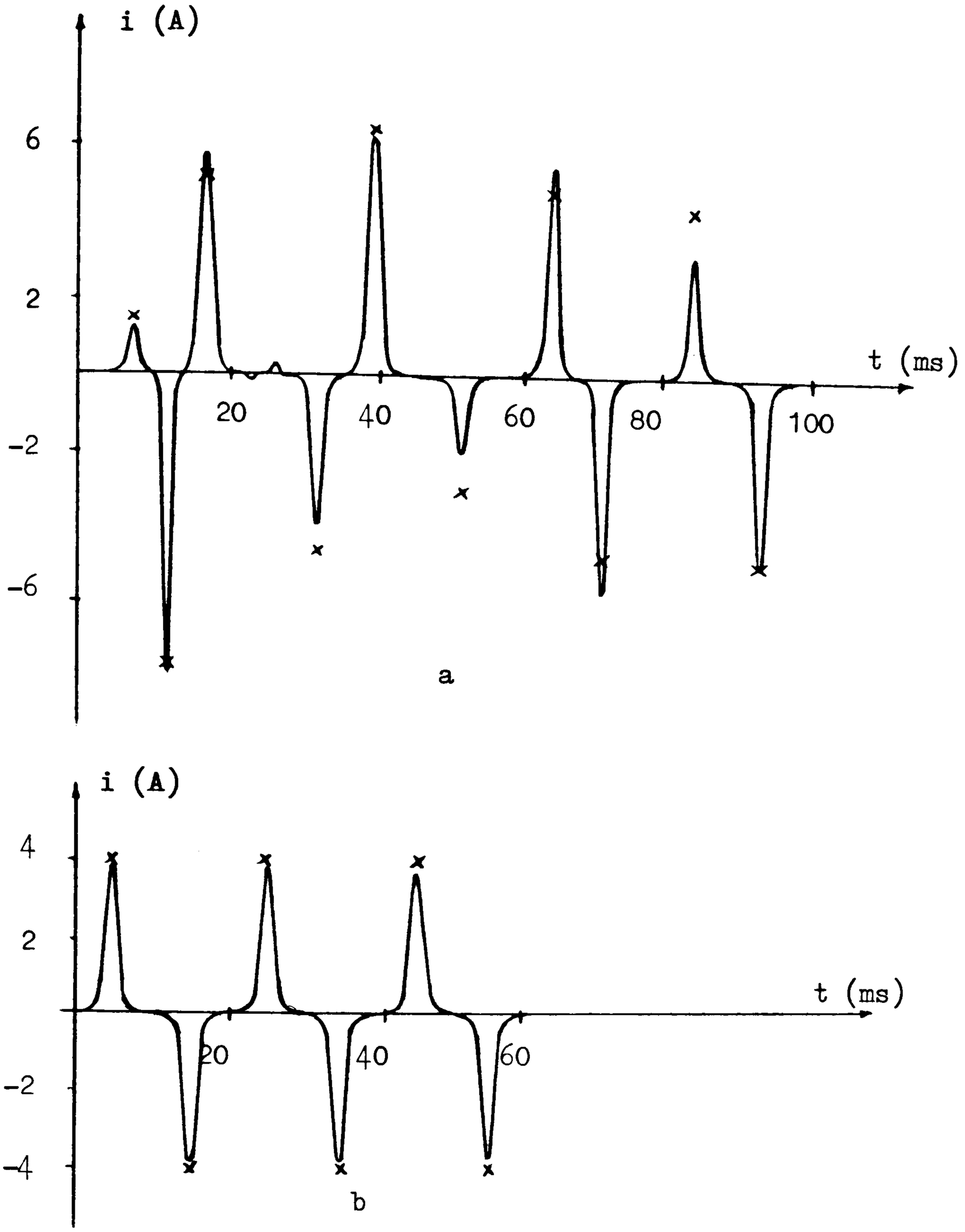

X Experimental point

\- Computed

a - Transient state

b - Steady state

Figure 4.17 Fundamental Ferroresonance Current Waveform

$R = 1.64\ \Omega$ $\ell = 2.65\text{mH}$ $C = 6.8\ \mu\text{F}$

$V = 200\ V$

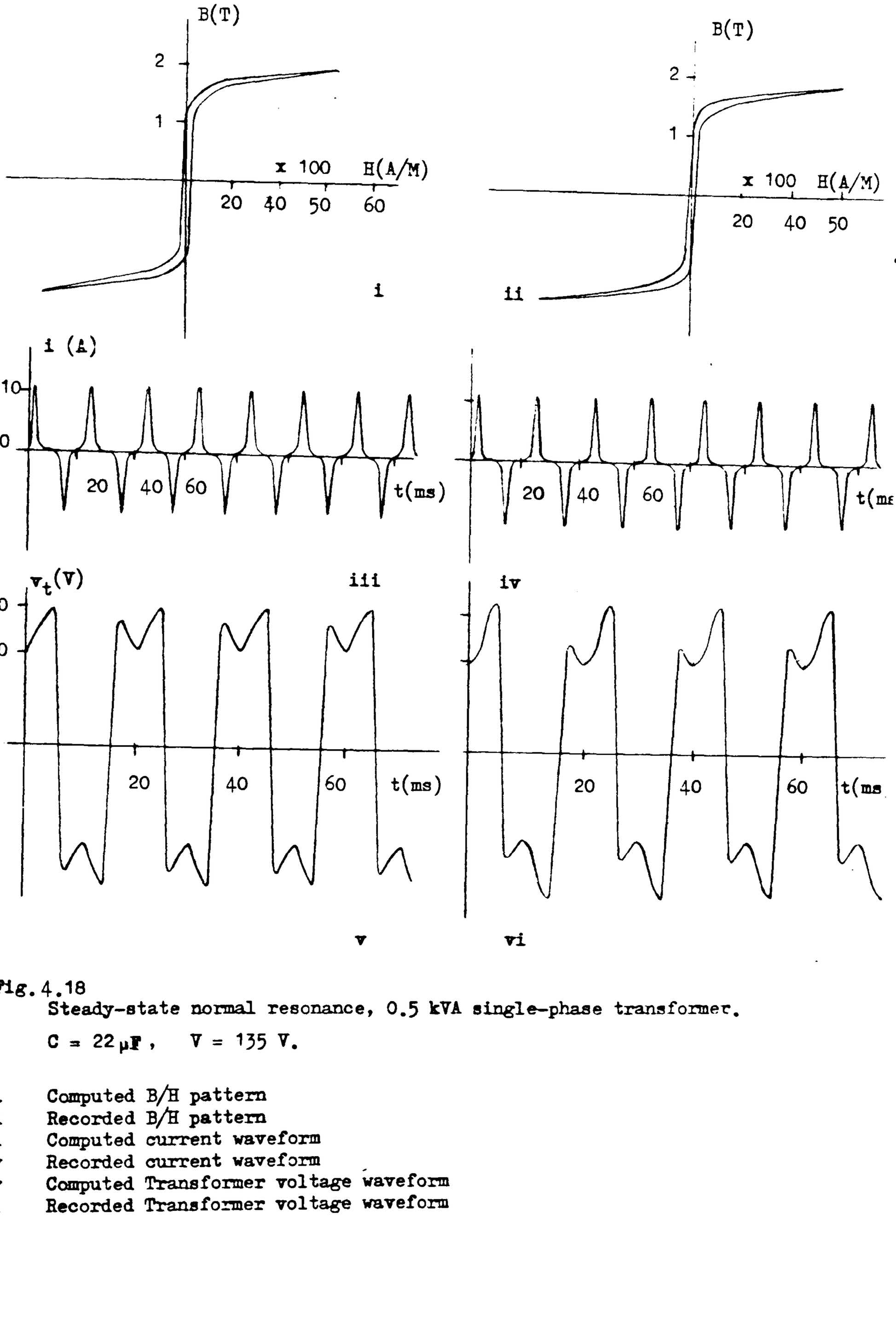

Fig. 4.18
Steady-state normal resonance, 0.5 kVA single-phase transformer.
C = 22 μF , V = 135 V.

i	Computed B/H pattern
ii	Recorded B/H pattern
iii	Computed current waveform
iv	Recorded current waveform
v	Computed Transformer voltage waveform
vi	Recorded Transformer voltage waveform

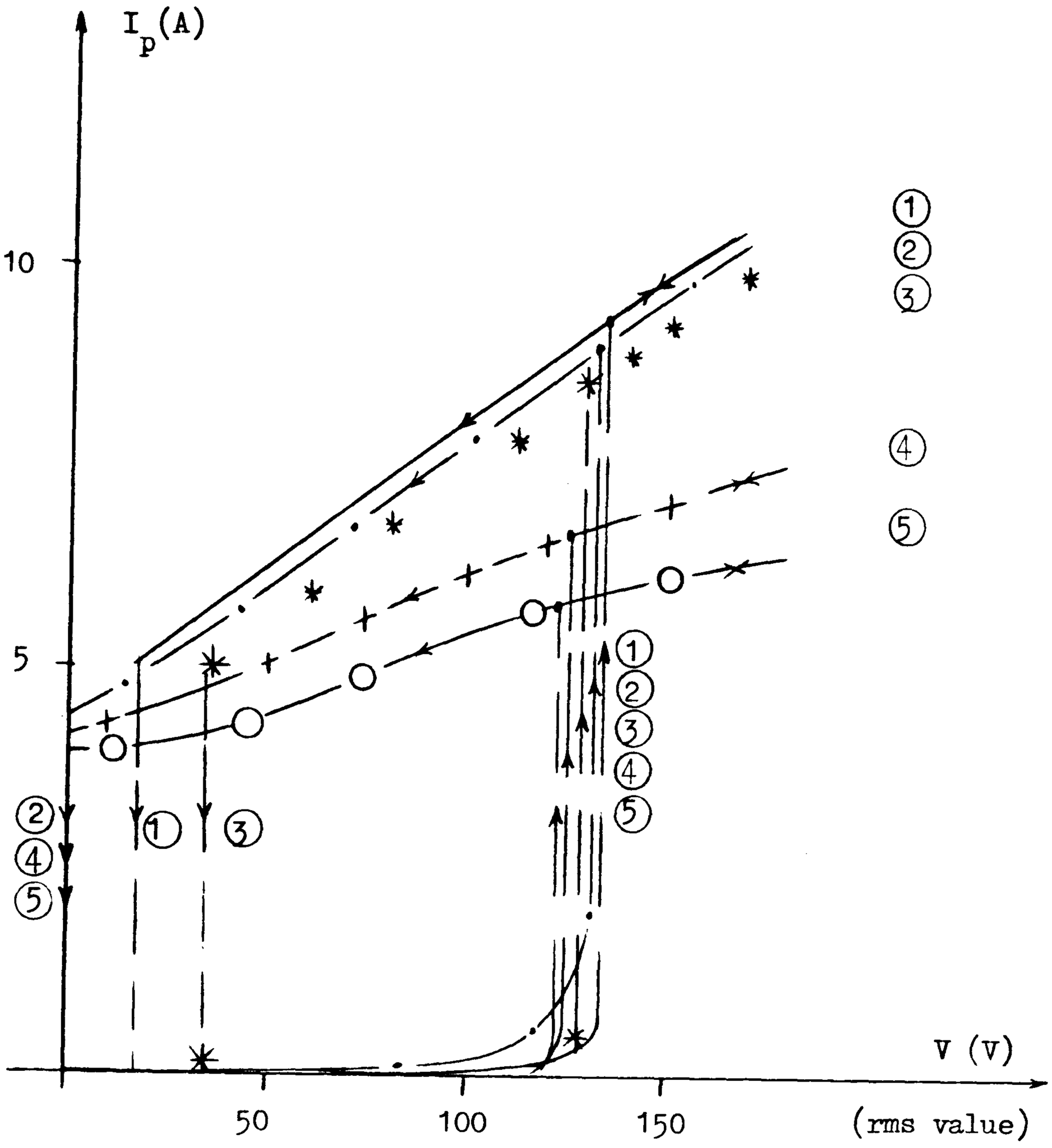

① Computed results using Preisach model for BH Loop

② Computed results using Exponential series for Magn.Curve

③ Experimental results.

④ Analytical results using two harmonics for flux linkages.

⑤ Analytical results using single harmonic for flux flux linkages.

$R = 1.64\Omega$ $C = 20\mu F$ $\ell = 2.65mH$

Figure 4.19 Current-Voltage characteristic of Fundamental Ferroresonance Circuit

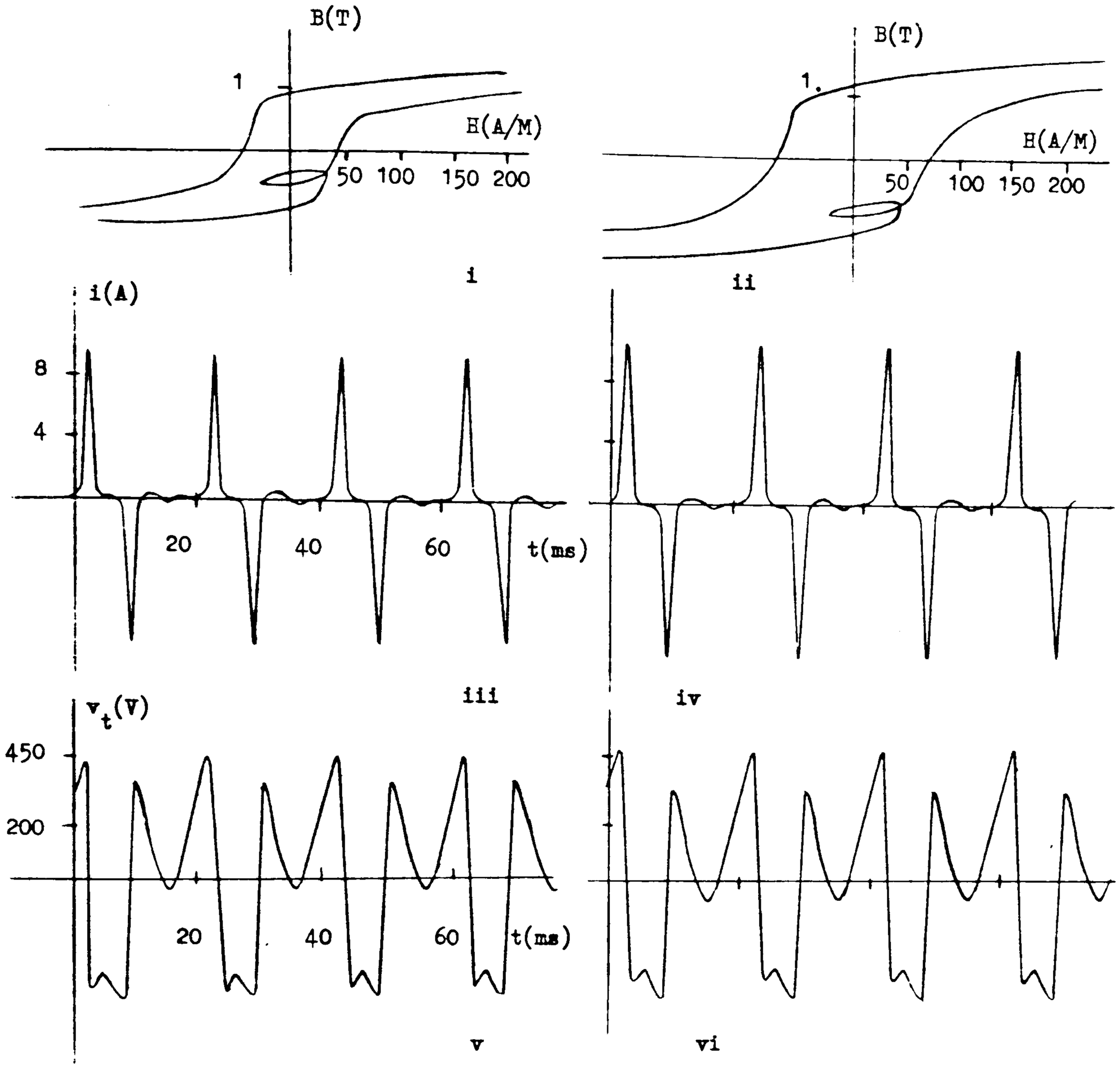

Fig. 4.20
Steady-state assymmetric resonant mode, 0.5 kVA.
Single-phase transformer. C = 10 μF. V = 275 V.

i Computed B/H pattern
ii Recorded B/H pattern
iii Computed current waveform
iv Recorded current waveform
v Computed transformer voltage waveform
vi Recorded transformer voltage waveform

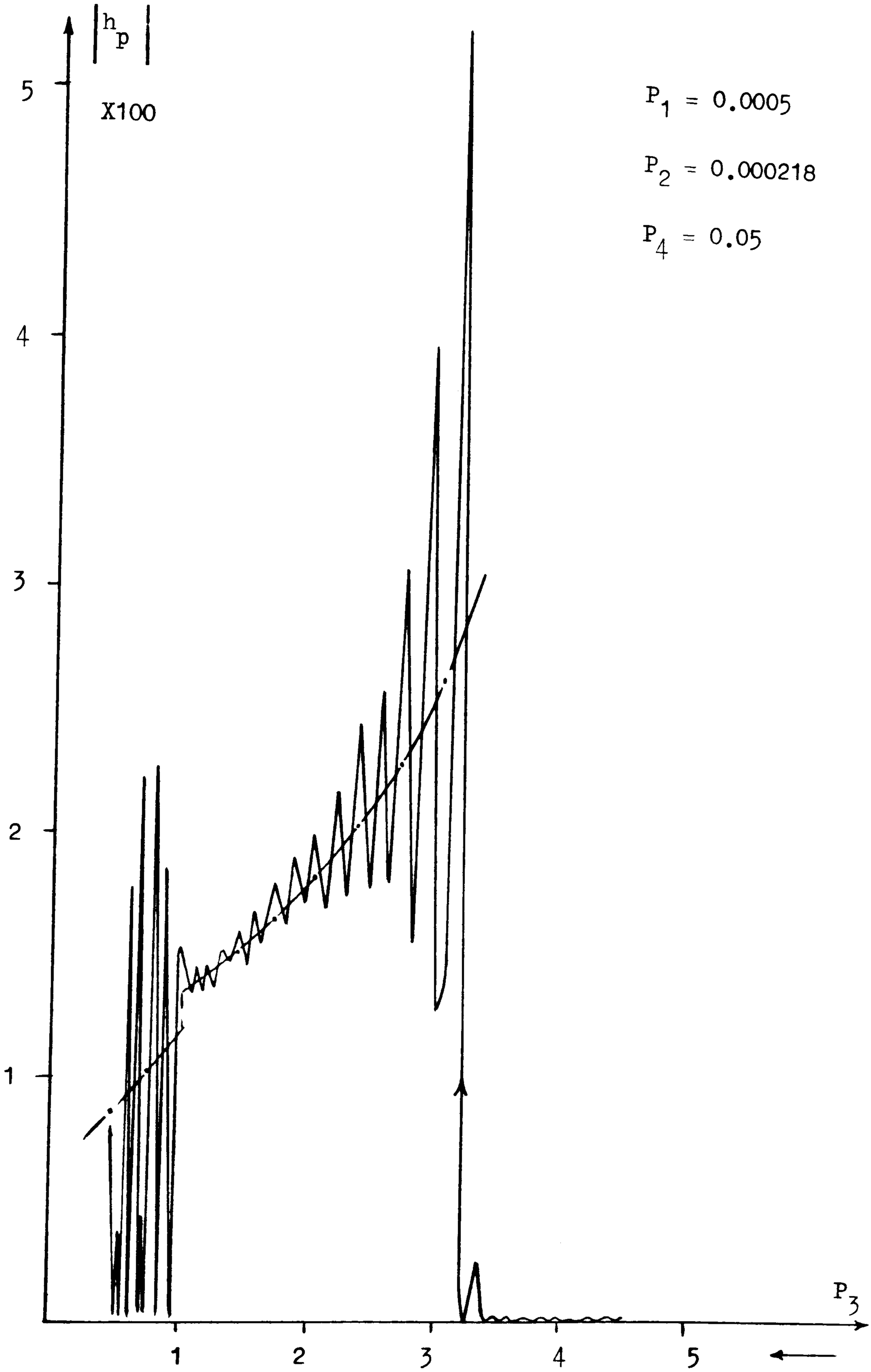

Figure 4.21 Variation of absolute value of h_p with generalized parameters

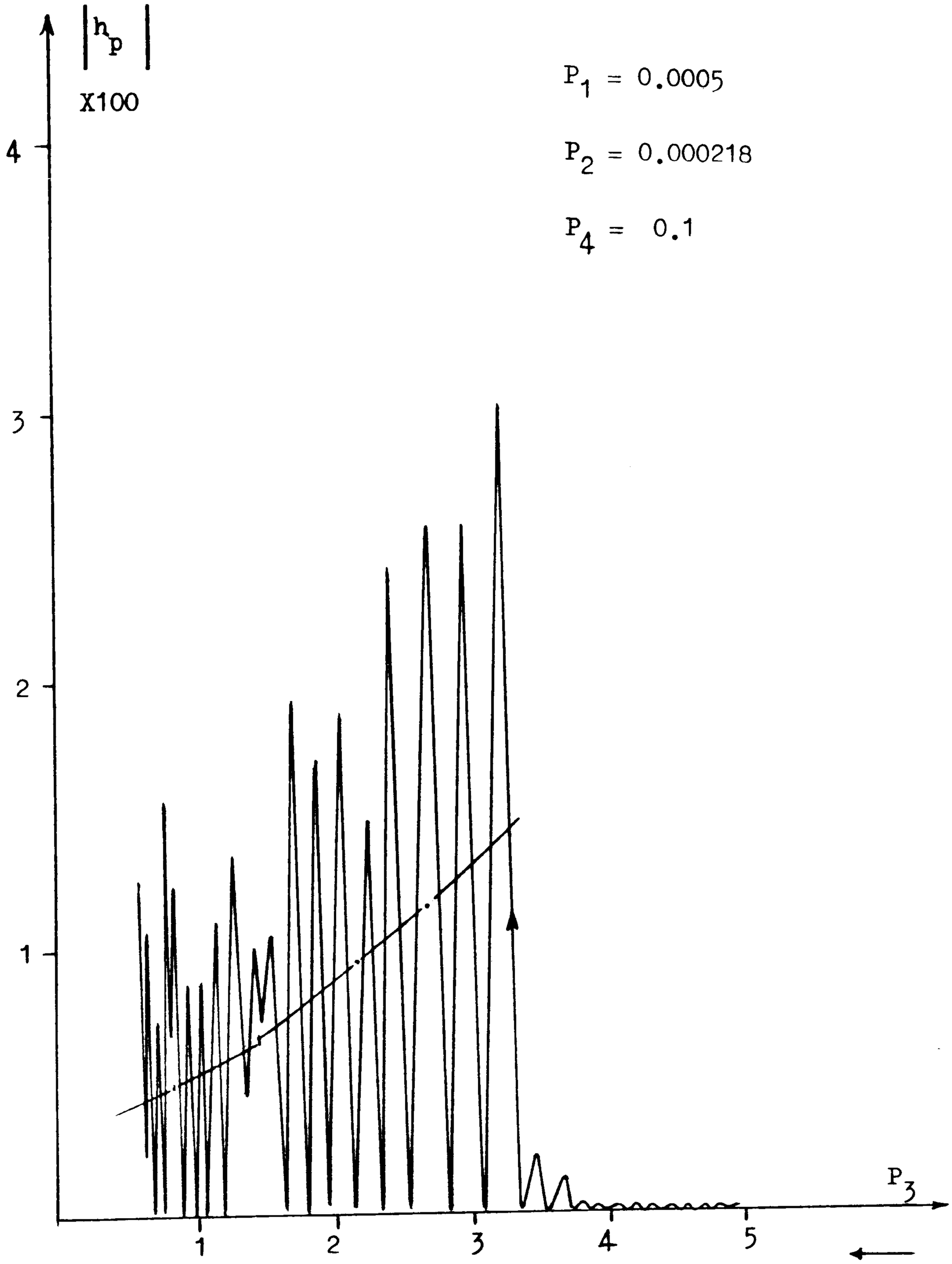

$P_1 = 0.0005$

$P_2 = 0.000218$

$P_4 = 0.1$

The value of P_3 is decreased from $P_3 = 5$

Figure 4.22 Ibid

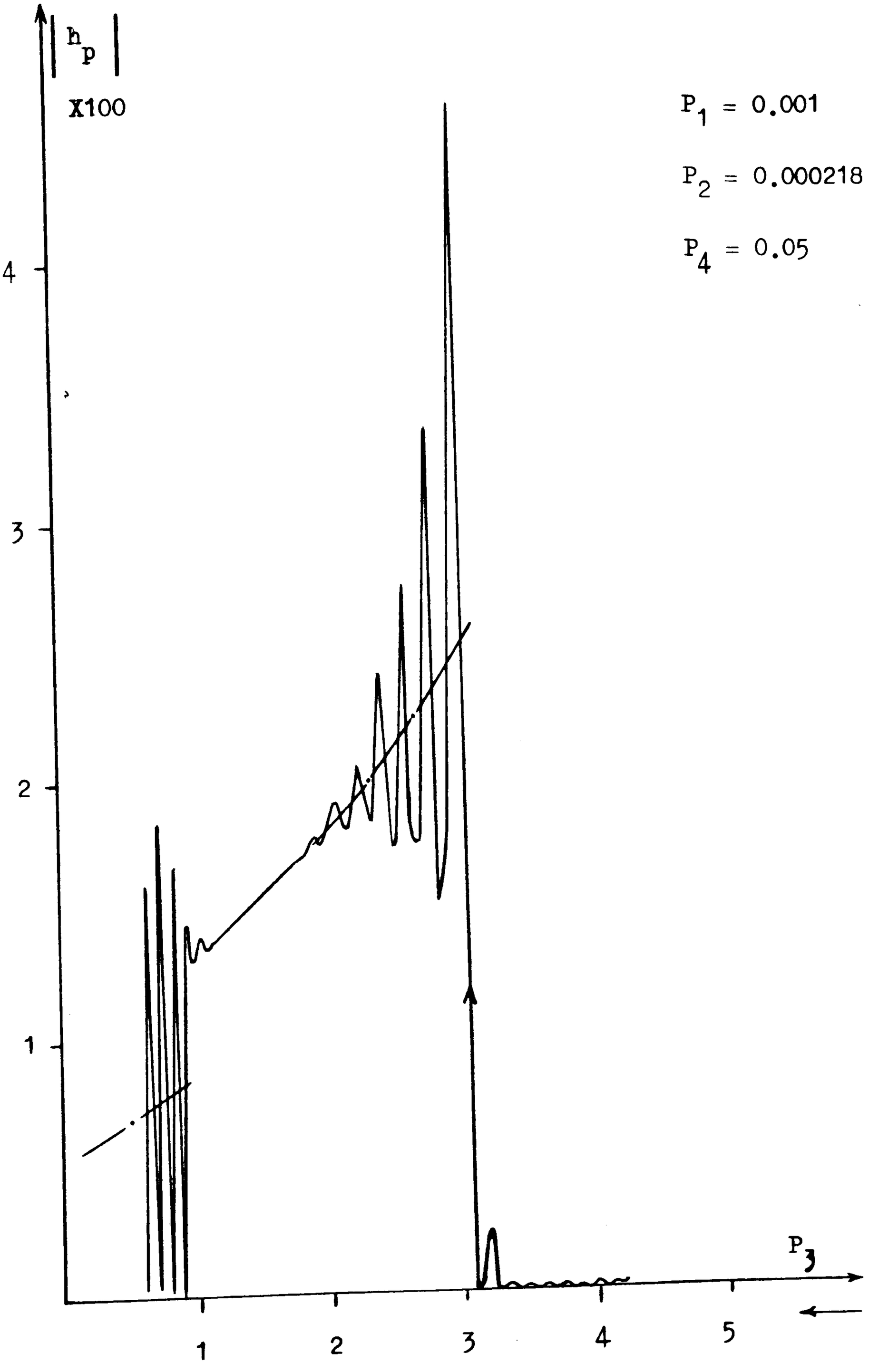

$P_1 = 0.001$

$P_2 = 0.000218$

$P_4 = 0.05$

The value of P_3 is decreased from $P_3 = 4$

Figure 4.23 Ibid

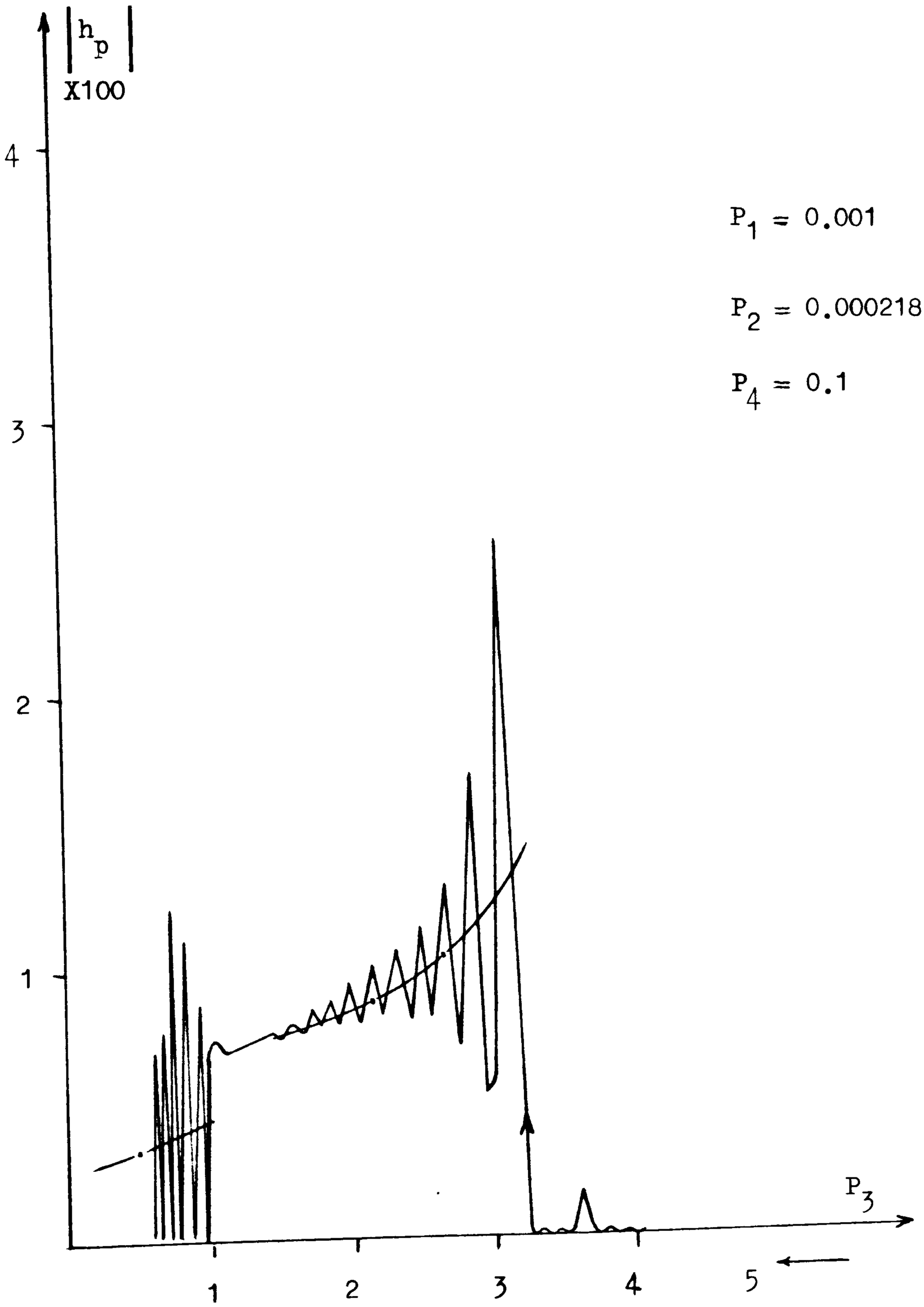

The value of P_3 is decreased from $P_3 = 4$

Figure 4.24 Ibid

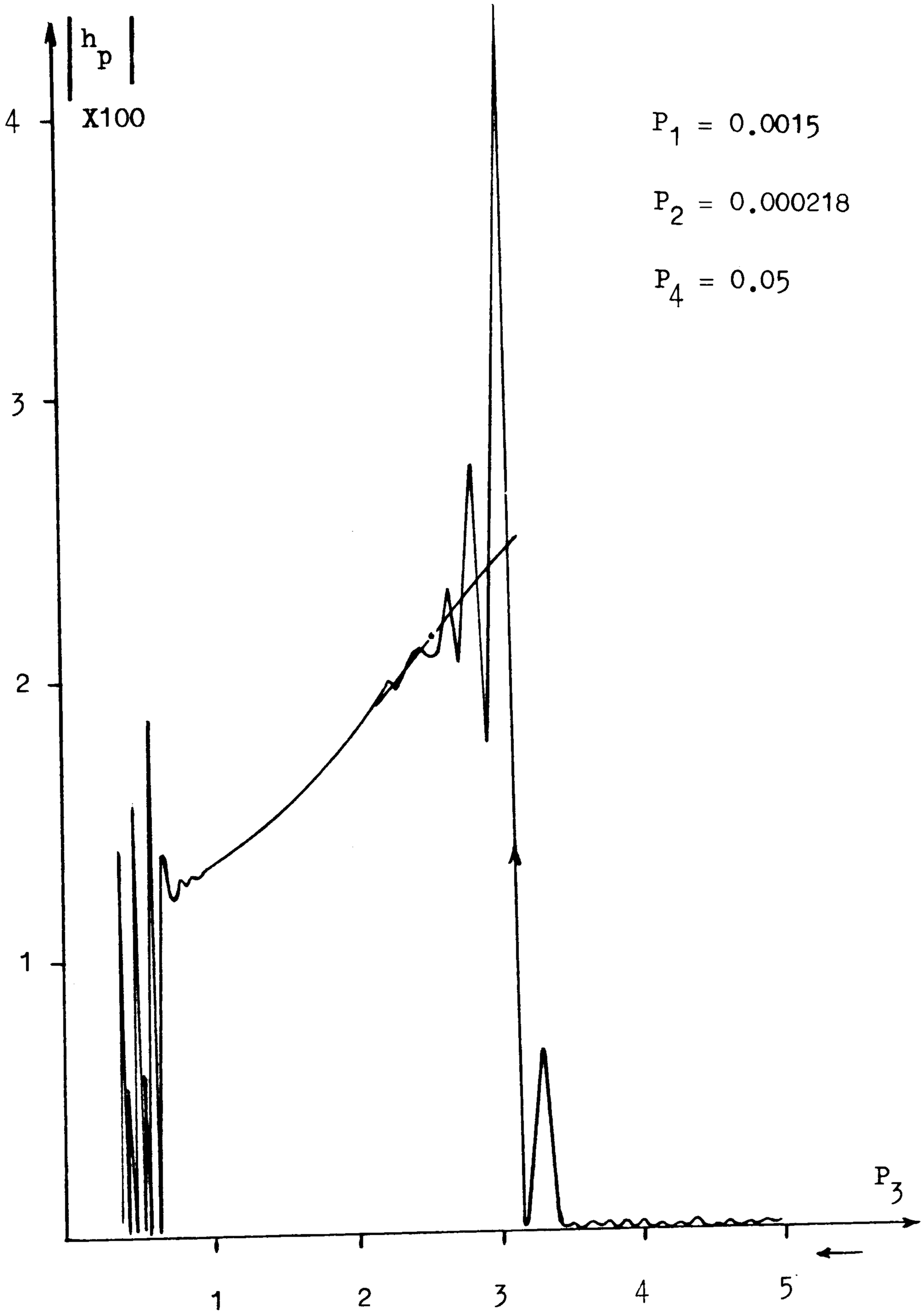

$P_1 = 0.0015$

$P_2 = 0.000218$

$P_4 = 0.05$

The value of P_3 is decreased from $P_3 = 5$

Figure 4.25 Ibid

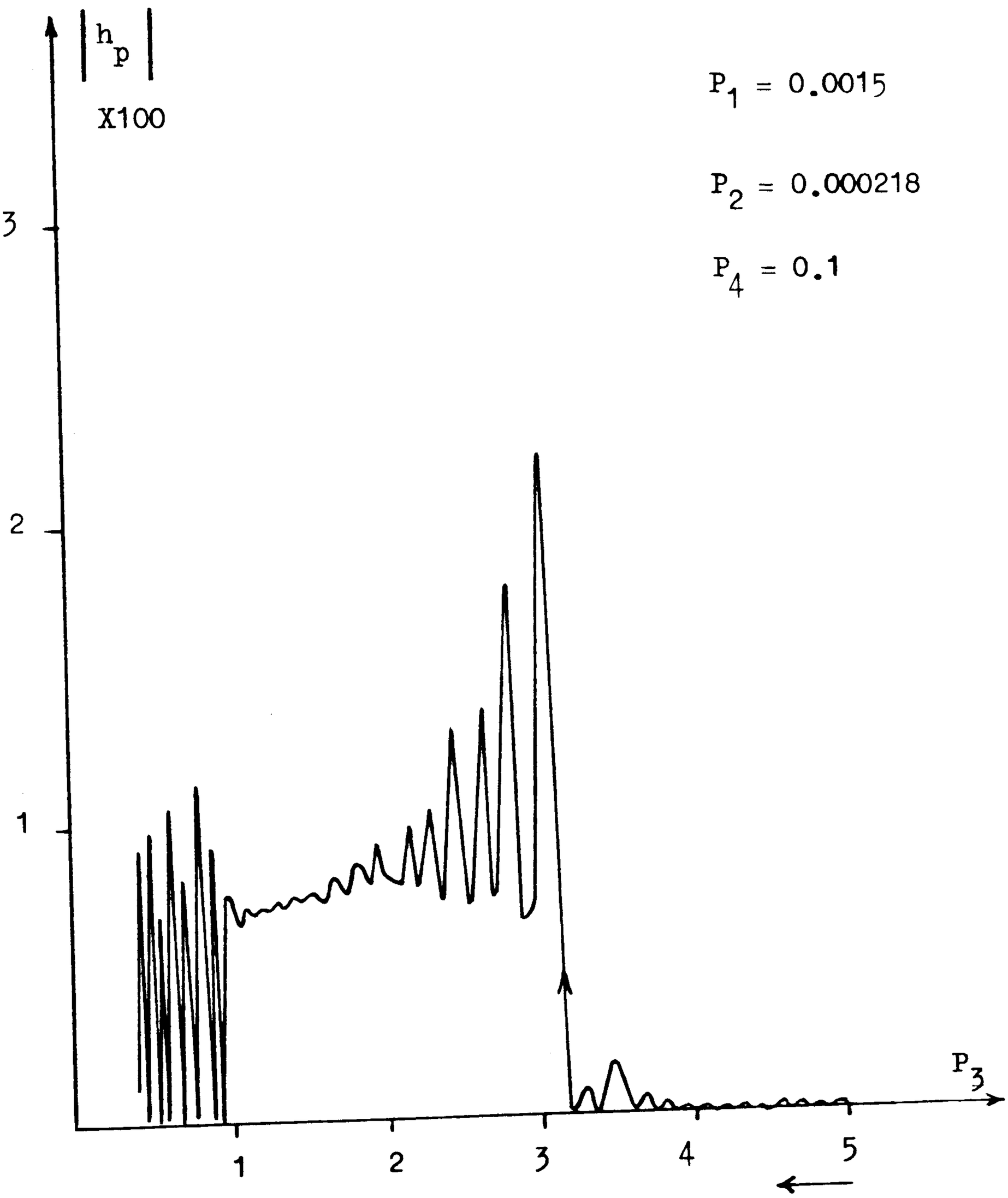

The value of P_3 is decreased from $P_3 = 5$

Figure 4.26 Ibid

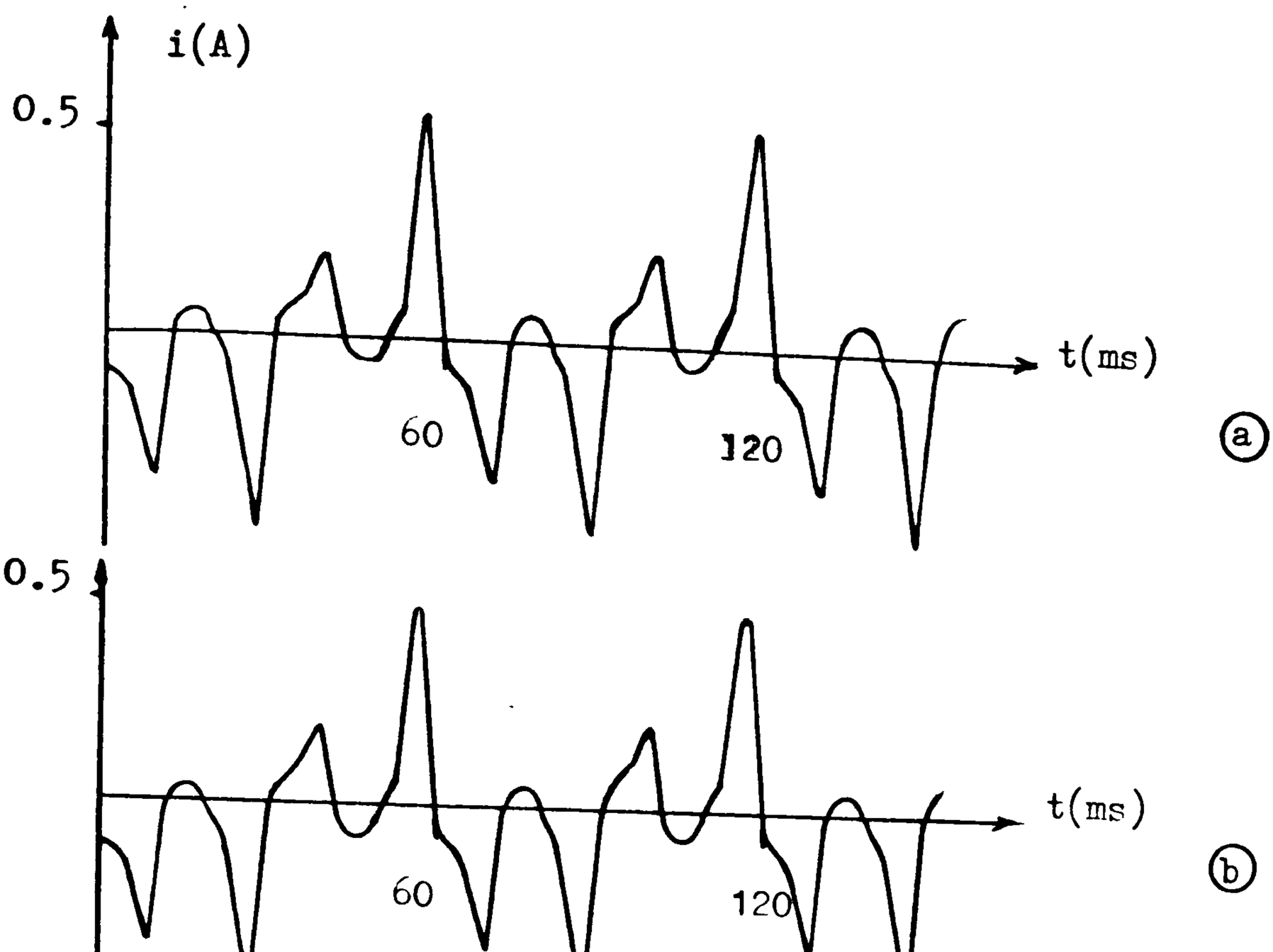

V = 70V, C = 22 μ F, R = 1.64 Ω ℓ = 2.65mH

ⓐ Recorded current waveform

ⓑ Computed current waveform - with hysteresis

ⓒ Computed current waveform - no hysteresis

Fig. 5.8 Effect of hysteresis on subharmonic Ferroresonance.

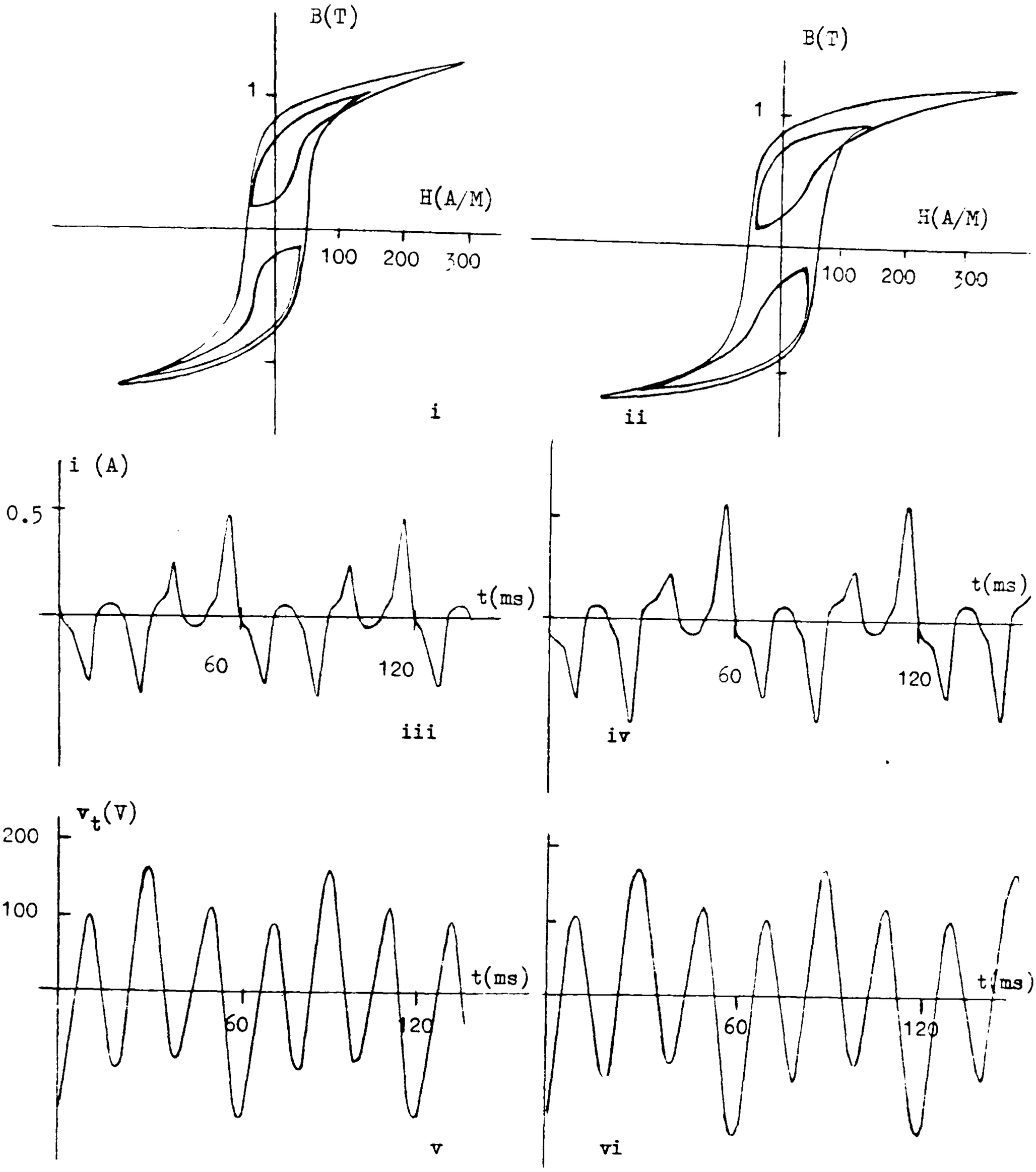

Fig. 5.9
Steady-state subharmonic resonance in a 0.5 kVA, single-phase transformer.
C = 22 μF. V = 70 V.

i Computed B/H pattern
ii Recorded B/H pattern
iii Computed current waveform.
iv Recorded current waveform
v Computed transformer voltage waveform
vi Recorded transformer voltage waveform

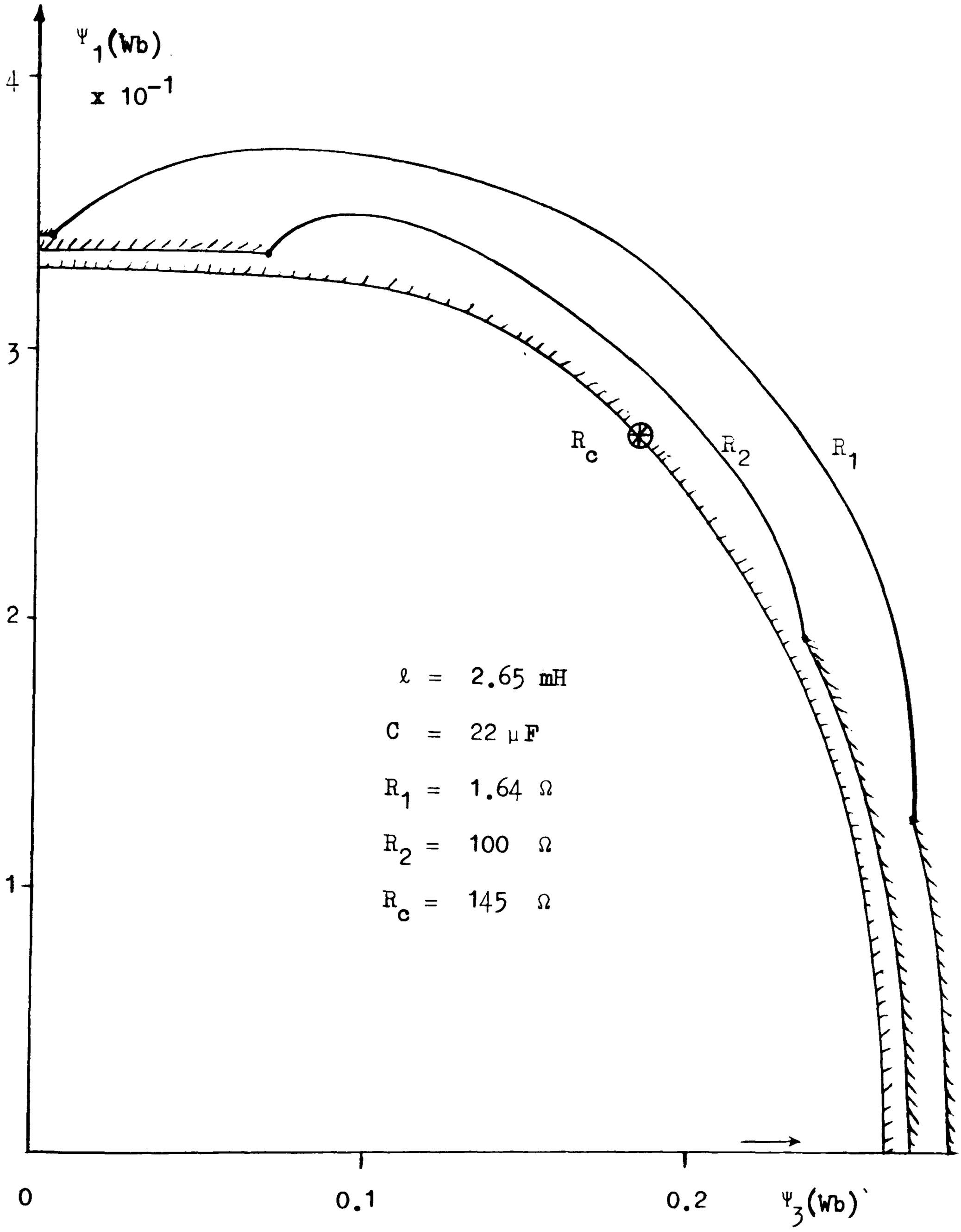

Fig. 5.10 Variation of Ψ_1/Ψ_3 characteristic with the resistance of the circuit

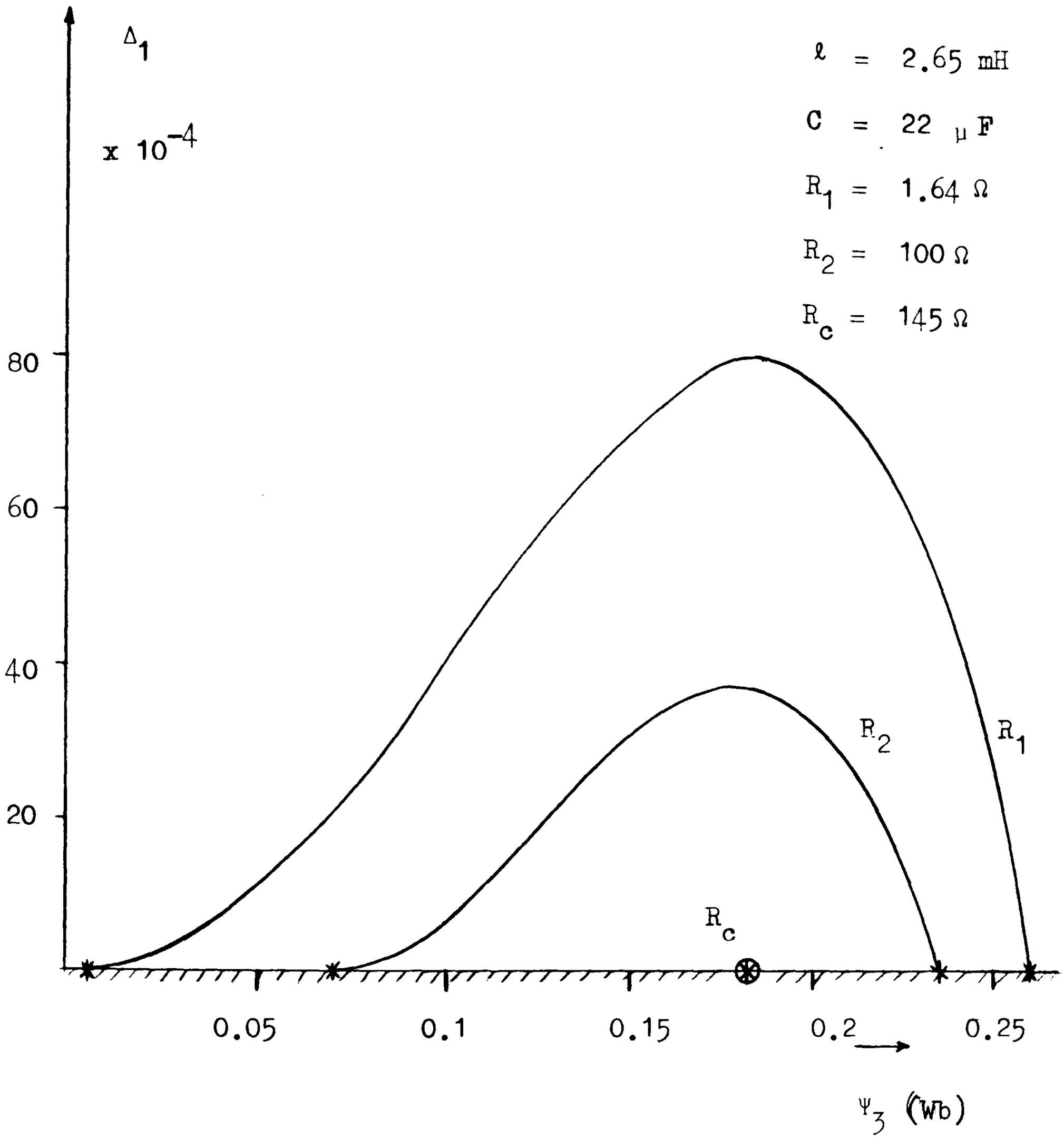

Fig. 5.11 Variation of Δ_1/Ψ_3 characteristic with the resistance of the circuit.

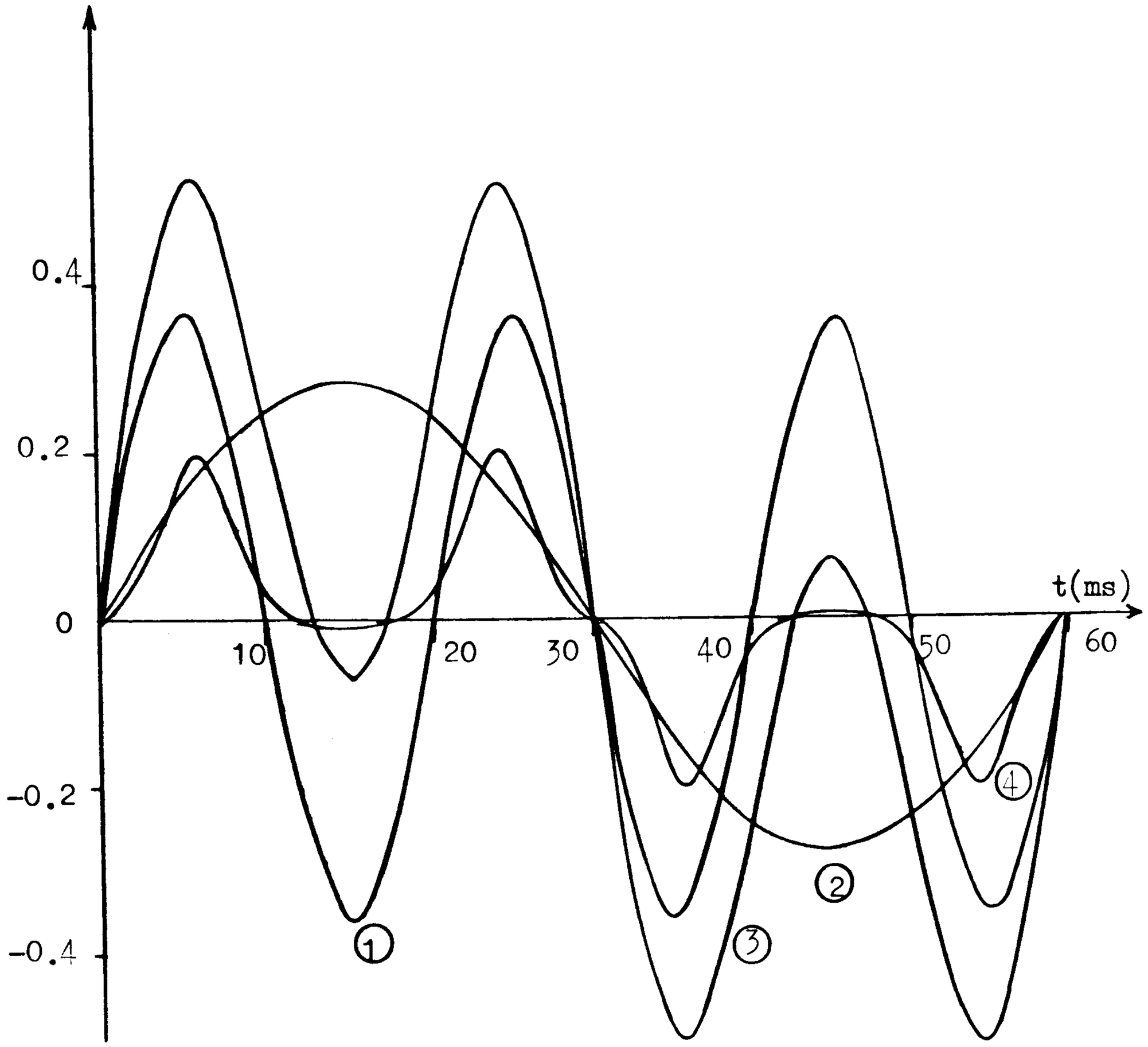

① $\Psi_3(t)$

② $\Psi_1(t)$

③ $\Psi(t) = \Psi_1(t) + \Psi_3(t)$

④ $i(t)$

The waveform of $\Psi_1(t)$, $\Psi_3(t)$, $\Psi(t)$ and $i(t)$ obtained from analytical solution $C = 22\ \mu F$, $V = 70V$, $R = 1.64\Omega$, $\ell = 2.65$ mH

Fig.5.12

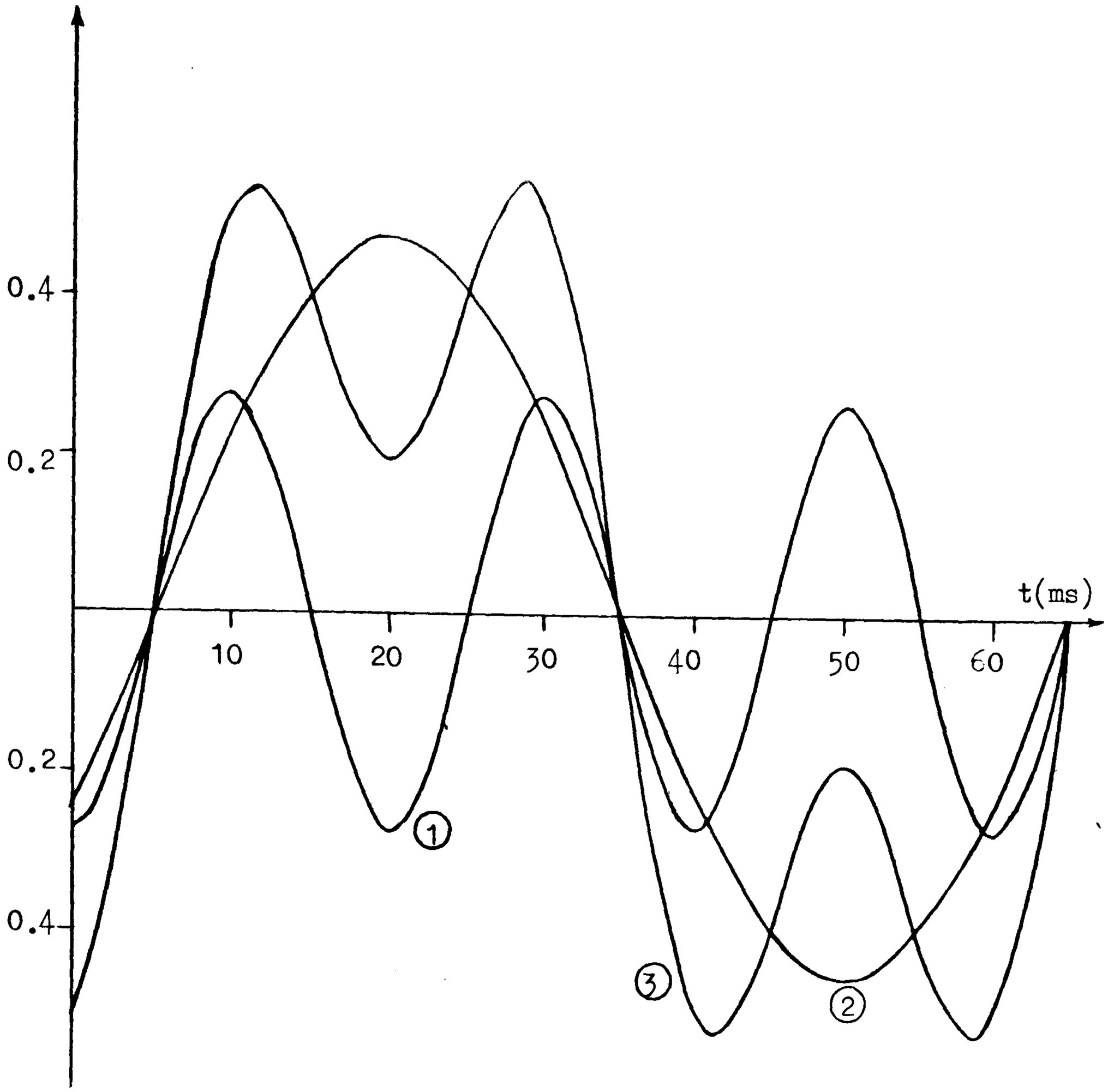

① $\Psi_3(t)$

② $\Psi_1(t)$

③ $\Psi(t) = \Psi_1(t) + \Psi_3(t)$

The waveform of $\Psi_1(t)$, $\Psi_3(t)$, $\Psi(t)$ obtained from analytical solution $C = 22\,\mu F$, $V = 50V$, $R = 1.64\Omega$ $\ell = 2.65$ mH

Fig. 5.13

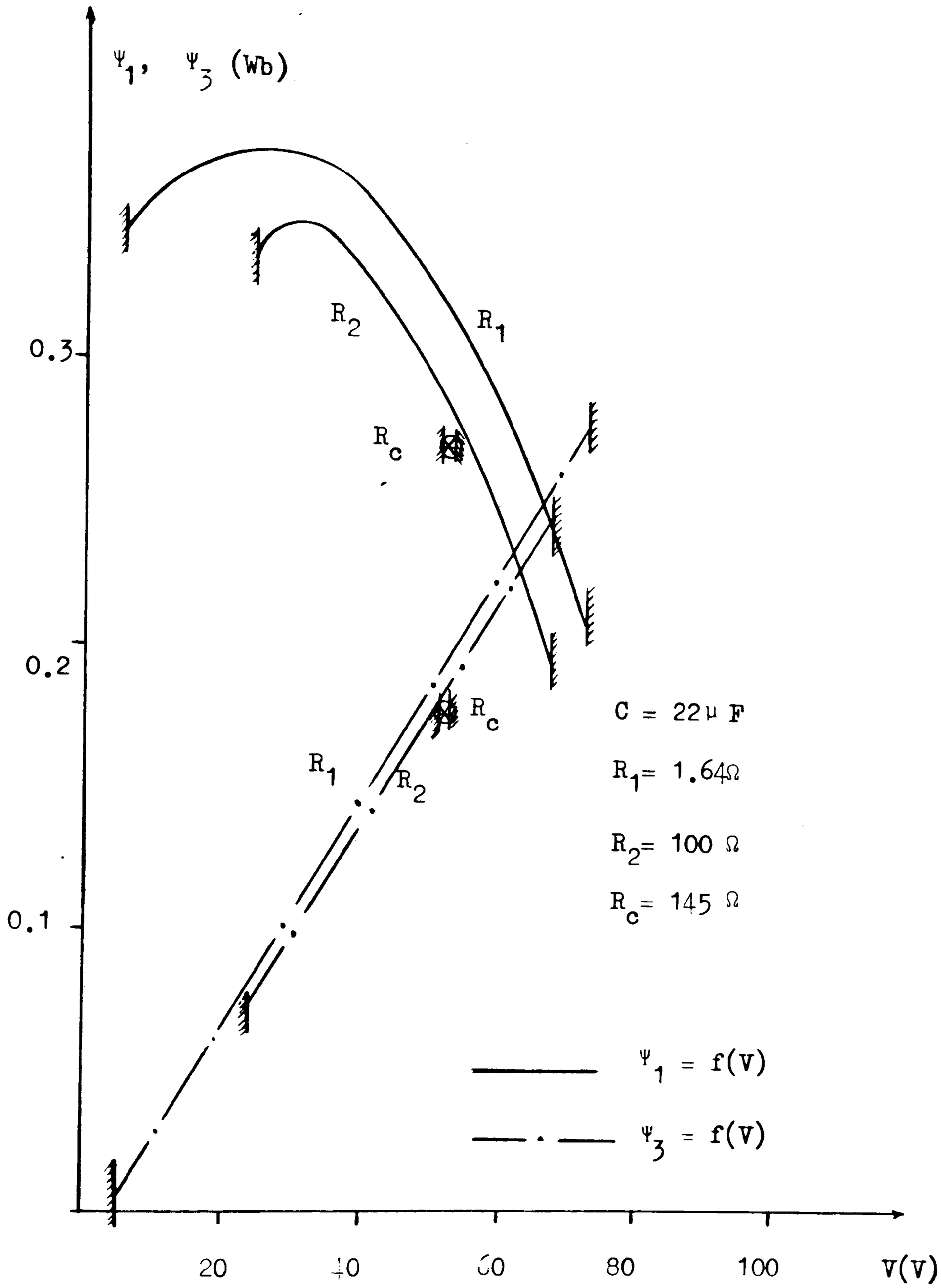

Fig. 5.14 Variation of Ψ_1 and Ψ_3 with the applied voltage

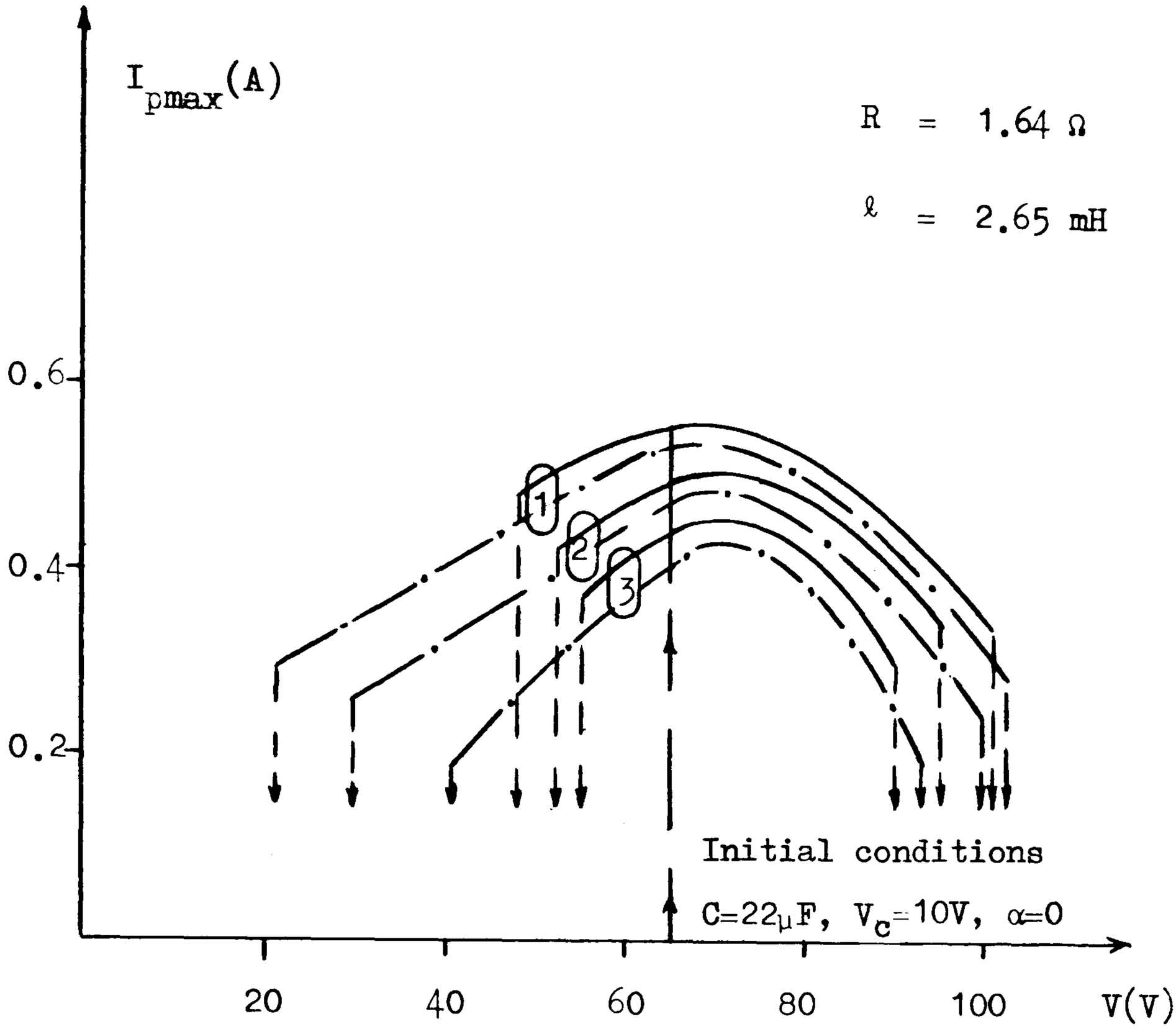

1 C = 24 μ F

2 C = 22 μ F

3 C = 20 μ F

——— Experimental results

——.—— Computed results (by Preisach model)

Fig. 5.15 The effect of the variation of capacitance on sustained I_{pmax} (maximum peak value of current) Voltage (RMS) value) characteristic.

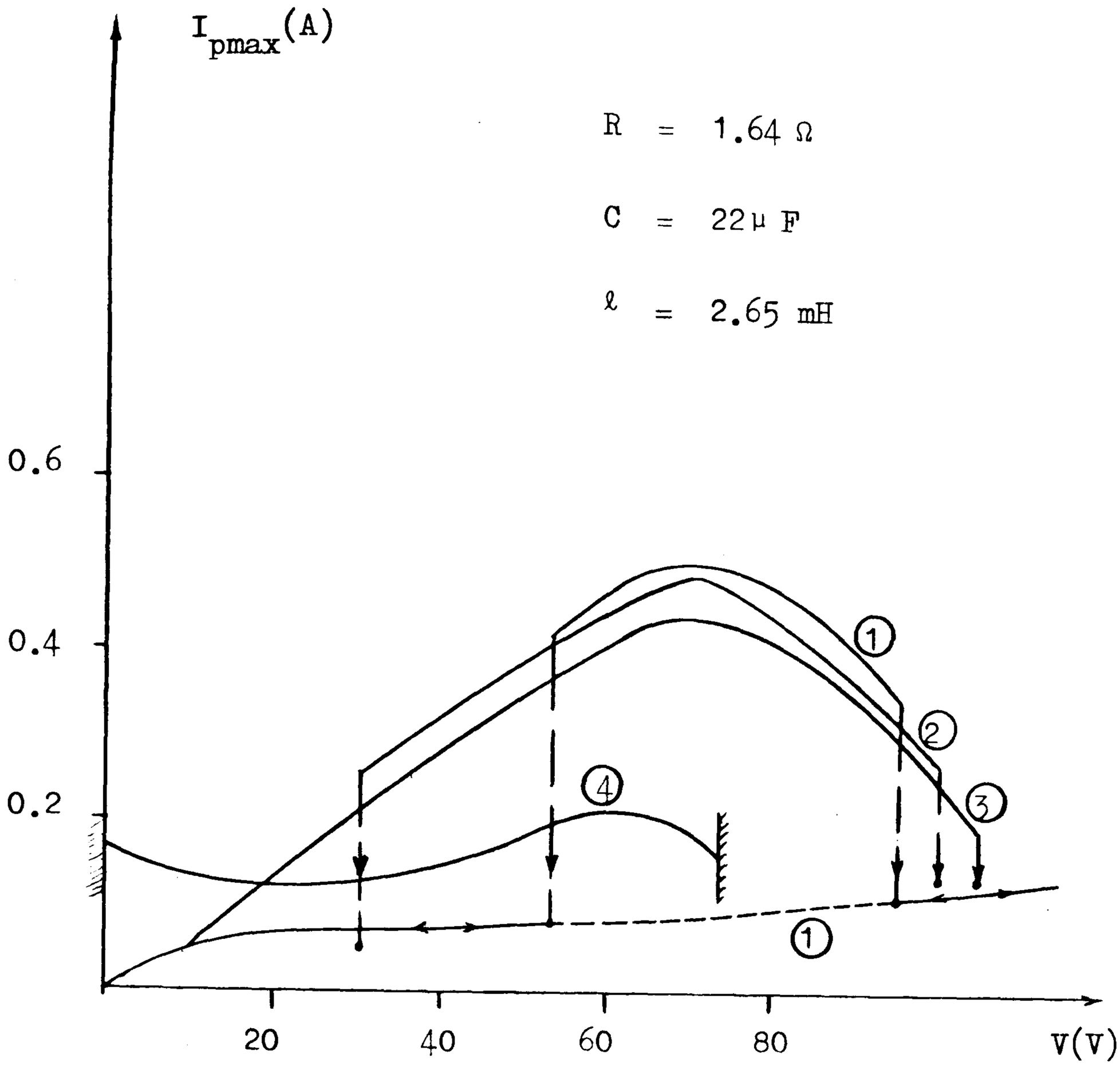

① Experimental results

② Com puted results obtained using Preisach model for BH loop representation

③ Computed results obtained using Exponential Series method for mag. curve representation

④ Analytical results

Fig. 5.16 I_{pmax} (maximum peak current) - Voltage (RMS value) characteristic